Effects of sodium benzoate on the innate immune response to gram-negative bacteria and Toll-like receptor stimulation

By

Andre Luis Ribeiro Ribeiro

A thesis submitted to UCL for the degree of

Doctor of Philosophy

Eastman Dental Institute

Department of Microbial Disease

2018

I, Andre Luis Ribeiro Ribeiro confirm that the work presented in this thesis is my own. Where information has been derived from other sources, I confirm that this has been indicated in the thesis.

non scholae sed vitae discimus

Abstract

Sodium benzoate (NaB) is a sodium salt that is widely used in the pharmaceutical, cosmetic and food industries. This widespread use results in almost everybody in the world being exposed daily to this compound. Currently very little is known about the effects of NaB can have on the immune response, even though it has been associated with the clinical course of chronic inflammatory diseases, such as orofacial granulomatosis and neurodegenerative disorders. Here, I show that THP-1 cells, a monocytic human cell line presents an altered immune response when exposed to NaB. Immunologically stimulated THP-1 cells in the presence of NaB secreted reduced levels of IL6 and IL1β and higher levels of TNF, while other cytokines such as IP10 and IL8 were unaffected. The inhibitory effect in IL6 and IL1β secretion was a consequence of a free radical scavenging characteristic of NaB, which neutralizes the reactive oxygen species (ROS) generated downstream of TLR activation. This resulted in the impairment of a secondary signalling event, which is required to fully activate the cells immune response. The use of microarray analysis in combination with q quantitative proteomic analysis revealed that NaB has a significant effect on the THP-1 cells beyond the alteration in cytokine secretion. NaB also interferes with cellular amino acid metabolism and has a major attenuating effect on the immune response. Taken together, these results suggest that NaB is not inert and has a major effect on a cells ability to mount an immune response. These findings could have major implications in how NaB is used in the future and in particular if it can be beneficial as a treatment for chronic inflammatory diseases, such as diabetes, atherosclerosis, rheumatoid arthritis, neurodegenerative disorders, and so on. On the other hand, by disturbing the inflammatory response, NaB could have a negative impact on other conditions such as orofacial granulomatosis. Further work will be needed to determine the role NaB plays in human inflammatory diseases.

Impact statement

Sodium benzoate (NaB) is widely used by pharmaceutical, cosmetic and food industries, resulting in a routinely daily exposure to most people worldwide. It is added to processed food as a preservative to control microbial growth and can be found in soft drinks, fruit juices, beers, salad dressings, but also occurs naturally in many fruits and vegetables: apples, tomatoes, strawberries, and dark green vegetables. An individual's exposure to NaB has the potential to be very high and cumulative due to the diverse sources of ingestion. Even though our ingestion of this compound is so high we know very little about how NaB affects the immune response. NaB has been associated with chronic inflammatory diseases, such as orofacial granulomatosis (OFG) and neurodegenerative disorders, such as Parkinson's disease and Alzheimer's disease. My findings will have the potential to have an impact on a whole spectrum of industries that routinely include NaB in their products.

The Oral Medicine department in the Eastman Dental Hospital is a reference service in the country to treat patients with OFG, and even though using all the resources available, only 70% of the patients had a complete resolution of their problems in a 10-year period. The treatment is usually based on immunomodulatory drugs, which have many side effects. Studies have shown that changing the patient diet for a benzoate-free type without any medication, achieves a resolution in between 50-70% of the cases, which is not too different to that observed with current medications. My results provide a plausible mode of action for NaB and how it may influence disease state in OFG. Therefore, the implementation of benzoate free diets may be used more frequently for this group of patients.

My results may have an impact on the regulatory bodies and governments that conduct routine toxicity tests on food additives and set national and international guidelines. The toxicity tests prior to approval to human consumption are usually made in a controlled environment under physiological conditions. However, in everyday life, people are exposed to many stimulatory substances and microbial agents that can stimulate the immune system and alter metabolic processes. Although the regulatory agencies require the companies to describe what is in their products

(benzoates in Europe are under the numbers E210-E219), the population should be aware of the negative effects associated with these substances.

My work has also demonstrated that using techniques such as microarray and proteomics has the potential to improve our understanding of how a compound can influence the cellular response in a non-biased way.

NaB (or any other substance capable of neutralizing ROS) which reduce the release of IL6 and IL1β can potentially work as a therapy for many chronic inflammatory diseases such as diabetes, atherosclerosis, rheumatoid arthritis, neurodegenerative disorders, and so on. It is therefore possible that my results will have an impact on a diverse array of clinical specialities and researchers who specialize in the treatment of these conditions.

Contents

Table of Figures

Table of Tables

Acknowledgements

This work was supported by the Capes Foundation, Ministry of Education of Brazil. I would like to thank and acknowledge the following people who have contributed to this body of work:

- Mrs Neuza Ribeiro, Mr Marcos Ribeiro and Mr Cezar Ribeiro – my mother and brothers for their unconditional support.
- Dr Andrew M Smith – for his supervision, guidance and support.
- Professor Stephen Porter – for his support and supervision.
- Professor Anthony W Segal – for his critical opinion.
- Dr Julio Martinez-Torres – for the uncountable thoughts shared about science and life, and for many out of hours of work together that helped to reach this point.
- Dr Adam P Levine – for his support with bioinformatics.
- Professor Kathryn Lilley, Dr Claire Mulvey, and Dr Tracey Hurrell – for their help with the proteomics study.
- Dr Houjiang Zhou – for his help with a phosphoproteomics study.
- Dr Thean Soon Chew – for his help with cell culture and orientation during the beginning of my studies.
- Dr Helen Petersen – for her help with *P. gengivalis* preparation and preliminary study with OFG patients
- Ms Juliet Foote – for her help with confocal microscopy and cellular pH measurements.
- Mr Riccardo Wysoczanski, for his help with flow cytometry.
- Ms Sabrina Pacheco, Ms Janne Plugge, and Dr Francesca Semplicci – for their technical support, and excellent laboratory management.
- Mr Bahman - Nedjat-Shokouhi – for his support with qRT-PCR
- Dr Joao Pinheiro – for his critical opinion and orientation always present in many moments of my career
- Mrs Erni Marlina, Ms Mathena Pavan, and Mr Abdulaziz Ghannam – my PhD colleagues that were always willing to help whenever necessary

- To all my colleagues and staff members at the Division of Medicine and Eastman Dental Institute - for their contribution to this work
- Mrs Sophia Joyce – for her administrative support.

Statement of Collaborative Work

A number of aspects of the work presented in this thesis were conducted as part of a collaboration. These include:

- Quantitative proteomics by mass spectrometry was performed by Professor Kathryn Lilley, Dr Claire Mulvey, and Dr Tracey Hurrell, Cambridge Centre for Proteomics, University of Cambridge.
- Quantitative phosphoproteomics by mass spectrometry was performed in collaboration with Dr Houjiang Zhou, Cambridge Centre for Proteomics, University of Cambridge. Although this piece of work is not included here, it helped to guide the cell signalling investigation and introduced me to proteomics study
- Intracellular pH measurements using confocal microscopy was performed by Ms Juliet Foote, Division of Medicine, University College London

List of Abbreviations

AD	Alzheimer's disease
ADP	adenosine diphosphate
AMP	adenosine monophosphate
ANCOVA	analysis of covariance
ANOVA	analysis of variance
AP1	activator protein 1
APC	antigen-presenting cells
APOA1	apolipoprotein A1
APOC1	apolipoprotein C-I
ARE	antioxidant response element
ASK1	apoptosis signal-regulating kinase 1
ATCC	American Type Culture Collection
ATG16L1	autophagy related 16 Like 1
ATP	adenosine triphosphate
BBB	blood-brain barrier
BCA	bicinchoninic acid
BDNF	brain-derived neurotrophic factor
BSA	bovine serum albumin
BSS	balanced salt solution
BTNL2	butyrophilin like 2
cAMP	cyclic adenosine monophosphate
CAT	catalase
CCK-8	Cell Counting Kit-8
CCL	chemokine (C-C motif) ligand
CCR	C-C chemokine receptor
CD	Crohn's disease
cDNA	complementary DNA
CDx	cluster of differentiation number
CGD	chronic granulomatous disease
CLR	C-type lectin receptors
CNS	central nervous system
CO_2	carbon dioxide
CoA	coenzyme A
CREB	cAMP response element-binding protein
CXCL	C-X-C chemokine ligand
DAAO	D-amino acid oxidase
DAVID	Database for Annotation, Visualization and Integrated Discovery
DC	dendritic cells
DMTU	N,N'-dimethylthiourea
DNA	deoxyribonucleic acid
dNTP	deoxyribonucleotide triphosphate

DTT	dithiothreitol
EAE	experimental allergic encephalomyelitis
EDTA	ethylene diamine tetraacetic acid
EGTA	ethylene glycol tetraacetic acid
ELISA	enzyme-linked immunosorbent assay
ERK	extracellular signal–regulated kinases
FBS	foetal bovine serum
FDA	Food and Drug Administration
FLG	filaggrin
GI	gastrointestinal
GPX	glutathione peroxidases
H_2O_2	hydrogen peroxide
HC	healthy control
HCL	hydrochloric acid
HD	Huntington's disease
HEPES	4-(2-hydroxyethyl)-1-piperazineethanesulfonic acid
HkEc	heat-killed *E. coli*
HkPg	heat-killed *Porphyromonas gingivalis*
HLA	human leukocyte antigen
HMOX1	heme oxygenase 1
IBD	inflammatory bowel disease
IFN	interferon
Ig	immunoglobulin
IKBa	nuclear factor of kappa light polypeptide gene enhancer in B-cells inhibitor, alpha
IKK	inhibitor of nuclear factor kappa-B kinase
IKKε	the inhibitor of kappa light polypeptide gene enhancer in B-cells
IL	interleukin
IL6r	IL6 receptor
iNOS	inducible nitric oxide
IP10	interferon gamma-induced protein 10
IRAK	interleukin-1 receptor-associated kinase
IRF	interferon regulatory factor
IRGM	immunity-related GTPase M
JNK	c-Jun N-terminal kinase
KEAP1	kelch-like ECH-associated protein 1
KEGG	Kyoto Encyclopaedia of Genes and Genomes
LB	Luria-Bertani
LC-MS/MS	liquid chromatography-tandem mass spectrometry
LPS	lipopolysaccharide
LRR	leucine-rich repeat
LTA	lipoteichoic acids
MAPK	mitogen-activated protein kinase
MAPKK	MAP kinase kinases

MD2	lymphocyte antigen 96
MDM	monocyte-derived macrophages
MEK	MAPK/ERK kinase
MHC	major histocompatibility complex
MIC	minimum inhibitory concentration
MIG	monokine induced by gamma interferon
MMP	matrix metalloproteinase
MOI	multiplicity of infection
MPTP	1-methyl-4-phenyl-1,2,3,6-tetrahydropyridine
mRNA	messenger RNA
MRS	Melkersson-Rosenthal syndrome
MS	multiple sclerosis
mSP65	mycobacterium stress protein 65kd
MTT	3-[4,5-dimethylthiazol-2-yl]-2,5-diphenyl tetrazolium bromide
MYD88	myeloid differentiation primary response gene 88
NaB	sodium benzoate
NAC	N-acetyl-L-cysteine
NADPH	nicotinamide adenine dinucleotide phosphate
NCTC	National Collection of Type Culture
NDD	neurogenerative diseases
NFkB	nuclear factor kappa-light-chain-enhancer of activated B cells
NK	natural killer cells
NLR	NOD-like receptor
NMDAR	N-methyl-D-aspartate receptor
NO	nitric oxide
NOD	nucleotide oligomerisation binding domain
NOX	NADPH oxidase
NRF2	nuclear factor (erythroid-derived 2)-like 2
NT-3	neurotrophin-3
O_2^-	superoxide anion
OFG	orofacial granulomatosis
$OH^{\cdot}$	hydroxyl radicals
OTC	ornithine transcarbamylase
Pam3CSK4	trihydrochloride
PAMP	pathogen-associated molecular pattern
PBMC	peripheral blood mononuclear cell
PBM-DM	peripheral blood monocyte-derived macrophages
PBS	phosphate-buffered saline
PCA	principal component analysis
PCR	polymerase chain reaction
PD	Parkinson’s disease
pH	potential of hydrogen
PHGDH	phosphoglycerate dehydrogenase
PKA	protein kinase A

PMA	phorbol 12-myristate 13-acetate
PPIA	peptidylprolyl isomerase A
PRR	pathogen recognition receptor
PRX	peroxiredoxins
PSAT1	phosphoserine aminotransferase 1
PSPH	phosphoserine phosphatase
qRT-PCR	quantitative reverse transcription-PCR
RIG-1	retinoic acid-inducible gene I
rIL6	recombinant IL6
RIN	RNA integrity
RIPA	radioimmunoprecipitation assay
rLPS	rough LPS
RLR	RIG-I-like receptor
RNA	ribonucleic acid
RNS	reactive nitrogen species
ROO	peroxy radical
ROS	reactive oxygen species
RPMI	Roswell Park Memorial Institute
rTNF	recombinant TNF
SASP	senescence-associated secretory phenotype
SCA	spinocerebellar ataxia
SD	standard deviation
SDS	Sodium Dodecyl Sulfate
SDS-PAGE	SDS polyacrylamide gel electrophoresis
SEM	standard error of the mean
sLPS	smooth LPS
SMA	spinal muscular atrophy
SNARF	seminaphtharhodafluor
SOD	superoxide dismutases
SOS	superoxide dismutases
STAT	signal transducer and activator of transcription
TAK1	transforming growth factor-beta-activated kinase
TBK	TANK-binding kinase
TCR	T-cell receptors
TGF	transforming growth factor
TIR	Toll-interleukin 1 receptor
TIRAP	TIR domain-containing adaptor protein
TLR	Toll-like receptor
TMT	Tandem mass tag
TNF	tumour necrosis factor α
TNFR	TNF receptor
TRAF	TNF receptor-associated factor
TRAF6	TNF receptor-associated factor 6
TRAM	TRIF-related adaptor molecule

TRIF	TIR domain-containing adaptor protein inducing interferon-β
Trx	thioredoxin
UC	ulcerative colitis
UCD	urea cycle disorders
UCL	University College London
UCLH	University College London Hospitals
UCP	mitochondrial uncoupling protein
UK	United Kingdom
USA	United States of America
UV	Ultra Violet
WHO	World Health Organization

Chapter 1 Introduction

Sodium benzoate (NaB) is a sodium salt that has antifungal and antibacterial activity. It is widely used in the food and cosmetic industry as a preservative[1,2] and is also an approved drug for the treatment of urea cycle disorders[3]. NaB and its derivates have been implicated in human diseases, showing an improvement in disease progress[4], memory, cognition[5] and overall symptoms of diverse neurodegenerative disorders[6,7,8]. On the other hand, and of special interest in this study, patients with orofacial granulomatosis are associated with the initiation of symptoms due to ingestion of benzoate-containing diets[9,10,11]. Although there is large scale usage of benzoates and its known potential effects on human health, little is known about its effects on the immune system and especially on the innate immune response of macrophages.

1.1 Sodium benzoate (NaB) and benzoic acid

NaB is a salt with the chemical formula C_6H_5COONa and a molecular mass of 144.1 $g \cdot mol^{-1}$ (Figure 1-1A)[12]. This salt does not occur naturally and requires artificial manufacturing by chemical neutralization of benzoic acid with sodium hydroxide, sodium bicarbonate, or sodium carbonate. Benzoic acid is an aromatic carboxylic organic acid (Figure 1-1B) and the main source of NaB[13]. NaB and benzoic acid (C_6H_5COOH) differ only in a single atom, the hydrogen in the carboxyl group of benzoic acid is replaced by a sodium atom.

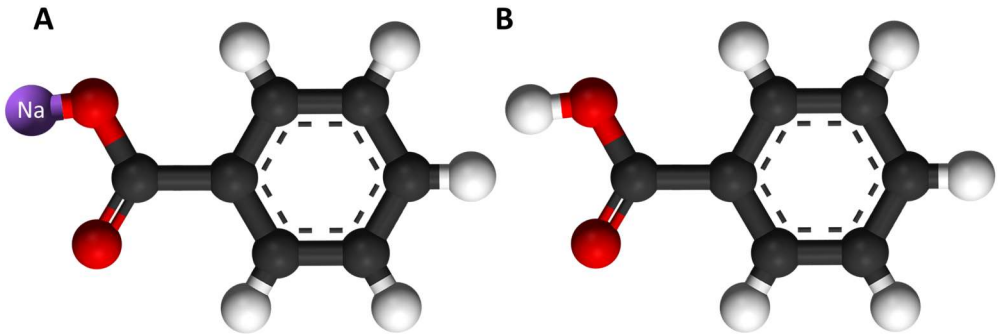

Figure 1-1: Chemical structure of sodium benzoate (A) and benzoic acid (B). Oxygen: red; Carbon: black; Hydrogen: white; and Sodium: purple. Downloaded from Google website under public domain rights.

Industrial production of benzoic acid is undertaken by oxidizing toluene with a molecular oxygen-containing gas in the liquid phase. Manganese and nickel are added to catalyse the reaction and heated up above 135 °C[14]. Sodium benzoate is the preferred form for commercialization because it forms a solid salt at room temperature (Figure 1-2), and also has a higher solubility in water when compared to benzoic acid[15]. The global production of sodium benzoate in 2015 was 72,750 tonnes[16].

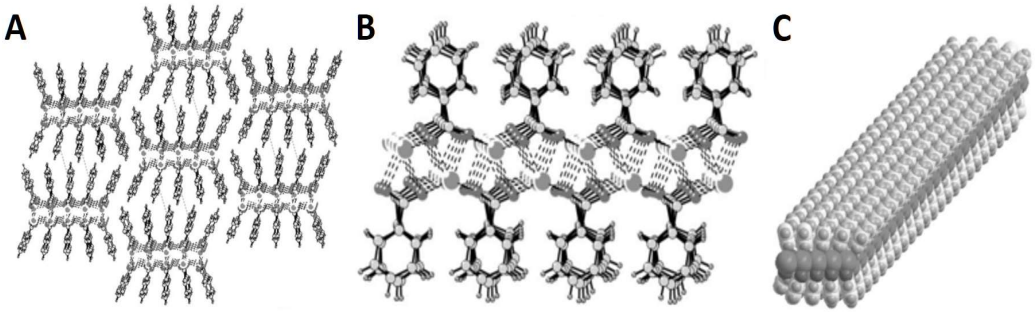

Figure 1-2: Molecular arrangement of NaB crystals. Hexagonal tapes showing π–π interactions between the tapes are dashed in grey (A). Side view of a single tape (B). Single tape representing a worm-like micelle (C). Adapted from Butterhof et al., 2013[15].

The antimicrobial activity of NaB is the main reason for its addition to foods. Furthermore, other important factors have contributed to its popularity, such as the ease of production and incorporation into products, low cost of production and low toxicity[17]. NaB has desirable properties for a food additive, such as it's colourless, odourless and a slight astringent taste, which is beneficial for minimal interference with the natural flavours and appearance of food[12].

NaB was the first chemical approved by the United States of America (USA) Food & Drug Administration (FDA) for using as a food preservative. The maximum level of NaB permitted in food is 1000 ppm (0.1% of total weight of approximately 7 mM) according to the FDA[13]. The amount of benzoates added to products in the United Kingdom (UK) is regulated by the European Union regulations and this amount is variable depending on the type of food. For instance, non-alcoholic drinks can contain a maximum of 150 mg/L, in liquid tea and fruits (600 mg/L), olives

and olive-based preparations (1 g/kg), in dietetic foods (1.5 g/kg), vegetables in vinegar, brine or oil (2 g/kg), semi-preserved fish products (2 g/kg), and concentrations as high as 6 g/kg in Crangon crangon[18]. NaB dissociates in aqueous solution to form benzoic acid. Benzoic acid and its derivatives; salts, esters and acids are generically known as benzoates and registered with E numbers E210-E219[9].

Benzoic acid occurs naturally in many fruits and vegetables: apples, prunes, cranberries, apricots, tomatoes, strawberries, peaches, avocado, dark green vegetables such as spinach, rocket and sage, and can be also found in spices such as cinnamon, and nutmeg[1,9,11,13,19]. Benzoic acid, or benzoates in general, is a food additive and used as preservatives in many processed foods such as fizzy drinks, fruit juices, beers, salad dressings, vinegar, sausages, dairy products, cocoa, hot chocolate, vinegar and pickles, prawns and some other shellfish[1,9,11,13,19,20]. Cosmetic and pharmaceuticals products are other important sources of benzoates that can contribute to the total intake dose of benzoates by humans (Figure 1-3)[21].

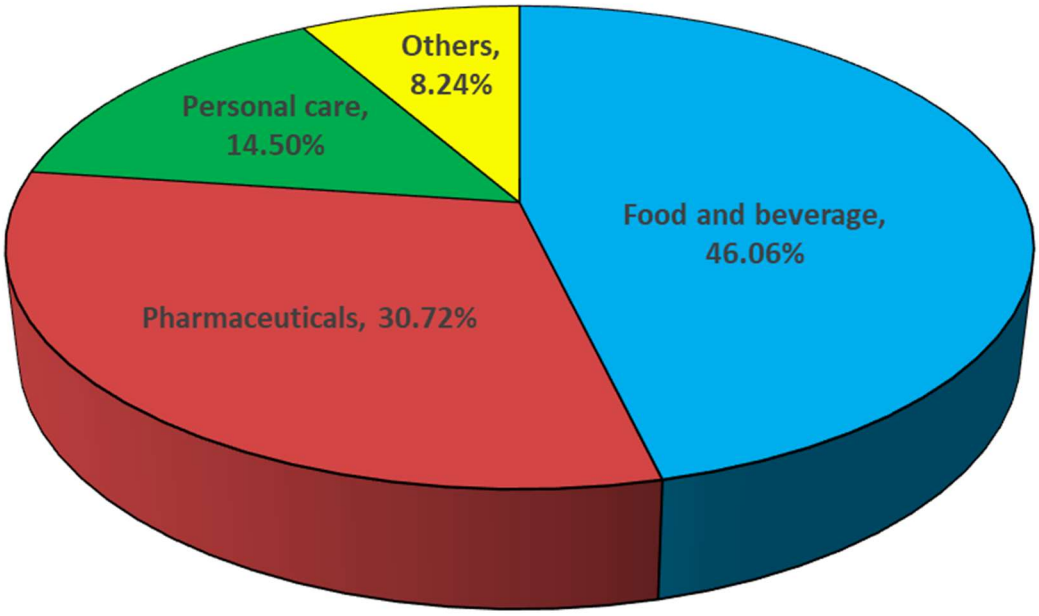

Figure 1-3: Global sodium benzoate market by application 2016. Data source from Technavio, 2017[21].

Benzoate consumption is rising worldwide. Food and beverages accounted for nearly 49% of world consumption of benzoic acid in the form

of sodium and potassium benzoate in 2013, increasing at an average annual rate of 10.7% compared to the 4 previous years.[22] While the rise in concerns about the use of synthetic preservatives, especially in Europe and North America caused a market decline, the Asia Pacific, Middle East and Africa markets are compensating, in part, due to a rise in the search for convenient food in these regions[16]. The Asia Pacific and Europe accounted for 64% and 22.5% world consumption respectively. China is the leading producer and consumer in the world, consuming more than 50% of the world production of benzoates[16].

1.1.1 Antimicrobial mechanisms of benzoates

The mechanisms of action of benzoates are pH-dependent. The antifungal and antibacterial activity of benzoic acid is carried out by its undissociated form, which varies from 93.5% at pH 3, 59.3% in pH 4, 12.8% in pH 5 and only 1.44% in pH 6, with a pKa of 4.204 at 25 °C[13]. The required concentration of benzoic acid to inhibit yeast growth increases as the pH becomes less acidic. At pH 3, the majority of yeast growth is inhibited with a concentration of 250 mg/L, whereas at pH 5, the concentrations required to control yeast growth to the same extent is between 500-750 mg/L, and at pH 7, all yeasts that tolerated this pH can grow even with a dose of 1200 mg/L of benzoic acid[23].

Several mechanisms are involved in benzoates microbial inhibitory growth effects. Benzoic acid, as a weak organic acid, has its maximum inhibitory activity at low pH. In low pH, the uncharged and undissociated benzoic acid is sufficiently lipophilic to traffic across the microbial cell membrane and enter the cell[24] (Table 1).

Table 1: Effect of benzoate concentration inside and outside the cell according to change in external pH. The concentration of benzoic acid was 0.01mM at pH below than 6.96 and 2mM in pH equal or higher than 6.96.

pH of external medium	Ratio [benzoate] in / [benzoate] out	pH in intracellular water
2.5	39.5	5.8
3.54	63.2	6.08
4.43	37.1	6.2
5.91	2.98	6.39
6.78	0.71	6.62
6.96	0.34	6.5
7.16	0.22	6.51
7.47	0.12	6.53

Data source: Krebs et al., 1983[24].

As an immediate effect, when the benzoic acid reaches a higher pH within the cell cytoplasm, the molecules dissociate and accumulate protons and anions inside the cell, changing the intracellular pH and other key metabolic reactions (Figure 1-4)[25].

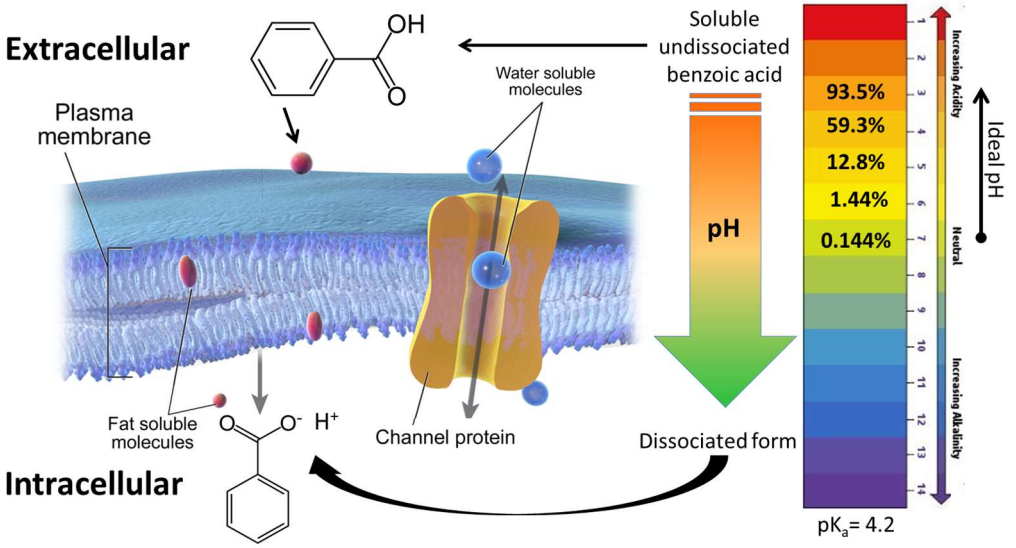

Figure 1-4: Schematic balance of benzoic acid in the intra and extracellular compartments. Undissociated benzoic acid is found in a higher percentage in acid conditions (see scale bar). In this medium, these lipophilic molecules can easily pass across the plasma membrane by simple diffusion, but when they reach a more neutral and stable intracellular pH, they dissociate and can interfere with cell metabolism. Adapted from Blausen.com staff.

The effects of intracellular pH-change after sodium benzoate administration was evaluated in *Bacillus subtilis*, results showed that after the administration of NaB, there was a reduction of intracellular pH and only mild and transient changes in the extracellular pH. A transcriptome analysis was carried out and showed that the main changes observed in gene expression profile were related to pH homeostasis and similar to those observed in external pH reduction induced by acid. The pH stress genes included important acid reversal mechanisms, such as formate dehydrogenases and amino acid transporters[26]. Furthermore, resistance against weak organic acids is associated with genes known to regulate cytosolic pH. Resistance to organic acid preservatives has been reported for the following species of yeasts: *Saccharomyces cerevisiae, Zygosaccharomyces bailii*, and *Zygosaccharomyces rouxii*. These species upregulate the expression of H^+ ATPases to control the cytosolic pH[27].

It is believed that weak acid preservatives will diffuse into the cell until anions and cations reach an equilibrium with the pH gradient across the membrane[25]. The metabolic changes induced by benzoates include inhibition of fermentation due to ATP depletion; interference with the permeability of the microbial cell membrane causing reduced transport of amino acid and cell starvation; and inhibition of specific enzyme systems within cells[13,25]. The changes in intracellular pH cause an energetic expensive stress response to the cell attempts to restore the homeostasis resulting in limited energy availability for cell division and other metabolic functions[25].

Krebs et al. 1983[24] investigated the effects of benzoates in a strain of baker's yeast (*Saccharomyces cerevisiae*) to elucidate their antifungal mechanism. The authors found that there was a relationship between intracellular pH, phosphofructokinase inhibition and CO_2 production. They concluded that benzoates accumulate inside the cell at low pH affecting the function of phosphofructokinase and causing glycolysis inhibition and ATP depletion and subsequently growth restriction (Figure 1-5).

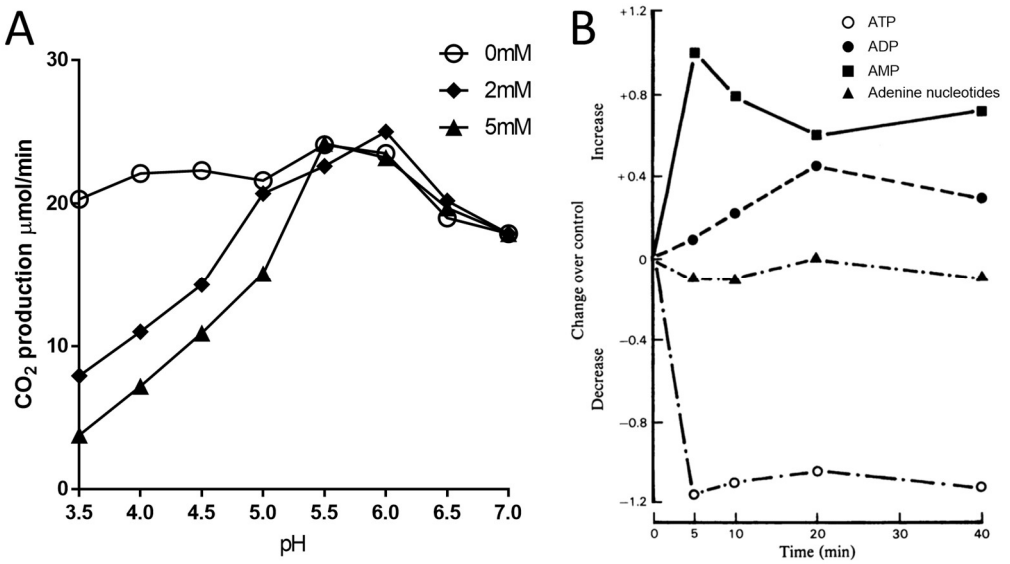

Figure 1-5: Effects of benzoate in intracellular anaerobic CO_2 production (A) and on adenine nucleotides during anaerobic fermentation (B). CO_2 production is reduced in pH <5 with concentrations of 2 mM and 5 mM in a dose-dependent manner. The effect of 5mM benzoic acid is eliminated at pH 5.5 (A). The ATP concentration fell dramatically after 5 minutes exposure to 10 mM of benzoic acid. An almost similar proportional increase was observed in the concentration of AMP, while the ADP showed a slight increase. It suggests an important inhibition in ATP synthesis caused by benzoic acid. Data source (A) and adapted image (B) from Krebs et al. 1983[24].

Increased CO_2 production in low pH is a property common to all weak acids preservatives and does not explain all the antimicrobial effects of these substances, otherwise, the antimicrobial properties of all acid preservatives would be directly related to their dissociation properties, which is not true[28]. Stratford and Anslow 1998[28] investigated the effect of some weak acids on growth inhibition of many yeast species and found that the minimum inhibitory concentration (MIC) differ among them. They showed that yeast species that were more sensitive to ethanol, a known solvent capable of disrupting membrane compounds, were also more sensitive to specific weak acid preservatives, especially to sorbic acid and benzoic acid. This result suggests that benzoic acid may act as a hybrid compound, acting as a proton donor and as a membrane-active compound[28]. A possible effect mechanism involving anion toxicity has also been suggested[27,29].

1.1.2 Food spoilage

Food loss and waste is a massive burden on the whole society. Food loss happens in all stages of the food chain and involves losses in production site; post harvesting, handling and storage; processing and packing; distribution and retail stores; and finally at the consumer level[30]. It is estimated that one-third of all food produced along the entire food chain in the world is lost or wasted, this counts for 1.3 billion tons per year[31].

The percentage of food lost in the food chain vary according to the type of food (Figure 1-6), but independent of the type of food, the main losses happen of the bottom of the chain at the consumer level[30].

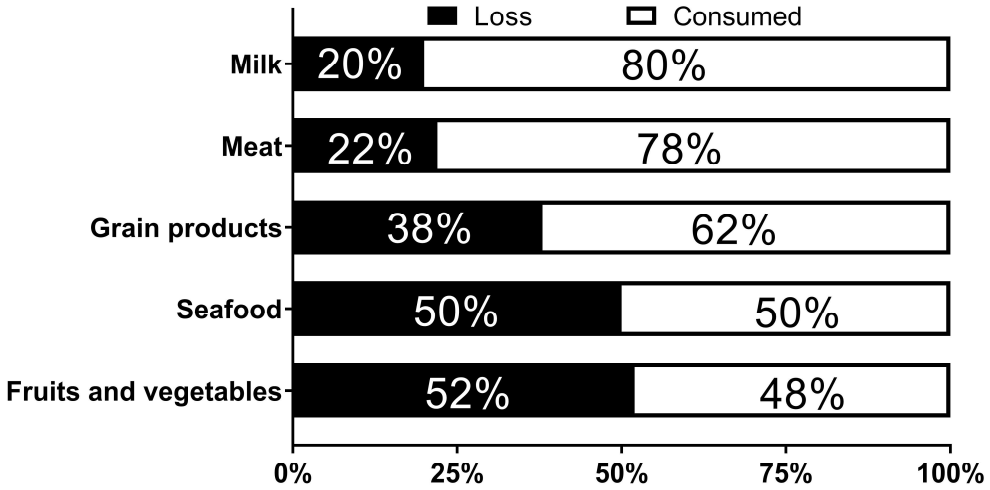

Figure 1-6: Percentage of food consumed and food loss in United States, Canada, Australia and New Zealand. Data source Food and Agriculture Organization of the United Nations, 2011[31].

Consumers are responsible for an average 58% of all losses in the food chain and two-thirds of these losses are due to spoilage[30]. A report from the UK Waste & Resources Action Programme has estimated that a reduction in 50% of food waste would save around 300 billion US dollars per year. The USA and Europe are responsible for 60% of food waste and from it, 21% is due to spoilage[32]. Microbial growth is the main factor that causes food spoilage and on the top of the economic burden, food spoilage is a world health problem responsible for foodborne intoxication[33].

According to the World Health Organization (WHO), there were 600 million cases of foodborne illnesses and 420,000 deaths due to foodborne diseases in 2010. Among these deaths, one-third were children, who account for only 9% of the entire population. Low-income countries have the highest rate of foodborne disease, with a high prevalence in Africa, followed by Southeast Asia[34].

In the UK, the Food Standards Agency estimates that around 1 million people suffer some type of foodborne illness, with 20,000 people requiring hospital treatment and 500 deaths per year. This consumes around £1.5 billion of the public funds yearly[35].

Many strategies can be used by the food industry to prevent microbial spoilage, which includes low-temperature storage, heat treatment, rich CO_2 atmosphere, modified atmospheric packing system, pH control and preservatives[36]. Food preservatives, such as benzoates and sorbic acid are convenient products due to the low cost and easy manipulation and addition to food products. NaB had a growing market valued at US$ 122.94 million in 2015[16].

1.2 Sodium benzoate and human diseases

Sodium benzoate has been linked to human diseases in many ways, as a therapeutic drug to treat urea cycle disorders[37,38], as an antioxidant[39], as an immunomodulator in neurogenerative diseases (NDD) [1,6,40], and also as a trigger for symptoms in patients with orofacial granulomatosis (OFG) [9,11,41]. OFG and NDDs are both characterized by chronic inflammation, however, they show a completely different response to benzoate. Although some studies have tried to understand the effects of NaB on the immune system, these effects are still poorly understood.

1.2.1 OFG and sodium benzoate

OFG is a rare chronic inflammatory granulomatous disorder that causes enlargement of the orofacial soft tissues, with clinical characteristics similar to the oral manifestation of Crohn's disease (CD)

and sarcoidosis[42,43,44,45]. The causes of OFG are unknown and many theories have been postulated to explain its aetiology, but none of them has provided convincing evidence to date[43,46]. However, there is a growing evidence that supports an allergic cause and NaB is the most common allergen associated with OFG[9,47].

Currently, OFG is considered a distinct entity, which should be differentiated from oral CD, tuberculosis and sarcoidosis[45]. OFG presents with localized oral granulomatous lesions similar to granulomatous cheilitis and Miescher's cheilitis; and characteristics that may overlap with the triad of Melkersson-Rosenthal syndrome (MRS) (orofacial swellings, facial nerve palsy and fissure tongue)[48,49]. Oral inflammation with indistinguishable features of OFG usually precedes CD, especially in adolescent patients[50,51].

The term OFG was first described in 1985 by Wiesenfeld *et al*., which encompassed two previously described entities: MRS and cheilitis granulomatosa[48]. OFG may present with different phenotypes, which include facial and lip swelling (upper and/or lower lip), mucosal cobblestoning, gingival enlargement, oral ulceration, mucosal tags and oedema, angular cheilitis and median lip fissures[48,52,53,54]. The most common clinical feature of OFG is lip swelling, affecting more than 50% of patients[48,52,54]. Other common clinical signs are oral ulceration[48,52,54] and cobblestoning (Figure 1-7)[52,54]. Disfigurement of the face and/or lips due to tissue fibrosis after long-term swelling is the main complication of OFG and normally the reason why patients seek treatment[42,52].

Figure 1-7: Clinical features of OFG. Disfiguring upper and lower lip swelling (A) with mucosal fissures (B). Hyperplasic mucosal folds (C) and oral ulcers are frequently found. Another painful lesion associated with OFG is angular cheilitis (D). Images kindly provided by Prof Stephen Porter.

The prevalence of OFG is difficult to establish due to limited information. It appears that OFG is more common in developed countries, with the majority of publications coming from the United Kingdom and Ireland[9], with a possible higher prevalence in Scotland[55]. Although OFG is considered an uncommon disease, the increasing number of reports may suggest that its prevalence is rising[52].

The histopathological features of OFG are not pathognomonic and encompass a non-specific inflammatory infiltrate with non-caseating granulomas, the presence of multinucleated giant cells, lymphocytes and Langerhans cells. Oedematous changes of the superficial corium with dilated lymphatic and blood vessels may also be present[48,52,54]. The non-caseating granulomas are usually small and loose, with lymphocytes in the surrounding tissue[52,56]. Some authors have associated the formation of the granulomas in OFG with lymphocytes, specifically T-cells[57,58].

A higher number of $CD4^+$ T cells are found inside and outside the granulomas of OFG samples when compared to a control group of other granulomatous lesions that do not fit the inclusion criteria of OFG[58]. Furthermore, the T-cells found in the OFG lesion demonstrate a similar diversity of T-cell receptors (TCR) when compared to T-cells from

peripheral blood from OFG patients and healthy individuals[57]. According to the authors, the T-cell population surrounding OFG lesions do not undergo clonal expansion and are the result of a random influx of T-cells at the inflammation site rather than a response to a specific antigen[57].

The histopathological features of OFG are identical to the oral manifestation of CD[49] and sarcoidosis[43]. Indeed, the diagnosis of OFG should be established after excluding these diseases first[49,52]. The differential diagnosis of OFG may be quite complicated because the main clinical symptoms are sometimes indistinguishable from other granulomatous disorders such as CD, sarcoidosis, infectious disease (tuberculosis and leprosy), reactions to foreign bodies, and delayed hypersensitivity reactions[49].

Thus, some authors have established the criteria for a true diagnosis of OFG that include: the presence of one or more clinical signs, such as facial and/or lip swelling, mucosal cobblestoning, gingival enlargement, oral ulceration, mucosal tags and oedema, angular cheilitis and median lip fissures; presence of non-caseating granuloma in histopathology assessment (not mandatory), and exclusion of other systemic granulomatous diseases (CD, sarcoidosis, tuberculosis, etc) [49,52].

1.2.1.1 Causes of OFG

The aetiology of OFG is unknown and has been a matter of discussion since it was first described. Some theories have tried to explain the causes of OFG, but all failed to find a consensus. These theories have tried to characterize OFG as a result of genetic predisposition, infection, allergy or immunological disorder, but controversial concepts have also been raised[43,46].

The first attempt to link OFG to a genetic predisposition investigated the human leucocyte antigen (HLA) in OFG patients. The HLA phenotype of peripheral blood of a small population of 16 OFG patients in Scotland was compared to 516 control individuals from West Scotland and found that HLA types A2, A3, B7, DR2, DR3, and DR4 of OFG patients were found in higher frequencies than in the control group. According to the

authors, data from a meta-analysis showed that HLA-A2 carries an elevated risk for CD, whereas HLA-A11 showed a negative correlation. They showed that 25% of the OFG patients tested for HLA-A11 and half of them were also positive for HLA-A2. These results suggest a different genetics from Crohn's disease[59,60]. However, these results have never been replicated[61].

A Swedish cohort has investigated NOD2 polymorphisms in two groups of OFG patients, with (n=17) or without (n=12) CD and similar oral phenotype. Using DNA from buccal swabs the authors assessed the NOD2 variants Arg702Trp, Gly908Arg and Leu1007fsinsC, all previously linked to gastrointestinal CD. None of the OFG only patients showed any of the NOD2 variants polymorphism, whereas one-third of patients with CD had the NOD2 variant Arg702Trp. The authors concluded that OFG patients with or without CD had a similar oral phenotype but genotypic differences regarding NOD2[62].

In a larger cohort from the UK, 201 patients with OFG, also with or without CD, and 1023 healthy controls were genotyped for risk variants with some similarities to OFG: NOD2, IRGM, IL23R, ATG16L1 (CD), BTNL2 (sarcoidosis), and FLG (atopy). The results showed no association between known CD-risk variants of NOD2 and OFG. There was an association between NOD2 p.L1007insC and OFG with CD. When these groups were analysed together (OFG only and OFG + CD), there was an association with the CD-associated IL23R p.R381Q and the sarcoidosis risk variant rs2076530 in BTNL2. The authors suggested a genome-wide association scan to fully define the genetic architecture of OFG[61].

Another theory regarding the causes of OFG has linked it to infection. This theory relies on the implication of microorganisms in other granulomatous diseases with similar features, such as tuberculosis[43,46]. Apaydin *et al*. reported the presence of *Mycobacterium tuberculosis* in 3 of six biopsies of MRS/OFG patients and suggested a possible role of mycobacterium in the aetiology of OFG.[63] Using a different approach, Ivanyi *et al*. investigated the presence of mycobacterium stress protein 65kd (mSP65) in the serum of 10 patients, 6 OFG only and 4 with CD, and found positive levels of serum protein in 7, 4 CD and 3 OFG patients.[64] A

supposed case of OFG due to *Mycobacterium tuberculosis* was reported[65], however many of diagnostic criteria of OFG were not observed in this report. The current literature does not support the role of *Mycobacterium tuberculosis* in the pathogenesis of CD[66].

Another possible link of microorganisms in the cause of OFG relates to the beneficial response to antibiotic therapy. Five OFG cases were successfully treated with an azithromycin pulse therapy (an antibiotic scheme to treat inflammatory acne) and resulted in almost a complete improvement in all cases with a medium period of 3 months, according to the authors. They suggested that a continuous exposure to an unspecific antigen would be a possible cause, which may benefit from the antimicrobial effect as well as an additional anti-inflammatory and immunomodulatory properties of azithromycin. However, no evidence of microbial involvement was found in biopsies of these patients.[67]

On the other hand, two studies involving Scottish[68] and Irish[69] populations have searched for the presence of *Mycobacterium paratuberculosis* by polymerase chain reaction (PCR) in biopsy samples of 30 and 21 OFG patients respectively. Both failed to show the presence of Mycobacterium in these cases. Another study also failed to show the presence of *Borrelia burgdorferi* using a similar method in 12 patients[70]. Thus, there is insufficient and controversial support for a microbial role in the causation of OFG[43].

Inflammatory/immunological dysregulation as a cause of OFG has been postulated, mainly because of the histopathology of OFG that shows the presence of non-caseating granulomas, lymphoedema and an agglomeration of lymphocytes, all suggesting an altered immune response[43,46]. One report analysed the T-cell diversity on a patient with a history of 5 years swelling of the lips, gums and oral mucosa later diagnosed as OFG. This investigation was motivated by the similar histology of OFG to other granulomatous diseases that are characterized by a limited heterogeneity of alpha/beta and gamma/delta T cells. A high number of $CD4^+$ T-cells within and outside the granulomas was found in the lip biopsy of this OFG patient, along with elevated expression of T-cell-associated cytokines and chemokines, indicative of a T-cell mediated

immune response in this OFG patient that is similar to the inflammatory response observed in CD[58]. Another report has shown massive peripheral T-cell activation on an OFG patient, who had a similar TCR repertoire in lesion-associated lymphocytes and the peripheral blood lymphocytes, suggesting that there is a dysregulated T-cell response in OFG that causes a random influx of T-cells at the inflammation site[57].

On the other hand, clonal expansion of T cells was demonstrated in a single patient whose T-cells from the vicinity of the lesion used a limited repertoire of TCRVβ when compared to peripheral blood T-cells from the same patient, as well as mucosal T-cells from healthy individuals[71]. However, the role of T-cells in the causation of OFG remains unclear due to the reduced number of studies and lack of strong evidence[46].

An allergic reaction is another possible aetiology of OFG, which may be split into two main categories: allergy to dental materials; and allergy to food compounds. Few reports have been published associating OFG cases with an allergy to dental materials[72,73,74,75]. One case reported a two-year long swelling of the cheek and lips further diagnosed as OFG[74]. The patient showed a positive reaction on a patch test to mercury and had many amalgam dental fillings. After total replacement of amalgam fillings, all signs and symptoms disappeared after six months.

Tomka *et al*. reported 3 cases of OFG that were successfully treated after replacement of amalgam filling for other dental materials.[72] All patients showed high sensitivity to mercury on patch tests, which decreased after amalgam removal. Lazarov *et al*. showed two cases of OFG associated with an allergy to dental materials based on positive reactions on patch tests[75]. One case was positive for gold in a patient with gold crowns on the upper incisors, who experienced a full recovery after crowns replacement with different dental materials. The other case was diagnosed with an allergy to mercury, however, in this case, the patient refused to replace her amalgam fillings. After two years, there was a worsening of the disease. The authors attributed the increased signs of disease to the maintenance of her amalgam fillings[75]. A case with documented hypersensitivity to cobalt has also been reported.[73]

Besides the small number, all cases of hypersensitivity to dental materials were diagnosed by patch test. In an investigation of the role of allergy in mucosal diseases performed by patch tests, 264 out of a total of 1,252 patients had OFG. The OFG group showed 54% of hypersensitivity to food additives, 51% to benzoic acid and 38.3% to cinnamaldehyde.[76]

Many food compounds and food additives have been associated to OFG [9,41,43,46,77], although their specific role, as a primary causative agent or as an agent that just exacerbate symptoms of the disease, has not been fully elucidated. The possible association between food allergy is supported by the fact that the majority of documented allergies in OFG patients are a result of atopic allergy due to a hyperallergic state[76,78].

Benzoic acid is the most prevalent allergen associated with OFG patients.[9,76] The list of others common allergens include food additives (such as salicylic acid, glutamic acid, tartrazine, propylene glycol, etc), cinnamaldehyde, perfumes/flavourings, and chocolate[9]; and a number of less common agents such as wheat, dairy products, eggs, peanuts, piperitone, cocoa, carvone, carmoisine, sun yellow dye and monosodium glutamate, all have been associated with OFG[46].

Wray *et al*. investigated the role of allergy in mucosal diseases and found that benzoic acid was the most prevalent single allergen to cause positive allergic reactions in all patients (41.5%) with the highest prevalence (51%) in OFG patients. They have carried out two different allergy tests: contact urticaria and delayed hypersensitivity (standard patch test). The results showed that majority of reactions were Type I hypersensitivity (contact urticarial – 46%) compared to delayed hypersensitivity (7.1%), supporting the role of atopic allergy in OFG[76].

Patel *et al*. sought for clinical evidence of allergy in patients with OFG in view of the recent link between OFG and dietary sensitivity. Their methods included the application of a questionnaire, skin prick tests, total and specific serum IgE levels. OFG patients were compared with a series of patients with inflammatory bowel disease (IBD) without oral involvement and to healthy controls. They observed an almost 3-fold increase in allergy rates when comparing OFG to healthy individuals, concluding that there is compelling clinical evidence of an association of OFG with allergy[47]. In a

double-blind randomized controlled trial using a placebo-controlled challenge with sodium benzoate, Nettis *et al*. investigated recurrent episodes of urticaria/angioedema in 47 healthy individuals who had previously reported episodes of urticaria after ingesting food containing benzoates. The results showed that there was only 1 patient out of 47 who had a reaction after ingestion of 75 mg NaB, which reinforces the low allergy rates to benzoates in non-OFG patients[79].

Another piece of evidence that supports the role of food allergy in the clinical course of OFG relies on the effects of restriction of known allergens from the diet of patients. Some reports have shown that cinnamon and/or benzoate free diets lead to improvement of symptoms in about 70% of patients[11,19,80]. Taibjee *et al*. reported a case of a patient with a confirmed diagnosis of OFG, who experienced a worsening of symptoms after eating chocolate[81]. Patch testing identified a positive reaction to cocoa liquor; in addition, the patient experienced a flare-up of the disease during the patch test containing cocoa liquor, showing a clear association between the allergen and disease. Although reports of allergen-free diet have shown promising results, the mechanisms underlying this association have not been clarified.

The use of exclusive enteral nutrition is a recognized treatment for induction of remission for Crohn's disease and the efficacy of this therapy was investigated in a retrospective study for the management of OFG in children. From 22 children who completed 6 weeks of exclusive enteral nutrition, 19 showed clinical improvement in the OFG appearance[82].

1.2.1.2 Treatment and prognosis of OFG

The evolution of OFG is considered unpredictable and the majority of therapies focus on controlling the symptoms. Treatment choices are, in some instance, experience-based and follow the current hypothesis of OFG causation.

Controlling the immune response through the use of anti-inflammatory and immunomodulatory drugs is the commonest treatment and shows the most reliable evidence of a successful treatment[45,49,52,83,84].

Corticosteroids are common agents for treating OFG and may be used topically, intralesionally and in systemic therapy. The criteria for treatment selection depend on the severity of the disease. Mild and superficial lesions like ulcers, mucosal tags, cobblestoning, and mild swelling can be treated with topic corticosteroids; moderate to severe swellings and unresponsive cases may require systemic corticosteroids and/or intralesional injections, immunosuppressants, or anti-tumour necrosis factor (TNF) therapy[44,85,52].

Fedele *et al*. demonstrated an initial success rate of 64% using intralesional injections of triamcinolone, especially for controlling lip swelling. Patients who presented recurrence were responsive to new injections of corticoid and were able to achieve remission of the disease and keep symptomless for a similar mean period than those who were responsive at the first injection[42].

The authors who associate the course of the disease to an allergy to dental materials are supportive of the conduct of replacement of the dental material (allergen), which normally is succeeded by the remission of symptoms.[72,73,74,75] Failing to replace this material has been also linked to a worsening of the disease[75].

Even without clear evidence of microbial involvement in the pathogenesis of OFG, reports of successful treatment with antimicrobial agents have been encouraged[51,67,86]. A supposed reason for successful treatment of inflammatory conditions with antibiotics relies on the assumption that microbial components can modulate cytokine and chemokine secretion and thus be responsible for inflammatory events[87]. The anti-inflammatory and immunomodulatory effects of antibiotics would be responsible for controlling the inflammation[87,88].

A broad range of antibiotics agents has been used to treat OFG, such as metronidazole[86], azithromycin[67], tetracycline, isoniazid, minocycline and roxithromycin[88]. Since the treatment of OFG is mainly focused on controlling the symptoms, many authors have supported the theory that antibiotics are beneficial in the treatment of OFG based on successful control of symptoms using antibiotics in their clinical experience[67,86,87,88].

Dietary restriction is another popular therapy and has been employed with beneficial outcomes in 54-78% of patients[9]. These diets are based on benzoates restriction[11,77] or a more limited diet with the removal of phenolic acids[19]. Avoidance of cross-reactive foods to confirmed plant allergens as determined by prick test has also been recommended[10]. All these therapies have shown improvements in 23% of patients requiring no further treatment[9].

The beneficial effects of selective diets such as exclusive enteral nutrition and benzoate-free diet have been proven efficient in the management of OFG, and in the case of benzoate-free diet, the effects can last longer than the period of dietary treatment itself, especially after controlled reintroduction of a normal diet[19,82]. Moreover, the benefits of this treatment can avoid or, at least, reduce the necessity for immunomodulatory treatment which has known side effects[9,11]. The main problems associated with dietary therapies are the necessity of nutrient supplementation[19] and adherence of patients to the dietary restrictions[9,19].

Furthermore, others challenges are associated with dietary therapies, which include patient awareness about benzoate containing foods; the necessity of preparing individual meals, which is time-consuming and may increase costs; and limitations for eating out[19]. It is also important to consider that restricted diets may have no effects on individuals, which is a common problem associated with OFG with about 30% of patients remaining unresponsive to treatment[9,52].

The immunologically basis of OFG is poorly understood and more investigations are required[9]. The effects of benzoate-free diet are promising, achieving improvements in a similar rate to drugs-based treatments (≈70%)[9,52].

1.2.2 Neurodegenerative disease and sodium benzoate

NDD is an umbrella term to describe a series of conditions that affect the neurons in the human brain. NDDs are progressive and incurable diseases that cause serious movement problems and mental malfunctioning. NDDs include Alzheimer's disease (AD) Parkinson's

disease (PD) and PD-related disorders, Prion disease, Huntington's disease (HD), spinocerebellar ataxia (SCA), and spinal muscular atrophy (SMA) among other less common diseases[89].

Neurons are the main cell in the nervous system, considered, the building blocks of the nervous system. There are many hypotheses underlying the pathogenesis of NDDs and include genetic defects, altered membrane metabolism, trace element neurotoxicity, excitotoxicity, reduced energy metabolism, and free-radical-mediated damage[89].One important characteristic of neurons is that they differ from any other proliferative tissue in their lifespan and must survive for the entire lifetime of the organism. Thus, ageing plays a significant role in the pathogenesis of many NDDs[90], acting isolated or in combination with other factors (Figure 1-8)[91].

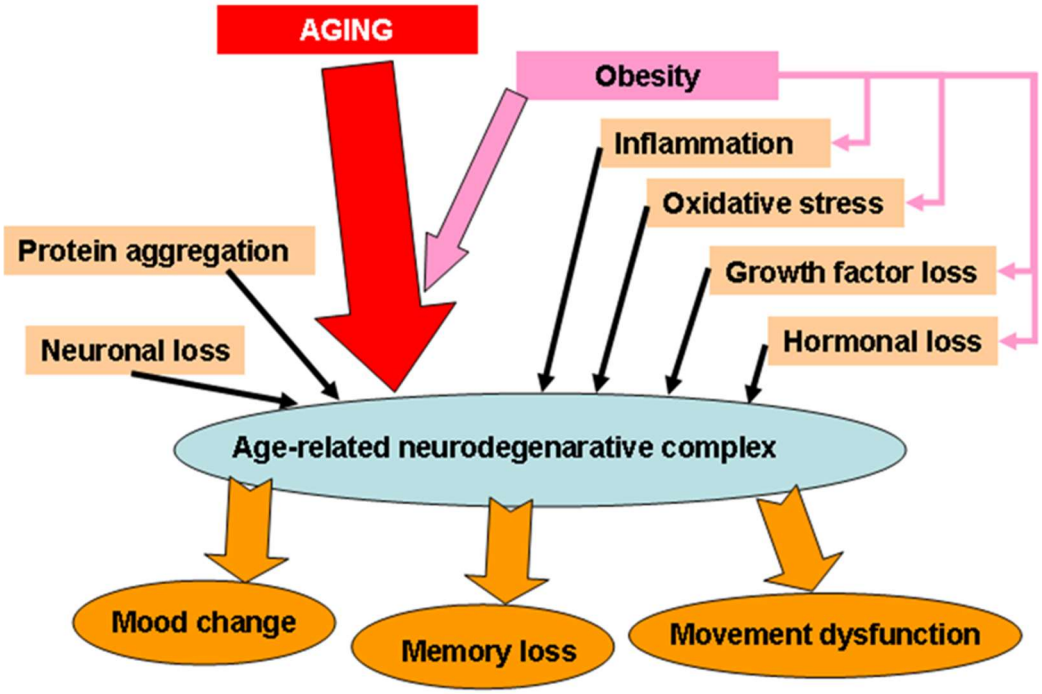

Figure 1-8: Age-related neurodegenerative diseases can be caused by isolated or a combination of factors. Image from Awada *et al*. (2013)[91].

A notable characteristic of NDD is the neuronal loss due to cell death, where apoptosis appears as an important contributor to neuronal death. Neuronal apoptosis occurs as a result of a biochemical cascade that involves oxidative stress, perturbed calcium homeostasis, mitochondrial dysfunction, and caspase activation[89].

Although the neuron is the primary target of NDD (AD, PD, HD, Prion's disease), other cells of the nervous system (astrocytes, microglial, Schwann cells) play important roles in the pathogenesis of these diseases. Astrocytes and microglia are known for their association with chronic inflammation in the central nervous system (CNS). With ageing, senescent cells secrete a variety of proinflammatory cytokines, chemokines, growth factors and proteases collectively termed as the senescence-associated secretory phenotype (SASP). These uncontrolled immune reactions contribute to neuronal dysfunction and death over time[92]. Figure 1-9 summarizes the current evidence for the role of different cell types in specific NDDs.

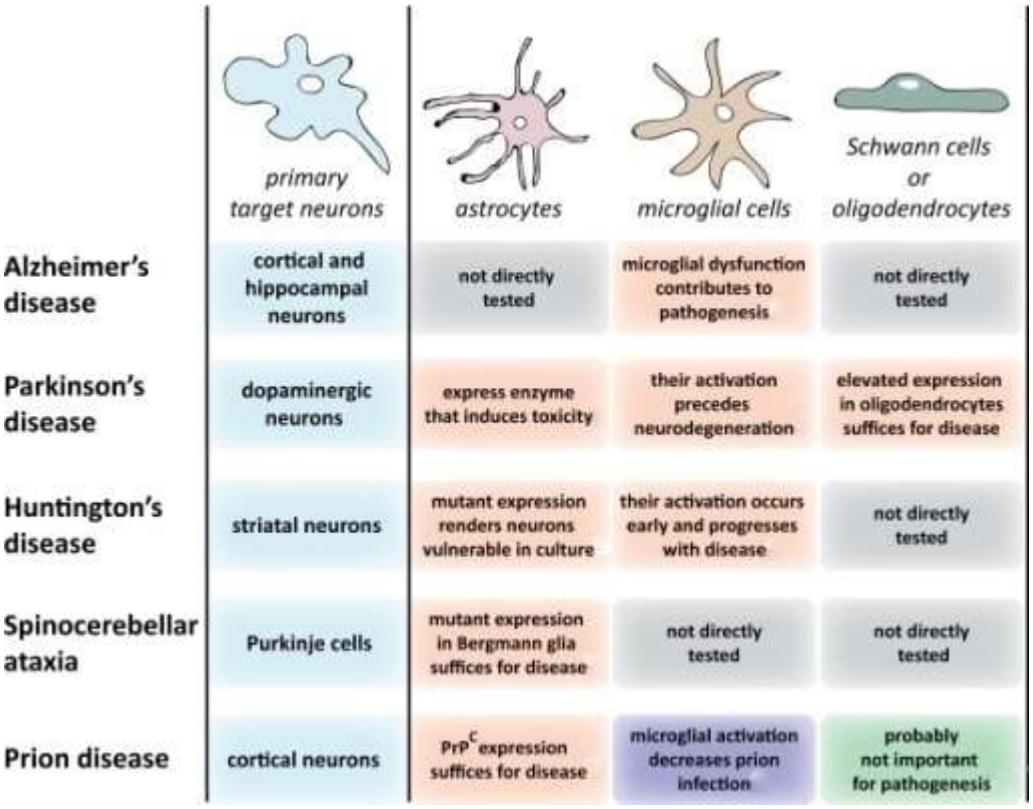

Figure 1-9: Summary of current evidence of contributor cells to the pathogenesis of neurodegenerative diseases. Adapted from Ilieva *et al*. (2009)[93].

Studies have shown that NaB may provide several beneficial effects on the CNS in different NDDs, including T-cell modulation (switching Th1 to Th2 cells and enriching Treg cells); modulation of innate immunity by knocking down proinflammatory cytokines and attenuating co-stimulatory molecules on the surface of microglia; controlling astroglia activation; and

suppressing disease progression in a mouse model of multiple sclerosis (MS)[4].

NaB attenuated the inflammatory markers, especially the secretion of proinflammatory cytokines, such as TNF and IL1β in mouse microglia after challenge with lipopolysaccharide (LPS) through inhibition of nuclear factor kappa-light-chain-enhancer of activated B cells (NFkB). NaB also inhibited the expression of inducible nitric oxide synthase (iNOS) in mouse microglia and primary human astrocytes[1].

IL1β was found to induce iNOS expression in mouse astrocytes in a mouse model of PD. Nitric oxide (NO) downregulated the levels of Parkin and DJ-1, proteins associated with survival of existing dopaminergic neurons. IL1β-induced iNOS caused a downregulation effect on Parkin and DJ-1 and this effect was neutralized by NaB. In summary, NaB altered dopaminergic neuronal protection, normalized striatal neurotransmitters, and improved motor functions by cinnamon in MPTP-intoxicated mice. These effects are suggested to be beneficial for PD patients[94].

Another beneficial effect of NaB to the CNS is an increase of neurotrophic factors; brain-derived neurotrophic factor (BDNF) and neurotrophin-3 (NT-3) in primary human neurons and astrocytes. Neurotrophic factors are molecules that stimulate and control neurogenesis and support the survival of existing neurons. NaB increased levels of neurotrophic factors occurred through activation of protein kinase A (PKA) and cAMP response element binding (CREB) protein[6].

Mice fed with NaB showed increased levels of NaB in serum and brain after oral ingestion, suggesting that NaB can reach the CNS after crossing the blood-brain barrier[6], which is an important property of NaB since it is an important challenge for therapeutic options that target the CNS[94].

NaB was tested in an experimental allergic encephalomyelitis (EAE), a mouse model of MS. NaB administration in drinking water ameliorated clinical symptoms and disease progression of EAE in recipient mice and suppressed the generation of encephalitogenic T cells in donor mice. It was achieved by reducing infiltration of mononuclear cells and demyelination in the spinal cord of mouse. NaB also switched the T cells

from Th1 to Th2 mode[95]. In another study, NaB also upregulated Tregs with a protective effect on a similar mice model of EAE. It was shown that NaB increased the expression levels of TGFβ, an important inducer of Tregs, through activation of STAT6. This mechanism has been attributed to the beneficial effects of NaB and predicted to be of therapeutic value for MS patients[8].

A few clinical trials have tested the efficacy of NaB on the treatment of neurological diseases[5,96,97]. NaB is considered a D-amino acid oxidase (DAAO) inhibitor, which can enhance the N-methyl-D-aspartate receptor (NMDAR) mediated neurotransmission. NMDAR is very important for memory and learning[5] and has an important role in the pathophysiology of schizophrenia[97].

In the AD, glutamatergic neurotransmission, particularly through the NMDAR, leads to neurotoxicity, especially in the late phase. Enhancing NMDAR activation by inhibiting the activity of DAAO could be beneficial for the early declining process of the AD. NaB, as a DAAO inhibitor, was administered at a concentration of 250-750 mg/day to 60 patients in the early phase of the AD in a double-blind randomized clinical trial. There were no adverse effects observed in the test group (NaB) after 24 weeks therapy. NaB treatment resulted in a better improvement than placebo in cognition and overall functions than control, considered a promising novel approach for the early dementing processes[5].

Two other clinical trials assessed the effects of NaB as an add-on drug[97] or as adjunctive therapy drug to sarcosine[96], a glycine transporter I inhibitor in patients with schizophrenia. In both trials, patients were kept under their antipsychotic drug therapy regimen on a double bind randomized clinical trial with doses not higher than 1000 mg/day. As an add-on drug, NaB adjunctive therapy significantly improved a variety of symptom domains and neurocognition in patients with chronic schizophrenia[97]. A similar effect was also observed when NaB was used as an adjunctive drug to sarcosine, with better results for cognitive function found on the group sarcosine plus NaB than on placebo or sarcosine alone. The authors suggest that the cognitive improvement can be primary without improvement in clinical symptoms[96].

Currently, there is an Australian clinical trial that aims to investigate the efficacy of NaB as an adjunctive treatment in early psychosis, using 2 doses of 500 mg/day of NaB[98].

1.2.3 Urea cycle disorders (UCD) and sodium benzoate

UCD represent a group of rare inherited metabolic disorders caused by deficiencies in any of six enzymes and two carrier proteins involved in the urea metabolism (Figure 1-10)[99,100]. The incidence is 1 in 30,000 births, with the most common enzyme affected the Ornithine Transcarbamylase (OTC) resulting in OTC deficiency[99]. The urea cycle is the main pathway for the disposal of waste nitrogen derived from catabolism of dietary and endogenous proteins[101]. The link between NaB and UCD is that NaB is an approved drug used in the treatment for hepatic metabolic defects associated with hyperammonemia[102].

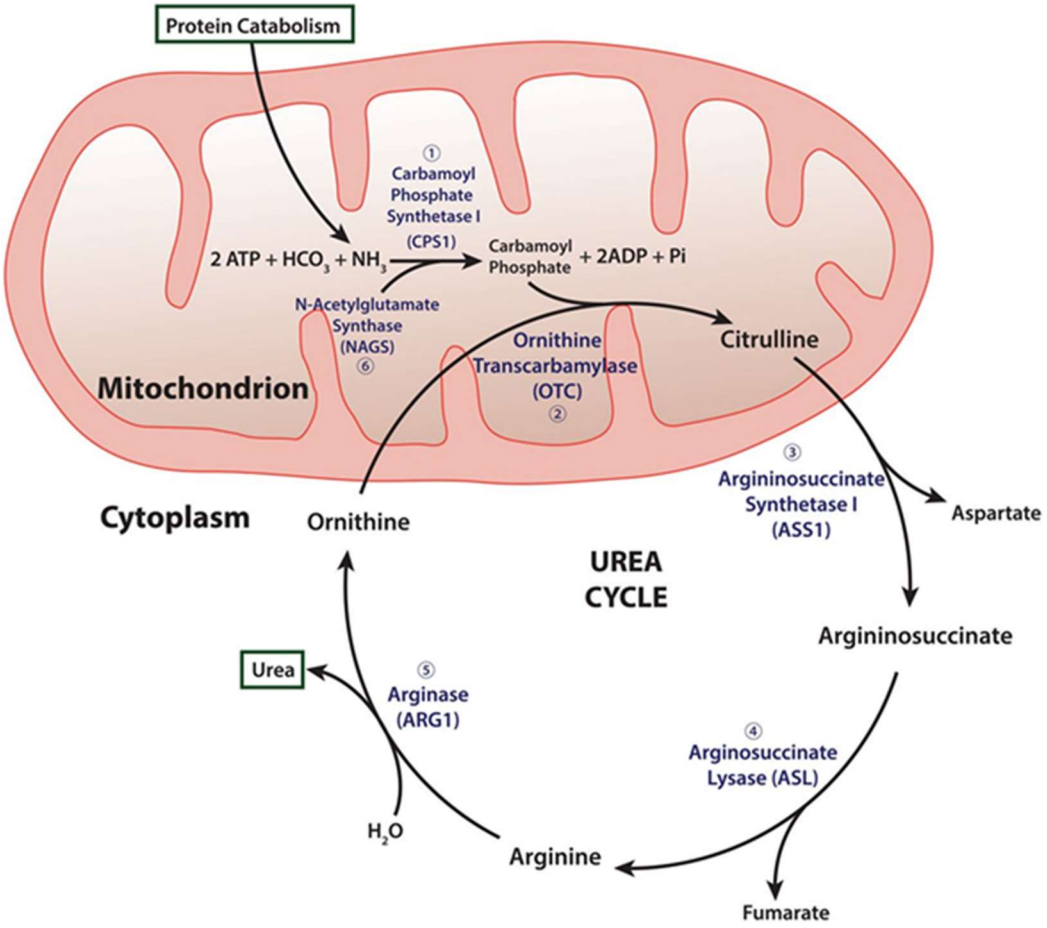

Figure 1-10: Schematic representation of the urea cycle. Nitrogenous products from protein or dietary catabolism are metabolized in the

mitochondria producing urea. Six enzymes participate in this pathway (numbered 1–6, with their associated gene in brackets). Image from Blair et. al. (2014)[37].

1.2.3.1 Sodium benzoate metabolism and nitrogen waste disposal

NaB salt quickly dissociates in an aqueous medium to form benzoic acid as previously explained. After oral ingestion, undissociated benzoic acid is quickly absorbed by the gastrointestinal tract and metabolized in the mitochondrial matrix in the liver and kidney. This process requires energy consumption and involves conjugation of benzoic acid with coenzyme A and glycine, which results in the formation of hippuric acid and rapidly secreted in urine (Figure 1-11)[103].

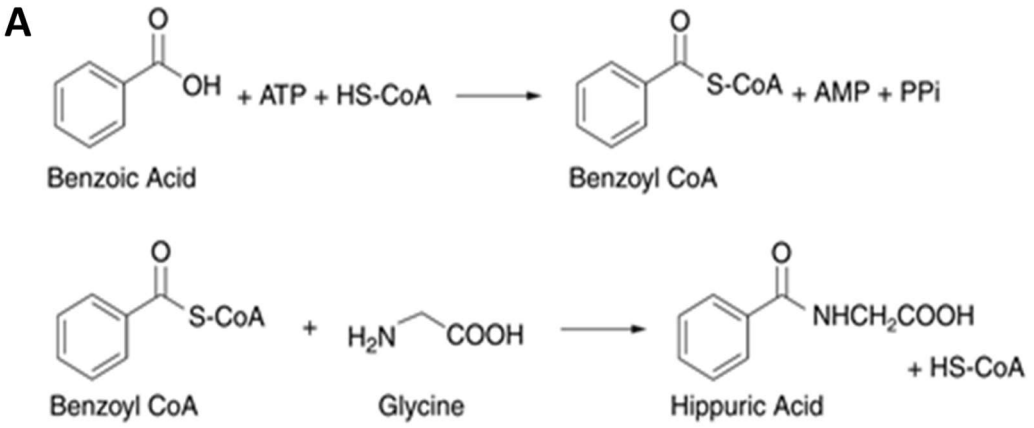

B

I- benzoic acid + ATP → benzoyl AMP + PPi

II- PPi + H_20 → 2 Pi

III- benzoyl AMP + HS-CoA → benzoyl CoA + AMP

IV- benzoyl CoA + glycine → hippuric acid + HS-CoA

∑: benzoic acid + glycine + ATP + H_20 → hippuric acid + AMP + 2Pi

Figure 1-11: Metabolism of benzoic acid in mammals. Benzoic acid reacts with HS-CoA to form benzoyl CoA. Then, benzoyl CoA reacts with glycine to form hippuric acid releasing free CoA (A). Reaction sequence of benzoic acid metabolism (B). Image 11A from Chipley (2005)[13].

Almost all of the administered NaB is metabolised to hippuric acid, only a small portion of non-metabolized NaB is detected in the urine (Figure 1-12). This metabolism is well established and the secretion of hippuric

acid in the urine reflects the intake of benzoates. Thus, elimination of hippuric acid after a challenge with NaB served as a clinical test for evaluating liver function[104].

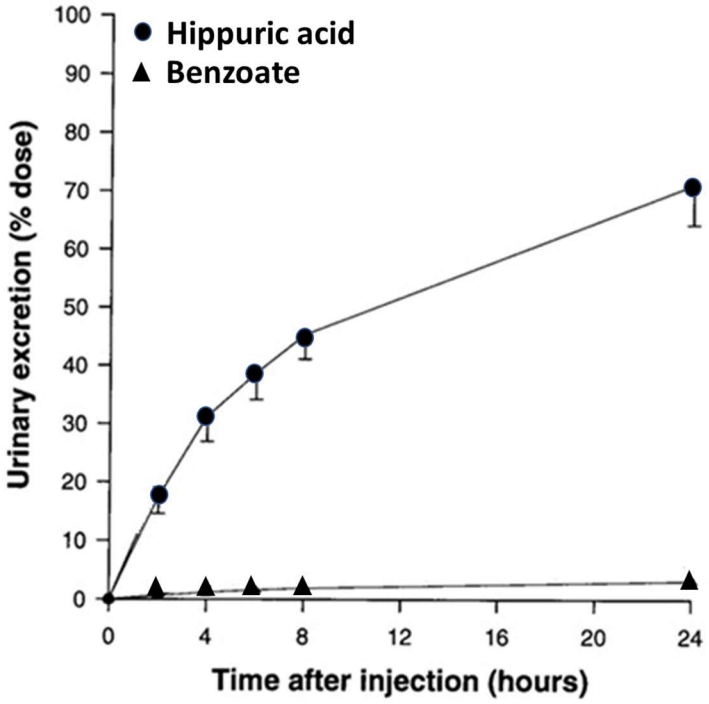

Figure 1-12: Urinary excretion of hippuric acid (circles) and benzoate (triangles) by normal control rats after intraperitoneal administration of 100 mmol of benzoate per 100 g body weight. Adapted from Krähenbühl *et al*. (1997)[105].

NaB decreases the levels of ammonium through the elimination of nitrogen as hippuric acid, which appears to occur at the expense of nitrogen that otherwise would have been eliminated as urea. Thus, NaB metabolism diverts the waste of nitrogen from the urea production[106].

It is believed that NaB alters the urea production by interfering in two sites of the ureagenesis pathway by inhibiting the pyruvate carboxylase and the N-acetylglutamate-dependent carbamoyl phosphate synthetase I[104,106,107]. Benzoate may block the urea cycle through sequestration of CoA via the accumulation of benzoyl-CoA, thus affecting the acetyl CoA-dependent reactions, especially the synthesis of N-acetylglutamate, the physiological allosteric activator of carbamoyl phosphate synthetase[108]. In the absence of glycine, there is an accumulation of benzoyl-CoA, an intermediate metabolite of NaB

metabolism, and consequent decrease in free CoA. The reduction of free CoA is the main mechanism responsible for NaB toxicity[13,105,106,107].

Although the toxicity of NaB is considered low, it needs to be used in moderation. Studies in animal models have shown that NaB can potentiate ammonium toxicity, increasing the levels of blood ammonia and mortality in mice[104,108]. In humans with cirrhosis, sodium benzoate caused an adverse effect increasing the basal and post-glutamine ammonia levels after treatment with high doses (10 g/day). Death after administration of high doses of NaB has also been reported[109].

1.2.3.2 Treatment of urea cycle disorders with sodium benzoate

Treatment of UCD with NaB is usually made in conjugation with sodium phenylacetate. Many cases have been reported with successful control of ammonium levels after administration of therapeutic doses of NaB, which is considered at 250 mg/kg/day[3,37,102]. A randomized trial study in healthy volunteers has demonstrated the efficacy of NaB in nitrogen secretion, with a better response when NaB was used in association with phenylbutyrate[101].

In an uncontrolled study that reported the 25-year experience of treatment of 299 patients with UCD using NaB, the authors reported an overall survival of 84%. There were 1181 episodes of hyperammonemia with a survival rate of 96%. Patients who were comatose at admission had a survival rate of 81%[3]. NaB isn't the sole therapy, it is usually used in combination with sodium phenylacetate and other therapies, such as intravenous arginine hydrochloride and a protein-restricted diet. Dialysis can also be used whenever necessary[3,37].

UCD is characterized by episodic life-threatening hyperammonemia. Mortality and morbidity are historically high, and survivors may experience devastating neurological sequelae[3,100]. NaB is one more therapeutic option to help to reduce nitrogenous waste, but to date, there is no treatment that has 100% efficiency to control the hyperammonemia and its complications, and patients are still dying from these disorders, especially neonates[3,38,100].

1.3 The immune system (General overview)

The immune system can be defined as an integrated body system of organs, tissues, cells, and cell products that differentiates self from nonself resulting in the neutralization of potentially pathogenic organisms or substances. The recognition and combined efforts in opposition to a potentially pathogenic organism are termed an immune responses[110].

In the battle against infection, the integrity of skin and mucosal surfaces plays a key role as the first line of defence, creating physical barriers against invading organisms. Microorganisms which breach these physical barriers initially encounter cells and molecules of the innate immune system[111].

Tissue-resident macrophages can recognise invading microbes and specific pathogen-associated molecules. Recognition results in the activation of the macrophage which results in microbial phagocytosis and the secretion of cytokines and chemokines. These molecules recruit additional cells from the innate immune system, such as neutrophils and monocytes, and initiate the inflammation process. Neutrophils are the first cells recruited and are followed later by monocytes, which rapidly mature into activated macrophages. The principal role of these cells is the engulfment and eradication of the microbial stimulant[110]. This coordinated defence attempts to eradicate the infection, however, if it is unsuccessful, the adaptive immune response is then initiated.

A specialized group of cells known as antigen-presenting cells (APC), which include macrophages and dendritic cells (DC), are capable of processing and presenting antigenic molecules to the adaptive immune system. Antigenic peptides are presented by APC through the binding to major histocompatibility complex (MHC) proteins and these antigen-loaded complexes are recognized by T-cells, which express antigen-specific TCRs. This interaction initiates T-cell activation, but for complete activation, a second signal is necessary. The second signal comes from the interactions between the co-stimulatory molecules (CD80 and CD86) expressed on the surface of APC and the T-cell expressed CD28. The

strength of T-cell activation is determined by a combination of antigen affinity to the TCR and the expression levels of the co-stimulatory molecules by the APC[110,111].

1.3.1 Anti-bacterial recognition and early response

The innate immune system is effective in dealing with a varied range of pathogens and achieves this through an invariant and limited repertoire of cellular receptors. Because of these receptors, macrophages, granulocytes, natural killer cells (NK) and DC can recognize simple molecules that are expressed by many microorganisms but are not expressed in host cells. These molecules contain conserved patterns (motifs) which are called pathogen-associated molecular patterns (PAMPs) and include mannose-rich oligosaccharides, peptidoglycans, LPS, nucleic acids, bacterial peptides, lipoproteins and others[110].

There are distinct groups of cell receptors used for recognition of PAMPs that are generally known as pathogen recognition receptors (PRR). They include four main groups: Toll-like receptors (TLR), nucleotide-binding oligomerization domain receptors or NOD-like receptors (NLR), C-type lectin receptors (CLR), and retinoic acid-inducible gene I (RIG-I)-like receptors (RLR)[112].

1.3.2 Toll-like receptors

The TLRs are a family of PRRs that play key roles in the immune system, as activators of the innate immune system, and also recruiting and activating the adaptive immune response[113]. TLRs belong to an ancient class of proteins that were first described in the fruit fly *Drosophila melanogaster*[114]. It was discovered that the Toll gene is required for *Drosophila* to defend against bacteria and fungi infection more than 100 years ago[113,114]. It is now known that Toll-homologues are present in almost all eukaryotes, such as plants, adult insects, and vertebrates, playing a pivotal role in facing pathogen invasion[115].

TLRs are type I transmembrane proteins with an extracellular amino (N)-terminal domain containing leucine-rich repeats (LRR), which give the TLRs their distinctive horseshoe-like shape; a transmembrane domain; and a cytosolic TIR domain, which interact with adaptor molecules for downstream signalling[114,116]. Adaptor molecules such as the myeloid differentiation primary response gene 88 (MYD88), Toll-interleukin 1 receptor (TIR) domain containing adaptor protein (TIRAP), TRIF-related adaptor molecule (TRAM) and TIR domain-containing adaptor protein inducing interferon-β (TRIF) bind to intracellular TLR domain and initiate a protein kinase cascade that will stimulate transcriptions factors such as NFκB, AP1 and IRFs, resulting in pro-inflammatory cytokines secretion and type I interferon response[116].

Thirteen TLRs (TLR 1-13) have been identified in human and mouse, there are 10 TLRs (TLR 1-10) found in human and 12 (TLR 1-9 and 11-13) in mice[114,115]. Each TLR recognizes a specific PAMP, which vary from bacterial components such as LPS and flagellin, viral and bacterial RNA and DNA, lipoproteins, peptidoglycan and so on (Figure 1-13)[114].

TLRs 1, 2, 4, 5, 6, and 10 are localized in the plasma membrane and the remaining TLRs (3, 7, 8, 9, 11, 12, and 13) are found in the membranes of intracellular vesicles. An exception is TLR4, which can be found in both locations[113,114,116]. TLRs located in the plasma membrane are more prone to recognize lipid or protein structures expressed on the surface of pathogens, while the intracellular TLRs are involved in the recognition of nucleic acids[116]. A general overview about the mammalian TLRs with their location, recognizing PAMP and signalling cascade can be found in Figure 1-13[117].

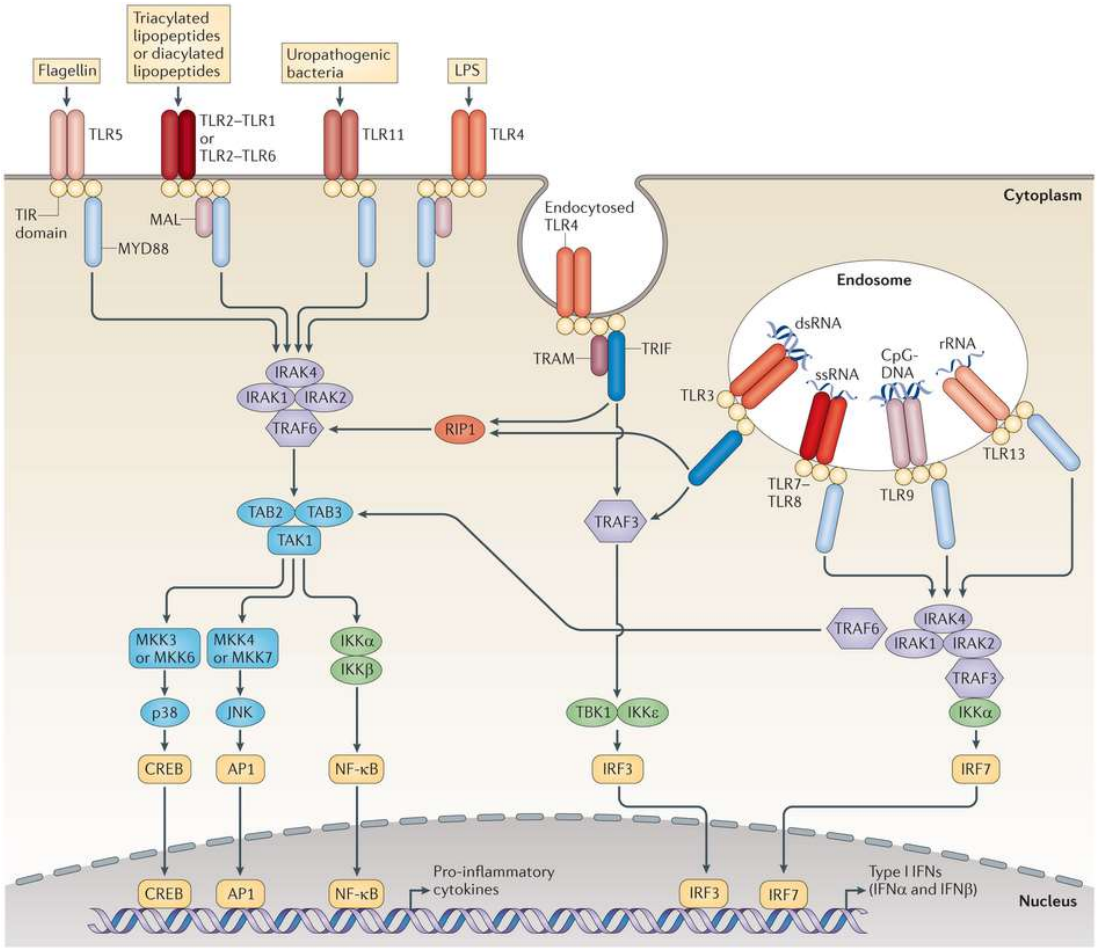

Figure 1-13: Schematic location of TLRs and signalling pathway. TLR signalling initiates ligand-induced dimerization. Homodimerization occurs for the majority of TLRs, except for TLR1-TLR2, TLR2-TLR6 and TLR7-TLR8 that form heterodimers. Signalling pathway uses adaptors proteins in a downstream cascade to activate transcriptor factors, which move to the nucleus to initiate transcription. Adapted from O'Neil *et al*. (2013)[117].

1.3.2.1 Toll-like receptors 1, 2 and 6

Lipopeptides or lipoproteins, the main TLR2 ligands, are recognized by TLR2 in complex with TLR1 or TLR6. TLR2-TLR1 heterodimer can recognize triacylated lipopeptide while TLR2-TLR6 complex recognises diacylated lipopeptide (Figure 1-14)[118,119,120]. TLR2 can recognize not only lipopeptides/lipoproteins but a variety of microbial components, which include: peptidoglycan and lipoteichoic acid from Gram-positive bacteria, lipoarabinomannan from mycobacteria, glycosylphosphatidylinositol anchors from *Trypanosoma cruzi*, a phenol-soluble modulin from

Staphylococcus epidermis, zymosan from fungi and glycolipids from *Treponema maltophilum*[121].

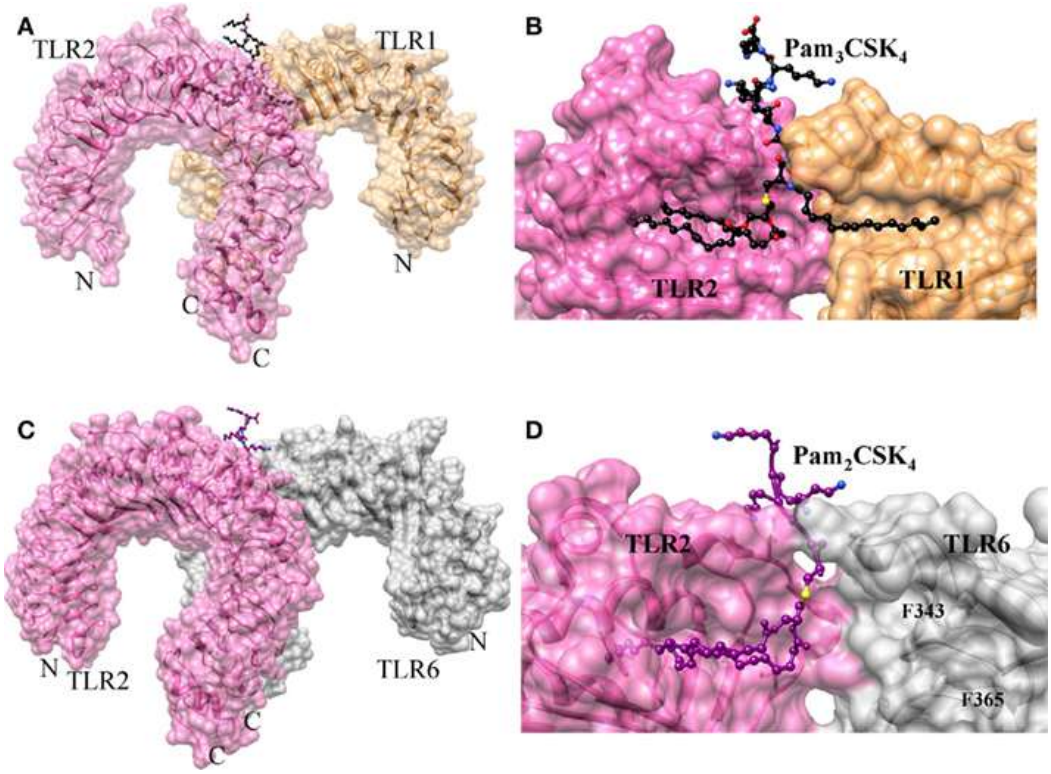

Figure 1-14: Structures of TLR2–TLR1/6 heterodimers induced by lipopeptides. (A) Crystal structure of TLR1/2–Pam3CSK4 complex. TLR1, TLR2, and Pam3CSK4 are coloured in sandy brown, hot pink, and black, respectively. (B) Lipid-binding pocket in TLR1/2–Pam3CSK4 complex (C). Crystal structure of TLR2/6–Pam2CSK4 complex. TLR2, TLR6, and Pam2CSK4 are coloured in hot pink, grey, and deep magenta, respectively. (D) Lipid-binding pocket in TLR1/2–Pam2CSK4 complex. Image from Manavalan *et al.*(2011)[118].

The mechanism of activation of TLR2-TLR1 and TLR2-TLR6 complexes are similar to other TLRs, interaction with an agonist on the extracellular domain, which either induces the formation of a receptor dimer or changes the conformation of a pre-existing dimer. This conformation change brings together two intracellular TIR domains and makes them interact physically and is capable of recruiting downstream adaptor signalling molecules[118].

TLR2-TLR1 and TLR2-TLR6 use the canonical MyD88 adaptor for pro-inflammatory signalling downstream of their activation. TIRAP adaptor protein is in the majority of cases, the link between MyD88 and the TLR complex TIR domain[122]. MyD88 activates IRAK family kinases, which in

turn, lead to a variety of downstream responses, including the MAPK pathway and the activation of transcriptor factors, Activator protein 1 (AP1) and NFkB, for proinflammatory cytokine responses, such as TNF, IL8, IL6, IL1β and IFNβ (Figure 1-15) [119,121,122,123].

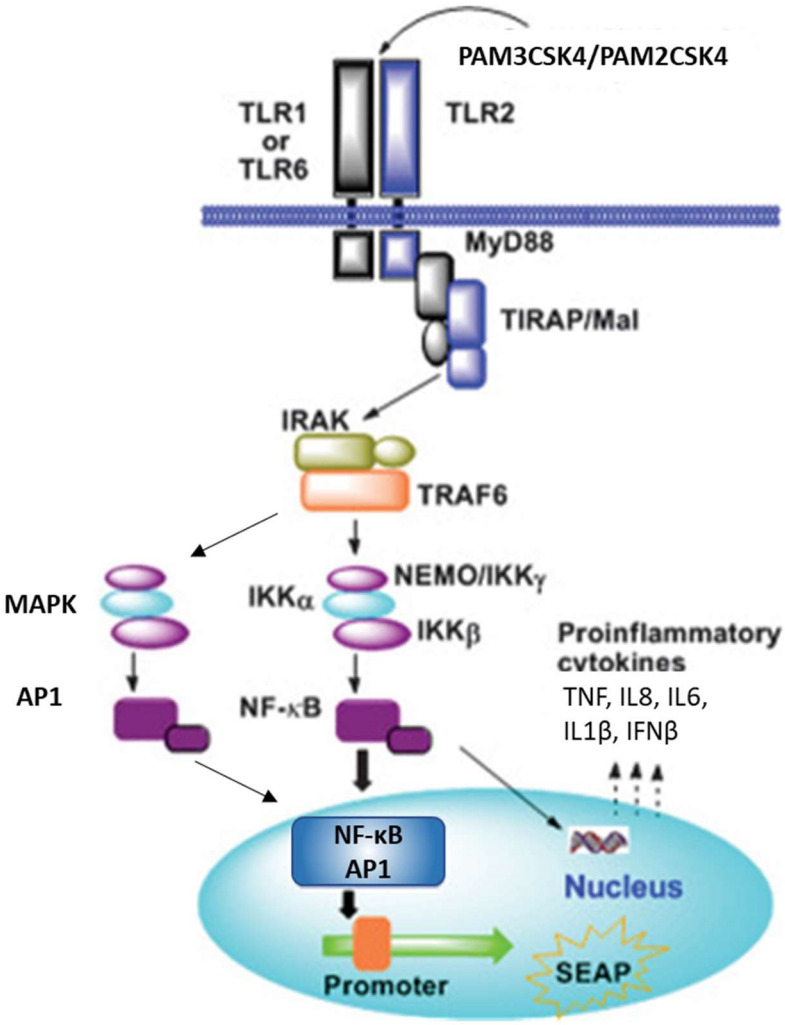

Figure 1-15: TLR2 signalling pathway. PAM3CSK4 (TLR2/1) and PAM2CSK4 (TLR2/6) ligands lead to the NF-κB and AP1 activation through the adaptor protein MyD88 and induce production of proinflammatory cytokines, such as TNF, IL8, IL6, IL1β and IFNβ. Adapted from Cheng *et al*. (2015)[123].

1.3.2.2 Toll-like receptor 4

The TLR4 recognizes LPS which forms part of the outer membrane of Gram-negative bacteria. TLR4 can also bind to lipoteichoic acids (LTA), viruses, fungi, and mycoplasma[110,124]. Activation of TLR4 by LPS leads to an acute inflammatory response with the release of a set of inflammatory

cytokines. An overly strong response to LPS can lead to a collapse of the circulatory and respiratory system which is known as septic shock[110,125].

A wide variety of pro- and anti-inflammatory cytokines and chemokines can be produced by macrophages after TLR4 activation such as IL-1, IL6, IL8, IL-12, IL-10, interferon gamma-induced protein 10 (IP10), monokine induced by gamma interferon (MIG) and TNF. This cocktail of inflammatory mediators results in the induction of inflammation and recruitment of inflammatory cells to the infection site[110,126].

TLR4 requires dimerization for effective activation and uses adaptor molecules not only for signalling but also for helping in this process. Dimerization occurs predominantly in its TIR domain after initial stabilization and recruitment of adapters proteins[127]. Besides that, two molecules are fundamentally important to TLR4 function, lymphocyte antigen 96 (LY96, also known as MD2) and the cluster of differentiation 14 (CD14). The complex formed by the TLR4 and MD2 (TLR4/MD2 complex) is critical for LPS full response (Figure 1-16)[128].

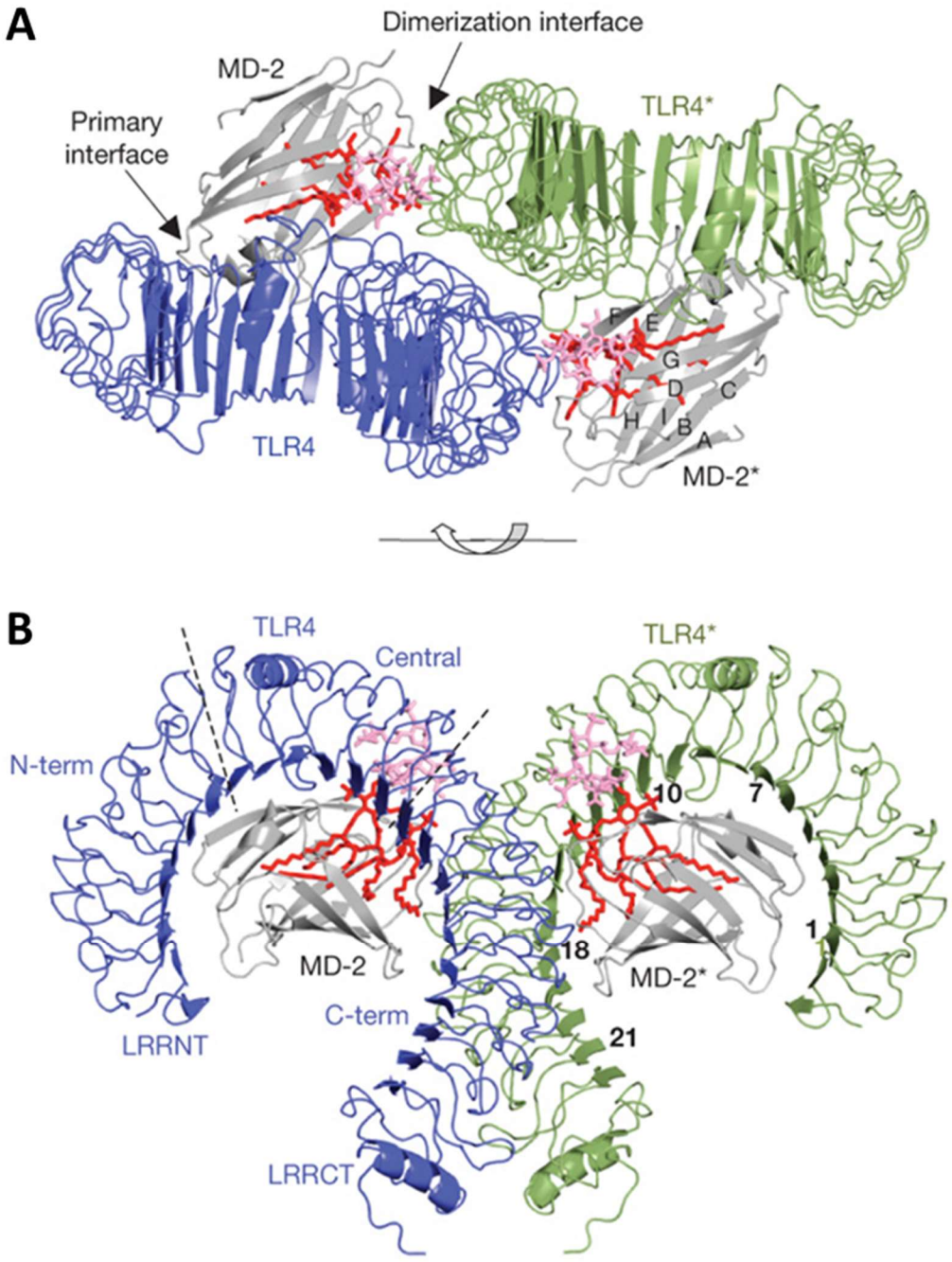

Figure 1-16: Overall structure of the TLR4-MD2-LPS complex. Top view of the symmetrical dimer of the TLR4-MD2-LPS complex (A). The primary interface between TLR4 and MD2 is formed before binding LPS, and the dimerization interface is induced by binding LPS. Side view of the complex (B). The lipid A component of LPS is coloured red, and the inner core carbohydrates of LPS are coloured pink. The module numbers of the LRRs in TLR4 and the names of the b strands in MD-2 are written in black. Image from Park *et al*. (2009)[129].

CD14 is considered a co-receptor of LPS and its presence is not mandatory for TLR4 signalling, however, it can enhance in many folds the

intensity of the signal.[130] An interaction between these molecules are crucial for initiating and modulating the inflammatory response to pathogens.

TLR4 signalling can lead to pro-inflammatory cytokines induction and/or a type I interferon response. It is dependent on the type of stimuli and the type of recruited adaptor proteins. Two main pathways follow TLR4 activation and are called MyD88-dependent and MyD88-independent pathway[114,131,132].

The MyD88-dependent pathway involves a complex formed by MyD88/TIRAP that binds to the TIR domain of the TLR4 and interacts with the protein kinases IRAK 1 and 4. Upon activation, IRAK4 phosphorylates IRAK1 that in turn causes ubiquitination of the TNF receptor-associated factor 6 (TRAF6)[133]. Then, TRAF6 can lead to activation of the transcriptor factor NFkB or a member of the MAPK family. MAPK signalling uses the AP1 as a transcriptor factor. Both cases will result in pro-inflammatory gene activation and the release of cytokines such as IL1β, IL6, IL12 and TNF[128,134]. The MyD88-dependent pathway can be modulated by CD14 but is CD14-independent when activated by the rough variant of LPS (Figure 1-17)[125].

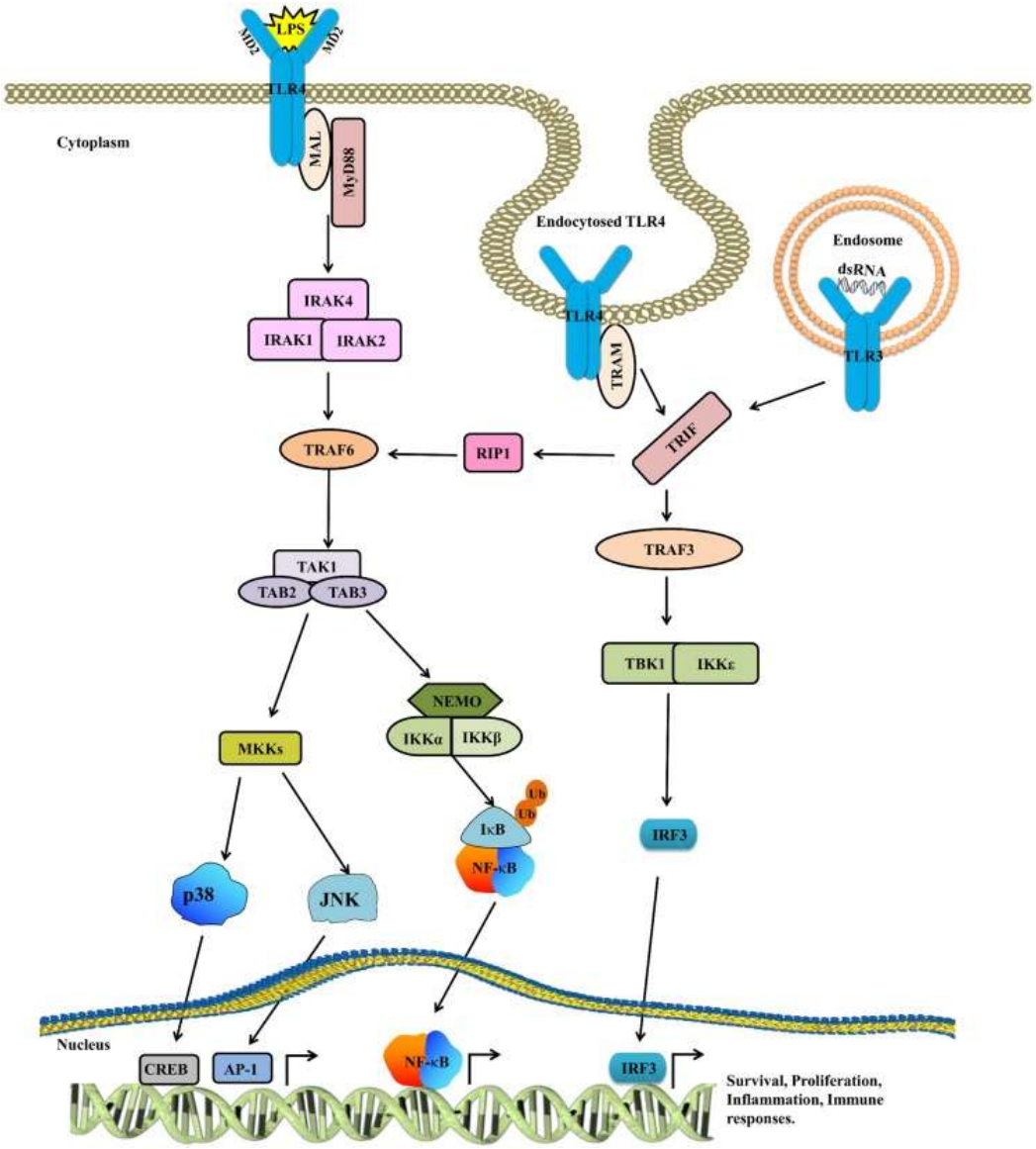

Figure 1-17: The TLR4 signalling pathway upon LPS activation. Upon ligand binding, TLR4 recruits downstream adaptor molecules such as MyD88/MAL and TRIF/TRAM to mount an inflammatory response. The activated MyD88/MAL then activates IRAK4, TRAF6, TAK1, and IKK complexes, while TRIF/TRAM signals through RIP1 to TRAF6/TAK1 and IKK. After this, both these pathways converge at NFκB. Besides activating NFκB, TAK1 also phosphorylates MAPKs to further reinforce the inflammatory response. TheTRIF/TRAM pathway not only activates NFκB but also triggers IRF3 to mount an antiviral response. Image from Yesudhas *et al*. (2014)[135].

On the other hand, the MYD88-independent pathway, also known as the TRIF pathway, responds via TRAM/TRIF adaptor molecules and is CD14-dependent for activation[125,130]. TRAM acts as a bridge between the TLR4-TIR-domain to TRIF, which in turn interacts with the effector proteins

TANK-binding kinase 1 (TBK1) and the inhibitor of kappa light polypeptide gene enhancer in B-cells (IKKε) to phosphorylate and dimerise IRF3 and to a lesser extent IRF7. The IRFs then translocate to the nucleus inducing IFN-α and IFN-β synthesis, and the subsequent release of IFN inducible chemokines such IP10 and MIG[130,136,137,138].

Furthermore, activation of the TRAM-TRIF signalling pathway induced by LPS requires TLR4 endocytosis[139]. This process is controlled by dynamin, which is a GTPase that regulates endocytosis by controlling the 'pinching off' of plasma membrane invaginations, which creates early endosomes[140]. LPS induces assembly of the ligand-binding complex consisting of CD14, MD-2 and TLR4 at the plasma membrane. From this location, which is probably a PtdIns(4,5)P2-rich subdomain of the plasma membrane, signalling is initiated and the receptor is endocytosed by a dynamin-dependent process[139].

Blockage of dynamin by dynasore, a highly specific inhibitor of dynamin, abolished the LPS-induced TRAM-TRIF-dependent phosphorylation of IRF3[139]. This process occurs later, after activation of TRAM/MyD88. Internalization of TLR occurs 60-120 minutes after LPS stimulation[141].

Internalized TLR in endosomes, colocalizes with MD2 and CD14 after LPS stimulation[141]. CD14 is an important molecule for ligand-receptor signalling, depending on the type of LPS. The LPS is composed of 3 parts and typically consist of a hydrophobic domain known as lipid A (or endotoxin), a nonrepeating "core" oligosaccharide, and a distal polysaccharide (or O-antigen)[142]. Modifications on LPS structure occurs on the O antigen, the outermost domain of the LPS molecule. The side O-chains are not required for cell survival and require energy expenditure. Thus, whenever the environmental conditions require, the bacteria stop the production of the O-chain. The "wild-type" and full form of LPS is called smooth LPS (sLPS), while the "mutant" form, lacking O-chains, is called rough LPS (rLPS)[143].

sLPS requires CD14 for efficient activation of TLR4, while the rLPS is CD14-independent (Figure 1-18)[125]. There are functional differences in immune activation between these forms of LPS, while rLPS releases high

amounts of TNF and IL1β, stimulation of mouse and human macrophages with sLPS show a reduced secretion of both cytokines[143,144]. On the other hand, interferon secretion is higher in sLPS compared to rLPS. CD14 deficient mice present a very low inflammasome and type I interferon response, suggesting that CD14 is required for their activation[143].

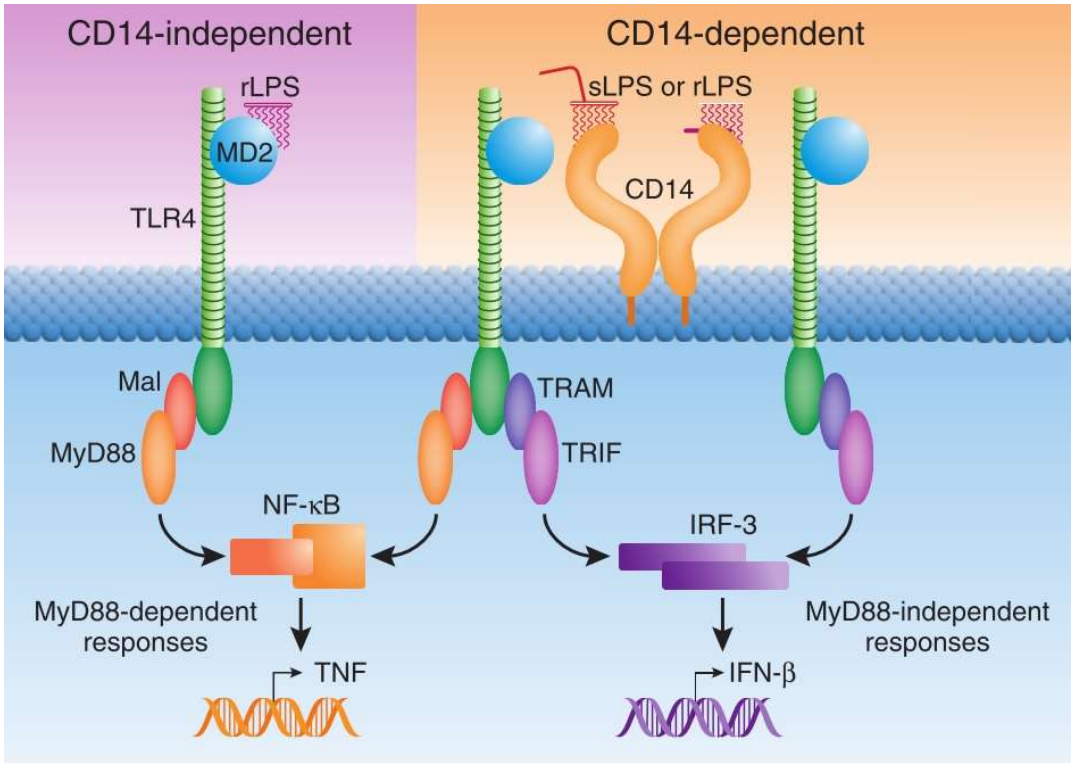

Figure 1-18: CD14-independent and CD14-dependent signalling by TLR4-MD2. TLR4-MD2 can bind rough but not smooth LPS without a requirement for CD14. Signalling by this complex is limited to the MyD88-dependent pathway, using the adaptors Mal and MyD88 to activate NF−κB, resulting in transcription of TNF. TLR4-MD2 can bind both rough LPS (rLPS) and smooth LPS (sLPS) in a CD14-dependent process. In addition to MyD88-dependent signals, these complexes also signal MyD88-independent responses via TRAM and TRIF, leading to IRF-3 activation and IFN-β transcription. Adapted from Godowski (2005)[125].

1.3.3 Reactive oxygen species (ROS)

ROS were historically viewed as purely harmful molecules that are byproducts of aerobic metabolism[145,146]. Nowadays they are recognized as important signalling molecules in several cellular processes and especially in inflammation[145,147]. ROS can be defined as partially reduced metabolites of oxygen that possess strong oxidizing capabilities and include the

superoxide anion (O_2^-), hydrogen peroxide (H_2O_2), and hydroxyl radicals ($OH^{\cdot}$)[145,147].

ROS production via nicotinamide adenine dinucleotide phosphate (NADPH) oxidase-dependent respiratory burst is a necessary effector response for the destruction of intracellular microbes by macrophages. This process takes place mainly in the mitochondria downstream of TLR activation[148].

ROS can be produced exogenously (pollutants, tobacco, smoke, drugs, or radiation) or intracellularly as result of multiple mechanisms. Although ROS can be produced by other mechanisms, the main generator is a family of membrane-bound enzymes; NADPH oxidases[146]. The superoxide forms from the one-electron reduction of molecular oxygen (O_2) and, within the cell, is rapidly converted by superoxide dismutases 1 and 2 (SOD 1 and 2) into H_2O_2[145]. This process is very unstable and nonenzymatic dismutation is rapid and can be accelerated 10-fold by SODs[149]. It prevents accumulation of superoxide that can damage and inactivate proteins[145]. H_2O_2, which is not a radical, is highly diffusible and relatively unreactive, but in the presence of a reduced transition metal as in Fenton chemistry, H_2O_2 can react to produce a hydroxyl radical. The hydroxyl radical is so reactive that it will oxidize any type of macromolecules and thereby damage molecules nearby[149]. The hydroxyl radical has a very short half-life within the cell due to its high reactivity, lasting around 10^{-9} seconds[150].

Finally, hydrogen peroxide can be reduced to water by catalytic enzymes such as glutathione peroxidases (GPXs), peroxiredoxins (PRXs), or catalase[151]. Figure 1-19 shows a summary of the production of ROS within the cell.

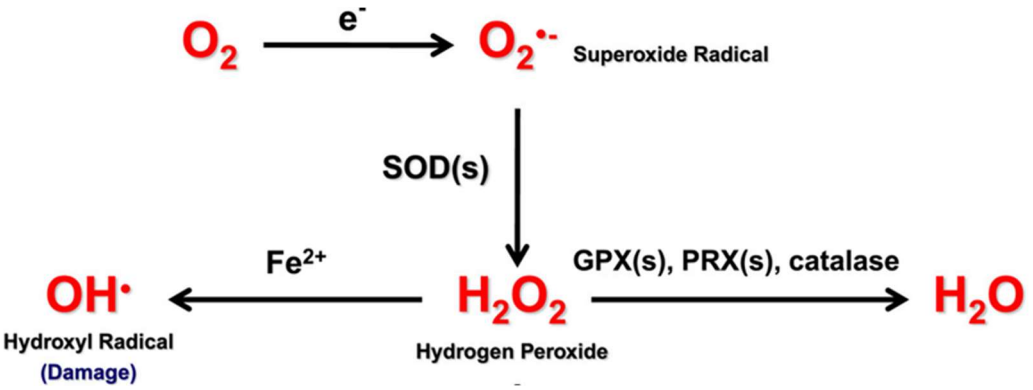

Figure 1-19: Production and interconversion of reactive oxygen species. O_2^- is formed from molecular O_2 by gaining a single electron from an NADPH oxidase (NOX) enzyme or from electron leak in the electron transport chain of the mitochondria. Superoxide dismutase enzymes convert two superoxide molecules into H_2O_2 and H_2O molecules. Hydrogen peroxide can undergo Fenton chemistry with Fe_2^+ to form $OH^{\cdot}$. Alternatively, hydrogen peroxide can be reduced to water by glutathione peroxidases, peroxiredoxins, or catalase. Adapted from Sullivan and Chandel (2014)[151].

Due to its stability, hydrogen peroxide is the main ROS signalling molecule during inflammation, activating NFkB via the MAP kinase pathways (ERK, JNK, and p38)[147]. ROS signalling has been shown to stimulate the secretion of proinflammatory cytokines; TNF, IL6 and IL1β[147].

1.4 Summary of investigations conducted and hypotheses

In this thesis, the effects of NaB on the innate response of monocytes/macrophages is characterized after bacteria and TLR ligand challenge. The effects of NaB was studied using assays to investigate gene transcription, cytokine secretion, cell signalling pathways, protein expression. Large-scale studies of genes and proteins were carried using gene expression microarrays and high-performance liquid chromatography-mass spectrometry-based proteomics, respectively. Intracellular location of proteins was investigated by using subcellular fractionation.

NaB is better recognized as a food preservative to reduce microbial growth in an acidic environment, but it has been also considered as a substance that helps the disposal of nitrogenous waste, a D-amino acid oxidase inhibitor, and a free radical scavenger. The link between NaB and the chronic inflammatory disorder OFG motivated this thesis to investigate whether NaB would interfere with the inflammatory response of monocytes/macrophages using the monocytic cell line THP-1.

Since the information available on the literature about the effects of NaB on monocytes is limited, the hypotheses were very general.

The hypotheses investigated in this thesis are:

1- What are the effects of NaB on the innate immune response after TLR stimulation?
2- What are the mechanisms of action of NaB that interfere with the immune response?
3- What are the consequences of changes caused by NaB on the immune response?
4- What is the overall change in the cell caused by NaB treatment before and after TLR challenge?

Chapter 2 Materials and methods

2.1 Cell culture

2.1.1 THP-1 cells

The THP-1 cell line (ATCC® TIB-202™), a cell line derived from the peripheral blood of a 1-year-old male patient with acute monocytic leukaemia, is a monocyte-derived and spontaneously immortalized cell line[152]. THP-1 cells were cultured and maintained in enriched RPMI/THP-1 culture medium. Cells were grown in flasks at a concentration of 2-4x10^5 cells/mL prior to being stimulated. THP-1 cells were maintained by addition or replacement of fresh medium of medium and split 3x times per week and kept no longer than 2 months.

2.1.1.1 THP-1 culture media

The THP-1 culture medium contained RPMI 1640 Medium, GlutaMAX™, plus 10% foetal bovine serum (Sigma F9665), 100 U/mL of Penicillin and 100 µg/mL Streptomycin (Gibco 15140-122), 20 mM HEPES solution (Sigma H0887), and 20 nM 2-mercaptoethanol (Gibco 31350).

2.1.2 Peripheral blood monocyte-derived macrophages (PBM-DM)

100 mL of peripheral venous blood was collected from healthy patients in 5 U/mL heparin by adding 300 µL of 1,000 IU/ml heparin sodium (Wockhardt) to each 50 mL syringe. Peripheral blood monocytes were isolated using Lymphoprep™ (Axis-Shield) by layering 25 mL of blood onto 15 mL of Lymphoprep in 50 mL Falcon tubes. Tubes were centrifuged at 900 g for 30 minutes at 20 °C with low brakes. The lymphocyte-monocyte layer at the interface of the serum at the top and the Lymphoprep in the middle was harvested and pooled into two 50 mL Falcon tubes. The cell suspension was topped up with PBS and centrifuged at 500 g for 5 minutes

at 20 °C with the brakes on. The cells were washed two further times with PBS but centrifuged at 500 g.

The cell pellet was resuspended in 10 ml of RPMI 1640 Medium GlutaMAX™ Supplement (Gibco) containing 100 U/mL of Penicillin and 100 µg/mL Streptomycin (Gibco) and 20 mM HEPES (Sigma) and plated onto 92 mm Nunclon™ surface coated tissue culture plates (Nunc). The cells were incubated in a humidified tissue culture incubator at 37 °C, 5% CO_2 for 2 hours in a Heraeus BB15 incubator (Thermo Scientific) to allow for monocyte adherence induced by serum starvation. After 2 hours, the RPMI media was tipped off, cells were washed with PBS once to remove non-adherent lymphocytes and fed with 10 mL of RPMI 1640 Medium GlutaMAX™ Supplement containing 10% FBS (Sigma), 100 U/ml penicillin, 100 µg/ml streptomycin and 20 mM HEPES. After 24 hours, cells were fed with a further 10 ml of RPMI containing 10% FBS and incubated for a total of 5 days to obtain adherent monocyte-derived macrophages as previously described[153].

After 5 days, MDMs were washed in PBS, scraped, counted and cultured overnight in X-VIVO™ 15 medium (Lonza) at $1x10^6$ cells/mL on tissue culture plates and were ready for stimulation on the following day.

2.2 Reagents for biological assays

2.2.1 NaB

Sodium benzoate BioXtra, ≥99.5% (B3420 Sigma-Aldrich) was diluted at 1 M concentration in Endotoxin-Free Ultra-Pure Water (TMS-011 EMD Millipore) and filtered with a Nalgene 0.45µm filter (Thermo Scientific 190-2545) to remove undissolved residue and stored at room temperature in 50 mL Falcon tube.

2.2.2 Heat-killed bacteria

2.2.2.1 Luria-Bertani (LB) broth and agar plates

20 g of LB Broth powder (L3022 Sigma) was added to 800 mL of dH2O, mixed with a magnetic stirrer and made up to 1000 mL then autoclaved and plated. LB broth was made up as above without the agar.

2.2.2.2 Heat-killed *Escherichia coli* (HkEc) stock

The fully antibiotic sensitive clinical isolate, *E. coli* NCTC 10418 was cultured by adding 1 µL of glycerol stock into 10 mL LB broth (Sigma L3022) and incubated at 37 °C, 250 rpm in an Innova™ 4000 incubator shaker (New Brunswick Scientific) overnight. *E. coli* was centrifuged at 3000 *g* for 20 minutes, room temperature in a Heraeus Multifuge X1R (Thermo Scientific), washed once with 20 mL PBS, resuspended in 1 mL PBS. The killing of *E. coli* was carried out by incubating 1 mL of bacteria in PBS at 60 °C for 1 hour in a Grant GD100 circulating immersion bath. The killing of *E. coli* was checked by plating 80 µL of HkEc onto LB agar plates with no antibiotics.

HkEc solution was counted at 1:20 dilution using a Cecil BioQuest™ CE2502 spectrophotometer. The *E. coli* optical density at 600 nm (OD_{600}) of 1×10^8 bacteria/mL in PBS is 0.365 as previously established in our laboratory. The concentration of *E. coli* in PBS was adjusted to 1×10^{10} bacteria/mL and stored at -20 °C.

2.2.2.3 Heat-killed *Porphyromonas gingivalis* (HkPg) stock

The *P. gingivalis* ATCC 33277 strain was kindly provided by Dr. Helen Petersen (Manchester University Hospital, UK) after being cultured from frozen stocks under anaerobic conditions (85% N_2, 10% H_2, 5% CO_2) into Trypticase soy broth supplemented with 1 mg of yeast extract/mL, 5 µg of hemin/mL, and 1 µg of menadione/mL. The killing of *P. gingivalis* was carried out by incubating 1 mL of bacteria in PBS at 60 °C for 1 hour in a

Grant GD100 circulating immersion bath. The concentration of *P. gingivalis* used to stimulate the cells was determined by titration, after stimulation of THP-1 cells with different concentrations of HkPg. The levels of the secreted IL8 was used as the output. The lowest concentration that showed the maximum secretion of IL8 was chosen as the working concentration, which was 1 µL/mL.

2.2.3 Mixed biological reagents

The list of reagents containing the description of each item, catalogue number, supplier, and usual working concentration can be found in Table 2. If in any case, the experiment required the use of a different concentration, this information will be available in the results description. The working concentration was established based on usual concentrations found in the literature and/or titrated and toxicity determined by MTT assay (see section 2.4.1).

Table 2: List of reagents containing the description, catalogue number, supplier, and usual working concentration.

Item description	Catalog #	Supplier	Work Conc	Preinc
Pam3Cys-Ser-(Lys)4, trihydrochloride	ALX-165-066	Alexis Biochemicals	10 µg/mL	
LPS from Salmonella abortus equi S-form	ALX-581-009	Alexis Biochemicals	200 ng/mL	
LPS from Salmonella Minnesota R595	ALX-581-008	Alexis Biochemicals	200 ng/mL	
N-Acetyl-L-cysteine	A7250	Sigma-Aldrich	1 mM	30’
TEMPO	214000	Sigma-Aldrich	1 mM	30’
N, N′-Dimethylthiourea	D188700	Sigma-Aldrich	2 mM	30’
Curcumin (high purity)	ALX-350-028	Alexis Biochemicals	12.5 µM	30’
HUMIRA® (adalimumab)		AbbVie Inc.	100 µg/mL	
Tyrphostin AG 490	T3434	Sigma-Aldrich	20 µM	30’
PD98059	tlrl-pd98	InvivoGen	20 µM	30’

Recombinant Human TNF	210-TA	R&D Systems	10 ng/mL	
Recombinant Human IL6	206-IL	R&D Systems	10 ng/mL	
Actinomycin D	A9415	Sigma	2 µg/mL	
Bafilomycin A1 from Streptomyces griseus	B1793	Sigma-Aldrich	200 nM	
Brefeldin A	B5936	Sigma-Aldrich	1 µM	
Ammonium chloride	A4514	Sigma-Aldrich	10 mM	
Monensin sodium salt	M5273	Sigma-Aldrich	2.5 µM	
z-Leu-Leu-Leu-CHO (MG-132)	I-130	Bio-Techne	10 µM	1h
12-myristate 13-acetate (PMA)	P8139	Sigma-Aldrich	2 µM	

Abbreviations: Catalog #, catalogue number; Work conc, working concentration; Preinc, preincubation

2.3 Cell stimulation

2.3.1 NaB treatment

THP-1 cells or PBM-DM were incubated with 5 mM NaB overnight pre-challenge with bacteria or TLR ligands. The cells were then harvested and centrifuged at 500 g for 5 minutes. The supernatant was removed, and the cell pellet was resuspended and washed 2X with PBS after centrifugation at 500 g for 5 minutes. The washing steps were also carried out with the cells that were not treated with NaB.

The cells pre-treated with NaB were resuspended in medium containing 5mM NaB at a concentration of 1 X 10^6 viable cells/mL. Cells were counted, and viability determined using the TC20™ Automated Cell Counter (Bio-Rad) with Trypan Blue (1450021 Bio-Rad).

2.3.2 Stimulation of cells

Cells were stimulated with HkEc with a multiplicity of infection (MoI) 20:1 (bacteria/cell). HkPg was added at a concentration of 1 µL/mL,

established after titration. The TLR ligands LPS (TLR4) smooth (200 ng/mL) and rough (200 ng/mL) types, and 10 µg/mL PAM3CSK4 (TLR1/2) were used for the immunological challenge of specific TLRs.

The list of all the biological reagents with their working concentration and time required of preincubation are described in Table 1. Any alteration in concentrations used in the described experiments will be documented in the results section.

2.4 Cell viability assays

2.4.1 MTT cell viability assay

2.4.1.1 MTT (3-[4,5-dimethylthiazol-2-yl]-2,5-diphenyl tetrazolium bromide)

A 0.5% solution of MTT (3-[4,5-dimethylthiazol-2-yl]-2,5-diphenyl tetrazolium bromide) was made by dissolving 500 mg of MTT (Sigma M2128) in 100 mL of PBS and stored at 4 °C in the dark. Cells were cultured in 96-wells plate within 100 µL of the medium under different conditions and time frames depending on the experimental protocol. The viability of the cells at the end of the protocol was determined by adding 30% of total volume of MTT (30 µL) to the wells and incubated for at least 4 hours.

2.4.1.2 MTT lysis solution

One litter of lysis solution was prepared using 900 mL of isopropanol, 47 mL of dH_2O, 50 mL of 10% sodium dodecyl sulfate (SDS) and 3 mL of concentrated HCl, which was kept at room temperature.

2.4.1.3 MTT assay

After MTT incubation, the plate was centrifuged at 8000 rpm for 5 minutes. The supernatant was removed with a multi-channel pipette and

100 µL of MTT lysis solution added to the cells and pipetted multiple times until all formazan crystals were dissolved. Results were read on a FLUOstar Omega microplate reader (BMG LABTECH) at 563 nm.

2.4.2 CCK-8 cell viability assay

The Cell Counting Kit-8 (B34306 Biotool) ready-to-use solution was added to each well to a concentration of 10% v/v and kept in a humidified tissue culture incubator at 37 °C, 5% CO_2 for 1 hour. Results were read on a FLUOstar Omega microplate reader (BMG LABTECH) at 450 nm.

2.5 pH measurements

The pH of solutions and medium were monitored after NaB solution preparation, pre and after addition to RPMI enriched medium using a pH meter from Mettler Toledo, type Delta 340 (Gemini bv) previously calibrated with standard pH solutions. pH changes of the THP-1 medium after HkEc ± NaB stimulation were also monitored over the next 3 days.

2.6 Cytokine assay

2.6.1 Enzyme-linked immunosorbent assay (ELISA) assay

Cytokine levels from supernatants or total cell lysates (see section 2.8.1.1) from cultured THP-1/PBM-DM cells under several conditions were collected and stored at -80°C prior to use. After removal of supernatants for storage, cell viability was assessed using the MTT assay. Total cell lysates were standardized prior to testing using the Pierce™ BCA Protein Assay Kit (23225 Thermo Fisher Scientific) and stored at -80°C. Samples were diluted with reagent diluent for ELISA. The ELISAs were carried out using Duo-Set ELISA kits according to manufacturers' instructions and read on a FLUOstar Omega or CLARIOstar microplate readers (BMG LABTECH). Microplate readers were set to 450 nm and 570 nm, the last used for wavelength correction, for ELISA kits supplied by R&D Systems.

The wavelength correction was done using MARS Data Analysis Software by subtracting readings at 570 nm from the readings at 450 nm for (Table 3). For ELISA kits provided by PeproTech, colour development was monitored and read on the plate readers at 405 nm with wavelength correction set at 650 nm (Table 3). The full description of each kit used is shown in Table 3.

Table 3: Description of ELISA kits used, catalogue number, supplier, and supernatant dilutions.

Kit	Catalog #	Manufacturer	Dilution
Human IL8/CXCL8 DuoSet ELISA	DY208	R&D Systems	1:40
Human TNFlpha DuoSet ELISA	DY210	R&D Systems	1:10
Human IL6 DuoSet ELISA	DY206	R&D Systems	1:10
Human IP10 DuoSet ELISA	DY266	R&D Systems	1:40
Human IL-1 beta DuoSet ELISA	DY201	R&D Systems	1:10
Human IP10 ELISA Development Kit	900-K39	PeproTech	1:40
Human IL-10 ELISA Development Kit	900-K21	PeproTech	1:10

Abbreviations: Catalog #, catalogue number

2.6.2 MSD® multiplex immunoassay

Supernatant from THP-1 cells stimulated with HkEc ± NaB for 24 hours was measured using the V-PLEX Proinflammatory Panel 1 Human Kit (K15049D-1 Meso Scale Discovery) containing the analytes IFNγ, IL10, IL-2p70, IL13, IL1β, IL2, IL4, IL6, IL8, and TNF. The assay was performed according to the manufacturers' instructions and read on a SECTOR® Imager 6000 (Meso Scale Discovery).

2.7 Gene expression

2.7.1 RNA purification

Total RNA was extracted and purified from THP-1 cells after several treatments. Cells were harvested, and the supernatant was removed (or collected) and 350 µL of RLT lysis buffer (Qiagen) with 1% 2-

mercaptoethanol (M3148 Sigma) was added and stored at -80 ºC prior to extraction. RNA was extracted using the RNeasy Mini Kit columns with RNase-free DNase treatment (Qiagen) and processed according to the manufacturer's instructions with a RNase-free DNase treatment (Qiagen) step. The concentration of total RNA in RNase-free H_2O (Qiagen) was measured with a NanoDrop ND-1000 spectrophotometer (Thermo Scientific) and/or Qubit 2.0 Fluorometer (Invitrogen). Additionally, OD_{260}/OD_{280} and OD_{260}/OD_{230} were measured, which assessed protein and solvent contamination. For microarray expression profiling, RNA integrity (RIN) was analysed by measuring ribosomal RNA band 28S/18S ratios using high-resolution electrophoresis on an Agilent Bioanalyzer (Agilent Technologies, Inc), samples which attained RIN scores which were >8 were taken forward for whole transcriptome analysis.

2.7.2 Complementary DNA (cDNA) synthesis

Total RNA was converted to cDNA using the Moloney Murine Leukemia Virus Reverse Transcriptase (M-MLV RT) kit (M1705 Promega). 500 ng of total RNA diluted in 15 µL of RNase-free water was added to 1 µL of oligodT primer (Sigma) and incubated for 10 minutes at 70 °C for primer annealing and then placed on ice for 5 minutes. After that, a master mix containing 1 µL of M-MLV Reverse Transcriptase, 5 µL of 5X Reaction Buffer, 1 µL Recombinant RNasin® Ribonuclease Inhibitor (Promega), and 2 µL of dNTP Mix (NU-0010-10 Eurogentec) was added to each RNA sample making a total volume of 25 µL. Samples were incubated at 40 °C for 10 minutes for DNA polymerization and heated at 70 °C for 5 minutes for enzyme deactivation on a DNA Engine Tetrad 2® Peltier Thermal Cycler (Bio-Rad). Samples were made up to 100 µL with RNase-free water and stored at -20 °C.

2.7.3 Gene Expression Microarray

1.5 ng of total RNA was amplified using the HumanHT-12 v4 Expression BeadChip Kit (Illumina) and normalised to 150 ng/µL. 750 ng

was hybridised to Illumina Human-WG6 v3.0 Expression BeadChips (Illumina) for 16 hours at 58ºC. After hybridization, BeadChips were washed and stained with streptavidin-Cy3 (GE Healthcare, Little Chalfont, United Kingdom), scanned using the BeadArray Reader (Illumina), and processed using Illumina Genome Studio software (Illumina).

The original expression data contained 47,213 probes under 6 different conditions: untreated, NaB treated, HkEc, HkEc + NaB, HkPg, and HkPg + NaB, stimulated for 4 hours and 4 replicates each split into 2 chips with duplicates in each. These data were log2 transformed and quantile normalised, and analysed using the LUMI and LIMMA packages in the R programming language (Bioconductor)[154155]. The probes were mapped and annotated using the BioMart and BioConductor package illuminaHumanv4[156].

Probes that reached a minimum detection P-value of < 0.01 in at least 50% of the samples were included in the subsequent analyses (n = 16,348). Batch effects were corrected using combating batch effects when combining batches of gene expression microarray data (ComBat) normalization and efficacy of normalization was verified by density x intensity plot[157]. Differential gene expression analysis was conducted using LIMMA software (Bioconductor)[155]. The P-value was adjusted for multiple testing as described by Benjamini and Hochberg[158].

2.7.4 Semi-quantitative PCR

cDNA originated as previously described were amplified by PCR with primers created using Primer3 (Table 4). Stock primers at 100 µM were diluted to 5 µM i.e. 50 µL per 1 mL of RNase-free water for and stored at -20 °C. The PCR reaction was made up of 12.5 µl of HotStarTaq Master Mix (1000 U), 1 µL forward primer, 1 µL reverse primer, 2 µL cDNA and 8.5 µL RNase-free water, to a total volume of 25 µl. The final concentration in each reaction volume was 1.25 U HotStar Taq DNA polymerase, 1X PCR buffer containing 0.75 mM $MgCl_2$, 100 µM of each dNTP, 0.25 µM of each primer and ~10 ng of RNA equivalent. The RT-PCR was activated at 95 °C for 15 minutes, denatured at 95 °C for 30 s, annealed at 60 °C for 45

s, extended at 72 °C for 60 s, for a total of 35 cycles, then extended for a final time at 72 °C for 10 minutes before being cooled to 4 °C on a DNA Engine Tetrad 2® Peltier Thermal Cycler (Bio-Rad). The annealing temperature of 60 °C was chosen after a temperature gradient was run for the primer pair.

After the PCR, 5 µL of 6X Orange Loading Dye (R0631 Thermo Fisher Scientific) and loaded on 1% agarose gel containing 0.01% ethidium bromide. The gels were cast on horizontal electrophoresis and ran at 100V for 25 minutes. Images were captured using Thermo Scientific MYECL Imager.

Table 4: List of primers used for PCR/qRT-PCR.

GENE	Forward primer	Reverse primer	Target exons
IL6	5’-CACTGGCAGAAAACAACCTG-3’	5’-TGTACTCATCTGCACAGCTCT-3’	3-4
CXCL10 (IP10)	5’-AGTGGCATTCAAGGAGTACC-3’	5’-TGATGGCCTTCGATTCTGGA-3’	1-3
IL1B	5’-ACTGAAAGCTCTCCACCTCC-3’	5’-CTCTCCAGCTGTAGAGTGGG-3’	4-6
IL8	5’-CAGTTTTGCCAAGGAGTGCT-3’	5’-CCAGTTTTCCTTGGGGTCCA-3’	2-3
TNF	5’-GGACCTCTCTCTAATCAGCCC-3’	5’-TGGTTATCTCTCAGCTCCACG-3’	2-4
CD80	5’-ATCTGACGAGGGCACATACG-3’	5’-GAGAGGTGAGGCTCTGGAAA-3’	2-3
CD86	5’-GAAGAAGAAGAAGCGGCCTC-3’	5’-TCACTTTTGTCGCATGAAGATG-3’	5-7
CXCL9 (MIG)	5’-GCCCTTCCTGCGAGAAAATT-3’	5’-GCTGACCTGTTTCTCCCACT-3’	2-4
TRAF3	5’-CAGCGTGTCAAGAGAGCATC-3’	5’-GGACGCACACATGGAAGTTC-3’	2-4
IKBKE	5’-TTCAGCACAGCCATCCCTAA-3’	5’-CCCCGAAACATTAGCTCCTG-3’	8-10
TRIF	5’-ACCTCCTGCATGCCATGGTTCT-3’	5’-TCAGCCAGCAGGTGGTACAA-3’	1
TLR4	5’-GTTTCCCAGAACTGCAGGTG-3’	5’-TGTCTCCACAGCCACCAG-3’	2-3
PPIA	5’-GTGTTCTTCGACATTGCCGT-3’	5’-CCATTATGGCGTGTGAAGTCA-3’	1-3

2.7.5 Quantitative reverse transcription PCR (qRT-PCR)

cDNA originated as previously described were amplified using several primers from Table 4. qRT-PCR was performed using the QuantiFast SYBR® Green PCR kit (Qiagen), in duplicate on a Mastercycler® ep *realplex* (Eppendorf). Stock primers at 100 µM were diluted to 5 µM i.e. 50 µl per 1 mL of RNase-free water for qRT-PCR and stored at -20 °C. The qRT-PCR reaction was made up of 12.5 µl 2× QuantiFast SYBR Green PCR Master Mix, 0.5 µl forward primer, 0.5 µl reverse primer, 2 µl cDNA and 9.5 µl RNase-free water, to a total volume of 25 µl. The final concentration in the reaction volume was 1× QuantiFast SYBR Green PCR Master Mix, 0.1 µM of each primer and ~10 ng of RNA equivalent per reaction. The PCR mix was activated at 95 °C for 15 minutes, denatured at 95 °C for 15 s and annealed/extended at 60 °C for 60 s, for a total of 40 cycles, then a melting curve was performed. The annealing temperature of 60 °C was chosen after a temperature gradient was run for each primer pair.

Normalized mean gene expression values ± SD were determined from duplicate cycle threshold (Ct) values for each gene and the housekeeping gene peptidylprolyl isomerase A (*PPIA*). Relative transcript levels were determined by the $2^{-\Delta\Delta Ct}$ method[159].

2.8 Immunoblot

2.8.1 Cell lysate preparation

2.8.1.1 Whole cell lysate preparation

THP-1 cells were plated in a 24-well plate with a cell count of 2 x 10^6 cells under several treatments. At the planned stimulation time, cells were scraped with sterile 24 cm cell scrapers (SLS 99002T) and transferred to Eppendorf tubes and centrifuged with a Beckman Coulter Microfuge 22R for 1 minute at 2500 rpm. The supernatant was discharged

(or collected and stored at -80 ºC) and the cell pellet resuspended and washed with 1 mL of ice-cold PBS and centrifuged again using the same settings. The PBS was removed by aspiration and cells were lysed in 250 µL of ice-cold radioimmunoprecipitation assay (RIPA) buffer containing protease inhibitor cocktail (Roche 11697498001) and PhosSTOP™ (4906845001 Sigma) and vortexed (Table 5).

The cell lysate was then sonicated using a MSE Soniprep 150 (MSE) for three 10 seconds burst with an amplitude of 7 microns intercalated with periods of 10 s on ice for disrupting cellular membranes, releasing the cell contents and shearing of DNA. After the sonication, the lysates were centrifuged for 10 minutes at 4 ºC at ≥ 10,000 rpm.

2.8.1.2 Cell fractionation preparation

Subcellular fractionation for separating nuclear and cytoplasmic cell fractions was carried out using different buffer and centrifugation steps. Cells were prepared similarly to described above until the washing step with PBS. The cytoplasmic fraction was extracted using a cytoplasmic lysis buffer (Table 5). 100 µL of cytoplasmic buffer was added to the cell pellet and incubate on ice for 3 minutes. Then, samples were centrifuged at 200 g for 4 minutes and the cytoplasmic fraction collect in a new tube. The pellet containing the nuclei was carefully resuspended and washed using a wash buffer (the same cytoplasmic buffer without the detergent IGEPAL) and then centrifuged at 200 g for 3 minutes. 100 µL of nuclear extraction buffer (RIPA buffer with a higher concentration of SDS 1%) and incubated for 10 minutes on ice. Both buffers contained protease inhibitor cocktail and PhosSTOP™.

The cell lysates were then sonicated using a similar protocol described above. After the sonication, the lysates were centrifuged for 10 minutes at 4 ºC at ≥ 10,000 rpm.

Table 5: Cell lysate buffers for immunoblot

RIPA EDTA/EGTA lysis buffer		
Reagent/Manufacturer	Stock	Final concentration
Trizma® base (T1503 SIGMA)	1 M	50mM
Sodium chloride (S3014 SIGMA)	5 M	150mM
Sodium-deoxycholate (D6750 SIGMA)	5%	0.50%
EDTA solution (03690 SIGMA)	500 mM	1mM
EGTA (E3889 SIGMA)	500 mM	0.5mM
IGEPAL® CA-630 (I8896 SIGMA)	100%	1%
SDS (L3771 SIGMA)	10%	0.10%
PBS (P4417 Sigma)	10X	1X
Cytoplasmic lysis buffer		
Reagent	Stock	Final concentration
HEPES (H0887 SIGMA)	1 M	10 mM
MgCl2 (M8266 SIGMA)	150 mM	1.5 mM
KCl (P9541 SIGMA)	1 M	10 mM
DTT (D0632 SIGMA)	0.5 M	0.5 mM
EDTA	100 mM	1 mM
IGEPAL	100%	0.05%
PBS	10X	1X

2.8.2 Sample preparation

The protein concentration of each sample was measured using the Pierce™ BCA Protein Assay Kit (23225 Thermo Fisher Scientific) according to the manufacturer's instructions and read on a CLARIOstar or FLUOstar Omega microplate reader (BMG LABTECH) at 562 nm. Samples were then standardized with appropriated amounts of cell lysate and lysis buffer. One volume of sample buffer mix made of 3 volumes of 4X NuPAGE® LDS Sample Buffer (NP0007 Thermo Fisher Scientific) and 1 volume of 2-mercaptoethanol (Gibco 31350) was added to 2 volumes of standardized lysis buffer and then boiled at 95 ºC for 5 mins and stored at -20 °C.

2.8.3 SDS-PAGE gels

Sodium dodecyl sulfate-polyacrylamide gel electrophoresis (SDS-PAGE) gels were cast using the Mini-PROTEAN® System (Bio-Rad) with 30% w/v Acrylamide/ProtoFLOWGel (SLS H16996), 1.5 M Tris-HCl pH 8.8 (resolving gel), 1 M Tris-HCl pH 6.8 (stacking gel), dH_2O, 10% SDS (Sigma L3771), freshly made 10% ammonium persulphate (Sigma A7460) in plastic tubes. TEMED (Sigma T9281) was added last, previous to addition to a gel casting apparatus.

10% SDS-PAGE gels were used and loaded onto 15-well SDS-PAGE gels and run in ~700 ml of 1X transfer buffer without methanol (Table 6) at 100 V (constant voltage) for 40 minutes.

Alternatively, precast Novex 4-12% Bis-Tris Midi Protein Gels (WG1403 Thermo Fisher Scientific) were used on XCell4 SureLock Midi-Cell Chambers and run in ~1000 mL of 1X NuPAGE MOPS SDS Running Buffer (NP0001 Thermo Fisher Scientific) at 120 V for 2 hours.

Table 6: Buffers for SDS-PAGE gels.

10X Tris-buffered saline (TBS) pH 7.4		
Reagent	Stock	Final concentration
Trizma® base	24.2 g	20 mM
NaCl	80.06 g	137 mM
dH2O		800 mL
HCl (H1758 SIGMA)	5 M	pH to 7.4
dH2O		top up to 1 L
10X Transfer buffer		
Reagent	Stock	Final concentration
Glycine (G8898 SIGMA)	144 g	191 mM
Trizma® base	30.2 g	25 mM
dH2O		top up to 1 L
10X Running buffer		
Reagent	Stock	Final concentration
Glycine	144 g	191 mM
Trizma® base	30.2 g	25 mM
SDS	10%	0.1%
dH2O		top up to 1 L

2.8.4 Protein transfer to membrane

Proteins were transferred from gels using a wet transfer system to methanol-activated Immobilon-P PVDF Membranes (IPVH00010 Millipore). 400 mL of 1X transfer buffer (Table 6) containing 20% methanol on a Novex™ Bolt™ Vertical Mini Blot Module (B1000 Invitrogen™) and Invitrogen™ Mini Gel Tank (A25977 Invitrogen™) at 20V for 1 h following the manufacturer's instructions.

The SDS-PAGE gel was removed from its mould in the transfer buffer, the stacking gel was gently cut off with spatulas and the gel was placed on the bottom layer of a sandwich formed by a sponge and a piece of blotting paper. The PVDF membrane was placed on the top of the gel and a roller was used to remove all the trapped bubbles. The membrane was topped by another layer of blotting paper and sponge. The Mini Blot Module was then closed and mounted in the tank and the chamber filled with transfer buffer and ran at 20 V for 60 minutes.

2.8.5 Antibody staining

Membranes were blocked with 5% BSA (A2153 Sigma) in TBS (Table 6) plus 1% Tween 20 for 1 hour. Membranes were probed with primary antibody overnight at 4 ^{o}C (Table 7) then washed 3 times for 5 minutes with TBS-Tween. Membranes were probed with secondary antibody for 1 hour at room temperature then washed 3 times for 5 minutes with TBS-Tween. Bound antibody was detected using Luminata Crescendo Western HRP substrate (WBLUR0500 Merck) and exposed to Hyperfilm ECL (Amersham) in a film cassette and scanned with an Epson Perfection V700 Photo or image capture using Thermo Scientific MYECL Imager. Band intensity was quantified and normalised to actin using Image Studio^{TM} Lite software (LI-COR).

Table 7: List of antibodies used for western blotting

Antibodies	MW (kDa)	Manufacturer	Catalog #	WB Conc	Secondary Ab
Cofilin	19	Cell Signalling	5175	1:1000	Rabbit
TNF	15	R&D System	MAB610	1 µg/mL	Mouse
IL6	26	Sigma	i7901	1:1000	Mouse
HMOX1	33	Abcam	ab52947	1:2000	Rabbit
UCP2	33	Abcam	ab67241	1:500/1000	Mouse
IkBa	39	Cell Signalling	9242	1:1000	Rabbit
P38	40	Cell Signalling	9218	1:1000	Rabbit
PSAT1	40	Abcam	ab96136	1:1000	Rabbit
p-P38	43	Cell Signalling	4511	1:1000	Rabbit
p-c-Jun (Ser73)	48	Cell Signalling	9164	1:1000	Rabbit
ERK 1/2	42 / 44	Cell Signalling	9102	1:1000	Rabbit
p-ERK 1/2)	42 / 44	Cell Signalling	9101	1:1000	Rabbit
α-Tubulin	50	Thermo	MA1-19162	1 µg/mL	Mouse
p-IRF3	45 / 55	Cell Signalling	4947	1:1000	Rabbit
p-SAPK/JNK	46 / 54	Cell Signalling	9255	1:2000	Mouse
AKT	60	Cell Signalling	9272	1:1000	Rabbit
p-AKT (Ser473)	60	Cell Signalling	9271	1:1000	Rabbit
Catalase	60	Cell Signalling	12980	1:1000	Rabbit
KEAP1	60-64	Cell Signalling	8047	1:1000	Rabbit
P62	62	Abcam	ab56416	1 µg/mL	Mouse
p-C-FOS (Ser32)	62	Cell Signalling	5348	1:1000	Rabbit
NFkB p65	65	Cell Signalling	8242	1:1000	Rabbit
p-NFkB p65	65	Cell Signalling	3033	1:1000	Rabbit
p67phox (NCF2)	67	Home prepared		1:2250	Rabbit
Lamin B1	70	Abcam	ab133741	1:1000	Rabbit
p-STAT3	79 / 96	Cell Signalling	12640	1:2000	Rabbit
STAT3	79 / 96	Cell Signalling	12640	1:1000	Rabbit
pTBK1/NAK	84	Cell Signalling	5483	1:1000	Rabbit
NRF2	97-100	Cell Signalling	12721	1:1000	Rabbit
p-STAT6	110	Cell Signalling	9361	1:1000	Rabbit
Vinculin	117	Milipore	MAB3574	1:1000	Mouse
iNOS	135	Abcam	ab3523	1:500	Rabbit
ASK1	155	Cell Signalling	3762	1:1000	Rabbit
p-ASK1	155	Cell Signalling	3765	1:1000	Rabbit

List of secondary antibodies used for western blotting

Antibodies	Manufacturer	Catalog #	WB Conc
Goat Anti-Rabbit	Dako	P044801-2	1:2500
ECL Anti-mouse IgG	Amersham	NA931	1:2500

2.9 Confocal microscopy

THP 1 cells were plated out in a 96-well plate at a density of 1 x 10^5 cells/mL in a total volume of 200 µL/well in RPMI enriched medium and stimulated with HkEc (MoI 20:1) and incubated in a humidified tissue culture incubator at 37 °C, 5% CO_2 for 1 hour, in the presence or absence of NaB. Two µL (1 µg) of a pre-diluted (50 µg vial in 100 µL of DMSO) carboxy-S-1 succinimidyl ester 5-(and-6)-Carboxy SNARF®-1, Acetoxymethyl Ester, Acetate (C1272 Thermo Scientific) was added to each well and incubated for 5 minutes.

The Ibidi µ slide 8 well ibiTreat (IB-80826 Thistle Scientific) chamber slide was used for plating the THP-1 cells prior imaging. The chambers were pre-treated with 200 µL of poly L-lysine for 20 minutes at RT, the excess of poly L-lysine was removed and washed twice with PBS and left for air-drying. After the stimulation and labelling step, the cells were harvested and washed twice in balanced salt solution (BSS) buffer (Table 8) and centrifuged at 500 g for 5 minutes to remove all the excess of SNARF®. Then, cells were resuspended in 200 µL of BSS buffer and added to the chambers and taken for imaging.

Cells were imaged with a Zeiss 710 confocal microscope using a 63× oil immersion. SNARF-1 fluorescence was excited at 555 nm and the emission was split between two detectors measuring fluorescence emission simultaneously between 560–600 nm and >610 nm.

The cytoplasmic pH was measured by confocal ratiometric fluorescence microscopy and the SNARF fluorescence ratios were calibrated to pH values using standard curves derived from separate calibration experiments as previously described[160].

Table 8: Recipe for preparation of BSS buffer.

Reagent	Stock	Final Concentration
NaCl	3 M	156 mM
KCl (P9333 Sigma)	250 mM	3 mM
$MgSO_4$ (M2643 Sigma)	250 mM	2 mM
KH_2PO_4 (P9791 Sigma)	1 M	1.25 mM
$CaCl_2$ (C5670 Sigma)	1 M	2 mM
Glucose (G7528 Sigma)		10 mM
Hepes (H4034 Sigma)		10 mM
NaOH (71687 Sigma)		Adjust to pH 7.4
dH_2O		Top up to volume
Filter sterilize 0.2 µm		

2.10 Hydrogen peroxide assay

The release of H_2O_2 by THP-1 cells stimulated with PMA (P8139 Sigma) or HkEc was assessed by Amplex® Red Hydrogen Peroxide/Peroxidase Assay Kit (A22188 Molecular Probes). The assay is based on oxidation of Amplex Red by hydrogen peroxide in the presence of horseradish peroxidase (HRP), which gives rise to a coloured product, resorufin on a stoichiometry reaction of the Amplex Red reagent with H_2O_2 in a proportion of 1:1.

Cells were plated in a 96-well flat-bottomed plate at a density of 10^5 cells/well. H_2O_2 production was measured at 37°C in the presence of 3 µM Amplex® Red (Molecular Probes), 0.1 U/ml horseradish peroxidase (HRP) (Sigma-Aldrich) and, where appropriate, 1 µg/mL PMA or HkEc 20:1 (MoI) in the presence or absence of NaB in sterile RPMI 1640 Medium without phenol red (Gibco 11835030) or BSS buffer. Measurements were taken on a CLARIOstar OMEGA microplate reader (BMG LABTECH Ltd.). Excitation was set at 544 nm and emission was set at 590 nm, with measurements taken at 30 seconds intervals for 1 hour. The rate of H_2O_2 production per hour (nM/h) was calculated on the exponential phase using the MARS Data Analysis Software (BMG LABTECH Ltd.).

2.11 ROS / Superoxide assay

Production of ROS/superoxide by THP-1 cells stimulated with HkEc was assessed by Cellular ROS/Superoxide Detection Assay Kit (ab139476 Abcam). The assay has two non-fluorescent cell permeable dyes, ROS detection dye (green probe) reacts directly with a wide range of reactive species, such as hydrogen peroxide (H_2O_2), peroxynitrite ($ONOO^-$), hydroxyl radicals (HO), nitric oxide (NO), and peroxy radical (ROO), yielding a green fluorescent product indicative of cellular production of different ROS/reactive nitrogen species (RNS) types. However, the sensitivity of the green probe for O^{2-}, as well as hypochlorous acid (HClO) and nitric oxide (NO), is very low relative to other free radicals. The superoxide detection dye (orange probe) is a cell-permeable probe that reacts specifically with superoxide (O^{2-}), generating an orange fluorescent product.

Cells were plated in a 96-well flat-bottomed plate at a density of 10^5 cells/well. H_2O_2 production was measured at 37°C in the presence of 2 nM of ROS/Superoxide dyes and, where appropriate, HkEc 20:1 (MoI) in the presence or absence of NaB in sterile BSS buffer.

To evaluate the immediate effect of sodium benzoate as a radical scavenger, a 2-phase experiment was performed. During phase 1, cells were stimulated as previously described for 90 minutes, allowing the formation of ROS/superoxide and then, during phase 2, titrated doses of NaB were added to the wells, with a similar amount of buffer added to controls. And the experiment carried out for a total period of 3 hours.

Measurements were taken on a CLARIOstar OMEGA microplate reader (BMG LABTECH Ltd.). Excitation was set at 490 nm and emission was set at 525 nm for the green fluorescein, and excitation was set at 550 nm and emission was set at 620 nm for the orange rhodamine with measurements taken at 3-minute intervals for 3 hours. The rate of ROS/superoxide production per hour were calculated on the exponential phase using the MARS Data Analysis Software (BMG LABTECH Ltd).

2.12 Proteomics profile using mass spectrometry

For liquid chromatography-tandem mass spectrometry (LC-MS/MS) analysis, whole protein lysates were analysed under reducing conditions and samples were labelled using the TMTsixplex™ Isobaric Label Reagent Set (90061 Thermo Fisher Scientific).

5 X 10^6 THP-1 cells were plated in 5 mL of enriched RPMI medium a 6-well tissue culture plate and stimulated with 200 ng/mL LPS (smooth) in the presence or absence of NaB. Samples were stimulated or not (untreated) for 2 hours, 4 hours, 6 hours, 12 hours, and 24 hours and lysed in SDS/Hepes buffer pH 7.4 (0.1% SDS, 50 mM Hepes (H0887 Sigma)) with 1 tablet of PhosSTOP and 1 tablet of cOmplete™, Mini, EDTA-free protease inhibitors cocktail (5892970001 - Sigma) in RNase free water for a total volume of 10 mL.

Briefly, 100 µg of total protein in 100 µL of lysis buffer was used for labelling each tagged sample. Samples were reduced in 10 mM DL-Dithiothreitol (DTT 43815 Sigma) for 1 hour at 37 ^oC, alkylated in 25 mM Iodoacetamide (I6125 Sigma) for 2 hours at RT protected from light and then precipitated overnight with 10 volumes of 100% acetone at -20 ^oC.

Samples were centrifuged at 16,000 g for 20 minutes at 4 °C. The supernatant was removed, and the pellet left to air dry to allow residual acetone to volatilize. The pellet was resuspended in 100 µl of 100 mM HEPES, pH 8.5 (pH adjusted with KOH), vortexed and sonicated for proper solubilization. Samples were digested in 2-steps with 2.5 µg of sequencing grade modified trypsin (V5111 Promega), the first step for 1 hour at 37 °C, and after a second aliquot of 2.5 µg trypsin was added to samples and incubated overnight at 37 °C (no longer than 16 hours). The TMTsixplex™ tags were resuspended in 53 µL of acetonitrile (1.00017 EMD Millipore) and samples were added to each tag for 2 hours at room temperature, with constant agitation.

The reaction was quenched with 8 µl of 5% hydroxylamine (100 mM HEPES; pH 8.5) for 1 hour at room temperature, on a shaker and further quenched with 100 µL H_2O overnight at 4°C. All six labels were pooled together and pelleted down at 200 g and dried on a Savant SpeedVac

System SPD1010 (SPD1010A-230 Thermo Fisher Scientific) overnight. Solid phase extraction clean-up step was done using SepPak C18 cartridges (WAT023590 Waters) prior to reversed-phase high-performance liquid chromatography (RP-HPLC).

Dried peptide samples combined into a total of 100 µl of 5% organic mobile phase (80% acetonitrile, 20 mM ammonium formate (78314 Sigma); pH 10). Fifty µL of sample was injected on a RP column (40°C) and run at a flow rate of 0.244 mL/minute over 75 minutes run using mobile phase A (20 mM ammonium formate; pH 10) and mobile phase B (80% acetonitrile, 20 mM ammonium formate; pH 10).

LC-MS/MS with the LTQ-Orbitrap mass spectrometer (Thermo Fisher Scientific), was performed as previously described[161]. Raw MS files were analysed by the Mascot search engine 2.3.02 (Matrix Science) and searched against a SwissProt human database 2013_10 (containing 39,696 entries including common contaminants). Mascot search analysis parameters included: trypsin enzyme specificity, allowance for 2 missed cleavages, peptide mass tolerance of 20 ppm for precursor ions and fragment mass tolerance of 0.8 Da.

2.13 Experimental conditions tested

2.13.1 Lysosomal inhibition and cytokine release

$1x10^6$ THP-1 cells were plated in 24-well tissue culture plates in RPMI enriched medium and stimulated for 24 hours with HkEc at a MoI of 20:1 ± 5 mM NaB, with 2.5 µM monensin, 10 mM NH4Cl, 50 µM chloroquine, 1 µM brefeldin A or 200 nM bafilomycin A (see Table 1).

After 24 hours, supernatants were collected and stored at -80 °C and ELISAs performed (see section 2.6.1).

2.13.2 Antioxidants

$1x10^6$ THP-1 cells were plated in 24-well tissue culture plates in RPMI enriched medium and stimulated for 24 hours with HkEc at a MoI of

20:1 in the presence of either 5 mM NaB (pre-treated overnight), 1 mM N-Acetyl-L-cysteine (NAC), 2 mM TEMPO, 2 mM N,N'-dimethylthiourea (DMTU), and 12.5 µM Curcumin (high purity). All the other antioxidants were pre-incubated for 30 minutes before HkEc stimulation (see Table 1). After 24 hours, supernatants were collected and stored at -80 °C and ELISA assays were performed (see section 2.6.1).
After the pre-treatment with the antioxidants (NAC, TEMPO, DMTU, and curcumin), the release of H_2O_2 by THP-1 cells stimulated with Phorbol 12-myristate 13-acetate (PMA) or HkEc was assessed by Amplex® Red (see section 2.10).

2.13.3 Immunomodulators Tyrphostin AG 490 and PD98059

The immunomodulators Tyrphostin AG 490 (AG490), a specific and potent inhibitor of the Janus kinase 2 protein and signal transducer and activator of transcription 3 (JAK2/STAT3) was used at a concentration of 20 µM and added 30 minutes prior to bacterial challenge. PD98059, a potent and selective inhibitor of MAP kinase kinases (MAPKK), MEK1 and MEK2, was used at a concentration of 20 µM and added 30 minutes before or 4 hours after HkEc stimulation (see Table 1).

2.13.4 Recombinant cytokines stimulation

$1x10^6$ THP-1 cells were plated in 24-well tissue culture plates in RPMI enriched medium and stimulated for 4 or 24 hours ± HkEc and/or NaB, 10 ng/mL of recombinant TNF or 10 ng/mL of recombinant IL6 were added to cell culture medium to investigate their effects on THP-1 cells cytokine production and release (see Table 1).

After the specific stimulation time, cells were harvested, and the supernatant was collected and stored at -80 °C and ELISAs were performed (see section 2.6.1). The cell pellet was placed in either RLT buffer (see section 2.7.1) or RIPA buffer (see section 2.8.1.1), for mRNA extraction or protein analysis respectively.

2.13.5 Cytokine neutralization assays

$1x10^6$ THP-1 cells were plated in 24-well tissue culture plates in RPMI enriched medium and stimulated for 24 hours ± HkEc and/or NaB, 100 µg/mL HUMIRA®, an anti-TNF medication, or 1 µg/mL of anti-IL6 antibody were added to cell culture medium to investigate the effects of these cytokines on THP-1 cells cytokine production and release (see Tables 1 and 5).

After the specific stimulation time, the supernatant was collected and stored at -80 °C and ELISAs were performed (see section 2.6.1 Enzyme-linked immunosorbent assay).

2.14 Statistical analysis

All data are presented as mean ± SEM using GraphPad Prism 7.0 (GraphPad Software, Inc). Statistical significance was calculated using paired or unpaired two-tailed Student's t-test when 2 groups were analysed. When more than two groups were analysed, statistical significance was calculated using one-way ANOVA with Tukey's multiple comparison test or Dunnet's multiple comparison test when a control/reference group was used. Simple linear regression analysis, area under the curve and analysis of covariance (ANCOVA) was used to compare to linear regressions were calculated using GraphPad Prism 7.0. Microarray and proteomic data were analysed using multiple testing in R program with the BioConductor and LIMMA packages.

2.15 Ethics

For the human study, ethics was approved by the Joint University College London (UCL)/University College London Hospitals (UCLH) Committee for the Ethics of Human Research (project numbers 02/0324) and the NHS National Research Ethics Service, London-Surrey Borders Committee (project number 10/H0806/115). The ethics committee approved consent forms were signed by all participants.

Chapter 3 Effects of NaB on immune response of THP-1 cells

3.1 Introduction

Although NaB is widely used by the food and cosmetic industry, little is known about the effects of this compound has at the cellular level. Just a few studies have been published using primary or immortalized cells that could help the basis of this investigation[39,94,95,162]. Besides that, the main motivation to study NaB was the link between the negative effects of benzoate-containing diets observed in patients with OFG[11,19,163]. Reports of patients with OFG experiencing flare-up of the disease symptoms after ingestion of NaB contrasts with the potential therapeutic benefits in reducing inflammation in NDDs[41,95]. To affect the CNS, NaB probably needs to be absorbed and distributed by the blood and cross the blood-brain barrier (BBB), whereas at sites such as the mucosal surfaces and on the skin NaB may act in a more localized manner. In support of this, NaB has been constantly reported as one of the main allergens responsible for contact urticaria and delayed hypersensitivity on contact skin tests[76].

Since the most commonly affected area of OFG involves the oral mucosa, it is possible that NaB could act directly through absorption in addition to being delivered through a systemic route. Another crucial factor that differentiates the effects of NaB in OFG from those potentially beneficial to NDDs, relies on the greater exposition of the oral mucosa to all sort of irritants and allergens, ranging from microorganisms to unaccountable variety of substances that can cause irritation and/or inflammation.

We have decided to investigate effects of NaB on human monocytes (THP-1) and its potential to cause systemic inflammation, which in patients with OFG, could be sufficient to trigger the flare-up of the disease. The first part of these results aimed to study the effects of NaB on the inflammatory response of THP-1 cells, especially when challenged with bacteria or TLR ligands.

3.2 THP-1 differentiation to macrophage-like cells

THP-1 is a human monocytic cell line that can be differentiated in to macrophage-like cells using low doses of PMA or immune activation. They are large rounded cells resembling circulating monocytes from peripheral blood (Figure 3-1A) and, upon stimulation and differentiation, they experience a massive change in shape and size (Figure 3-1B-D).

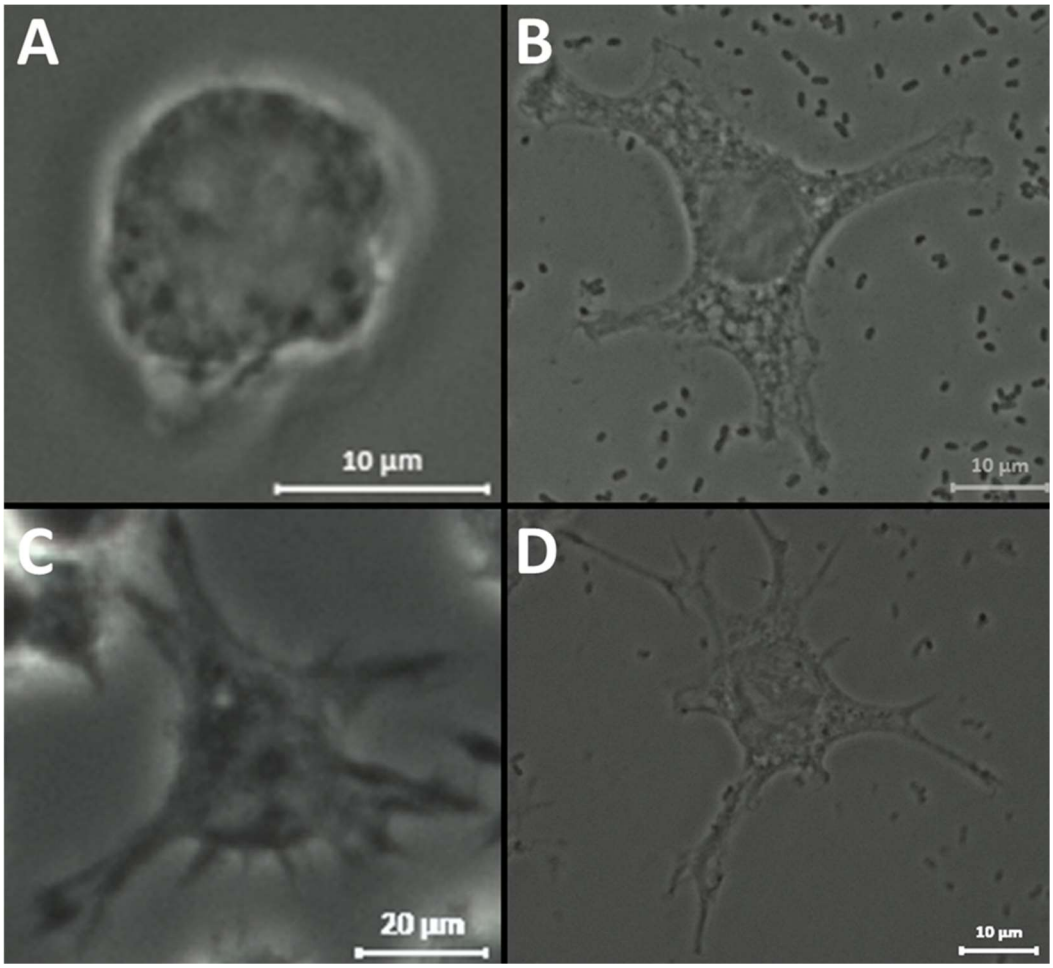

Figure 3-1: Phase-contrast microscopy images of the unstimulated THP-1 cells (A) and stimulated cells (B-D). Unstimulated THP-1 cells are rounded non-adherent cells (A). NaB alone does not differentiate the cells, keeping the round shape similar to untreated cells (data not shown). Upon HkEc stimulation, they differentiate in to macrophage-like cells, becoming adherent and spread on the glass surface (B). LPS stimulation also leads to THP-1 differentiation, but in a less intense way than with HkEc (C). NaB treatment does not affect differentiation of THP-1 cells into macrophage-like cells upon HkEc stimulation (D). Magnification 63X.

3.3 NaB toxicity

The toxicity of NaB on THP-1 cells was investigated using the MTT assay. In this assay, the MTT salt, 3-[4,5-dimethylthiazol-2-yl]-2,5-diphenyl tetrazolium bromide, is taken up by viable cells and reduced by the action of mitochondrial dehydrogenases into insoluble purple formazan that is colourimetrically measured. Purple formazan formation was used as a measure of cell viability. NaB toxicity worked in a dose- and time-dependent manner (Figure 3-2). THP-1 cells were cultured in different concentrations of NaB (0-80 mM) for 24 h (Figure 3-2A). NaB was very toxic to THP-1 cells at high concentrations ≥ 20 mM killing almost all the cells. The cell viability was tested at 4, 8 and 24 h after the addition of several concentrations (0-160 mM) of NaB, the absence or presence of immune stimulation (HkEc). There was no change in THP-1 viability at 4 h (Figure 3-2B), but by 8 h, a loss in cell viability was evident at concentrations above 80 mM (Figure 3-2C). By 24 h NaB concentrations above 5 mM reduced the viability of THP-1 cells (Figure 3-2D). Therefore, the concentration of 5 mM was established as our standard working dose.

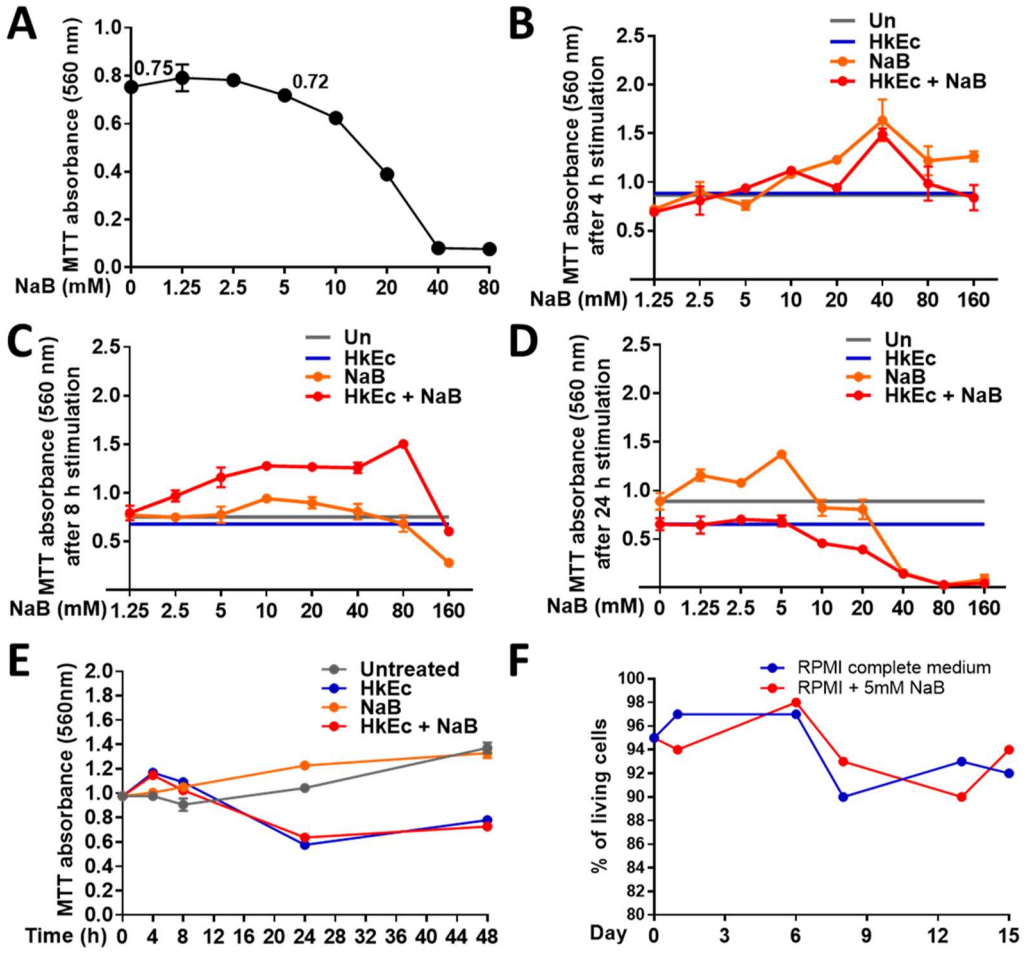

Figure 3-2: The effects of NaB on THP-1 cell viability using MTT assay. NaB is toxic to THP-1 cells at concentrations ≥ 10 mM after 24 h (A). THP-1 cells stimulated or not with HkEc in the presence of NaB (0-160 mM) were evaluated over 24 h (B-D). No cell loss was observed at 4 hours even at the highest NaB concentrations (B). At 8 hours of NaB exposure, cell viability started to decrease at NaB concentrations of 160 mM irrespective of HkEc stimulation(C). Over a period of 24 hours, concentrations above 5 mM showed a reduction in the number of viable cells irrespective of HkEc exposure (D). The straight grey and blue lines represent the average of the control groups (no NaB) for unstimulated and HkEc stimulated, respectively. Cell viability and proliferation rates were influenced by HkEc stimulation, but not for NaB treatment at 5 mM (E). THP-1 cells cultured in the absence or presence of 5 mM NaB were maintained and monitored for two weeks. There was no significant effect of 5 mM NaB on THP-1 cell viability, measured by Trypan blue exclusion test (F). Results shown are mean ± SEM of an individual experiment. The results of a single experiment are limited to establish a proper cause-effect of the experimental conditions.

We tested the effect on THP-1 cell proliferation of long-term exposure to 5mM NaB and observed that there was no alteration in cell viability or cell proliferation (Figure 3-2E). It is important to note that THP-

1 cells are spontaneously immortalized cancer cells, which proliferate indefinitely and double their population every 48-72 h. Upon activation with pathogens, HkEc for instance, these monocytes become activated, differentiate in macrophages, (Figure 3-2B), and stop proliferating (Figure 3-2E)[164]. At ≤5 mM, there was no change in cell proliferation or cell death due to NaB treatment (Figure 3-2). Changes in cell number resulting from bacterial challenge were not influenced by the presence of 5 mM NaB (Figure 3-2E). Finally, THP-1 cells were cultured in a tissue culture flask containing 5 mM NaB for 2 weeks in parallel with cells cultured in normal RPMI enriched medium. Whenever the cells needed to be subcultured, an appropriated volume was discharged and fresh medium containing the 5 mM of NaB was added to the flask. Cell viability was measured on automated cell counter based on cell density and Trypan blue exclusion, demonstrating that NaB is not toxic or capable of inducing maturation and cell cycle arrest in THP-1 cells at a concentration of 5 mM (Figure 3-2F).

3.4 THP-1 cytokine secretion response to HkEc stimulation

3.4.1 Cytokines secretion in THP-1 cells and effects of NaB exposure

Although there are some limitations when compared to primary monocytes, especially due to a lower expression of CD14, THP-1 cells are a good model for a basic translational study of primary monocytes. Upon activation with TLR ligands, these cells initiate an immune response and release a range of cytokines[165,166].

THP-1 cells were stimulated with HkEc (20:1 MoI) in the presence and absence of NaB. After 24 hours, the supernatant was collected and screened with a panel of inflammatory cytokines using a multiplex immunoassay (Figure 3-3).

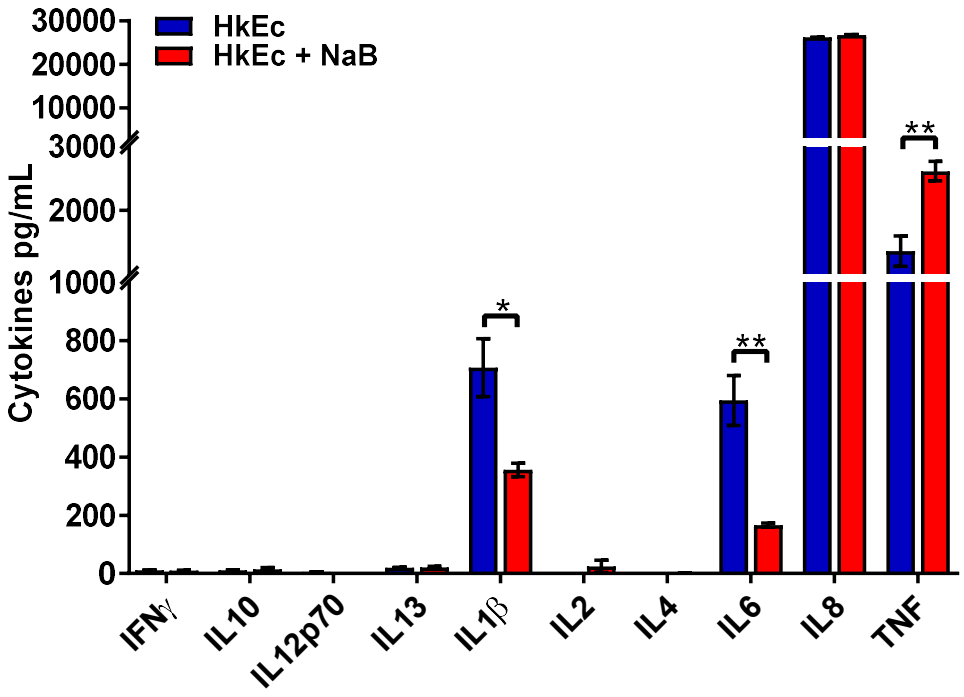

Figure 3-3: Stimulation of THP-1 cells with HkEc causes the release of IL8, TNF, IL6 and IL1β. NaB (5 mM) treatment caused a deregulation in pro-inflammatory cytokines secretion, with a reduction in IL6 and IL1β, and an increase in TNF. NaB had no effect on the release of IL8. All the other cytokines tested were either detected at a very low level or were below the detection limit of the high-sensitivity assay. Results shown are mean ± SEM, *p<0.05, **p<0.01, ***p<0.001, ****p<0.0001; n=1 individual experiment with 4 biological replicates, (two-tailed, unpaired t-test). This was a preliminary result that will be expanded later.

NaB treatment showed an ambiguous effect, reducing the levels of IL6 and IL1β in increasing the levels of TNF (Figure 3-3). This result suggests a selective effect of NaB on the innate immune response, which cannot be attributed to a purely anti-inflammatory effect or through the effects of an elevation in IL10 (Figure 3-3).

3.4.2 THP-1 cytokines response of TNF and IL6 to HkEc occurs in a dose- and time-dependence manner upon NaB treatment

To investigate if the effects on cytokine secretion were dependent on NaB dose, THP-1 cells were stimulated with HkEc for 24 h in the presence of a range of NaB concentrations (0-10 mM). IL6 levels were

reduced at very low concentrations (0.1 mM) and constantly reduced with increasing doses of NaB (Figure 3-4A). On the other hand, lower doses of NaB (0.1 – 2.5 mM) had no effect on TNF secretion, whereas 5 and 10 mM resulted in an elevation in TNF release (Figure 3-4B). The effects of NaB on IL6 secretion lasts even after NaB was removed from the medium (Figure 3-5).

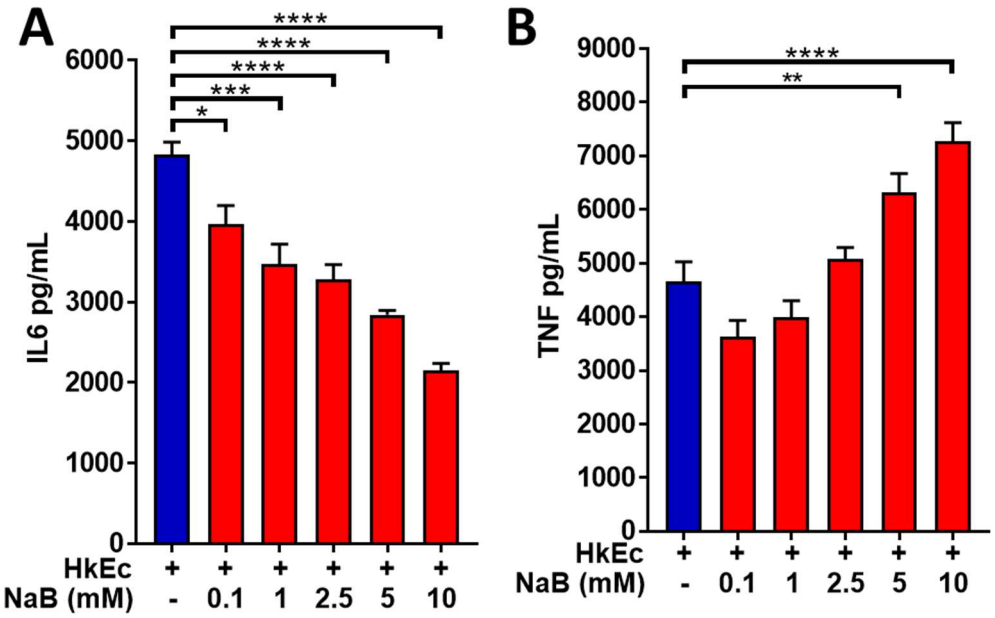

Figure 3-4: THP-1 cells stimulated with HkEc (MoI 20:1) for 24 hours were treated with increasing concentrations of NaB (0-10 mM) and the levels of IL6 (A) and TNF (B) measured by ELISA. An increase in the concentration of NaB correlated with an increase in secretion of TNF and inversely correlated with IL6 levels. Results shown are mean ± SEM, *p<0.05, **p<0.01, ***p<0.001, ****p<0.0001; n=1 individual experiment with 4 biological replicates, (two-tailed, unpaired t-test). The results of a single experiment are limited to establish a proper cause-effect of the experimental conditions.

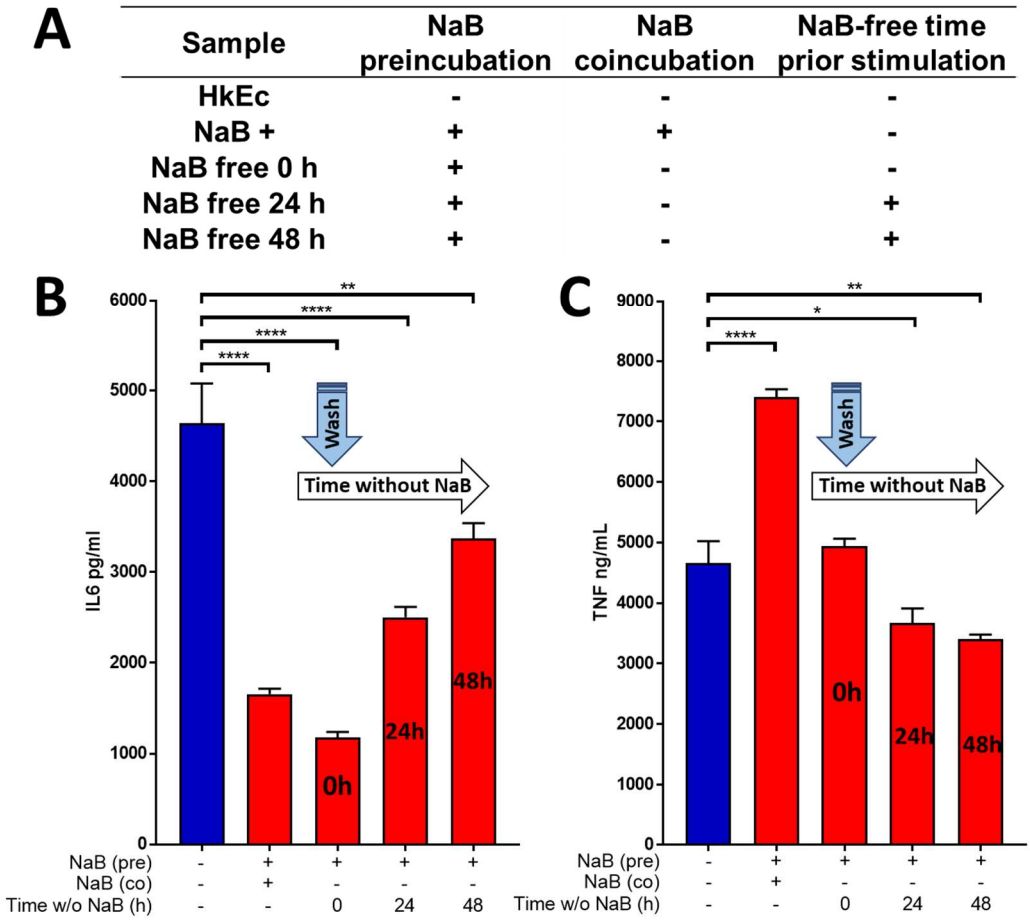

Figure 3-5: Effects of NaB on cytokine secretion after NaB removal from the culture medium. THP-1 cells were preincubated with NaB (5 mM), washed twice in PBS and stimulated in medium with either NaB (coincubation), replaced in a medium free of NaB and stimulated with HkEc (20:1 MoI) immediately (0 h) or left in the NaB-free medium for 24 and 48 hours prior stimulation (A). The total HkEc stimulation time was 24 hours in all samples. IL6 levels were reduced in all samples that were previously treated with NaB when compared with HkEc alone. TNF was increased only when THP-1 cells were costimulated in the presence of NaB. After removal of NaB, the levels of TNF returned to normal or even decreased over time. Results shown are mean ± SEM, *p<0.05, **p<0.01, ***p<0.001, ****p<0.0001; n=1 individual experiment with 4 biological replicates, (two-tailed, unpaired t-test). The results of a single experiment are limited to establish a proper cause-effect or if they were an accidental finding.

3.5 Transcriptome analysis of THP-1 cells upon bacterial stimulation

3.5.1 HkEc and HkPg stimulation of THP-1 cells and the effects of NaB

THP-1 cells were exposed to either 5 mM NaB, HkEc (20:1 MoI) or HkPg alone, or in combination for 4 hours. Unstimulated THP-1 cells were used as a reference for basal gene expression levels. Data from the 2 chips were merged and then analysed. Batch variation was minimised using ComBat (for a detailed description see section 2.7.3), an established R algorithm for minimizing batch effects in microarrays (Figure 3-6)[157].

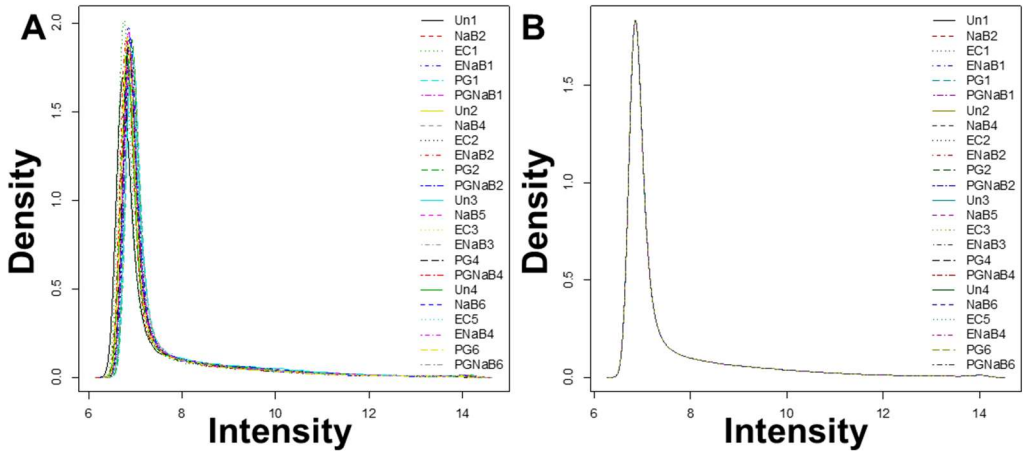

Figure 3-6: Density plot graph before (A) and after ComBat normalization (B). This normalization corrected variations between chips allowing the data to be merged and analysed.

A total of 47,213 probes were tested in the microarray chip, from those, 16,348 remained after quality control check and were further analysed. Bacterial stimulation regulated a specific number of genes (≈1%), with half of them commonly regulated in both, HkEc or HkPg stimulated samples (Figure 3-7). The cutoff p-value was set at $p<0.05$.

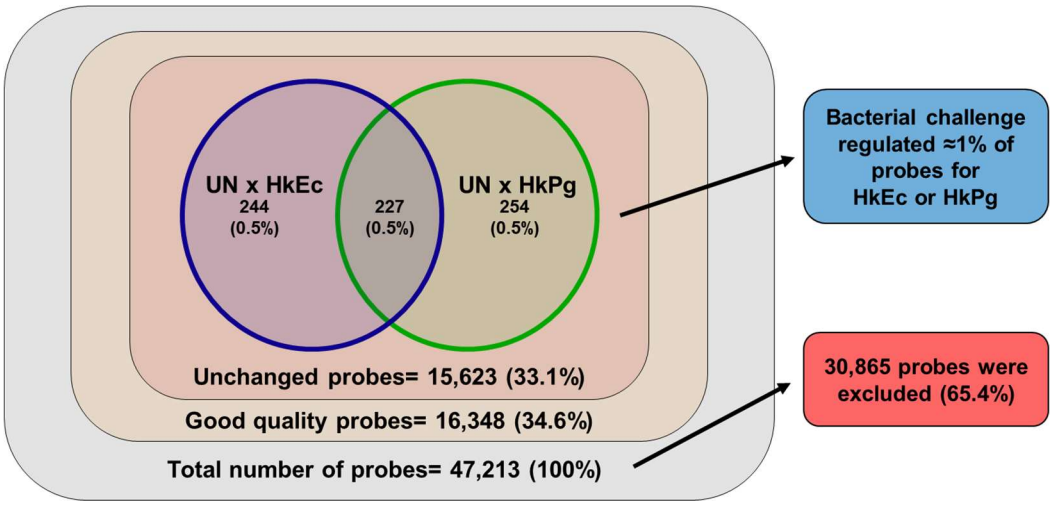

Figure 3-7: Venn diagram showing a summary of results obtained from whole gene transcriptomic analysis after quality control check (as described in section 2.7.3). Approximately 1% of the total probes were regulated by bacterial stimulation.

When we analysed the overall effects of NaB exposure on THP-1 cells, 1116 probes were affected across all three conditions: unstimulated, HkEc and HkPg stimulated. Thirty-six probes were statistically different in all three conditions (Figure 3-8).

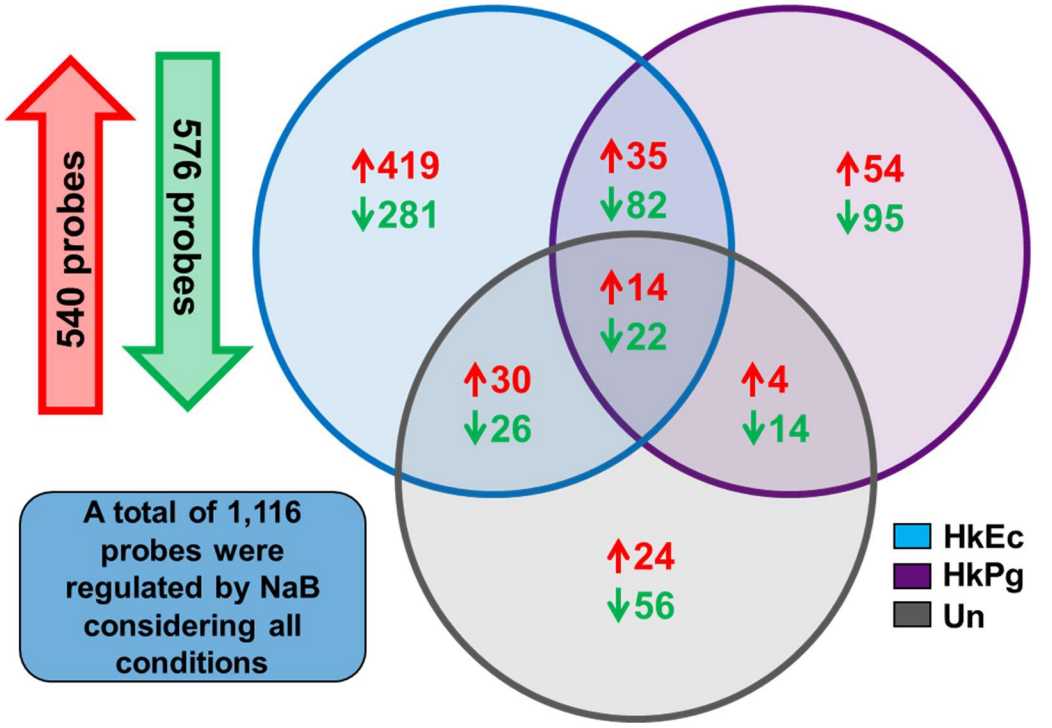

Figure 3-8: Venn diagram showing differences between expression profiles of the 3 different stimulation groups (Un, HkEc and HkPg) and the effects of NaB on gene expression. Unstimulated THP-1 cells treated with NaB showed changes in 200 probes with a predominant downregulating

effect (64%). Upon HkPg stimulation, NaB affected the expression of more genes (330) but downregulating effect still dominated (78% of the probes were downregulated). On the other hand, NaB regulated the expression of several genes after HkEc stimulation, but with predominance for an upregulation in genes expression (55% of the probes). In total, 36 genes were affected by NaB regardless of any other treatment (These are covered in more detail later).

Principal component analysis (PCA) was conducted to determine whether global gene expression profiles could be separated based on NaB or bacterial stimulation. PCA is a mathematical algorithm for reducing the dimensionality of datasets, by finding the principal components (directions) along which the variation is maximal. PCA analysis showed a clear difference between bacterial stimulation (Figure 3-9). A dendrogram showing the hierarchical clustering is shown in Figure 3-10.

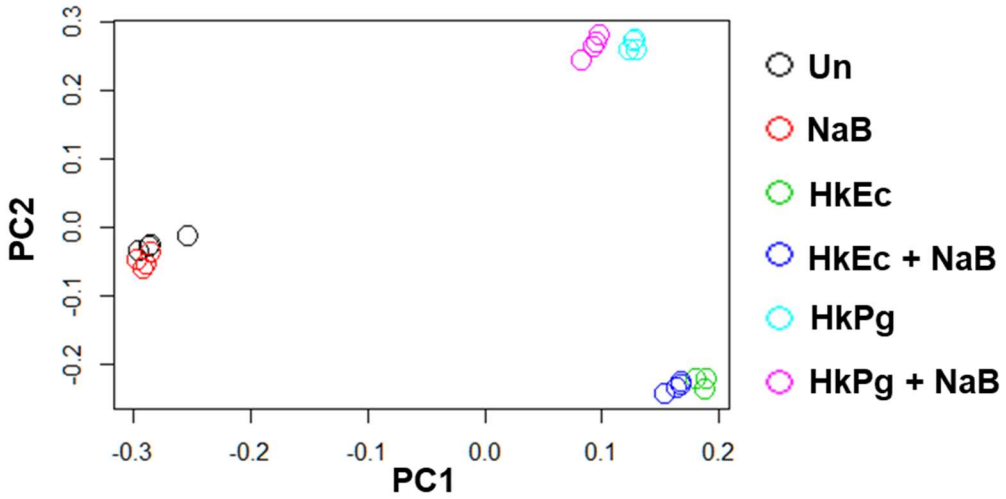

Figure 3-9: PCA plot for microarray data showing the relatedness between all samples. The plot clearly shows that most of the variance in the microarray data can be attributed to the bacterial stimulation. Slight changes can also be attributed to NaB treatment, which is observed as a shit to the left in the two bacterial stimulated samples in PC1.

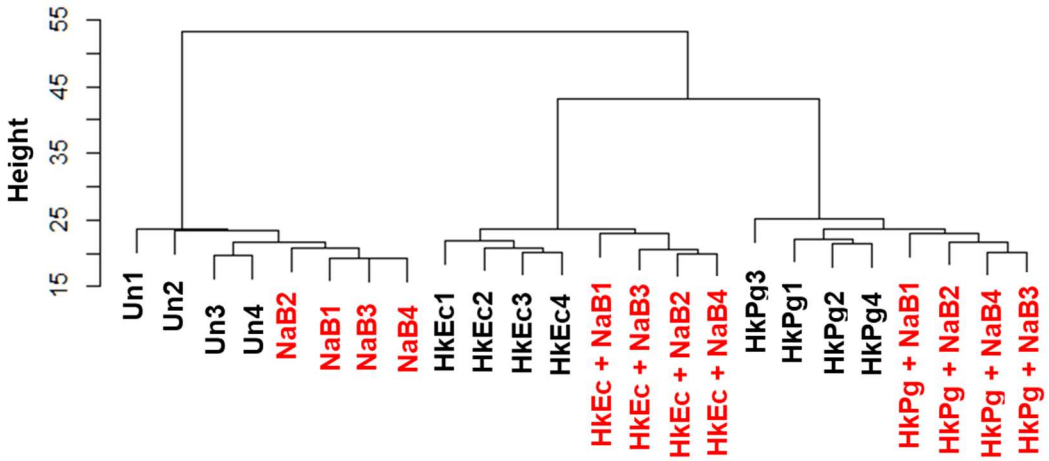

Figure 3-10: Dendrogram illustrating the hierarchical clustering of all microarray samples including all probes (16,348 probes) that passed the quality control. Three main clusters can be observed depending on the type of stimulation.

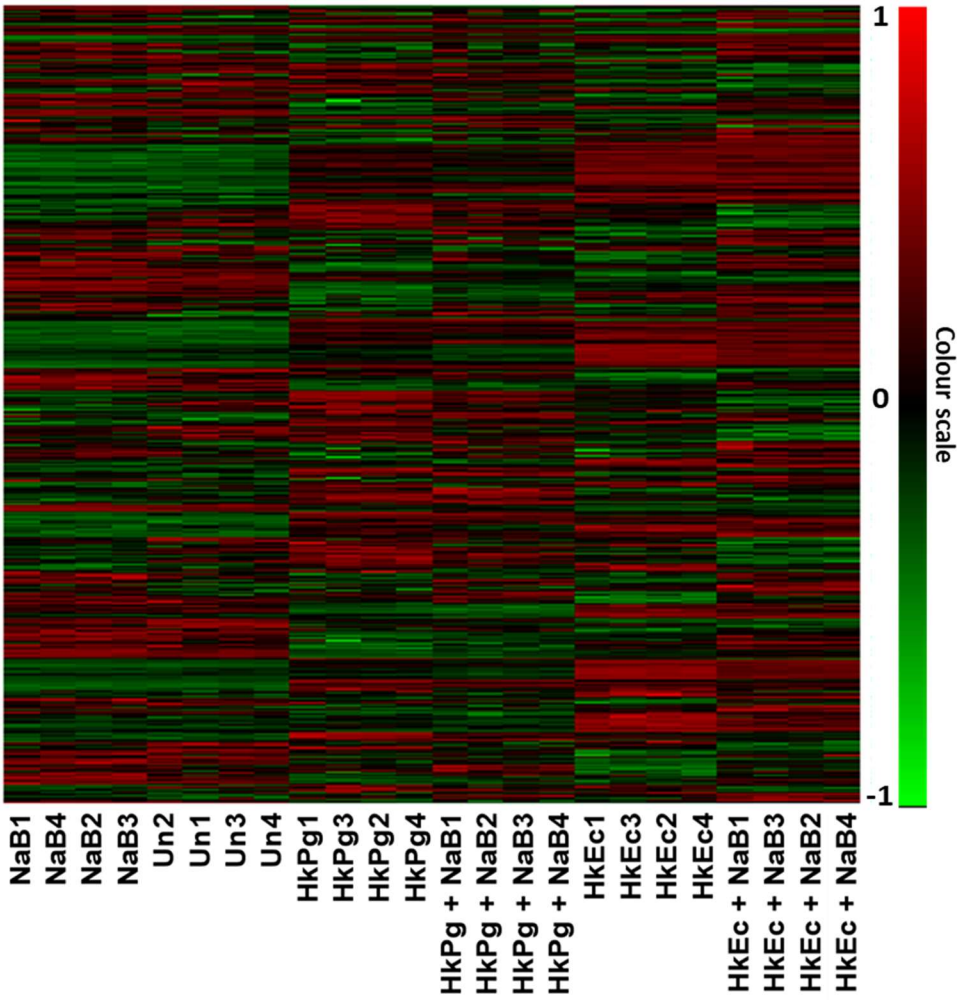

Figure 3-11: Heatmap of 1116 differentially expressed genes influenced by NaB treatment under 3 different conditions with an adjusted p-value less than 0.05 are shown. Hierarchical cluster generated based on gene

expression (rows). A dendrogram showing sample cluster (top) and colour scale coded values in the heatmap (right).

The list of all genes regulated by NaB was uploaded to the Database for Annotation, Visualization and Integrated Discovery (DAVID) v6.8 (http://david.abcc.ncifcrf.gov/) and the functional annotation tool was used to generate active pathways[167,168]. The top two pathways originated from the Kyoto Encyclopaedia of Genes and Genomes (KEGG) with the lowest p-value were related to the TLR ($p= 2.1E^{-4}$ KEGG path: hsa04620) and the cytokine-cytokine receptor interaction ($p=3.3E^{-4}$ KEGG path: hsa04060) pathways, with 19 and 15 genes involved in each pathway respectively, and 4 genes were found in both (Figure 3-12A). Another important pathway affected by NaB treatment was the glutathione metabolism ($p= 8.9E^{-2}$) pathway (Figure 3-12B).

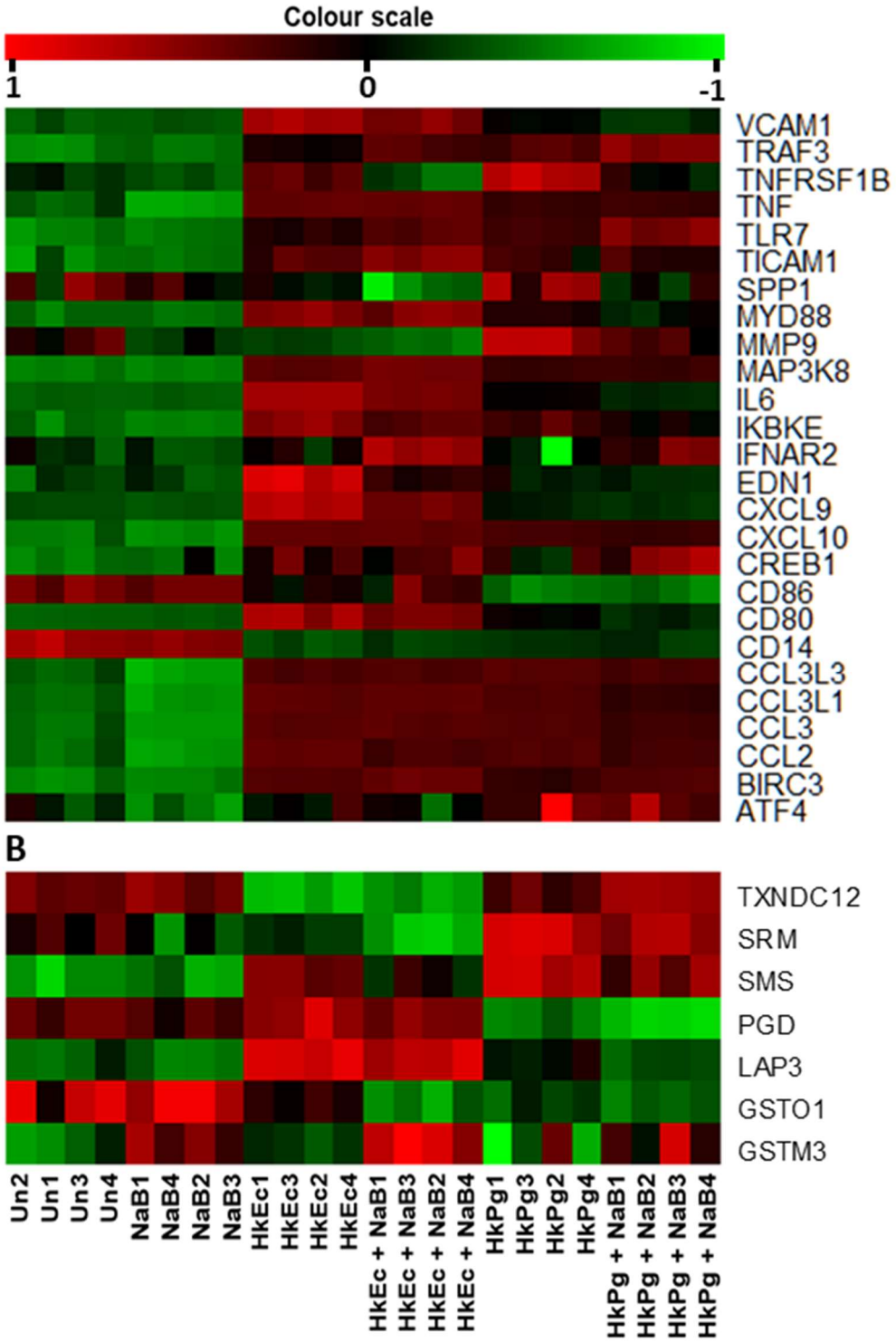

Figure 3-12: Heatmap of genes involved in TLR and cytokine-cytokine receptor interaction pathways (A) and glutathione metabolism (B). Many genes associated with TLR and TNF pathways have essential functions in innate immunity (A). The glutathione pathway is involved in amino acid metabolism, which includes glycine, and has an important role in redox regulation and detoxification reactions.

There were 32 genes that were controlled by NaB exposure and showed the same type of change, up- or downregulating gene expression regardless of the stimulation with bacteria or not. It suggests a strong link between NaB and these specific genes. Using DAVID Bioinformatics Resources and String (https://string-db.org/) online databases, these genes didn't show any significant interactions in terms of pathways or function, however, more than 50% of them shared the same nuclear location (Figure 3-13).

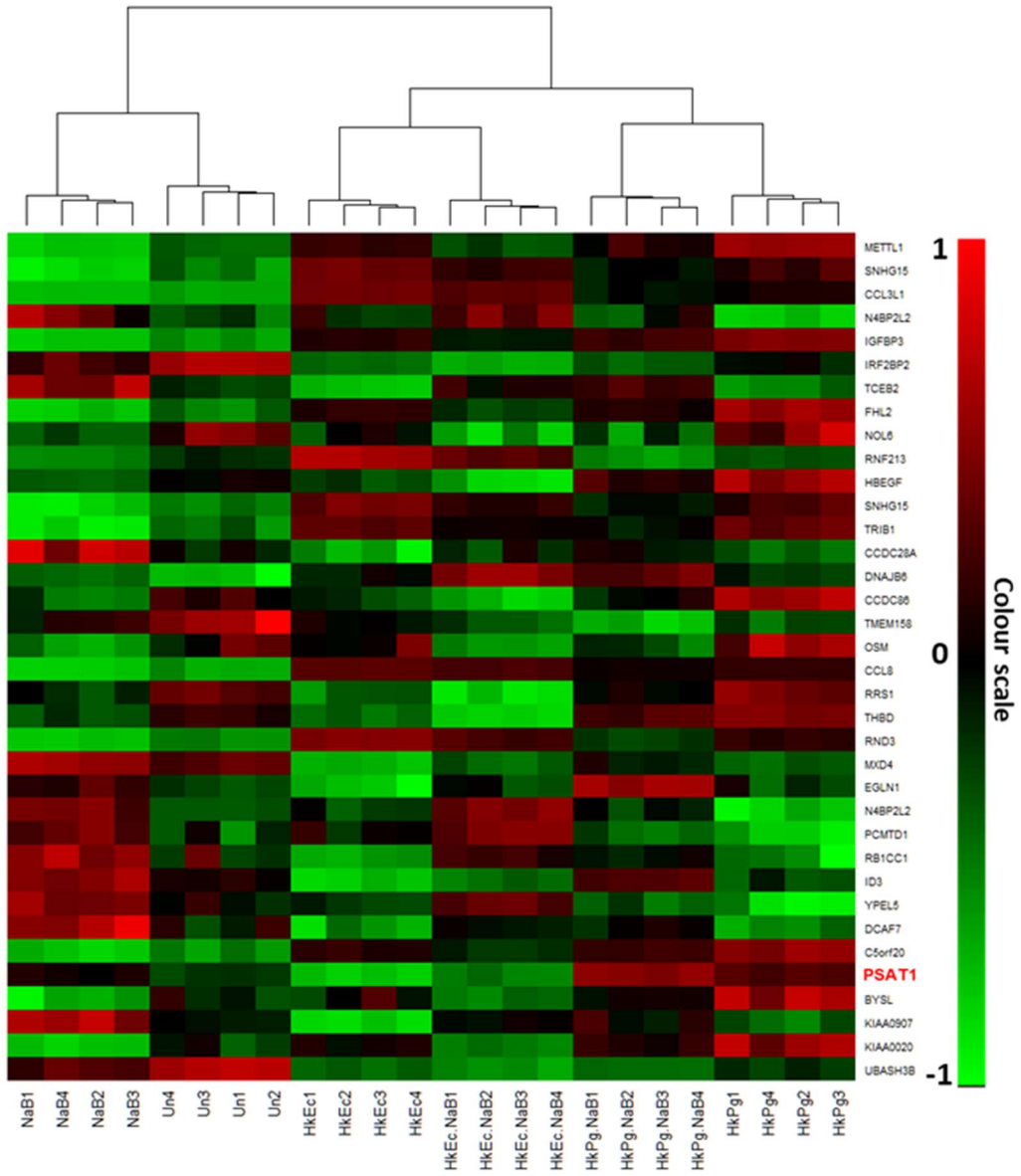

Figure 3-13: Heatmap of 36 genes controlled by NaB treatment regardless of bacterial stimulation. All of them had a similar pattern up- or downregulating gene expression regardless the type of stimulation. Nuclear location is a common feature to more than 50% of the genes. It is important to note that the hierarchical cluster now shows an increased

height when compared samples ± NaB. The phosphoserine aminotransferase 1 (PSAT1) is upregulated in all samples treated with NaB. The role of PSAT1 will be better explored in chapter 7.

PSAT1 is an enzyme that catalyses the reversible conversion of 3-phosphohydroxypyruvate to phosphoserine and plays a key role in the serine/glycine biosynthesis. So far, the results pointed to a more potent effect of NaB when THP-1 cells were stimulated with HkEc than with HkPg, in view of the number of genes regulated in these samples. To reduce the size of the thesis, HkPg groups were not included in further analysis.

3.5.2 Gene expression analysis of HkEc stimulation and the effects of NaB on THP-1 cells

In the previous section, the overall effect of NaB was evaluated in combination with other samples. Now, a more focused approach will investigate the alterations induced by NaB on the THP-1 immune response. From those genes regulated by NaB treatment, 909 out of 1,116 (81.4%) were observed upon HkEc stimulation.

Similar to what was seen in the previous section, the main pathways involved in HkEc response were related to important functions in innate immunity, particularly associated with the TLR4 pathway (Figure 3-14). The data was originated from microarray and further confirmed by qRT-PCR. Genes responsible for cytokines production and adaptor proteins showed statistical alteration in expression when THP-1 cells were stimulated with HkEc compared to HkEc plus NaB. IL6 was the gene with the second lowest p-value ($4.16E^{-07}$).

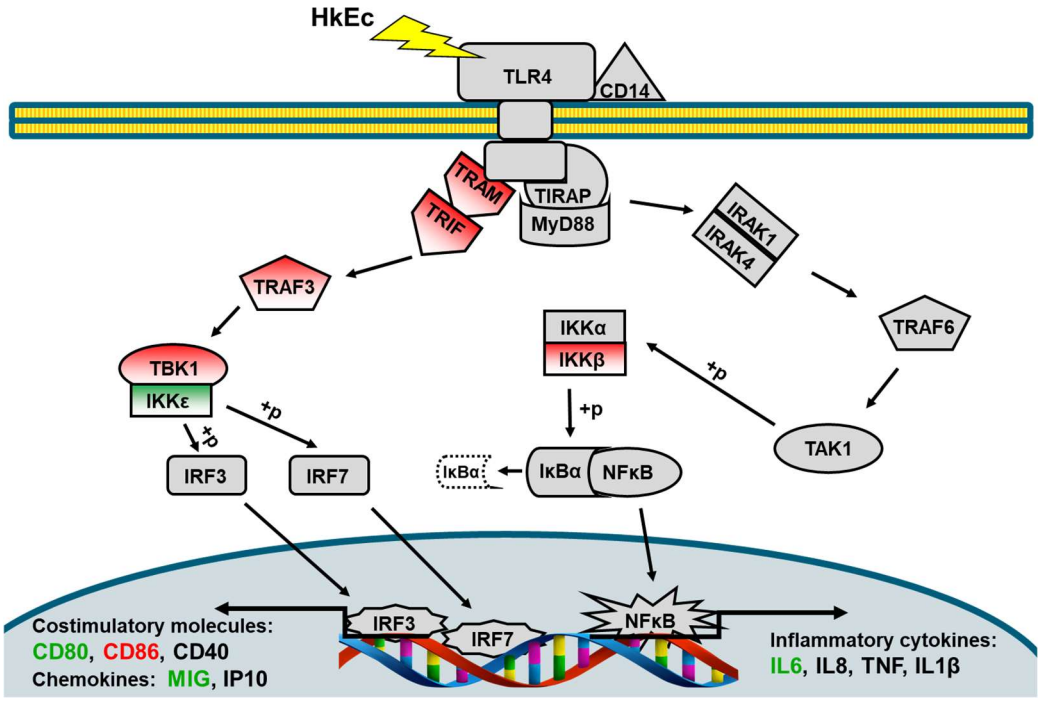

Figure 3-14: THP-1 gene expression in response to HkEc stimulation is altered by the co-incubation with NaB. Data originated from microarray analysis and further validated by qRT-PCR. The presence of NaB during a HkEc response resulted in the upregulation (red) of many adaptors proteins and downregulation (green) of important cytokines and chemokines. Simplified TLR4 signalling pathway adapted from DAVID Bioinformatics Resources website.

Another important pathway associated with the innate immunity was associated with genes from the cytokine-cytokine receptor interaction (KEGG pathway hsa04060) (Figure 3-15).

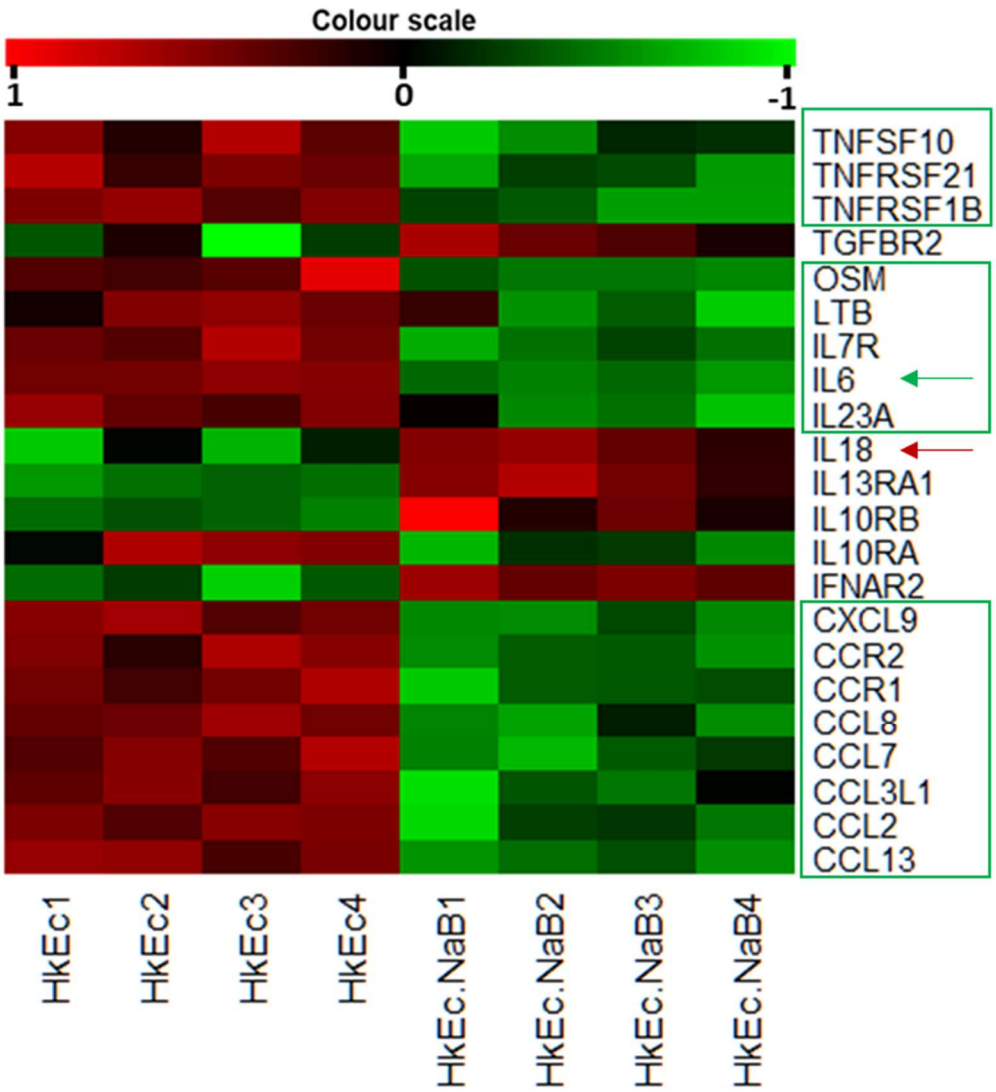

Figure 3-15: Heatmap of THP-1 gene expression comparing HkEc ± NaB in the cytokine/cytokine receptor pathway. NaB treatment downregulate many genes associated with the synthesis of pro-inflammatory cytokines. The TNFRSF1B gene is responsible for the synthesis of TNFR2, which is a soluble receptor and controls TNF activity by sequestering the cytokine and antagonizing TNF activity.

The CC chemokine family (from C-C motif ligands proteins) is involved in the acute inflammatory state in the recruitment and activation of polymorphonuclear leukocytes. Together with some CCL genes, the chemokine receptor family (CCR1 and CCR2) were downregulated by NaB, suggesting an attenuated response to these chemokines.

3.6 Characterization of pro-inflammatory cytokine dynamics in THP-1 upon HkEc stimulation and the effects of NaB

The early inflammatory process occurs immediately after recognition of antigenic stimuli and macrophages are very often the first cells to respond to these stimuli. This stage involves the production and release of pro-inflammatory cytokines in a coordinated response to harmful stimuli[110].

To characterize the cytokine dynamics to bacterial response, a time-course was carried out to investigate the cytokine secretion and gene induction of the main cytokines produced by THP-1 cells (Figure 3-2). The protein levels of IL8, IP10, TNF, IL6 and IL1β were investigated by ELISA and the gene induction by qRT-PCR (Figure 3-16).

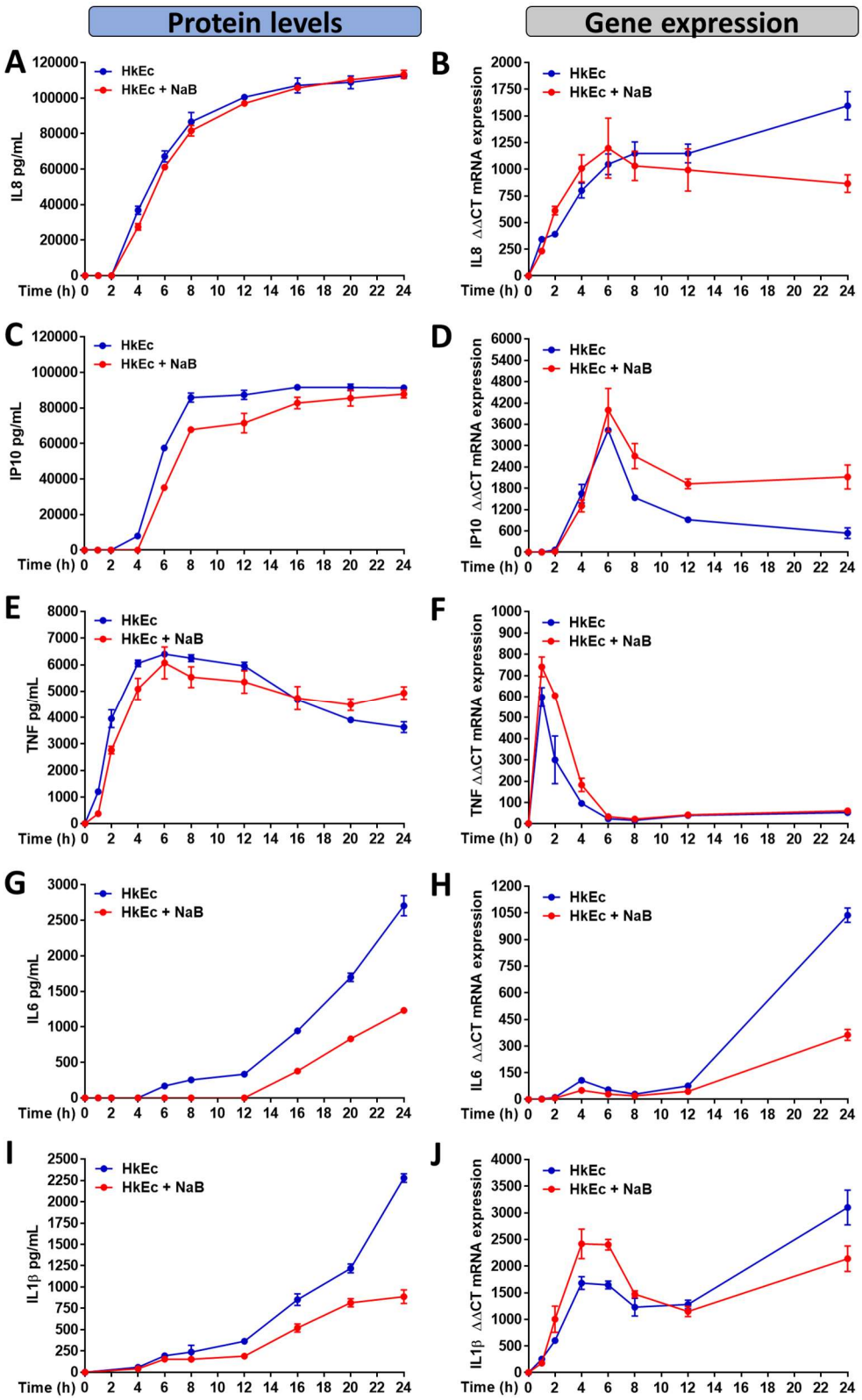

Figure 3-16: Time course of cytokine secretion (left panel) and gene expression (right panel) in THP-1 cells stimulated with HkEc ± NaB. The secretion of IL8 and IP10 are unaffected by NaB treatment (A and C), even though some differences in gene expression can be observed (B and D). TNF was detected as soon as in the first hour, reaching a peak at 6 hours, decreasing from this time and accentuated decline after 12 hours (E). The

message level rises very quickly peaking at one hour and then decreases with the almost complete loss of expression after 6 hours (F). NaB treatment showed an increased mRNA expression and a slower decline of the released TNF. The cytokines that demonstrated the greatest sensitivity to NaB at both the secretion and transcription level were IL6 and IL1β (G-J).

Taken together, these results suggest that NaB affects specific cytokines, downregulating IL6 and IL1β and deregulating TNF. Twenty-four hours after stimulation seemed to be the best point for investigating the majority of these cytokines, except for TNF, which showed an earlier gene induction that is practically gone after 6 hours. These data were used for planning further experiments.

3.7 NaB reduces IL6 and IL1β levels, and deregulate TNF in THP-1 cells upon HkEc stimulation

A few studies have shown a predominant anti-inflammatory effect of NaB, reducing the levels of IL6, IFNγ and TNF in splenocytes, and IL1β and TNF in microglia, both stimulated with LPS[1,169]. Here, monocytes were stimulated with HkEc for 24 hours in the presence or absence of NaB.

The induction and release of IL8 and IP10 in response to HkEc were unaffected by the presence of NaB (Figure 3-17). They are both induced downstream of TLR4 signalling but use different pathways. IL8 follows the MyD88-dependent pathway, while IP10 is linked to a type-I interferon response downstream a MyD88-independent/TRIF pathway[114,125,131,134]. On the other hand, IL6 and IL1β were negatively regulated by NaB and showed a reduced level of protein and mRNA expression (Figure 3-18). These reduced levels of IL6 and IL1β did not result in the increased expression of the anti-inflammatory cytokine IL10. Only a very low concentration (≈10 ng/mL) of IL10 was detected in HkEc ± NaB samples using the high-sensitivity multiplex immunoassay (Figure 3-3), whereas all attempts to detect IL10 with an ELISA failed. TNF secretion was increased in the presence of NaB (Figure 31-9), an evaluation of TNF induction and secretion will be detailed later in chapters 5 and 6.

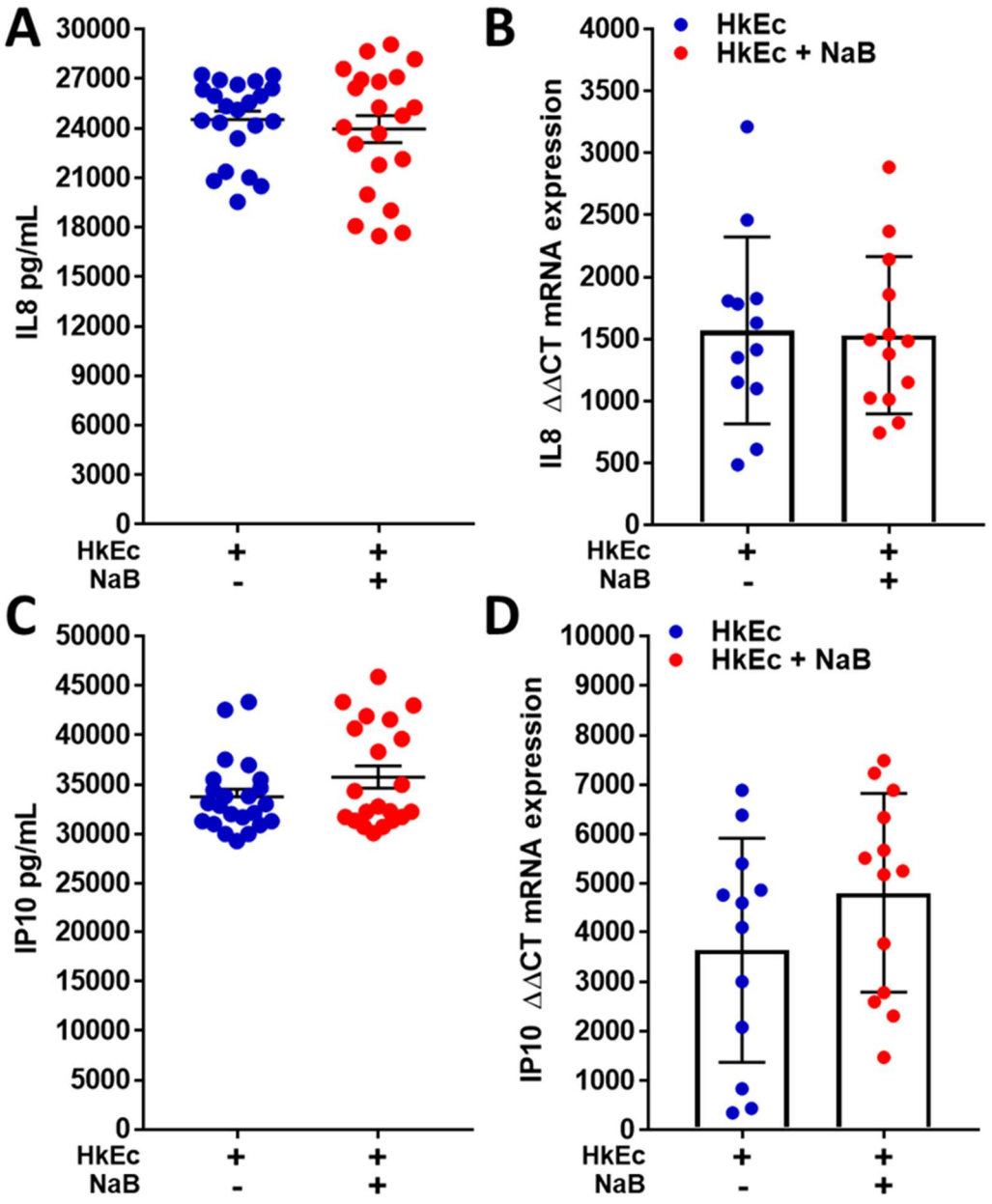

Figure 3-17: IL8 and IP10 secretion (A and C) and gene expression (B and D) in THP-1 cells stimulated with HkEc ± NaB. The addition of NaB had no significant effect on HkEc induced secretion of IL8 and IP10. Results shown are mean ± SEM, n= 5 and 3 independent experiments for protein levels and mRNA expression, respectively (two-tailed, unpaired t-test).

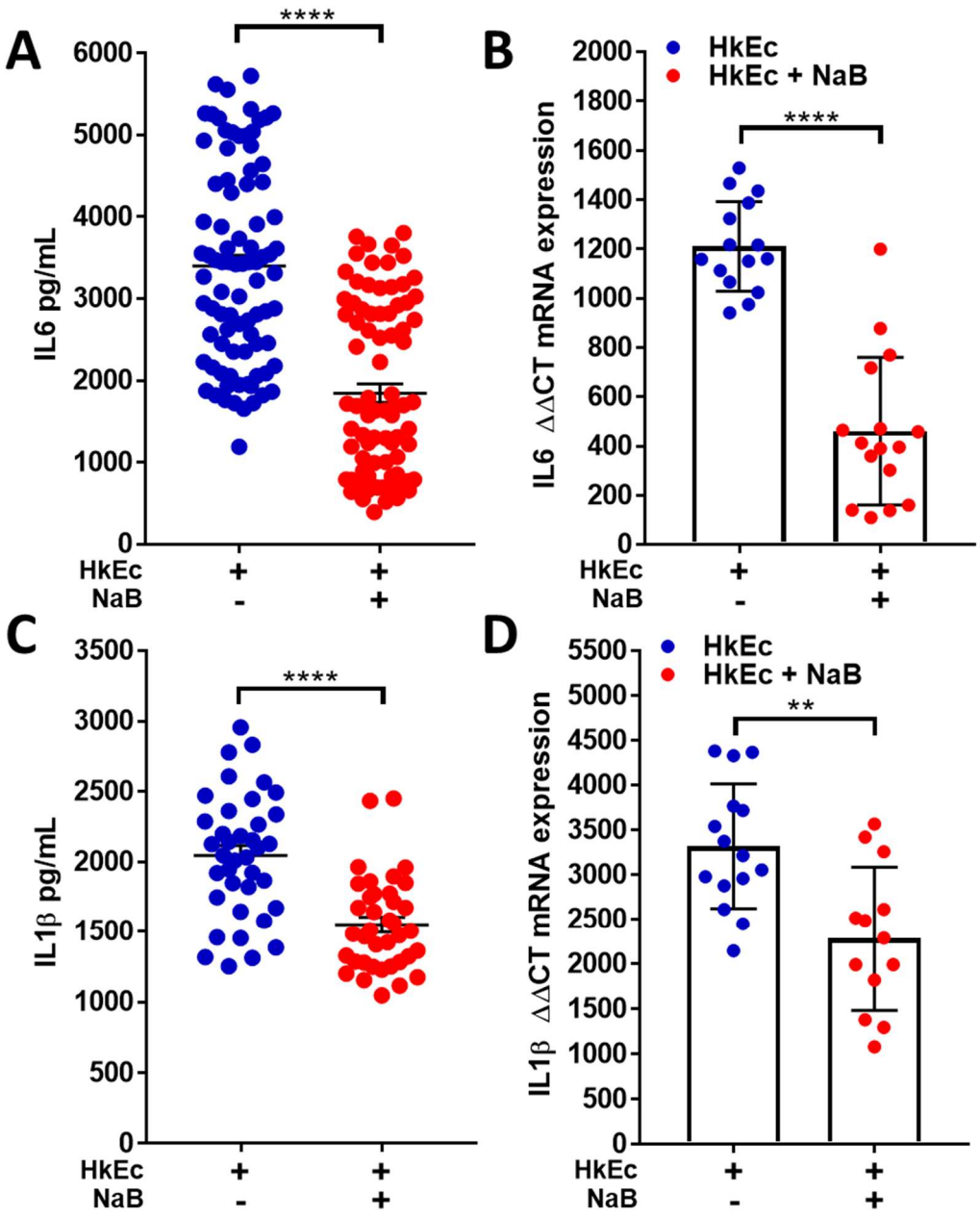

Figure 3-18: IL6 and IL1β cytokine secretion levels (A and C) and gene expression (B and D) in THP-1 cells stimulated with HkEc ± NaB. These cytokines were reduced in both levels as result of NaB treatment. n= 10 (IL6 protein), 5 (IL1β protein) and 3 independent experiments for protein levels and mRNA expression, respectively. Results shown are mean ± SEM, *p<0.05, **p<0.01, ***p<0.001, ****p<0.0001; (two-tailed, unpaired t-test).

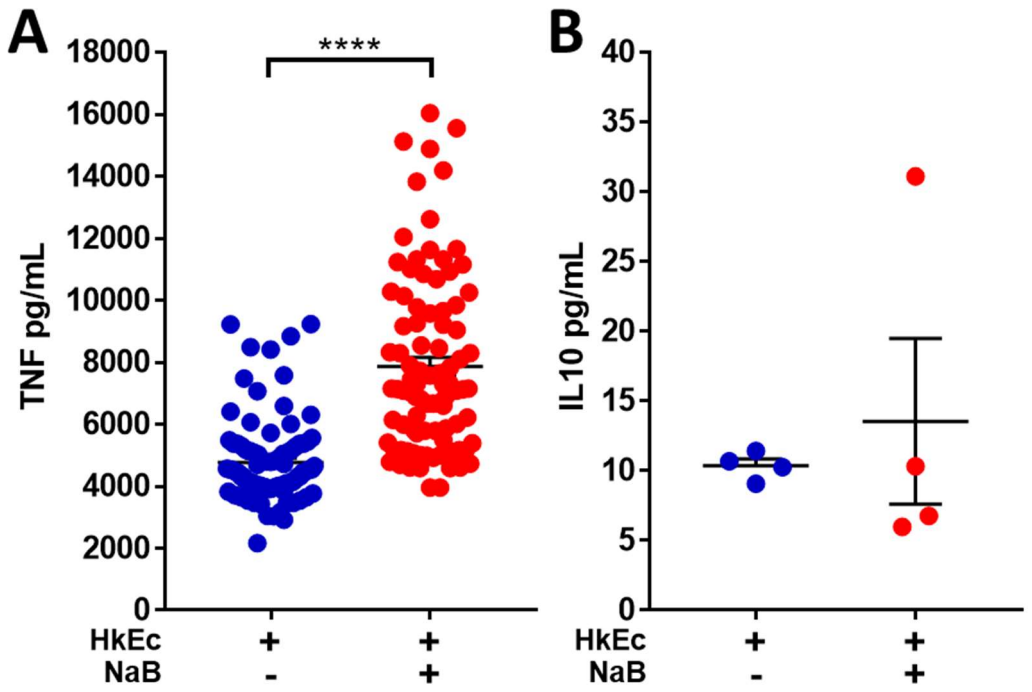

Figure 3-19: TNF (A, ELISA) and IL10 (B, MSD® multiplex immunoassay) cytokine secretion levels in THP-1 cells stimulated with HkEc ± NaB. TNF was increased because of NaB treatment. IL10 was not detected in ELISA (data not shown) and detected in a similar very low level. n= 10 (TNF) and n=1 (IL10) independent experiments. Results shown are mean ± SEM, *p<0.05, **p<0.01, ***p<0.001, ****p<0.0001; (two-tailed, unpaired t-test).

3.8 NaB reduces IL6 and deregulate TNF in THP-1 cells upon TLR4 and TLR1/2 stimulation

Heat-killing bacteria is a well-established method used to stimulate the immune system but maintain sterility in the culture dish and since the immune response is similar to that of the equivalent live bacteria it is assumed that most of the PAMPs are preserved[170,171,172]. However, they carry multiple antigens and generate a complex signal. HkEc is capable of activating multiple receptors including TLRs (TLR 1/2, 2/6, 4, 5,9), especially TLR4 and TLR2[173].

To investigate if NaB was affecting a particular pathway downstream TLR activation, the specific TLR ligands LPS (TLR4) and PAM3CSK4 (TLR 1/2) were used to stimulate THP-1 cells. The inclusion

of NaB downregulated IL6 and IL1β regardless of whether the cells were stimulated with LPS or PAM3CSK4 (Figure 3-20).

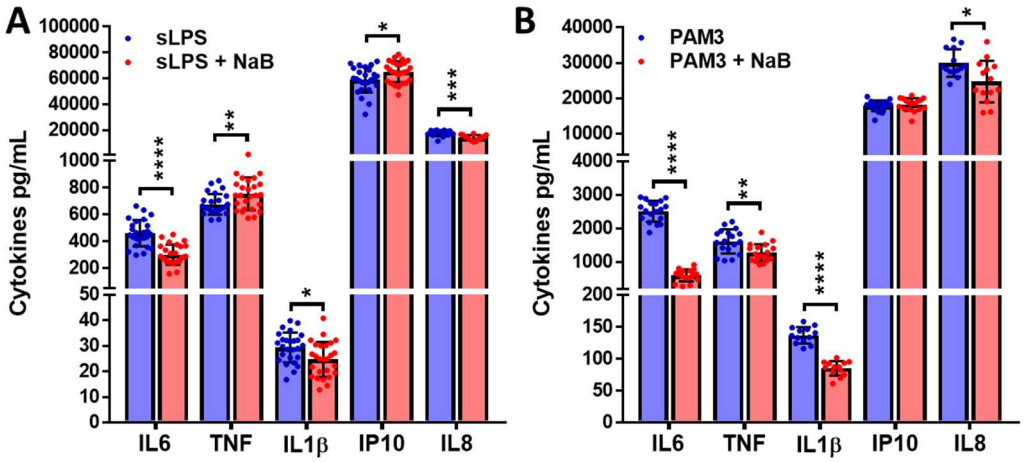

Figure 3-20: Cytokine secretion levels from THP-1 cells stimulated with LPS (A) or PAM3CSK4 (B) ± NaB. IL6 and IL1β secretion were reduced and showed the biggest effect size downstream of both TLR ligands by the inclusion of NaB. Results shown are mean ± SEM, for n= 5 (LPS) and n=3 (PAM3CSK4) independent experiments. *p<0.05, **p<0.01, ***p<0.001, ****p<0.0001; (two-tailed, unpaired t-test).

3.9 Initial TLR signalling downstream stimulation is not affected by the inclusion of NaB

In light of the reduced mRNA expression, the signalling pathway downstream of TLR4 and TLR2 were assessed to investigate if NaB could potentially interfere with the protein kinase cascade. Downstream of TLRs, the main signal to induce IL6 and IL1β follow the MyD88-dependent pathway and uses the transcription factors NFkB and AP1. NFkB is kept in the cytoplasm bound to its inhibitor nuclear factor of kappa light polypeptide gene enhancer in B-cells inhibitor, alpha (IKBa). When activated, the IKBa is ubiquitylated and degraded by the proteasome, releasing the activated NFkB that translocates into the nucleus and initiates gene transcription. Furthermore, the AP1 complex can also induce transcription of proinflammatory cytokines downstream of the MAPK pathway (Figure 1-15). The initial response to HkEc stimulation seemed to be unaffected by NaB, which suggests that NaB does not interfere with this initial TLR signalling (Figure 3-21).

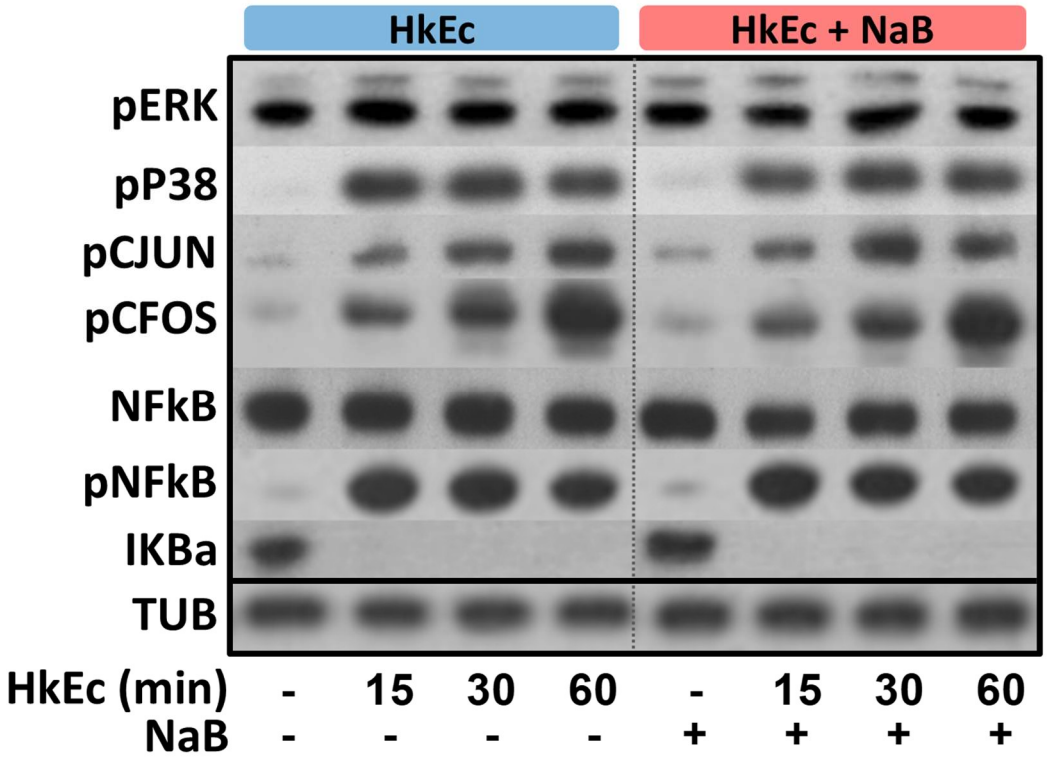

Figure 3-21: The major signal molecules downstream of TLR stimulation were visualized after HkEc stimulation. There was no obvious difference in any of the major signalling molecule during the initial TLR response between HkEc and HkEc plus NaB. Immunoblots for the phosphorylated MAPKs P38 (pP38) and ERK (pERK), and the subunits of the AP1 complex, phospho-c-JUN (pC-JUN) and phosphor-C-FOS (pC-FOS), showed a similar phosphorylation pattern. The NFkB response was also not affected by NaB treatment, as determined by increased phosphorylation (phospho-Ser536) and degradation of its inhibitor IKBa. α-tubulin is shown as loading control. Results shown are representative of 3 independent experiments.

3.10 Protein transport and lysosomal inhibition

Inhibition of lysosomal proteases has been shown to increase intracellular cytokine levels in HkEc stimulated human MDMs[174]. Monensin is an antibiotic derived from *Streptomyces cinnamonensis* and is an ionophore that disrupts intracellular Na^+ and H^+ gradients, affecting the final stages of secretory vesicle maturation from Golgi apparatus[175]. Bafilomycin A is an antibiotic that specifically inhibits the vacuolar-type H^+-

ATPase and prevents acidification and fusion of autophagosome-lysosome, which can lead to cytokine degradation[176].

Brefeldin A is a macrocyclic lactone produced by a variety of fungi and appears to inhibit protein secretion early in a pre-Golgi compartment (between the endoplasmic reticulum and Golgi)[175]. NH_4Cl is a weak base and has been shown to accumulate in acid intracellular compartments such as in lysosomes raising the vacuolar pH and inhibiting lysosomal enzymes [177].

To investigate if the deregulated secretion of cytokines caused by NaB is replicated through the use of known blockers of protein secretion THP-1 cells were stimulated with HkEc in combination with either 5 mM NaB, 2.5 µM monensin, 10 mM NH_4Cl, 2.5 µM brefeldin A or 200 nM bafilomycin A and IL6 and TNF release determined (Figure 3-22).

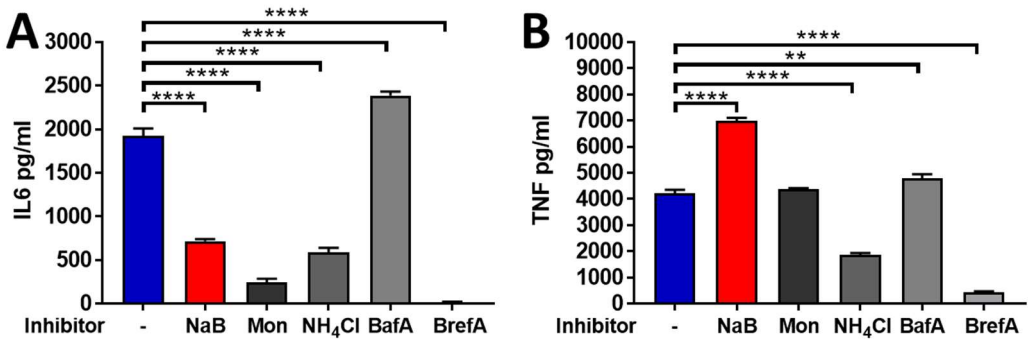

Figure 3-22: IL6 (A) and TNF (B) secretory levels were measured after 24 h HkEc stimulation upon exposure to either NaB, monensin, NH_4Cl, bafilomycin A, and brefeldin A. Results shown are mean ± SEM, *p<0.05, **p<0.01, ***p<0.001, ****p<0.0001 (one-way ANOVA with Dunnett's test, control group HkEc).
Abbreviations: Mon, monensin; BafA, bafilomycin A; BrefA, brefeldin A.

The effects of NaB on IL6 and TNF secretion was not replicated by the inclusion of any of the classic trafficking inhibitors (Figure 3-22). The results did demonstrate that IL6 and TNF respond differently to monensin suggesting that IL6 is highly dependent on the generation of an intracellular Na^+ and H^+ gradient, which facilitates the final stages of secretory vesicle maturation from Golgi apparatus[175]. TNF release was unaltered in the presence of monensin and therefore is not dependent on the intracellular Na^+ and H^+ gradient. IL6 and TNF secretion were reduced in the presence

of NH_4Cl and brefeldin A demonstrating a shared requirement for ER to Golgi transport and acidification of intracellular organelles. Finally, inhibition of the vacuolar-type H^+-ATPase and autophagosome-lysosome fusion elevated both IL6 and TNF. This demonstrates that an active autophagy pathway may have a regulatory role in IL6 and to a lesser extent TNF secretion. None of the inhibitors replicated the cytokine secretion response of NaB suggesting that it is acting via a different mechanism.

3.11 Differences in IL6 and TNF cytokine levels resulting from NaB exposure are a consequence of altered synthesis rather than secretion

Brefeldin A is a potent inhibitor of IL6 and TNF secretion in THP-1 cells since it blocks the vesicle formation and fusion involved in ER to Golgi transport[175]. The total amount of IL6 and TNF synthesised upon HkEc ± NaB stimulation can be determined by the inclusion of brefeldin A, which trapping the cytokines inside the ER and builds up the intracellular levels.

THP-1 cells were stimulated with HkEc in the presence of either NaB, brefeldin A or a combination of both. In this experiment, cells were stimulated for 6, 12 and 24 hours and the supernatant collected, the cell pellet washed and lysed in RIPA buffer, and extracellular (supernatant) and intracellular (cell lysate) cytokines measured by ELISA. When brefeldin A was used, it aimed to trap the cytokines for specific periods of time, always starting from the previous time point. For instance, when samples were collected at 6 hours, brefeldin A was added at time 0 with HkEc. Samples collected at 12 hours, were stimulated with HkEc at time 0 and the cells were kept without brefeldin A for 6 hours, allowing the normal cytokine secretion until brefeldin A was added to the culture medium. Similarly, samples that were collected at 24 hours had HkEc added at time 0 and were kept without brefeldin A for 12 hours. At 12 hours initial stimulation with HkEc, brefeldin A was added to the culture medium (Figure 3-23).

This approach permitted the investigation of cytokine synthesis and secretion for the periods of 0-6, 6-12 and 12-24 hours. Figure 3-23

summarizes the experiment design and the results are shown in figures 3-24 to 3-26.

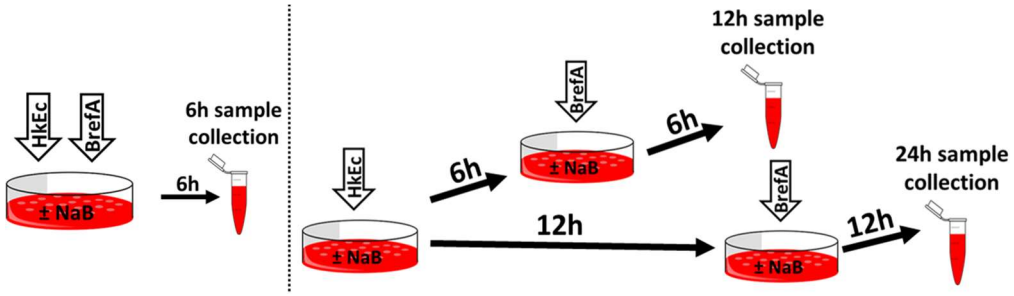

Figure 3-23: Experiment design to investigate the cytokine synthesis and secretion over specified time periods in unstimulated and HkEc stimulated THP-1 cells ± NaB. Brefeldin A (BrefA) was used to trap cytokines intracellularly. This experiment was performed in parallel with samples without addition of brefeldin A.

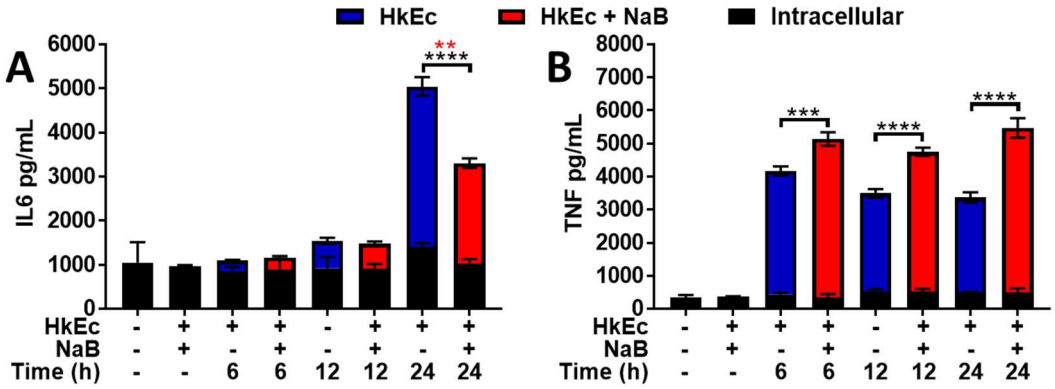

Figure 3-24: IL6 (A) and TNF (B) levels were measured by ELISA in HkEc stimulated THP-1 cells ± NaB in the supernatant and whole protein lysates, for the secreted and intracellular levels, respectively. The intracellular levels of both IL6 and TNF remained constant, suggesting that the cytokines produced are released or degraded as quickly as they are synthesised without accumulating intracellularly and NaB had no obvious effect on intracellular trafficking. IL6 is mainly released after 12 hours (A), while almost all the TNF was produced and released during the first 6 hours (B). In HkEc samples only, TNF decreases after 6 hours, while upon exposure to NaB, it showed an increase after 12 hours, suggesting a second peak in TNF induction. Results shown are mean ± SEM, *p<0.05, **p<0.01, ***p<0.001, ****p<0.0001; for comparisons between the same time point (two-tailed, unpaired t-test). Black asterisks, intracellular levels; red asterisks, secreted levels.

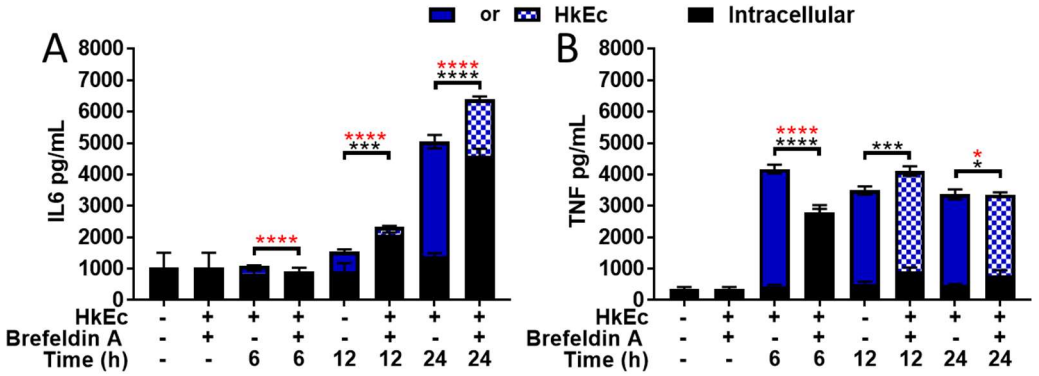

Figure 3-25: IL6 (A) and TNF (B) levels were measured by ELISA in HkEc stimulated THP-1 cells ± brefeldin A. The supernatant and whole protein lysates were quantified for the secreted and intracellular levels, respectively. By using brefeldin A and trapping the cytokines inside the cell, it is possible to understand their dynamics. IL6 started to be synthesised between 6 and 12 hours and showed a massive increase between 12 and 24 hours. On the other hand, all TNF was produced and secreted within the first 6 hours. Addition of brefeldin A at later time points had limited effect on the secretion and intracellular levels of TNF. Black asterisks, intracellular levels; red asterisks, secreted levels.

Brefeldin A effectively blocked the secretion of both cytokines when the cells were exposed to it. The stacked bar graph shows secreted levels of HkEc in top blue bars, secreted levels of HkEc + brefeldin A in top blue and white bars, and the intracellular levels of both groups in black bottom bars.

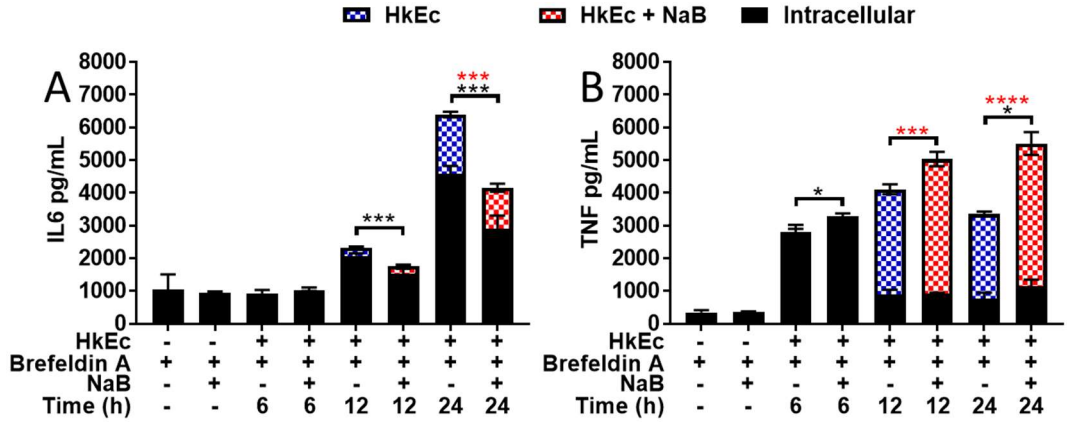

Figure 3-26: IL6 (A) and TNF (B) levels were measured by ELISA, in HkEc stimulated THP-1 cells exposed to brefeldin A ± NaB. The supernatant and whole protein lysates were quantified for the secreted and intracellular levels, respectively. NaB exposure led to an impaired synthesis of IL6, which is subsequently observed as reduced secretion of this cytokines (see figure 3-24). Conversely, TNF was synthesized in higher amount upon exposure to NaB (B, 6 hours) and resulted in higher secretion levels when

compared to HkEc alone (B, 12 and 24 hours). Results shown are mean ± SEM, *p<0.05, **p<0.01, ***p<0.001, ****p<0.0001; for comparisons between the same time point (two-tailed, unpaired t-test). Black asterisks, intracellular levels; red asterisks, secreted levels.

Through the use of brefeldin A it has been shown that IL6 and TNF are synthesised and secreted at a similar rate and at any given time there is only a limited amount of intracellular cytokines. NaB does not seem to alter this cellular transit and seems to be acting almost exclusively at the level of transcription and translation.

3.12 NaB and pH changes

External pH can influence the intracellular pH[177], and thus hinder the cytokine trafficking and release[174]. To investigate if NaB would be acting by simply changing the concentration of protons, the pH of the THP-1 medium was directly measured with a calibrated pH meter under different conditions (Figure 3-27).

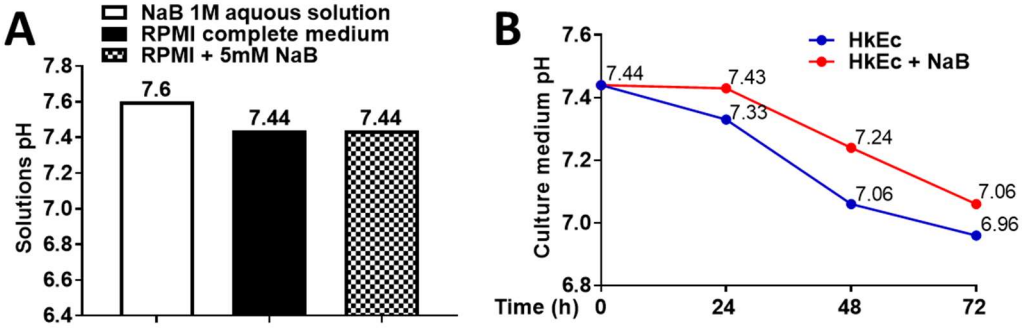

Figure 3-27: pH measurements of NaB solutions. The pH was measured in 1 M solution and 5 mM NaB in RPMI enriched medium (A). 1 M NaB aqueous solution was slightly alkaline. The pH of the complete RPMI medium was 7.44 and did not change after addition of 5 mM NaB. THP-1 cells were stimulated with HkEc ± NaB and the pH measured over 3 days. The pH continuously dropped in the NaB-free medium after the first 24 hours, while in 5 mM NaB, the pH seemed to be more stable and a reduction was observed after 48 hours stimulation. Results shown are of a single measure. The results of a single experiment are limited to establish a proper cause-effect of the experimental conditions.

Addition of 5mM NaB to RPMI complete medium was buffered in solution resulting in no change to the pH. The inclusion of stimulated THP-

1 cells in RPMI ± 5 mM NaB demonstrated that the NaB reduced the acidification of the media over time. This demonstrated that NaB may be acting as a buffer during stimulation or because it affects the immune response activity of the THP-1 cells, resulting in a reduced acidification of the extracellular medium. Confocal microscopy was used to measure the intracellular pH using SNARF®, a fluorescent dye that changes the colour according to pH. No changes in cytoplasmic pH were observed due to NaB exposure (Figure 3-28).

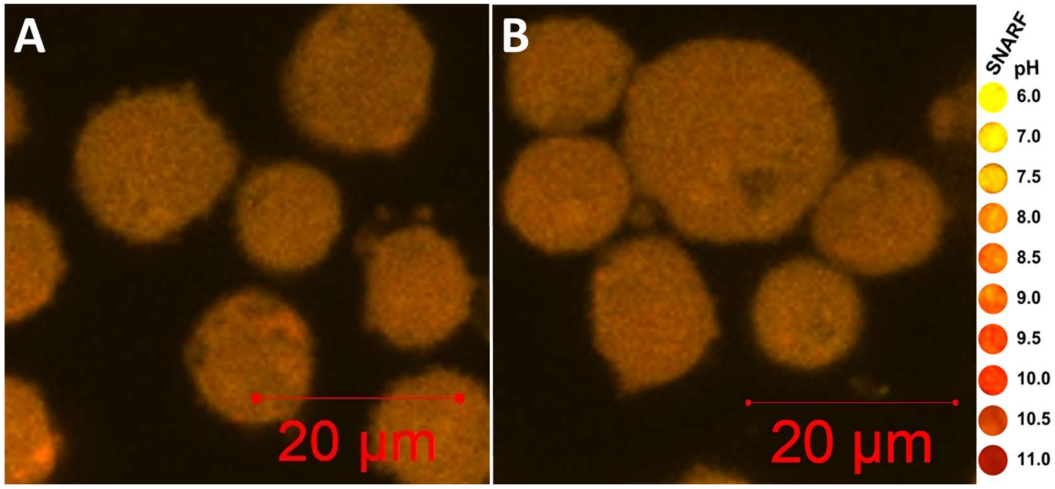

Figure 3-28: Confocal microscopy image of THP-1 cells stimulated with HkEc for 1 hour ± NaB using SNARF®. There was no major difference between HkEc stimulation (A) and NaB exposure (B). Comparable results were observed in untreated and NaB exposed THP-1 cells when compared to any condition (data not shown). pH colour scale on the right.

Taken together, these results suggest that NaB may have a different mechanism of action rather than simply altering cytosolic pH in THP-1 cells.

3.13 Deregulated cytokine secretion caused by NaB treatment may interfere with the whole innate immune response

An orchestrated early immune response is required for an adequate bacterial clearance and may prevent the development of chronic inflammation. Defective production of pro- and anti-inflammatory cytokines can have a profound effect on human health and is known to contribute to the pathogenesis of CD [174,178]. The release of the pro-inflammatory cytokines IL6 and TNF demonstrate a strong positive linear correlation in

monocyte-derived macrophages (MDM) from healthy individuals and this correlation was shown to be significantly perturbed in MDM from patients with CD (Figure 3-29A)[178].

NaB exposure was found to reduce IL6 and increase the TNF levels in THP-1 cells stimulated with HkEc, which caused a major disruption in the expected correlation between these two cytokines (Figure 3-29B).

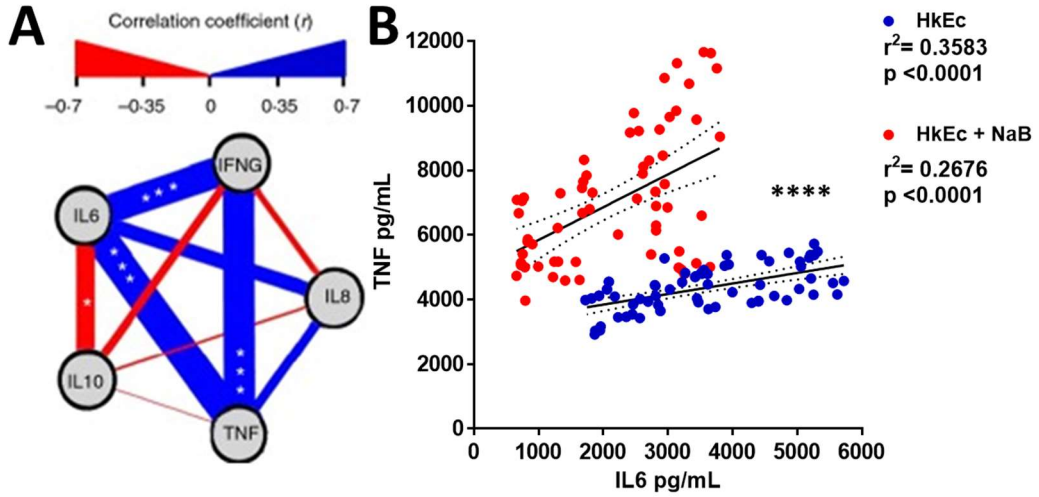

Figure 3-29: The positive linear correlation between IL6 and TNF is disturbed by NaB exposure. The Linear correlation between cytokines release in MDM stimulated with HkEc (A). NaB-treated HkEc-stimulated THP-1 cells showed reduced IL6 and increased TNF levels when compared to HkEc alone. Regression lines are different in HkEc compared to HkEc plus NaB. Results shown in B used simple linear regression analysis and ANCOVA for 10 individual experiments, *p<0.05, **p<0.01, ***p<0.001, ****p<0.0001, (ANCOVA). Image A adapted from Smith *et. al.* (2014)[178].

In view of the different dynamics in cytokine production and secretion, the relationship between IL6 and TNF, I hypothesized that NaB would act in 3 distinct phases (signals). The first signal, downstream of TLR activation and responsible for the early TNF induction. The second signal comes from the formation of intracellular ROS in combination with an autocrine/paracrine TNF signal via TNF-receptors. This signal would play a key role in IL6 and IL1β induction. Finally, the third signal originated from the autocrine/paracrine IL6 secretion and activation of the JAK/STAT3 signalling pathway which regulates TNF secretion (Figure 3-30). The

following chapters will deal with understanding these signalling events and how NaB alters them.

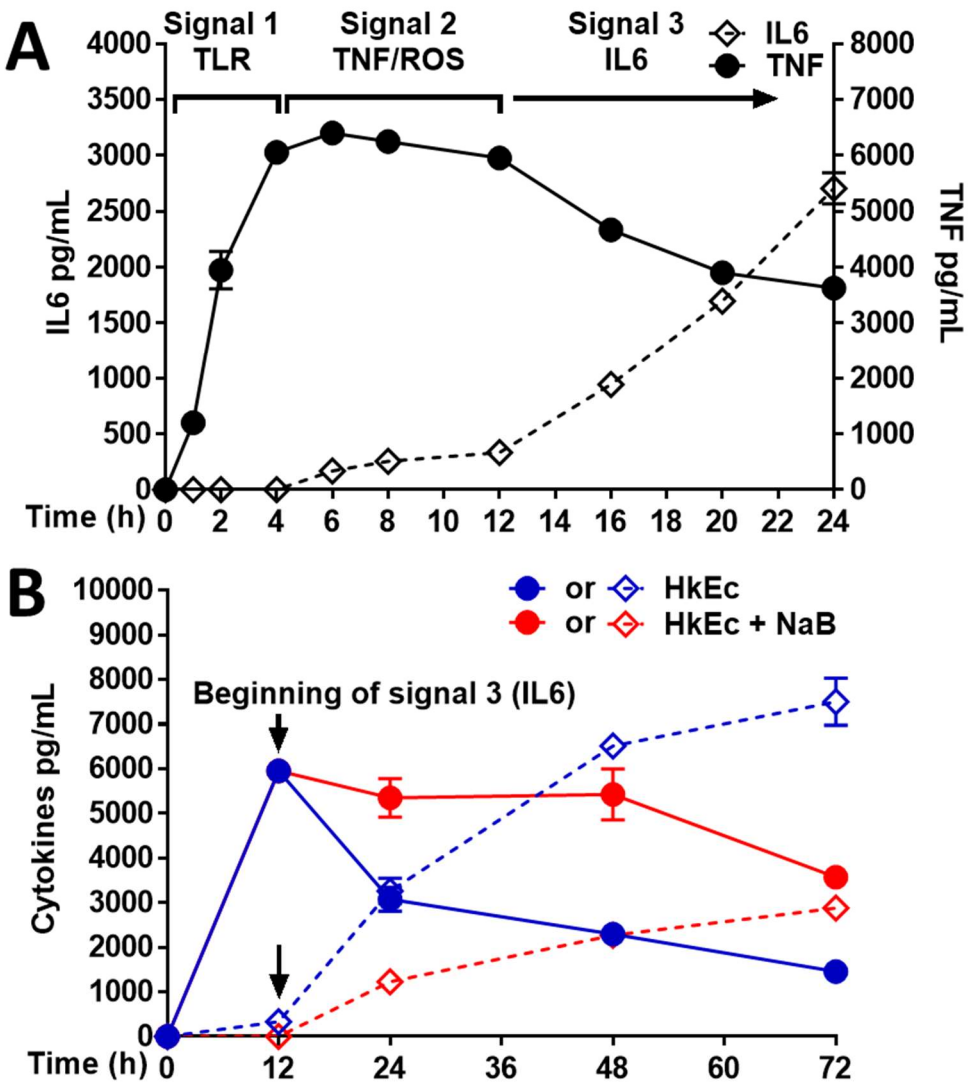

Figure 3-30: Relationship between IL6 and TNF dynamics and possible mechanisms underlying NaB disruption of cytokine secretion. THP-1 cells stimulated with HkEc would undergo three distinct signals that would influence the immune response. These signals would contribute to cytokine induction and regulation (A). Signal 1 originated downstream TLR activation, signal 2 comes from intracellular ROS formation and autocrine/paracrine TNF stimulation, and a third signal originates from IL6 binding to its receptor IL6R and activating the JAK/STAT3 pathway. THP-1 cells were stimulated with HkEc ± NaB for a total period of 72 hours. The third signal starts with the secretion of IL6 and controls the secretion of TNF. Because NaB treatment reduces IL6, the third signal is impaired, resulting in an elevation in the secretion of TNF. Filled circles and continuous line shows levels of TNF. Empty diamonds and dashed lines, IL6 levels.

3.14 Discussion

In this chapter, the main effects of NaB on the immune response were investigated. NaB exposure deregulated the cytokine response at mRNA and protein levels in THP-1 cells stimulated with heat-killed bacteria or TLR ligands, despite a similar initial signal downstream of TLR activation. To date, our literature search suggests we have conducted the first transcriptomics analysis upon NaB exposure, which showed that NaB regulated 1% of probes upon heat-killed bacterial stimulation.

NaB was found to have a toxic effect on THP-1 cells in a dose- and time-dependent manner, with a concentration of 5 mM being well tolerated by these cells, even after 15 days of exposure, which includes approximately 7 cell-cycles. The FDA approved concentration of NaB in foods is 0.01% of total weight, which is around 7 mM. However, it is difficult to know how it would affect the human body: it could conceivably work locally on the mucosal surfaces of the gastrointestinal tract, or systemically after absorption and distribution around the body. Most of the NaB ingested is metabolized in the mitochondrial matrix within the liver and kidney to hippuric acid and secreted in the urine[103,105]. Nevertheless, it is currently impossible to say how it is distributed to the diverse tissues in the body. In any case, from absorption to metabolism, NaB will be distributed through the bloodstream and will be available to circulating monocytes.

The gene expression profile showed that NaB affects many genes related to the TLR signalling and cytokine-cytokine receptors pathways after bacterial stimulation. Upon HkEc stimulation and NaB exposure, there was an attenuation of the overall response due to partial activation or deactivation of genes related to innate immunity compared to HkEc stimulation only. Furthermore, this effect targeted specific genes rather than the whole cell immune response, which suggests that NaB is a selective modulator of the immune response.

Another important finding was that NaB exposure required metabolic adaptations of the cell. Changes in gene expression of amino acid synthesis, especially involving glycine biosynthesis, suggest that the NaB uptaken results in its conversion to hippuric acid as previously shown to

occur in the liver and kidney[103,105]. This detoxification/clearance of NaB requires a metabolic adjustment within the THP-1 cells, which could account for the toxicity of this compound. The toxic levels may in part correspond with the cells ability to up-regulate the glycine biosynthesis pathway. If this is the case, then the sensitivity to NaB may differ depending on the cell type. The role of NaB metabolism will be better investigated in Chapter 7.

NaB exposure caused a profound change in IL6 and IL1β induction and secretion, significantly reducing the expression of these cytokines. A few studies that investigated the effects of NaB in cell types, such as mouse microglia, astroglia, splenocytes, and primary human astrocytes, have shown a similar reduction in IL6 and IL1β[14169]. To date, all reports have shown an inhibitory effect of these two cytokines, suggesting that NaB might involve a similar inhibitory mechanism that is independent of the cell type or stimulant.

While these inflammatory cytokines are important to initiate an adequate immune response and control bacterial infection[179180181], deregulation of cytokine secretion from the normal physiology is fundamental in diseases associated with chronic inflammation, such as in NDDs[92,182]. IL6 and IL1β play a pivotal role in neuroinflammation, which is underlying the pathogenesis of many NDDs[182,183,184], and the ability of NaB to reach the CNS after crossing the blood-brain barrier[6] suggest that it may be beneficial in controlling neuroinflammation. Despite any side effect associated with NaB ingestion, this versatility of NaB in attenuating IL6 levels in multiple cell types is potentially useful for many diseases associated with chronic inflammation, such as atherosclerosis[185], cancer, diabetes, and rheumatoid arthritis[186].

On the other hand, we found increased levels of TNF at a concentration of 5 mM NaB, while the previous reports have found a reduced level of TNF upon LPS stimulation in mouse microglia (1 mM NaB) and astrocytes (≈7 mM NaB)[1,169]. In THP-1 cells, TNF hypersecretion was dose-dependent and observed at concentrations of 5 and 10 mM, concentrations below 5 mM were unable to increase TNF secretion. The regulation of TNF by NaB will be further investigated in Chapter 5.

The alterations in cytokines seemed to be associated with their induction since their intracellular trafficking and secretion seemed to be unaffected by NaB. Our results showed that there was no accumulation of IL6 and TNF intracellularly and almost all the synthesized proteins were secreted. If any degradation occurs, it is not affected by NaB. It is important to mention that NaB alone, without any bacterial or TLR ligand stimulation, did not induce any inflammatory response, all the effects observed in cytokine release were found after TLR/bacterial stimulation.

In THP-1 cells, the changes in cytokines secretion should be seen not only in isolation but as a major disruption of the innate immune response. There is a positive correlation between IL6 and TNF, which is found in primary MDM[178] and also observed in THP-1 cells, which was disturbed by NaB exposure (Figure 3-29). Disruption of inflammatory signals is associated with disease status and severity in conditions characterized by chronic inflammation[178,187,188]. Dysregulation of cytokine release may be behind some of the negative effects observed on NaB consumption in patients with OFG. This condition will be analysed in more detail in Chapter 8.

Chapter 4 Effects of NaB on the THP-1 cell immune response (Signal 2)

4.1 Introduction

NaB exposure caused an altered innate immune response because of a deregulated secretion of pro-inflammatory cytokines in human monocytes, as demonstrated in chapter 3. A reduced secretion of IL6 and IL1β has been shown in other cells rather than monocytes, such as microglia[1,4] and splenocytes[169]. However, the mechanism by how NaB affects the immune response is unknown.

In the previous chapter, it has been shown that the altered cytokine secretion is mainly because of their synthesis and not due to any major impairment in intracellular trafficking or a deficiency in the secretory mechanism. There was also no abnormality in the early signals downstream of TLR activation, generating a hypothesis that a second signal would be responsible for a boost in IL6 and IL1β that is reduced or lacking due to NaB exposure.

TNF has been shown to induce the secretion of pro-inflammatory cytokines IL6 and IL1β through MAPK signalling pathway[189,190,191], mainly via TNFR1[192]. In breast cancer cells expressing a dominant negative form of the ERK1, TNF-induced IL6 production was blunt, suggesting that TNF induction of IL6 is mediated via ERK1 activation[191].

ROS have an established role in inflammation and are predominately produced from mitochondrial respiration[145,147] and NADPH oxidase in professional phagocytic cells such as neutrophils and macrophages[149,193]. ROS generated downstream TLR activation lead to pro-inflammatory cytokine production[194] especially IL6 upon LPS stimulation[195].

In this chapter, the mechanisms underlying NaB inhibition of cytokine synthesis were investigated, with a focus on ROS generation and TNF receptor signalling.

4.2 NaB acts as a free radical scavenger and impairs IL6 production by neutralization of ROS

4.2.1 Characterization of ROS induction

ROS function as mediators in many cell-signalling pathways under normal conditions. However, harmful stimuli such as those generated by microbial antigen significantly induce the generation of ROS which, causes the level to exceed body's antioxidant defence system[196]. HkEc-induced ROS was investigated by evaluating the expression of proteins associated with ROS using western blot (Figure 4-1).

ROS are critical components of the antimicrobial repertoire of macrophages. Macrophages, as professional phagocytes, generate ROS using the NADPH oxidase complex during the respiratory burst. Here we show that the $P67^{phox}$ (NCF2 gene), one of the subunits of the NADPH oxidase complex is overexpressed upon HkEc stimulation. Under oxidative stress, there is an increase in ROS that the cell tries to compensate. The mitochondrial uncoupling proteins (UCP) 1–3 are mitochondrial anion carrier proteins that are overexpressed to minimize ROS emission from the electron transport chain. ROS or their by-products are thought to activate UCP proteins to induce proton leak, thus providing a negative feedback loop for mitochondrial ROS production[197,198]. The UCP2 has been found to be activated by ROS[197].

Signals generated by ROS can activate the apoptosis signal-regulating kinase (ASK1), through oligomerization and, autophosphorylation[198]. ASK1 is one of the mechanisms responsible for the activation of the MAPK signalling pathway[146,199].

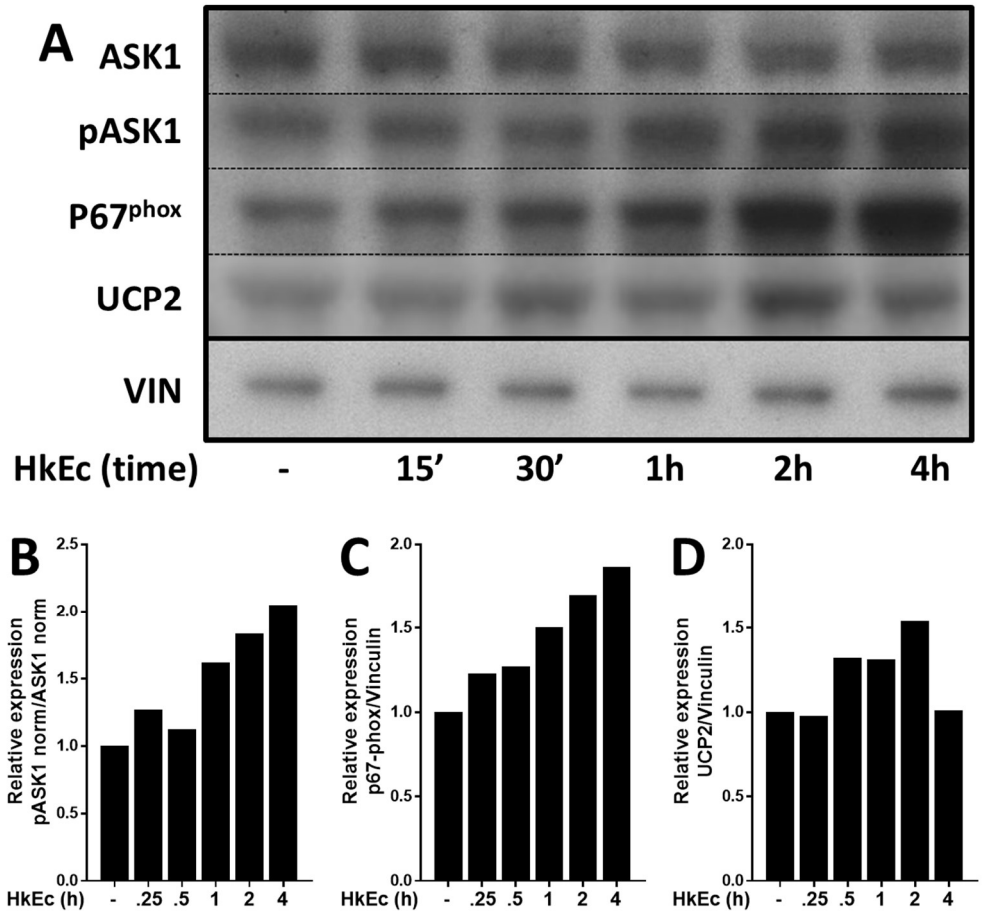

Figure 4-1: Immunoblots showing the expression of ROS-associated proteins in THP-1 cells stimulated with HkEc. Upon bacterial challenge, there was an increase in the phosphorylation of ASK1 and increased expression of $P67^{phox}$. At 30 minutes of stimulation, there was an increase in the expression of the UCP2, suggesting an attempt of the cells to compensate the extra ROS produced. Protein quantification for pASK1 (B), $P67^{phox}$ (C), and UCP2 (D). iNOS expression was not identified in any of the immunoblots performed (Data not shown). Vinculin was used as a loading control.

4.2.2 ROS formation and effects of NaB

To investigate the competence of NaB to act as a radical scavenger and thus, neutralize the ROS generated by bacterial stimulation, two assays were used: the Amplex® Red, which indirectly measures the superoxide/peroxidase activity by reacting with hydrogen peroxide released by the cell; and the Cellular ROS/Superoxide assay, which has two dyes that reacts selectively with ROS (green dye) and specifically with superoxide (red dye). These two assays test different aspects of ROS

activation, while the Amplex® Red uses an impermeable dye and only reacts with extracellular H_2O_2, the Cellular ROS/Superoxide assay uses two cell permeable dyes, which allows the formation of intracellular ROS/superoxide to be determined. By combining these two assays, it was possible to understand the mechanism underlying ROS moderation by NaB.

Activation of macrophages by pathogens leads to the generation of ROS in a process called respiratory burst. In this process, there is a marked increase in non-mitochondrial oxygen consumption and generation of superoxide (0^-) by the NADPH-oxidase complex[200]. Superoxides are very unstable molecules and are quickly dismutated by enzymatic and nonenzymatic reactions, resulting in oxygen-derived species such as H_20_2 (see Figure 1-19). Thus, monitoring the release of H_20_2 is an established method to evaluate the respiratory burst[201].

THP-1 cells were stimulated with either phorbol 12-myristate 13-acetate (PMA), an activator of NADPH oxidase, or HkEc ± NaB and the generation of extracellular H_20_2 measured using Amplex® Red (Figure 4-2).

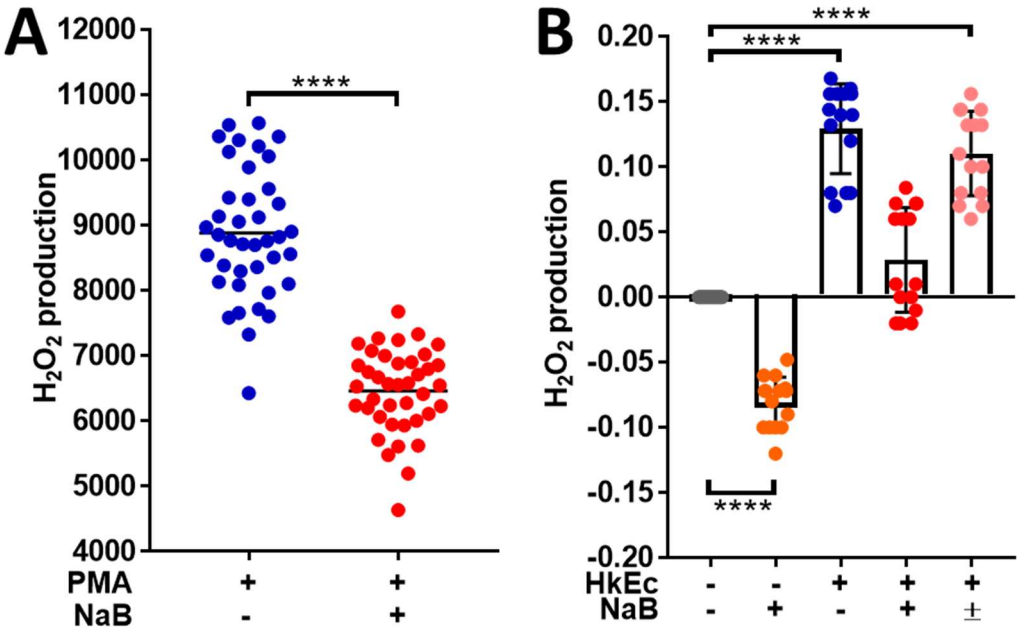

Figure 4-2: H_2O_2 production by THP-1 cells stimulated with PMA (A) or HkEc (B) ± NaB. NaB exposure reduced the levels H_2O_2 upon stimulation with PMA (A). Upon HkEc stimulation, there was an increase in H_2O_2 production, which is neutralized when NaB was in the culture medium.

Cells pre-incubated with NaB were washed 2X with PBS and assayed without the presence of NaB (± NaB). By doing it, the decomposing effect of NaB was abolished, which suggests that NaB reacts with H_2O_2. Results shown are mean ± SEM of 4 (A) and 2 (B) independent experiments, *p<0.05, **p<0.01, ***p<0.001, and ****p<0.0001 (two-tailed, unpaired t-test; one-way ANOVA with Dunnett's test)

To investigate the specific production of ROS and superoxide, the ROS/Superoxide assay was used. The ROS dye can react mainly with H_2O_2 and HO^- and is permeable to the cell membrane, reacting with the intracellular and extracellular ROS (Figure 4-3).

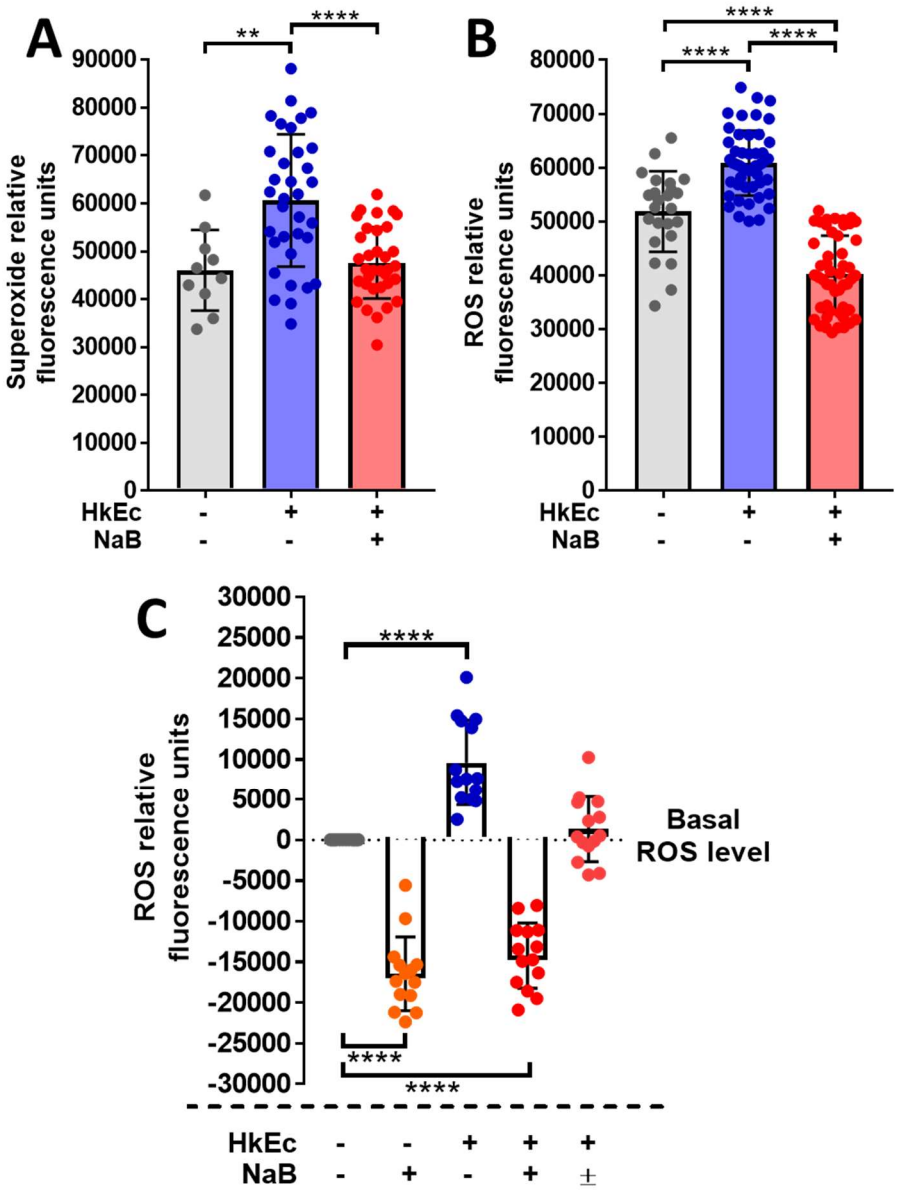

Figure 4-3: ROS and superoxide production was investigated in THP-1 cells stimulated or not with HkEc ± NaB. Upon stimulation, there was a

significant increase in superoxide and ROS production. NaB exposure neutralized the burst in superoxide production (A) and decreased the levels of ROS below than recorded in unstimulated cells (B). NaB strongly reduced the levels of ROS in stimulated and unstimulated cells. Cells pre-incubated with NaB were washed 2X with PBS and assayed without the presence of NaB (± NaB). This experiment aimed to exclude the effects of the NaB from the medium and determine the role of the intracellular NaB previously uptaken by the cell on ROS levels (C). Removal of NaB from the medium had minimal effect on the ability of intracellular NaB to restrict the levels of HkEc-induced ROS production. Results shown are mean ± SEM of 4 (A and B) and 2 (C) independent experiments and analysed using one-way ANOVA with Tukey's test (A and B) and Dunnett's test (C). In C, the basal level of ROS was established based on the control group of unstimulated cells (*p<0.05, **p<0.01, ***p<0.001, and ****p<0.0001).

To test the scavenging capability of NaB, THP-1 cells were stimulated with HkEc and ROS production was monitored using the ROS/superoxide assay. At 1 hour of stimulation, the experiment was paused and several concentrations (0-40 mM) of NaB were added to the cells and the ROS production was monitored for an extra hour (Figure 4-4).

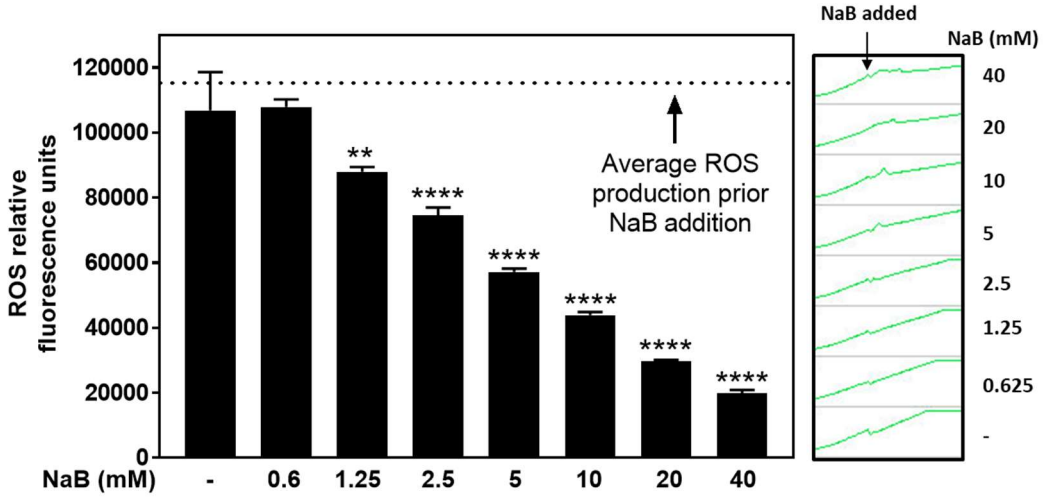

Figure 4-4: ROS scavenging activity of NaB is dose-dependent and occurs almost immediately of NaB addition. THP-1 cells were stimulated for 1 hour with HkEc and the ROS production was monitored. At 1 hour, the experiment was paused and concentrations from 0-40 mM of NaB were added (black arrow) and ROS production was monitored for an extra hour. Concentration from 1.25 mM and above showed significant ROS scavenging activity of NaB in a dose-dependent manner. At 40 mM NaB, almost all the ROS generated was decomposed. Results shown are mean ± SEM of 3 independent experiments and analysed using one-way ANOVA with Dunnett's test, (*p<0.05, **p<0.01, ***p<0.001, and ****p<0.0001).

Next, a range of antioxidants was used to determine their effects on cytokine secretion. NAC, a prodrug to L-cysteine that is a precursor to the biologic antioxidant glutathione; 2,2,6,6-tetramethylpiperidine-N-oxyl (TEMPO), an intracellular scavenger of superoxide anion[39]; and curcumin, a phenolic compound naturally found in some plants and known for its H_2O_2, HO^-, ROO^-, O^{2-} scavenging activity[202,203] (Figure 4-5).

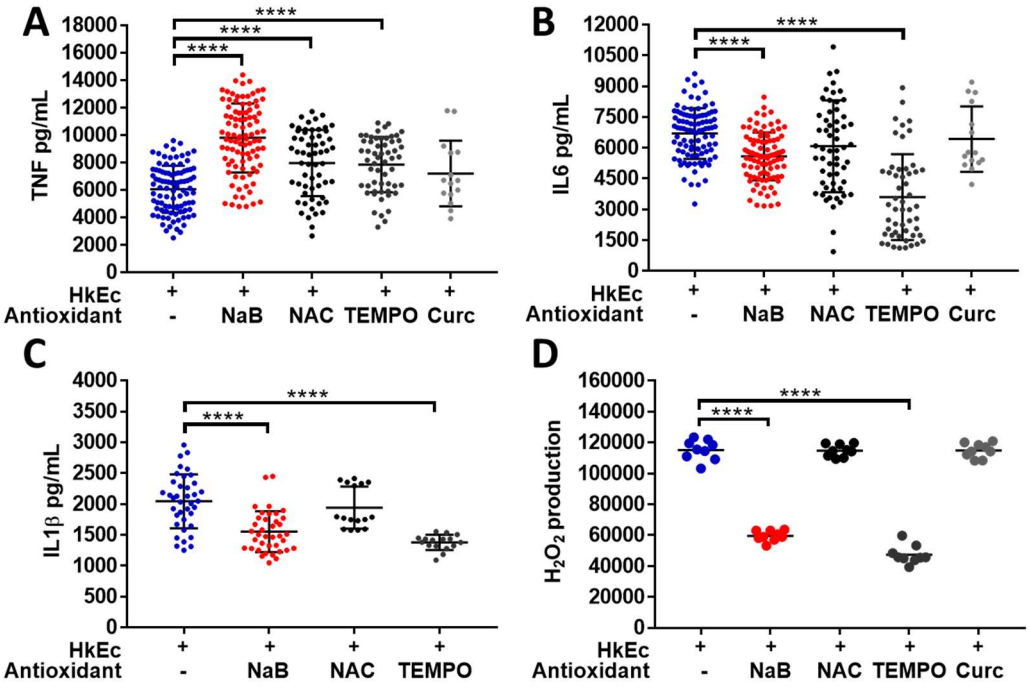

Figure 4-5: THP-1 cells were incubated with either NaB and known antioxidants NAC, TEMPO and curcumin, and stimulated with HkEc. The cytokine levels of TNF, IL6 and IL1β were measured by ELISA (A-C). The H_2O_2 production was measured using the same antioxidants. NaB and the antioxidants NAC and TEMPO induced a hypersecretion of TNF (A). However, only NaB and TEMPO showed a reduction of IL6 and IL1 β (B and C). Similarly, only these two compounds showed an effective scavenging activity and reduced H_2O_2 production (D). Results shown are mean ± SEM of 9 (A and B), 4 (C) and 1 (D) independent experiments, *p<0.05, **p<0.01, ***p<0.001, ****p<0.0001, (one-way ANOVA with Dunnett's test, HkEc as control group).

In the results shown in Figure 4-5, only the antioxidants NaB and TEMPO that effectively reduced the H_2O_2 production were capable of reducing the secretion of IL6 and IL1 β. It suggests a correlation between H_2O_2 production and IL6 and IL1 β release.

Taken together, these results suggest that ROS is required for maximal induction of IL6 and IL1β upon immune stimulation. Effective inhibition of HkEc-induced superoxide/ROS generation causes a reduction in IL6 and IL1β secretion. On the other hand, NAC and TEMPO treatment resulted in a hypersecretion of TNF, but the mechanisms behind this response are not clear.

To examine if the reduced levels of ROS found in NaB treated samples were caused by any deficiency of the NADPH oxidase complex or if it could potentiate the expression of antioxidant enzymes, the expression of genes associated with key elements of this system was carried out (Figure 4-6).

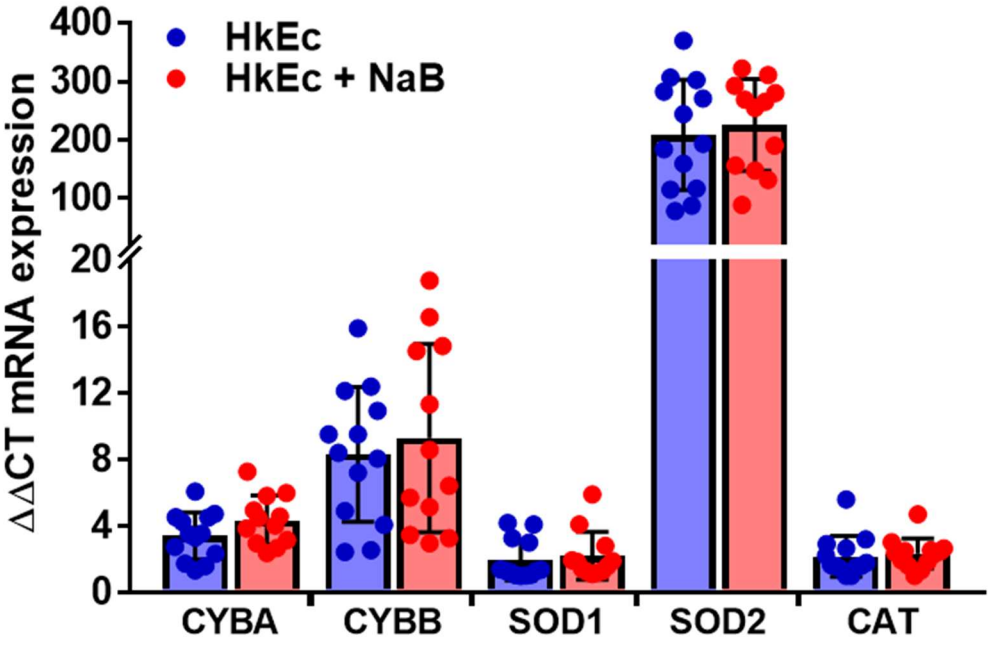

Figure 4-6: mRNA Expression analysis of ROS associated genes in THP-1 cells stimulated with HkEc ± NaB for 24 hours evaluated by qRT-PCR. The expression of cytochrome b genes (CYBA and CYBB) and the antioxidant enzymes SOD1, SOD2 and catalase were similar. Results shown are mean ± SEM for 3 independent experiments, *p<0.05, **p<0.01, ***p<0.001, ****p<0.0001; (two-tailed, unpaired t-test).

4.3 TNF induces IL6 production, but it is similarly affected by NaB exposure

Experiments were designed to investigate the role TNF plays in IL6 induction using recombinant TNF (rTNF) and neutralizing antibodies.

THP-1 cells were stimulated with either HkEc, LPS, rTNF or a combination of these ± NaB. HUMIRA® (adalimumab), an anti-TNF therapeutic drug used for several inflammatory conditions (e.g. rheumatoid arthritis, polyarticular juvenile idiopathic arthritis, psoriatic arthritis, ankylosing spondylitis, CD), is a recombinant human IgG1 monoclonal antibody that binds to TNF, preventing it from binding to and activating TNF receptors[204]. Recombinant TNF induced IL6 secretion in the absence of TLR stimulation (Figure 4-7A). THP-1 cells stimulated with HkEc in the presence of HUMIRA® for 24 hours, demonstrated the efficiency of this monoclonal antibody to bind and block TNF (Figure 4-7B). The effects on IL6 secretion resulting from TNF were tested in THP-1 cells stimulated with LPS for 24 hours (Figure 4-7C).

TNF is a major inducer of IL6 downstream of LPS stimulation and blocking TNF results in a substantial reduction in IL6 release. The stimulation of THP-1 cells with rTNF and NaB resulted in more than 2-folds increase, while blocking TNF abrogated IL6 secretion, therefore demonstrating that TNF signalling is a major inducer of IL6 upon LPS stimulation (Figure 4-7D).

The effects on IL6 levels resulting from TNF were tested in THP-1 cells stimulated or not with HkEc ± NaB for 24 hours (Figure 4-8). The influence of TNF on IL6 secretion downstream of HkEc was still observed but was not as dramatic as seen with LPS. There was no secretion of IL6 when rTNF was added in combination with NaB. TNF-induced ROS generation was reduced by NaB exposure (Figure 4-9).

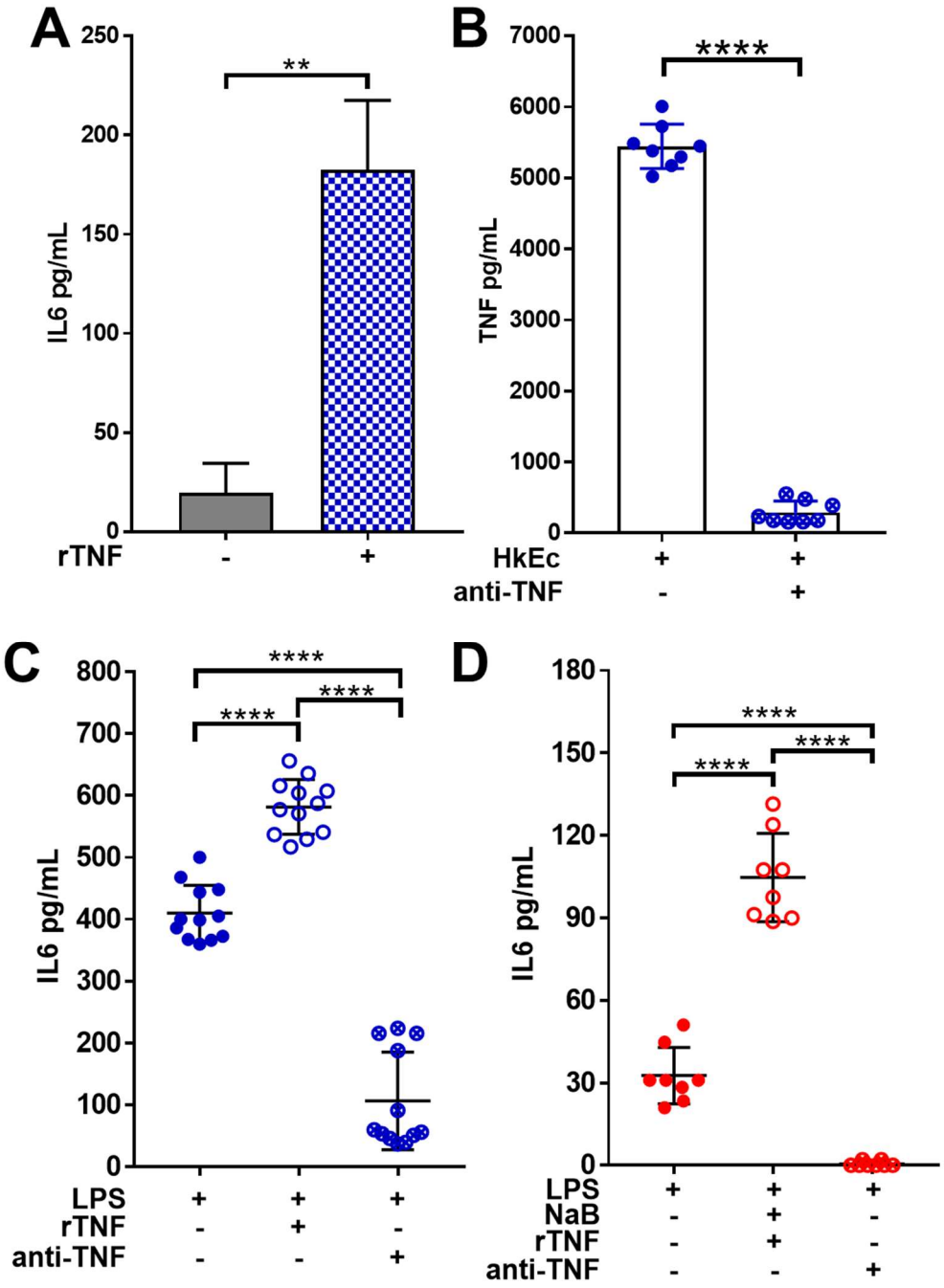

Figure 4-7: The effects on IL6 secretion upon TNF manipulation. THP-1 cells were stimulated with TNF (A), HkEc plus an anti-TNF antibody (B), LPS in combination with rTNF and anti-TNF (C and D), and in the presence of NaB (D). The levels of IL6 (A, C and D) and TNF (B) were measured by ELISA. Results shown are mean ± SEM of 2 independent experiments, *p<0.05, **p<0.01, ***p<0.001, ****p<0.0001, (two-tailed, unpaired t-test).

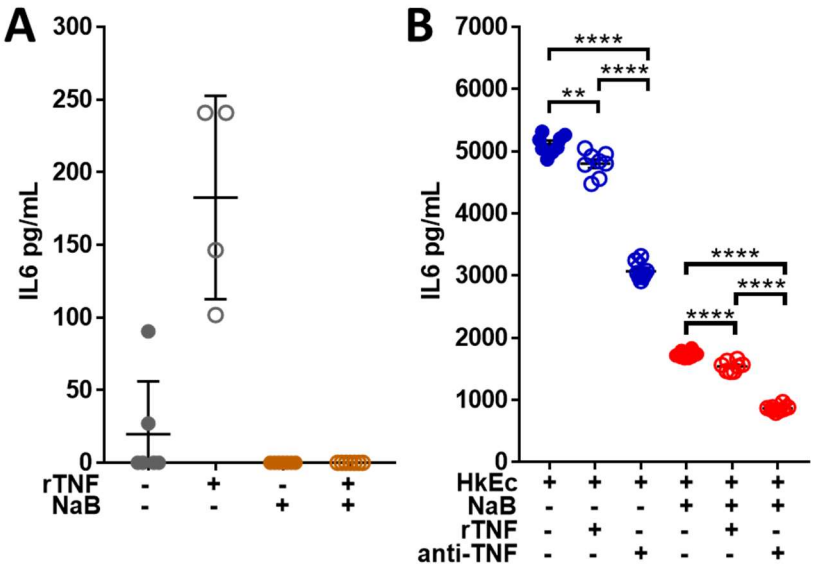

Figure 4-8: THP-1 cells were stimulated with HkEc ± NaB for 24 hours with either TNF or anti-TNF antibody, and the levels of IL6 were measured by ELISA. TNF induction of IL6 was completely inhibited by NaB. Addition of TNF to HkEc stimulated cells even reduced the levels of IL6, regardless of NaB treatment. However, neutralization of TNF reduced the secretion of IL6. Results shown are mean ± SEM and analysed using one-way ANOVA with Tukey's test (B). In B, statistical analysis was applied separately depending on NaB exposure (*p<0.05, **p<0.01, ***p<0.001, and ****p<0.0001).

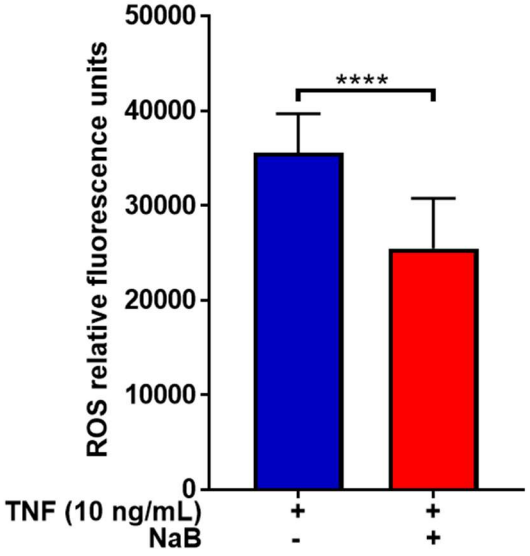

Figure 4-9: ROS production in THP-1 cells stimulated with recombinant TNF and measured by ROS/Superoxide assay. TNF generates ROS that is partially neutralized by NaB. Results shown are mean ± SEM of 2 independent experiments, *p<0.05, **p<0.01, ***p<0.001, ****p<0.0001, (two-tailed, unpaired t-test).

These results suggest that TNF plays a role in the IL6 production, which is clearly observed when the cells were stimulated with LPS. TNF induction of IL6 seemed to be related to the generation of ROS, which is neutralized by NaB (Figure 4-9). HkEc stimulation already induces very high levels of TNF (8 times more than LPS), that is the probable reason why no additional effect was observed by the supplementary TNF.

4.3.1 ROS reduction induced by NaB attenuates the oxidative stress response signalling pathway KEAP1 -NRF2

The Kelch-like ECH-associated protein 1 (KEAP1)-nuclear factor (erythroid-derived 2)-like 2 (NRF2) regulatory pathway plays a central role in the protection of cells against oxidative stress. Under normal conditions, NRF2 is bound to the endogenous inhibitor KEAP1 that facilitates the ubiquitination and proteasomal degradation of NRF2[205,206]. Under oxidative stress, modifications in cysteine residues of KEAP1 (e.g. via oxidation of sulfhydryl groups or phosphorylation) apparently weakens the interaction with NRF2, and NRF2 can no longer be ubiquitylated and degraded. This saturates KEAP1 and allows the newly-synthesized NRF2 to accumulate and translocate to the nucleus[205]. In the nucleus, NRF2 forms heterodimers with other transcription factors such as c-Jun and small Maf proteins (G/F/K), binds to the antioxidant response element (ARE) and regulates the expression of more than 200 genes involved in cellular antioxidant defence[207] (Figure 4-10).

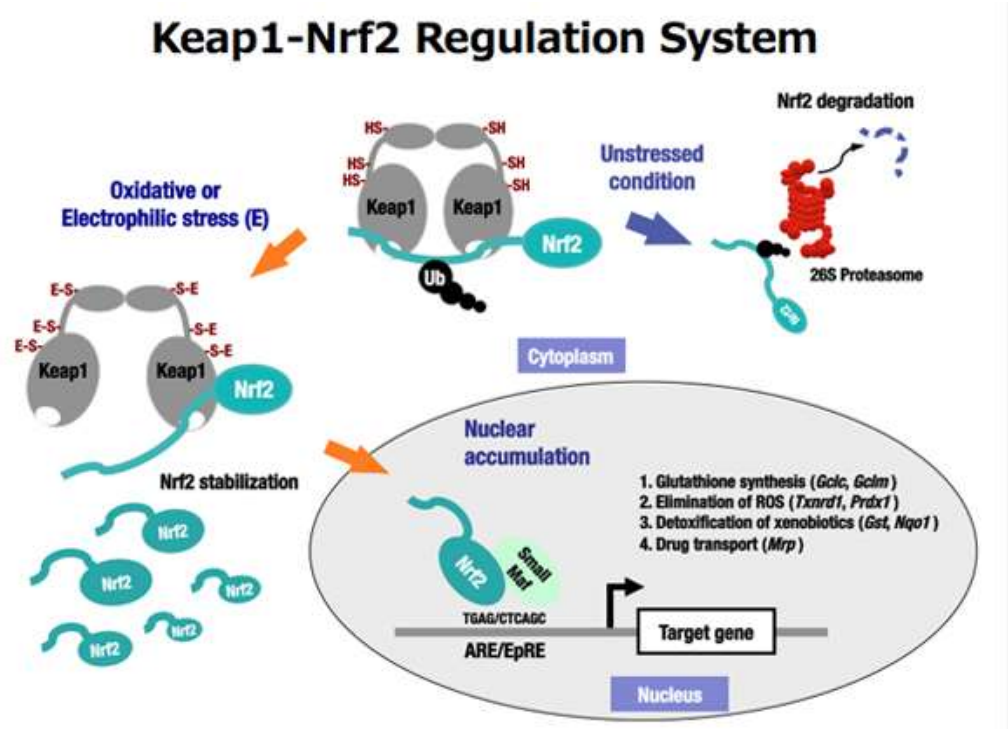

Figure 4-10: KEAP1 -NRF2 regulatory system. Under normal condition, KEAP1 is bound to NRF2 and facilitates NRF2 ubiquitination and proteasome degradation. Oxidative stress causes conformation changes that inhibits polyubiquitylation of NRF2, that accumulates and saturates KEAP1 . Newly synthesized NRF2, can translocate to the nucleus and activate the antioxidant response elements. (Image was taken from http://multiple-sclerosis-research.blogspot.com/2015/06/tecfidera-and-nrf2.html, accessed on 16/11/2017)

To investigate the effects of reduced ROS in consequence of NaB exposure, subcellular protein fractions were prepared to analyse the expression of nuclear and cytoplasmic expression of the KEAP1 -NRF2 signalling pathway (Figure 4-11).

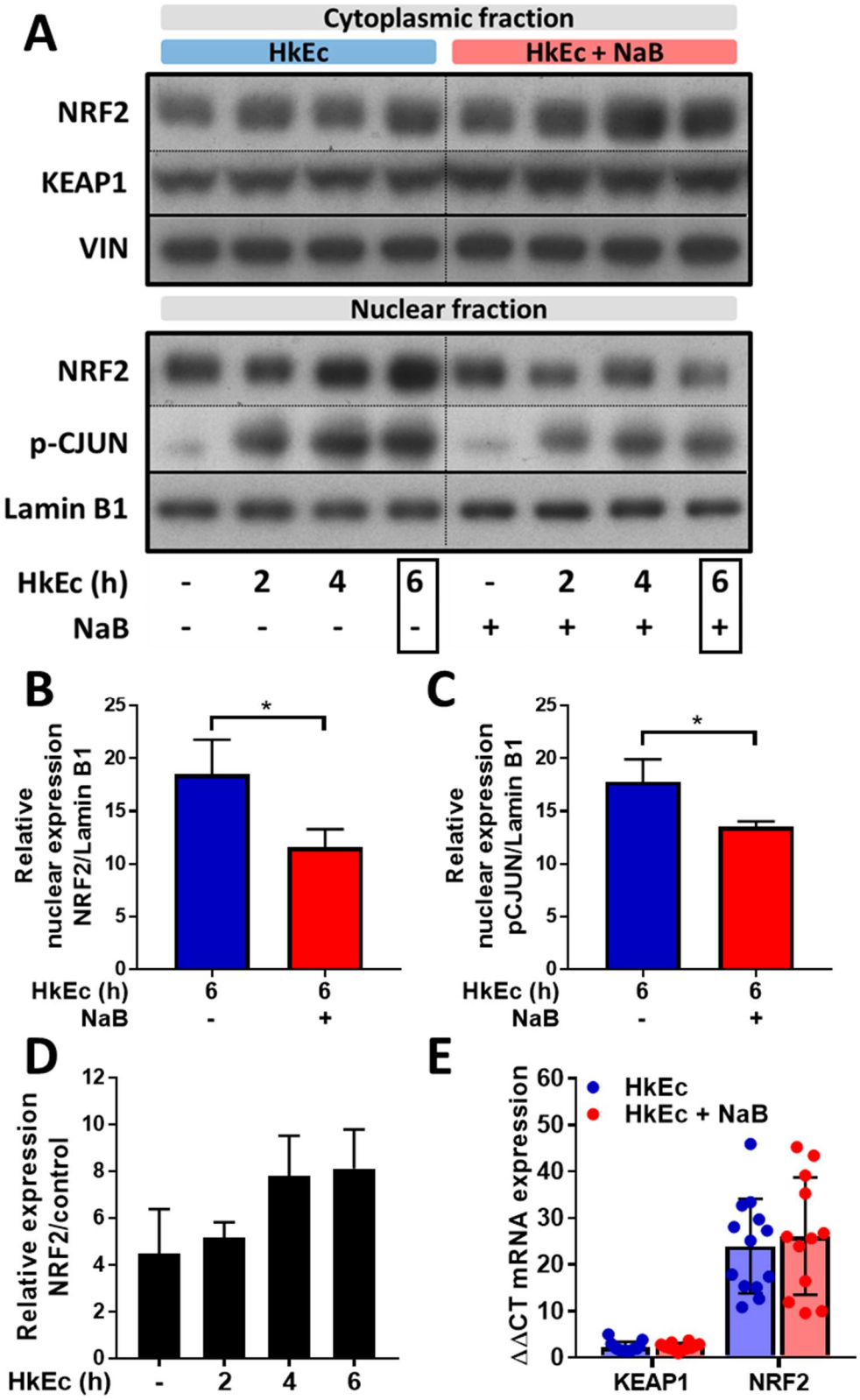

Figure 4-11: Immunoblot showing the protein expression of the cellular fractions: cytoplasmic (A, top) and nuclear (A, bottom) of THP-1 cells stimulated with HkEc ± NaB. 10 µM of the MG132, a proteasome inhibitor, was used 1-hour prior stimulation. Cellular fractions were prepared using differential centrifugation steps (see section 2.8.1.2). Quantification is

shown in B-D. qRT-PCR mRNA expression of KEAP1 and NRF2 in THP-1 cells stimulated with HkEc ± NaB for 24 hours (E). Protein expression of the KEAP1 /NRF2 complex in the cytoplasmic fraction is maintained relatively stable over time (A, top). HkEc stimulation NRF2 total expression (D) and nuclear translocation (B) to initiate transcription of antioxidant responsive elements (ARE). This NRF2 nuclear translocation is attenuated on NaB treatment. Expression of phosphor-C-JUN in the nucleus was also attenuated in NaB samples. At 6 hours, the expression level of nuclear NRF2 and p-C-JUN is significantly weaker on NaB exposure (C). Gene expression levels of NRF2 increased more than 20 times (compared to untreated control, not shown) the presence of HkEc after 24 hours, but NaB had no effect on message levels (E). Loading controls for the cytoplasmic and nuclear fractions used were vinculin and lamin B1, respectively. Results shown are mean ± SEM of 3 independent experiments, *p<0.05, **p<0.01, ***p<0.001, ****p<0.0001, (two-tailed, unpaired t-test).

Immunoblots of nuclear and cytoplasmic fractions showed an attenuated NRF2 nuclear expression upon NaB exposure, whereas there was no difference in the cytoplasmic expression of KEAP1 and similar mRNA levels of both proteins, NRF2 and KEAP1. NRF2 is the main protein responsible for an antioxidant response, activating several genes related to antioxidant defence[207]. These results suggest that, by buffering ROS, NaB reduces the need for a robust antioxidant response, resulted in the reduced levels of NRF2 in the nucleus and higher nuclear expression of c-JUN, a downstream target of NRF2 activation.

Activation of NRF2 regulates the expression of numerous cytoprotective genes, including antioxidants. Genes involved in the synthesis and regeneration of glutathione, detoxifying molecules, regulators of transcription factors and growth factors. Heme oxygenase 1 (HMOX1) is one of those proteins regulated by NRF2 and degrades heme, generating biliverdin and CO[208]. HMOX1 expression appeared to be lower on exposure to NaB (Figure 4-12).

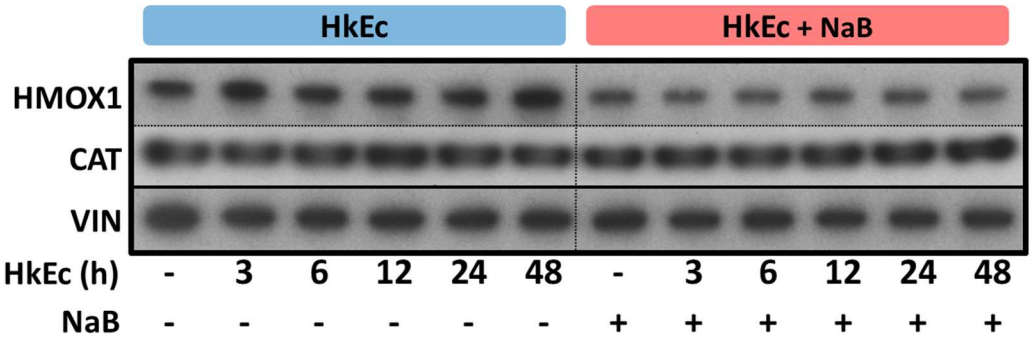

Figure 4-12: Immunoblot showing the protein expression HMOX1 and Catalase after an extended period of THP-1 cells stimulation with HkEc ± NaB. HMOX1 is one of the main antioxidant proteins induced by NRF2 activation. HMOX1 expression appears to be reduced in all NaB treated samples irrespective of stimulation. However, catalase (CAT), a well-expressed protein that participates in degradation of hydrogen peroxide, was similarly expressed in both samples. Results shown are for 1 experiment.

4.3.2 Effects of ERK1/2 signalling pathway on cytokine secretion

There is a strong link between ROS generation and the MAPK ERK1/2 since it participates in the ROS signalling cascade inducing cytokines synthesis[193], and increasing NRF2 protein expression[206]. Signals generated by ROS through the MAPK pathway, activate the transcription factor AP1. C-JUN is one of the subunits that form the AP1 complex, and upon its phosphorylation, C-JUN translocates to the nucleus to initiate transcription. Phospho-C-JUN was found overexpressed in the nucleus at 6 hours in HkEc stimulated cells compared to HkEc + NaB (Figure 4-11). A rise in the intracellular production of ROS, dependent or not of the NADPH oxidase machinery, results in activation of the ERK1/2 pathway[149].

To investigate the participation of the ERK pathway, downstream of HkEc exposure and IL6 secretion, PD98059 was used. PD98059 is a potent and selective inhibitor of MAP kinase kinases (MAPKK), MEK1 and MEK2. By adding PD98059 to THP-1 cells there was an abolishment of ERK1/2 phosphorylation and strongly reduced phosphorylation of its downstream transcription factors C-JUN and C-FOS (Figure 4-13).

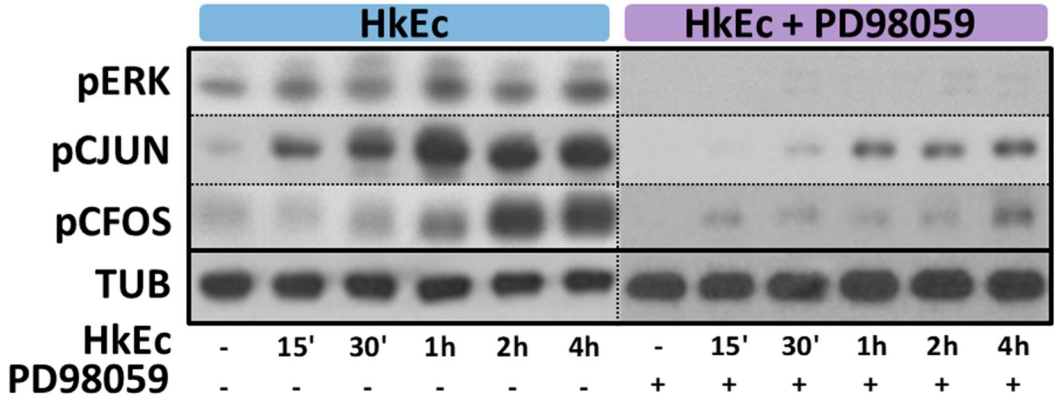

Figure 4-13: Immunoblots showing the phosphorylation of ERK1/2 and the AP1 transcription factor subunits C-JUN and C-FOS in HkEc ± PD98059.PD98059 abolished ERK1/2 phosphorylation and reduced the phosphorylation of C-JUN and C-FOS. This shows that PD98059 is a potent inhibitor ERK1/2 and, therefore, reduces the phosphorylation of downstream proteins. α-tubulin was used as a loading control. Results shown are for 1 experiment. α-Tubulin was used as a loading control.

An experiment was designed to identify the temporal effect of p-ERK1/2 using PD98059 in cytokines secretion. PD98059 was added to the cells at two specific time points during HkEc stimulation: the first, 30 minutes prior to HkEc stimulation in order to block ERK1/2 signalling at the beginning of the bacterial stimulation. The second, 4 hours after HkEc stimulation, allowing the initial signalling downstream of TLR activation and aimed to investigate if ERK1/2 would be activated later by a second signal. The total stimulation period was 24 hours for all samples (Figure 4-14).

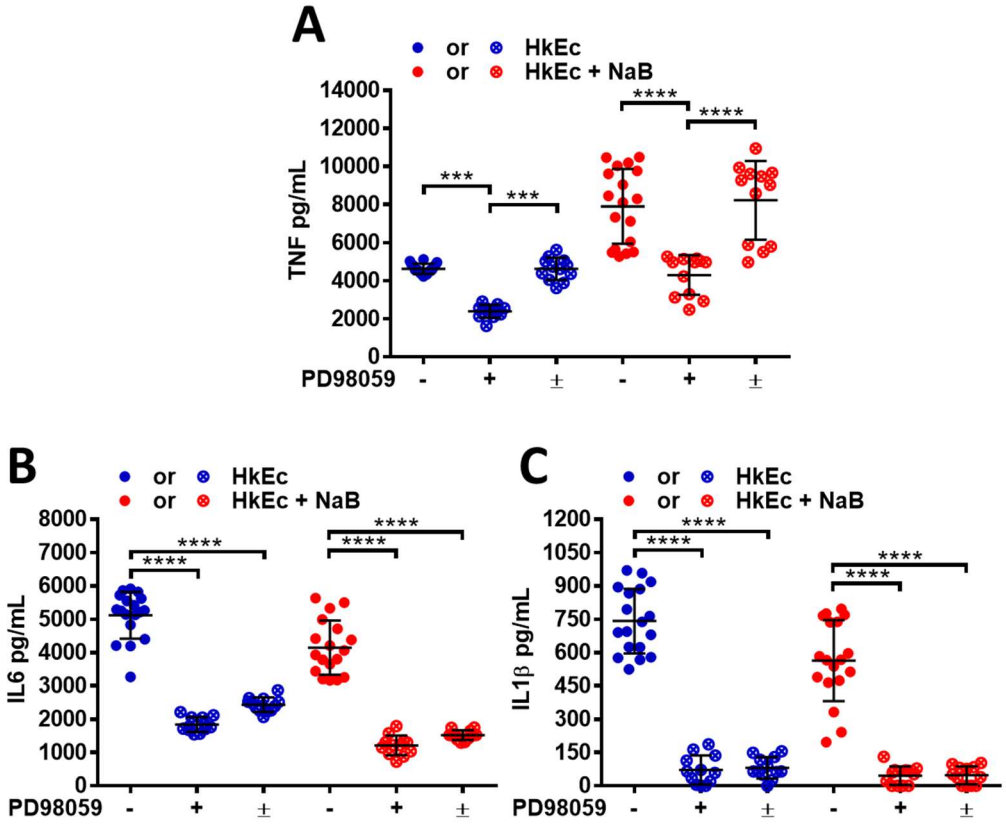

Figure 4-14: THP-1 cells were treated with ERK1/2 inhibitor PD98059, 30 minutes prior bacterial stimulation (+) or 4 hours after HkEc stimulation (±), in the presence or absence of NaB. The cytokine levels of TNF, IL6 and IL1β were measured by ELISA. PD98059 reduced the levels of TNF when added prior stimulation, but had no effect when it was added after 4 hours regardless NaB treatment (A). However, the levels of IL6 and IL1 β were similarly reduced regardless the time when PD98059 was added. Results shown are mean ± SEM of 3 independent experiments for comparisons between groups ± NaB, *p<0.05, **p<0.01, ***p<0.001, ****p<0.0001, (one-way ANOVA with Tukey's test).

These results showed that ERK1/2 signalling is important to TNF, IL6 and IL1β but with important temporal differences. While TNF induction requires ERK1/2 signalling during the first 4 hours, for IL6 and IL1β secretion it is important at later stages, since inhibition of ERK1/2 signalling by PD98059 had a similar effect if applied prior or 4 hours after bacterial stimulation.

4.4 Discussion

In this chapter, the mechanism underlying NaB inhibition of IL6 and IL1β was revealed. NaB acts as intra and extracellular free radical scavenger neutralizing ROS induced by immune activation. NaB can react with hydrogen peroxide and other intermediate by-products of oxidative stress. We demonstrated that ROS is generated in THP-1 cells upon TLR and TNF signalling and NaB reacts with and sequesters ROS, resulting in a diminished induction of IL6 and IL1β. IL8 and IP10 were not affected by NaB upon HkEc stimulation, suggesting these cytokines are less reliant on ROS signalling and use alternative activation pathways.

ROS are important signalling molecules in inflammation[145,147] and are generated by aerobic respiration in response to harmful stimuli[196]. ROS are constantly generated under aerobic conditions and their levels are controlled by the body's antioxidant defence system[196]. Upon HkEc stimulation, there is an increase in non-mitochondrial oxygen consumption (respiratory burst) through the NADPH oxidase complex[200], which is necessary for the digestion and clearance of intracellular microbes by macrophages[148].

In order to understand the role of NaB in the ROS regulation we used a range of approaches, which included, bioassays for direct measure of ROS and its by-products, indirectly evaluation by investigating the cellular response for ROS generation, HkEc stimulation increased ROS production which acted as a secondary signal that boosted IL6 and IL1β and in THP-1 cells is completely dissociated from TNF induction.

Our results showed that upon HkEc stimulation, there was an increase in $P67^{phox}$ expression, one of the subunits of the NADPH oxidase complex. An increasing phosphorylation of ASK1, which is a protein kinase that is a known ROS dependent signalling molecule that regulates downstream effectors such as the C-JUN. ROS and ASK1 phosphorylation were evident upon HkEc stimulation. ASK1 is kept inactivated by thioredoxin (Trx) in a redox-dependent interaction. ROS leads to direct oxidation of Trx and its subsequent dissociation from ASK1[146], which oligomerizes and autophosphorylates, becoming activated[198]. To control

the excessive ROS production, cells trigger an antioxidative mechanism to decrease ROS production through uncoupling mitochondrial proteins that cause a leakage of protons bypassing the ATP synthase and decreases the mitochondrial inner membrane's potential[197]. We showed that there was an induction in the expression of UCP2, one of the mitochondrial uncoupling proteins, in an attempt to curtail ROS production in THP-1 cells stimulated with HkEc.

In order to gain a greater insight into the role of NaB on ROS regulation, we used a combination of bioassays that directly measure a variety of ROS products. Using Amplex® Red, a cell-impermeable fluorescent dye that reacts with extracellular H_2O_2, NaB reduced the levels of H_2O_2 by about a third. When the cells previously treated with NaB were washed before being assayed, removing all the NaB from the supernatant, the levels of H_2O_2 were similar to those observed in cells that were stimulated with HkEc only. These results confirmed the ability of extracellular NaB to react with released H_2O_2 and suggest that this process is similar in THP-1 cells stimulated with HkEc irrespective of NaB.

Another bioassay that uses two different cell-permeable dyes that identify intracellular levels of superoxide and ROS was used, NaB exposure neutralized the superoxide production induced by HkEc stimulation resulting in similar levels to that seen in unstimulated cells. The ROS levels are even below the basal of unstimulated cells. In contrast to the Amplex® Red assay removing NaB from the supernatant maintained the ability of intracellular NaB to restrict the levels of HkEc-induced ROS production. This confirms the uptake of NaB and its accumulation in the cells, which maintains its ability to block ROS induced signalling in THP-1 cells. A similar residual effect was observed in IL6 cytokine secretion when NaB was removed from the supernatant.

The antioxidant activity of NaB was identified as the probable cause of the reduced IL6 and IL1β secretion through the use of a range of additional antioxidants. The inclusion of either NaB or TEMPO, an intracellular scavenger of superoxide anion[39], were capable of reducing the secretion of IL6 and IL1β. Interestingly, at the concentrations used in these experiments, NAC and curcumin had no effect on ROS levels or IL6 and

IL1β secretion. The ROS neutralization ability of NaB is immediate and dose-dependent and stimuli-independent. It suggests that NaB could interfere with any cell type that uses ROS as a second messenger.

ROS increases the expression of macrophage scavenger receptor type I, which was shown to be negatively regulated by the use of antioxidants including NaB[39]. Superoxide, but not hydrogen peroxide, has been shown to induce IL6 secretion in human bronchial epithelial cells. TNF-induced IL6 secretion was suppressed by the use of several antioxidants, which reinforces the role of ROS in IL6 induction[209].

So far, we have shown that HkEc stimulation increases the generation of ROS, which is actively linked to the rise in expression of ROS-associated proteins. One of the major cellular processes associated with immune activation is a rise in the antioxidant response in order to protect the cells from the ROS. The main antioxidant response mechanism is the KEAP1 /NRF2 pathway[207]. Briefly, NRF2 is bound in the cytoplasm by KEAP1 in non-oxidative stress condition. This results in NRF2 ubiquitylation and proteasomal degradation. Under oxidative stress, the interaction between KEAP1 /NRF2 is weakened resulting in the loss of NRF2 ubiquitylation and degradation. NRF2 is then able to translocate to the nucleus and induce transcription of proteins associated with the antioxidant response[205]. The inclusion of NaB during a HkEc stimulation resulted in a reduction in NRF2 nuclear localisation. This attenuated response of NRF2 provides additional evidence that NaB sequesters intracellular ROS and this is sufficient to alter the cellular response to bacterial stimulation.

Translocation of NRF2 to the nucleus and bindings to the ARE orchestrates the antioxidant defence response[207]. NRF2 regulates genes related to anti-oxidant, anti-inflammatory and detoxifying proteins such as HMOX1[208], which was found to be reduced in all NaB treated samples irrespective of stimulation. In NRF2 knockout mice, a range of inflammation markers, including inducible IL6, TNF and microglia activation, is increased compared with wild-type littermates[210]. The brain is particularly susceptible to oxidative damage because this organ consumes about one-third of the inspired oxygen in humans[211]. Inability to deal with oxidative stress through

NRF2 is underlying the mechanisms of neuroinflammation in this model[205,207,210].

Aggregation of misfolded proteins is a hallmark of neurodegenerative diseases in a disease-specific manner[90]. This aggregation of misfolded proteins leads to the activation of microglia, which results in an increased generation of ROS and release of pro-inflammatory cytokines, especially IL6[90,182,183]. NaB has the potential to control these two pivotal problems associated with NDDs.

Finally, it was shown that IL6 induction requires activation of the ERK1/2 signalling pathway. It occurs in the later stages of an immune response and needs ROS as a secondary signal for full activation. There is a strong link between ROS and ERK1/2, which was evident when PD98059 an ERK1/2 inhibitor was shown to block ROS generation and cytokine induction[147]. Therefore, in THP-1 cells exposed to NaB and an immune stimulant, the reduction in ROS could have a profound effect on the ERK1/2 effect accounting for the diminished activation of IL6 and IL1β.

In this chapter, we have provided strong evidence of ROS generation upon HkEc stimulation, and superoxide and ROS neutralization by NaB. ROS neutralization by NaB attenuates the cell's response to oxidative stress, resulting in a suboptimal signal through the ERK1/2 pathway and a diminished activation of the immune response especially the release of IL6 and IL1β. This ability of NaB as a ROS scavenger and immune suppressor has potential therapeutic benefits on diseases that have been shown to over-activate these molecules.

Chapter 5 TNF is hyper-secreted in the early stage of the immune response and is linked to ERK1/2 signalling pathway (Signal 1)

5.1 Introduction

In chapter 4, it was shown that the antioxidants NAC and TEMPO have a similar hypersecretion of TNF as seen with NaB, and this hypersecretion is not related to generation/scavenging of ROS (Figure 4-8). It was also shown that TNF requires ERK1/2 signalling during the first 4 h to a proper TNF response, which was strongly reduced by the addition of the MEK1 and MEK2 inhibitor PD98059 prior to bacterial stimulation (Figure 4-14).

In view that TNF is a cytokine that participates in the very early immune response, being induced and secreted during the first 6 hours after bacterial sensing (Figure 3-16), experiments were designed to focus on this period. In this thesis, the early immune response is considered the period dominated by TLR signalling after bacterial or ligand stimulation and encompasses the first 4 hours. The late immune response starts after the 4th hour when other signals, such as ROS and cytokines, start to play important roles.

5.2 NaB itself disturb the phosphorylation state of ERK1/2

To investigate the signal for induction of TNF, an in-depth look at the signalling cascade downstream of TLR activation was carried out (Figure 5-1).

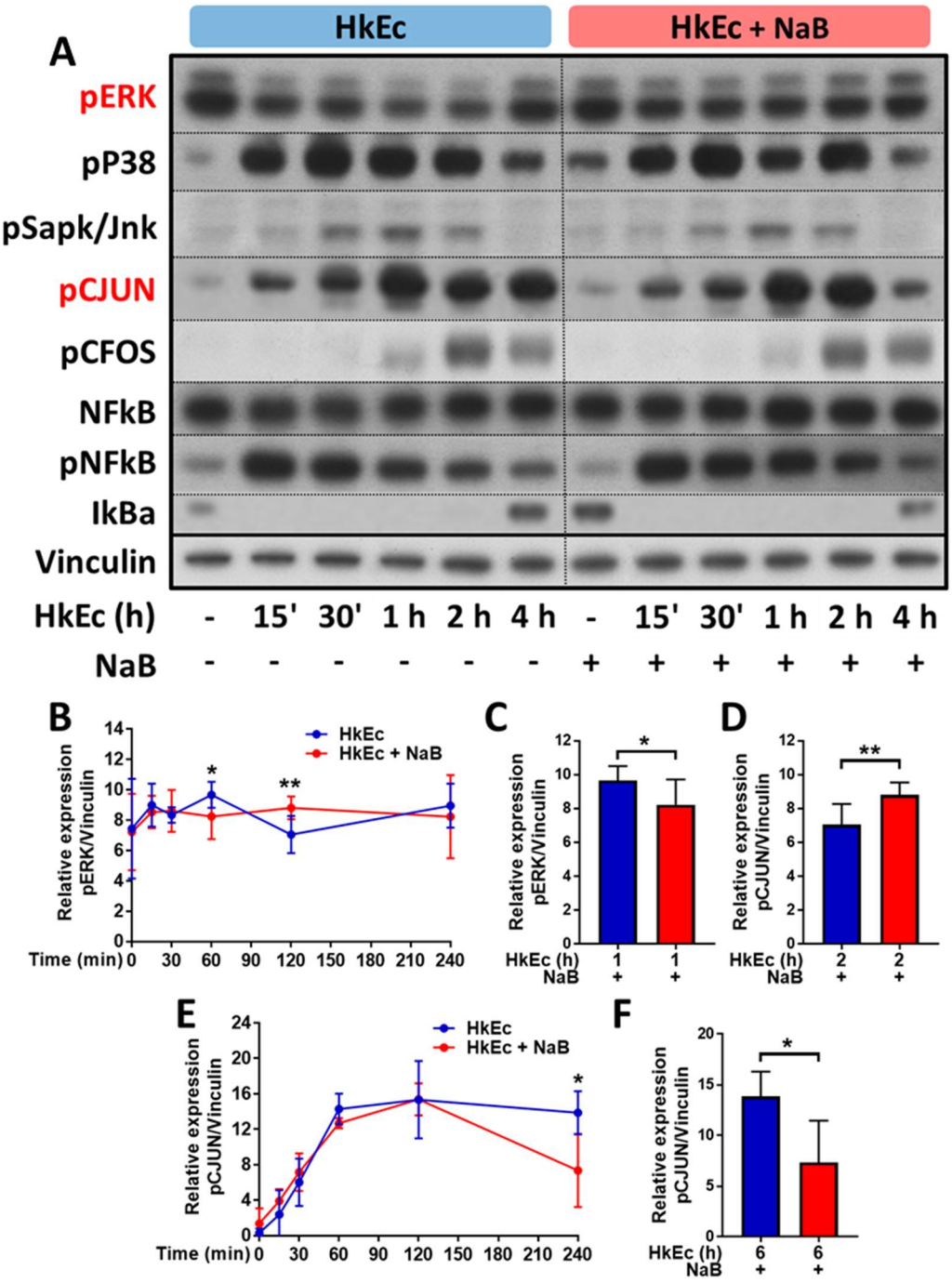

Figure 5-1: The major signal molecules downstream of TLR stimulation were visualized after HkEc stimulation for a total time of 4 h (A). There were differences in the phosphorylation pattern involving the ERK/C-JUN signalling pathway between HkEc and HkEc plus NaB. The phosphorylation pattern of ERK1/2 seems to fluctuate up and down in HkEc, but it is always high upon NaB exposure (B-D). At 4 h, the expression of phospho-C-JUN was less intense on HkEc plus NaB samples. Vinculin was used as a loading control. Results shown are mean ± SEM of 4 independent experiments, *p<0.05, **p<0.01, ***p<0.001, ****p<0.0001, (two-tailed, paired t-test).

In Figure 5-1 demonstrates that the majority of the signalling molecules downstream of TLR activation showed a similar pattern regardless of NaB treatment. While pERK1/2 showed a fluctuating pattern during the initial 4 hours after HkEc stimulation, treatment with NaB stabilized ERK phosphorylation, which may be involved in a deregulated TNF secretion upon NaB exposure.

To provide supporting evidence of an effect of NaB on ERK1/2 signalling, an experiment was designed using a higher concentration of NaB (20 mM) to try and exaggerate its effect (Figure 5-2).

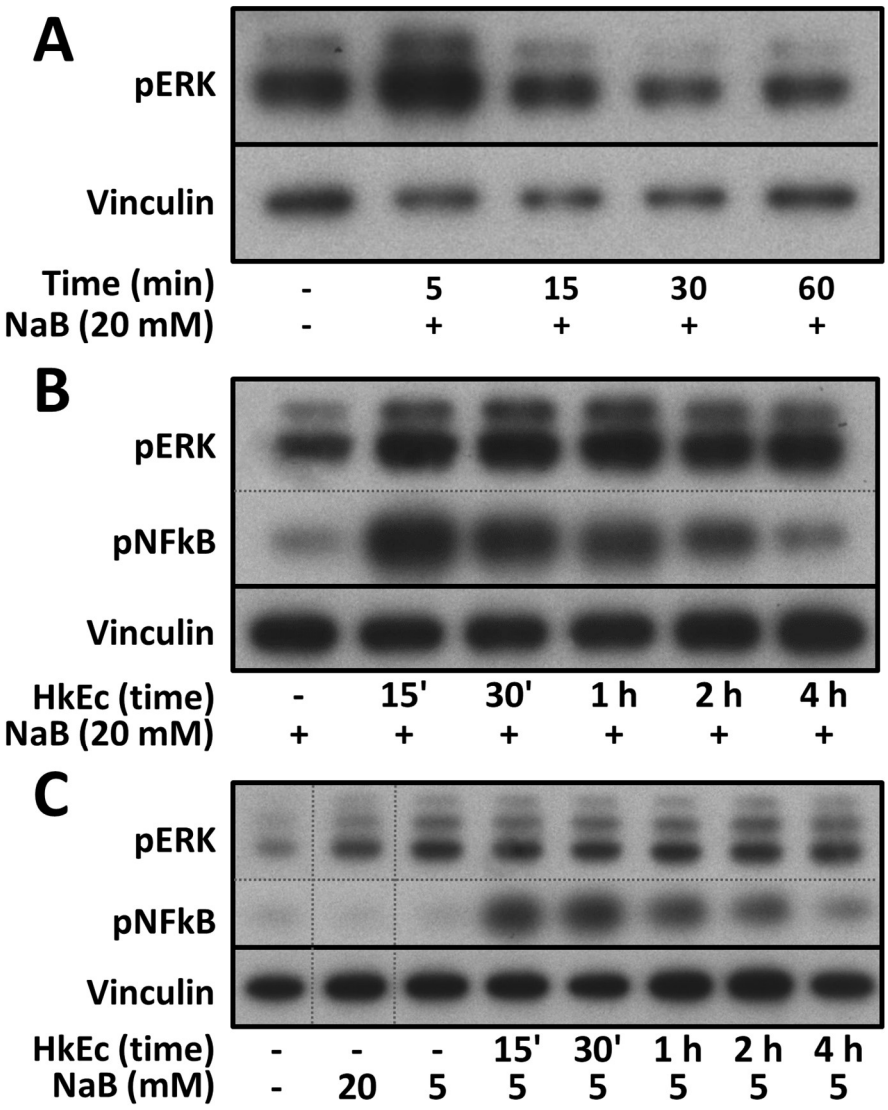

Figure 5-2: Immunoblots showing a time course using 2 different concentration of NaB (5 mM and 20 mM) and stimulated or not with HkEc. Cells were stimulated with 20 mM NaB without any bacterial challenge (A). At 5 minutes, there was an increase in the phosphorylation of ERK1/2 upon addition of NaB that decreased over time, showing that NaB itself disturbs

ERK1/2 signalling. Upon HkEc stimulation using a concentration of 20 mM of NaB, a steady-state of phosphorylation is observed in ERK1/2. At 20 mM, NaB itself does not cause activation of NFkB and does not disturb the NFkB phosphorylation pattern after HkEc stimulation (B). The basal level of phospho-ERK1/2 is higher with 5 mM and 20 mM of NaB when compared with untreated THP-1 cells (C). After HkEc stimulation, the same steady-state of ERK1/2 phosphorylation is observed when using either 5 mM or 20 mM NaB (B and C). Vinculin was used as a loading control. Results shown are of a single experiment. The results of a single experiment are limited to establish a proper cause-effect of the experimental conditions.

Figure 5-2 showed that NaB itself is capable of inducing phospho-ERK1/2 and upon HkEc stimulation the presence of NaB seems to stabilize the pERK signal. In contrast, the pattern of NFkB activation (pNFkB) was not influenced by NaB. It appears that ERK1/2 may be an important target of NaB exposition.

5.3 Message and protein levels of TNF are elevated on NaB samples

Although subtle, the disturbance in ERK1/2 signalling caused by NaB seems to have an effect on TNF regulation. So far, it has been shown that for a full induction, TNF requires ERK activation and NaB seems to disrupt the phosphorylation state of ERK, keeping it hyperactive (Figures 4-14 and 5-2). NaB in combination with HkEc increases the TNF mRNA

levels and results in higher TNF secretion than HkEc alone (Figures 5-3 and 5-4).

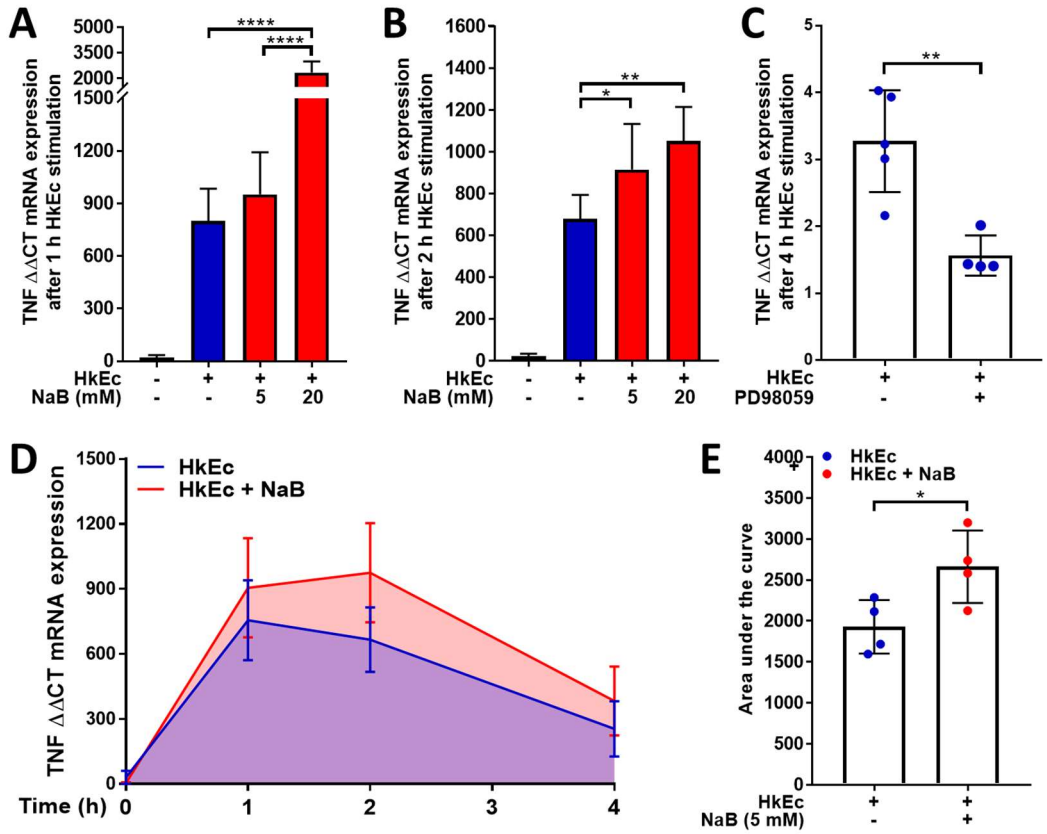

Figure 5-3: TNF gene expression measured by qRT-PCR. TNF mRNA expression is higher in HkEc + NaB than in HkEc alone. Increasing the NaB concentration from 5 mM to 20 mM intensify TNF expression at 1 h and 2 h (A and B, respectively). Inhibition of ERK1/2 signal reduces TNF expression (C). TNF gene expression occurs mainly during the first 4 hours and is almost completely lost after 6 hours (see Figure 3-16F). The cumulative effect on TNF gene expression is significantly higher upon NaB exposure (D and E). Results shown are mean ± SEM of 2 (A-C) and 4 (D and E) independent experiments, *p<0.05, **p<0.01, ***p<0.001, ****p<0.0001; (one-way ANOVA with Tukey's test (A and B); two-tailed, unpaired t-test (C and E); area under the curve (D)).

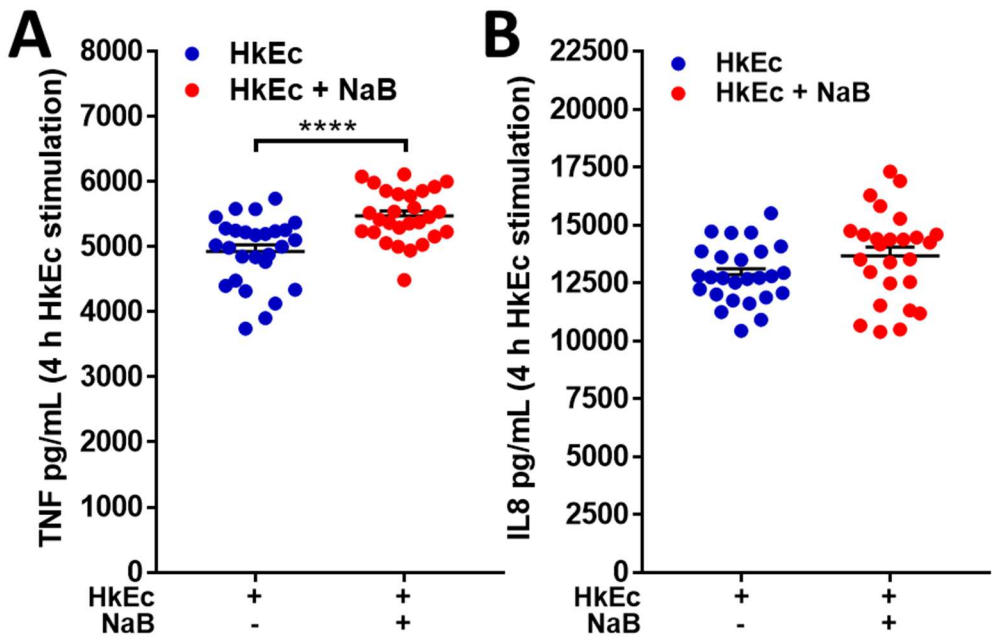

Figure 5-4: TNF (A) and IL8 (B) cytokine secretion levels in THP-1 cells stimulated with HkEc ± NaB for 4 h and measured by ELISA. TNF was increased because of NaB treatment, while IL8 levels were similar and used as a control. Results shown are mean ± SEM for 5 independent experiments., *p<0.05, **p<0.01, ***p<0.001, ****p<0.0001; (two-tailed, unpaired t-test).

5.4 NaB does not interfere with mRNA stability

In view of a high TNF mRNA level upon NaB exposure, an experiment was designed to test if the mRNA stability would be affected by NaB exposure. Actinomycin D, a chemotherapy medication used to treat a variety of cancers, was used to stop transcription and test if NaB exposure would interfere with TNF mRNA decay. Actinomycin D does this by binding DNA at the transcription initiation complex and preventing elongation of RNA chain by RNA polymerase[212].

THP-1 cells were stimulated with HkEc for 4 hours to induce TNF transcription. At 4 hours, samples were treated with either actinomycin D or NaB plus actinomycin D and the mRNA levels were investigated over time (Figure 5-5).

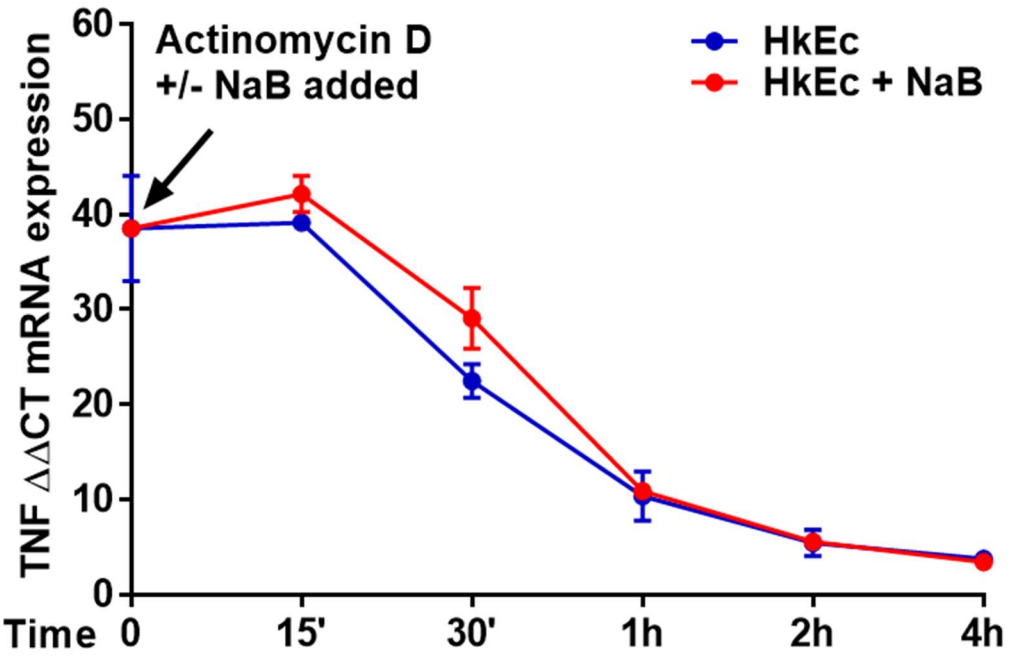

Figure 5-5: TNF gene expression measured by qRT-PCR. THP-1 cells were stimulated with HkEc for 4 h (Time 0) and either actinomycin D or NaB plus actinomycin D added to evaluate the mRNA decay. Addition of NaB did not change the speed of TNF mRNA decay (not significant). Results shown are mean ± SEM of 1 independent experiment, *p<0.05, **p<0.01, ***p<0.001, ****p<0.0001; (two-tailed, unpaired t-test).

5.5 Discussion

Our previous experiments demonstrated that TNF is hyper-secreted upon NaB exposure and it is induced very early after HkEc stimulation. The TNF mRNA levels reach a peak one hour after bacterial challenge and in 6 hours, almost all the message is gone. It was also shown that the MEK1 and MEK2 inhibitor PD98059 blocks ERK1/2 phosphorylation and it causes an important reduction in TNF levels when added prior to bacterial stimulation, and has no effect when added 4 hours after bacterial challenge, suggesting that the initial induction of TNF occurs mainly downstream of TLR activation.

Focusing on this early stage of the immune response, we observed that secretion of TNF is elevated upon NaB exposure after 4 h HkEc stimulation. This elevated secretion was a consequence of an increased message cumulated during the first 4 hours of stimulation. These facts led

us to have in-depth look at the signalling cascade downstream of TLR activation.

We found that NaB, at 20 mM without any bacterial challenge, disturbs ERK1/2 phosphorylation and becomes hyper-phosphorylated 5 minutes after NaB addition, with the strength of this signal decreasing over time.

THP-1 cells have an already high basal level of phosphor-ERK1/2, which might be linked to their malignant nature, and upon HkEc stimulation this phosphorylation state fluctuates over time. However, upon NaB exposure, phosphor-ERK1/2 remains always highly phosphorylated.

Lack of activation of ERK1/2 results in defective TNF secretion, which results in an inadequate transcriptional and post-transcriptional TNF induction[213,214,215,216]. Tumour Progression Locus 2 (TPL2) is a member of the serine/threonine protein kinase family and is required for LPS-induced, TLR4-mediated activation of the MAPK/ERK pathway in macrophages; being critical for TNF production. Peritoneal macrophages from TPL2 knockout mice showed no activation of ERK1/2 and defective TNF secretion. TPL2 is important for transport TNF mRNA from the nucleus to the cytoplasm[213]. Blocking of ERK1/2 was also found to interfere with TNF biosynthesis in human monocytes and macrophages, at both the transcriptional and post-transcriptional levels[215].

Full TNF secretion was dependent on ERK1/2 signalling. NaB exposure resulted in elevated TNF secretion and an increase in TNF mRNA levels, which was potentiated by a higher concentration of NaB. Taken together, these results suggest that ERK1/2 signalling plays a crucial role in TNF response. The disturb once induced by NaB exposure in the early ERK1/2 phosphorylation and maintenance of hyper-phosphorylated state during HkEc stimulation might be the cause of the disordered TNF synthesis induced by NaB exposure. However, more studies are required for elucidation of this question.

Chapter 6 IL6 deficiency contributes to TNF deregulation upon NaB exposure (Signal 3)

6.1 Introduction

Cytokines are signalling molecules that are very important immunomodulatory agents. The immune system depends on cytokine signalling to recruit new cells to a site of infection and for modulating the immune response. IL6 is mainly considered a pro-inflammatory cytokine, but studies have shown that IL6 also has anti-inflammatory activity[179,180,217].

IL6 is one of the major inducers of acute phase proteins and participates in many situations when there is a homeostatic perturbation. For instance, IL6 knockout mice release higher levels of TNF than WT animals in endotoxemia models[180]. The IL6 family include: IL6, IL11 and IL31 that share a common receptor and signal transducer subunit, the membrane glycoprotein gp130. The signal initiates when IL6 binds to the membrane IL6 receptor (IL6r), and subsequently, IL6/IL6R complex associate with gp130, leading to the gp130-homodimer formation and signal initiation[179]. This complex transduces IL6 signals resulting in the activation of the JAK/STAT3 signalling pathway.

In chapter 3, it was shown that NaB exposure reduces the secretion of IL6 (Figure 3-18A) and increases TNF (Figure 3-19A) after HkEc stimulation. TNF secretion peaked at 6 hours and gradually decreases after HkEc stimulation, but it is kept elevated upon NaB treatment (Figure 3-30). Although hyper-secretion of TNF is observed at the early stages of the immune response in the presence of NaB (Figure 5-4), it is unclear why the levels of TNF do not decrease at the same rate as that seen with HkEc alone. The second mechanism of TNF regulation must be disturbed by the inclusion of NaB and may relate to the loss of IL6 secretion and a feedback mechanism via IL6R/gp130 (Figure 6-1).

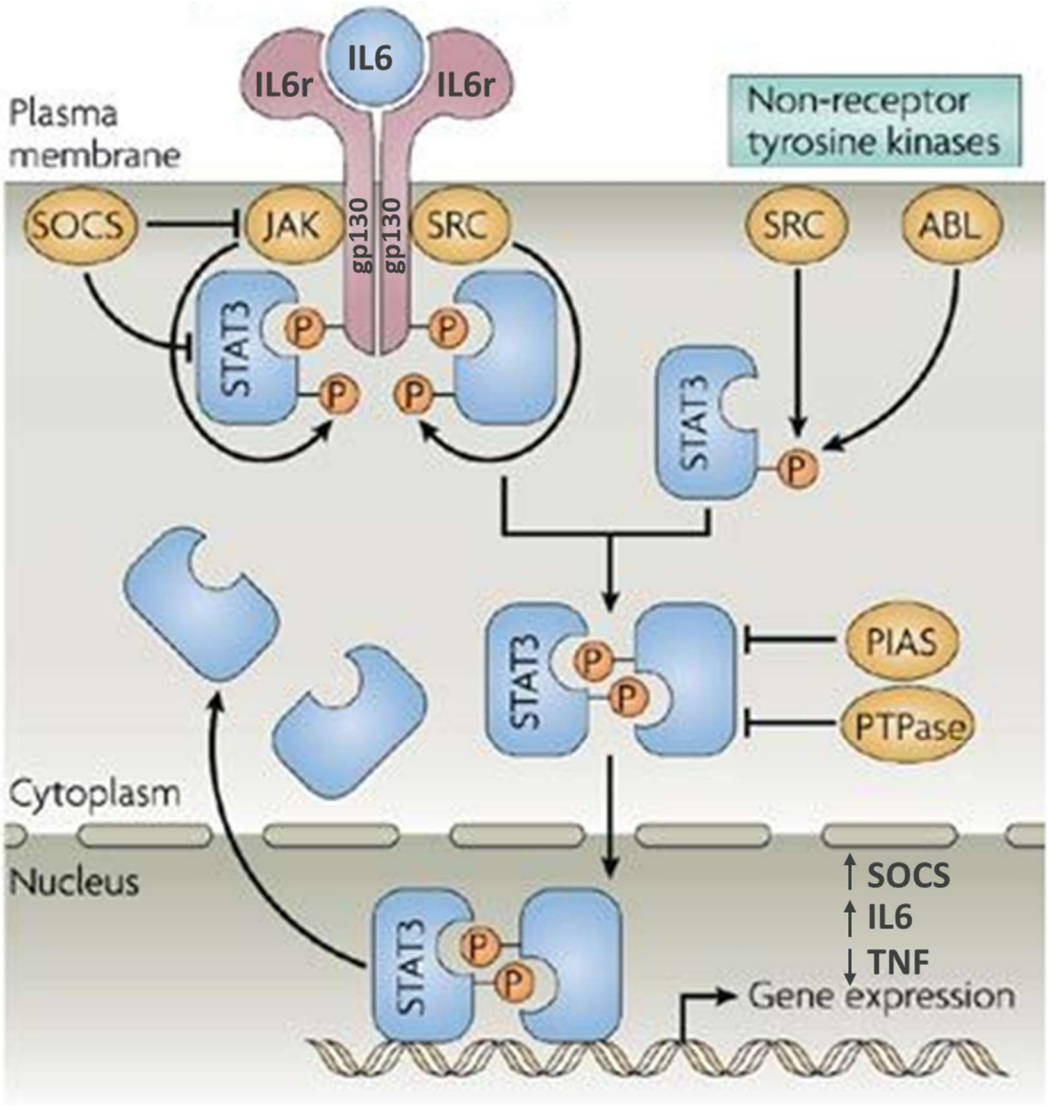

Figure 6-1: IL6 signalling cascade. IL6 initially binds to the non-signalling IL6 receptor, this complex binds to two molecules of gp130. Engagement of the IL6r to gp130 promotes a rearrangement of gp130 that leads to autophosphorylation of JAK and promotes the recruitment and phosphorylation of STAT3. STAT3 translocates to the nucleus and initiates/inhibits transcription of target genes. Image adapted from Yu *et. al.* (2007)[218].

6.1.1 STAT3 is phosphorylated by IL6 stimulation and by cytokines released upon HkEc challenge

STAT3 is the main transcription factor downstream of IL6/IL6r signalling. To investigate the role of IL6 in TNF regulation, IL6/STAT3 signalling was studied using agonists and inhibitors of STAT3. Firstly, THP-

1 cells stimulated with IL6 demonstrate STAT3 phosphorylation which peaks between 30 and 60 mins (Figure 6-2).

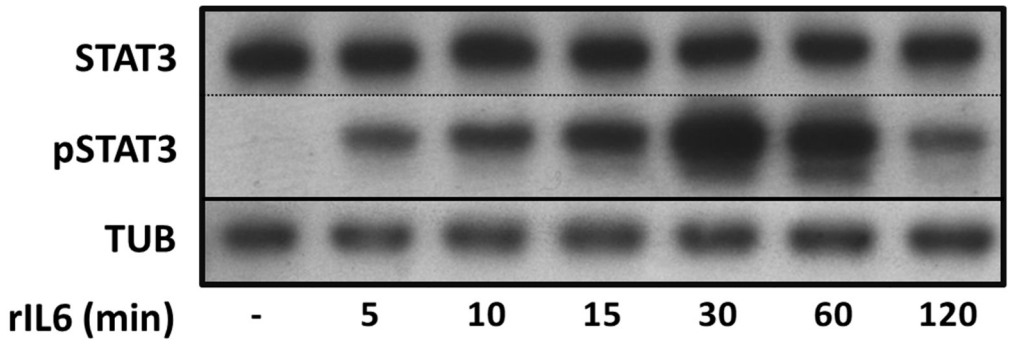

Figure 6-2: Phosphorylation of STAT3 was evaluated upon stimulation with 10 ng/mL of recombinant IL6. Phosphorylation was detected at 5 minutes and peaked at 30 minutes of IL6 stimulation. Results shown are representative of 2 independent experiments.

Secondly, STAT3 is phosphorylated upon HkEc stimulation (Figure 6-3). Since STAT3 is mainly activated downstream of cytokines-cytokine receptors interactions, brefeldin A was used to inhibit cytokines secretion and the phosphorylation of STAT3 was investigated in the early and late immune response (Figure 6-4).

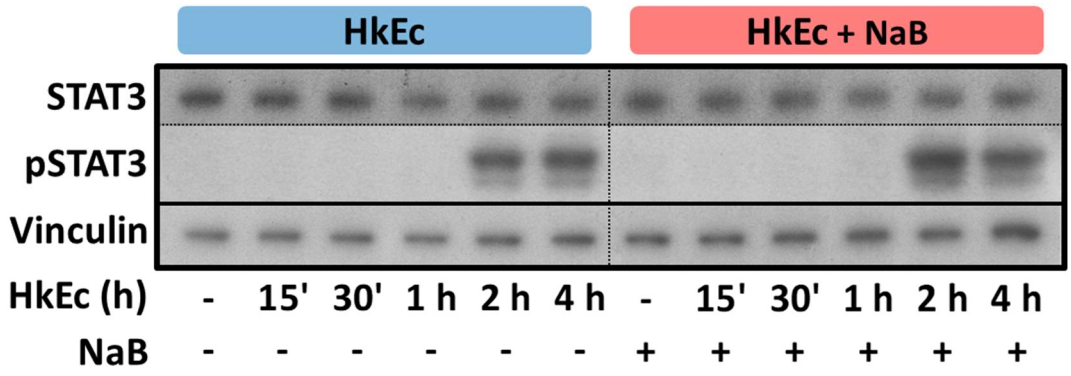

Figure 6-3: Phosphorylation of STAT3 is observed at 2 h HkEc stimulation, regardless the NaB exposure. Results shown are representative of 4 independent experiments.

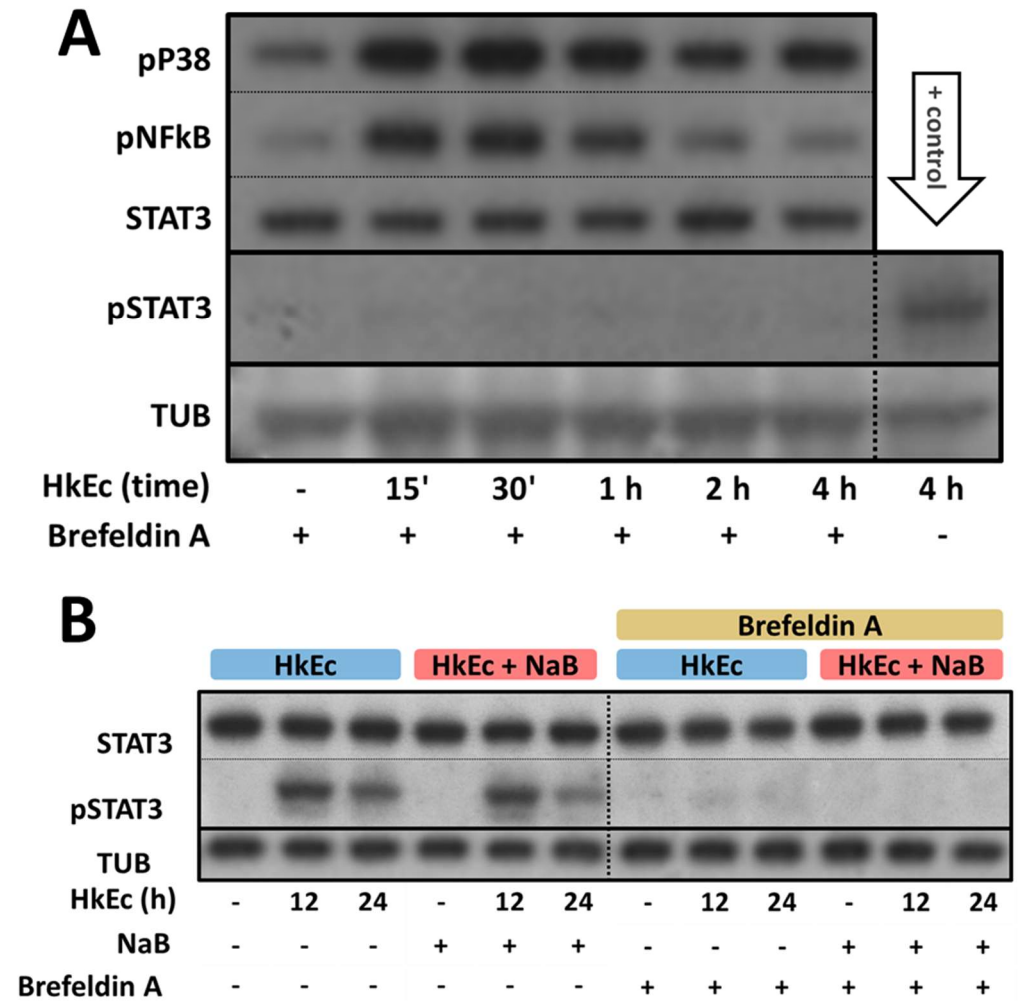

Figure 6-4: Blockage of cytokine secretion by brefeldin A inhibits STAT3 phosphorylation. Brefeldin A does not affect the signal directly downstream of TLR after HkEc stimulation, as observed by normal P38 and NFkB phosphorylation, but STAT3 activation is completely abolished in the short (A) and long-term (B). This suggests that STAT3 is indirectly activated upon HkEc stimulation, probably through the release of cytokines. Results shown are representative of 1 (A) and 3 (B) independent experiments.

In view of the fact that IL6 is first observed in the supernatant of HkEc-stimulated THP-1 cells at 6 hours (Figure 3-16) and the peak in STAT3-phosphorylation happens after 12 hours (Figure 6-4), the role IL6 plays in this response was investigated (Figure 6-5).

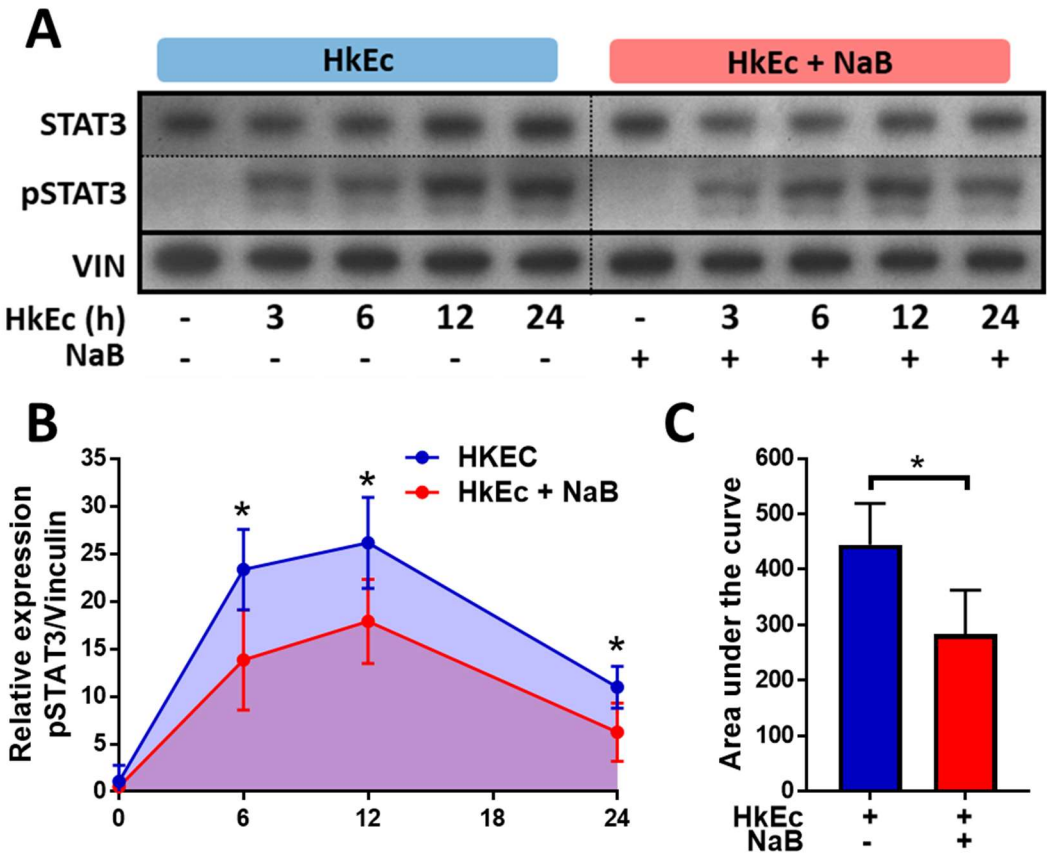

Figure 6-5: Phosphorylation of STAT3 was evaluated upon HkEc stimulation ± NaB over a 24 h period. Phosphorylation levels were found to be diminished with the inclusion of NaB at 6, 12 and 24 hours (A). This was confirmed when the cumulative levels of p-STAT3 were calculated (B and C). Results shown are representative of 4 independent experiments and shown as mean ± SEM, *p<0.05, **p<0.01, ***p<0.001, ****p<0.0001; (area under the curve; two-tailed, unpaired t-test).

6.1.2 STAT3 activation negatively regulates TNF induction and secretion

To investigate the participation of STAT3 signalling on TNF regulation, AG490, a JAK2 inhibitor that blocks the JAK/STAT3 signal, was used. The effect of IL6 on TNF release was also studied through the use of recombinant IL6 and a neutralizing anti-IL6 antibody.

Inhibition of STAT3 by AG490, led to an increase in gene expression and release of TNF and reduced secretion of IL6, while IP10 remained unchanged (Figure 6-6).

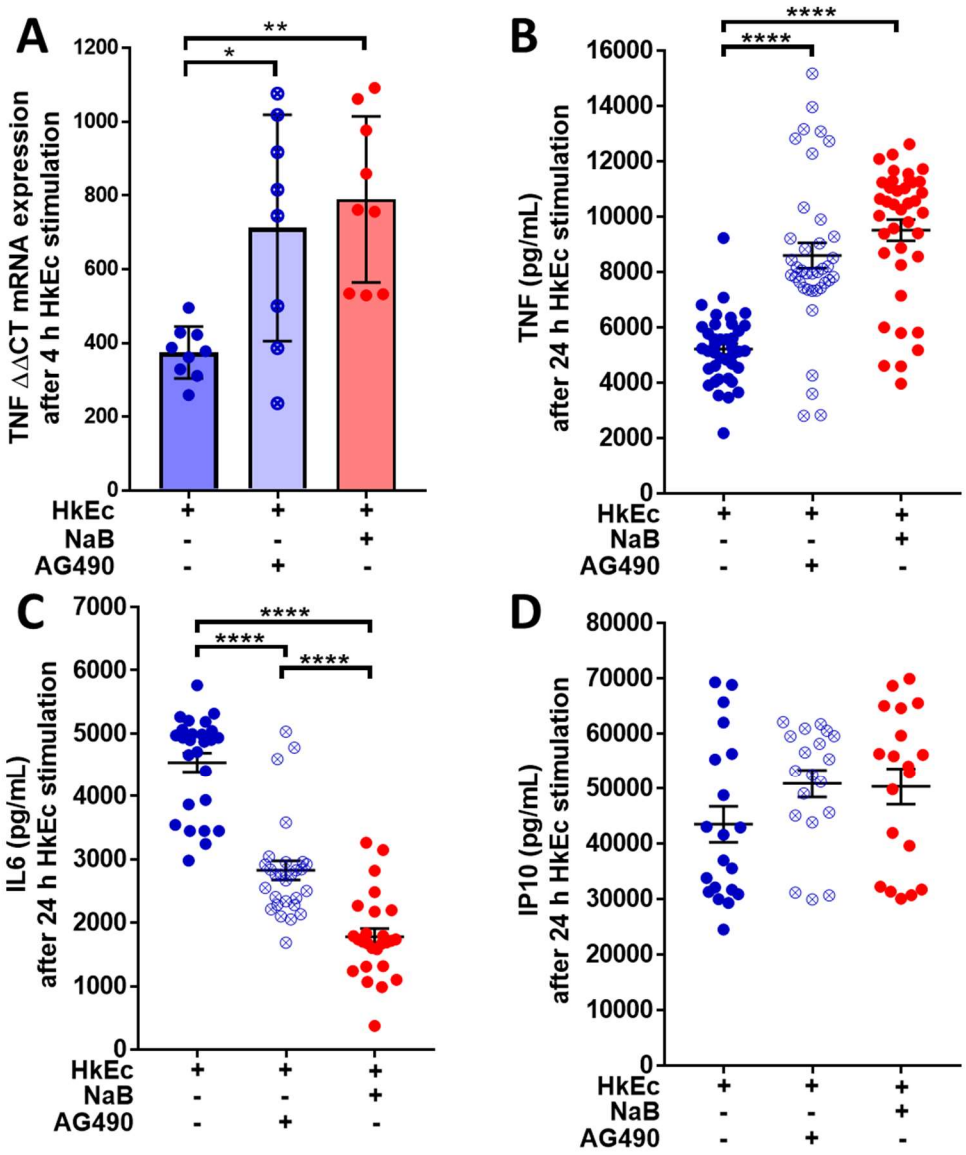

Figure 6-6: mRNA (TNF, A) and cytokine levels (B-D) after HkEc in combination with either NaB or AG490. STAT3 inhibition increased TNF gene expression (A) and cytokine secretion (B) to a similar level as observed with NaB. Furthermore, it reduced the levels of IL6 (C) and had no effect on IP10 secretion (D). Results shown are mean ± SEM, n= 3 (A) and n=5 (B-D) independent experiments and analysed using one-way ANOVA with Tukey's test (*p<0.05, **p<0.01, ***p<0.001, and ****p<0.0001).

Since the use of inhibitors may interfere with other cellular functions, the effect of IL6 on STAT3 activation and regulation of TNF was tested using a neutralization assay with an anti-IL6 antibody, which binds and sequesters the secreted IL6 by antigen/antibody reaction. The efficiency of the anti-IL6 antibody to bind to the cytokine was evaluated by measuring

the IL6 levels after HkEc stimulation (Figure 6-7A). Similar to the STAT3 inhibitor AG490, neutralization of IL6 by addition of an anti-IL6 antibody increased the release of TNF (Figure 6-7B).

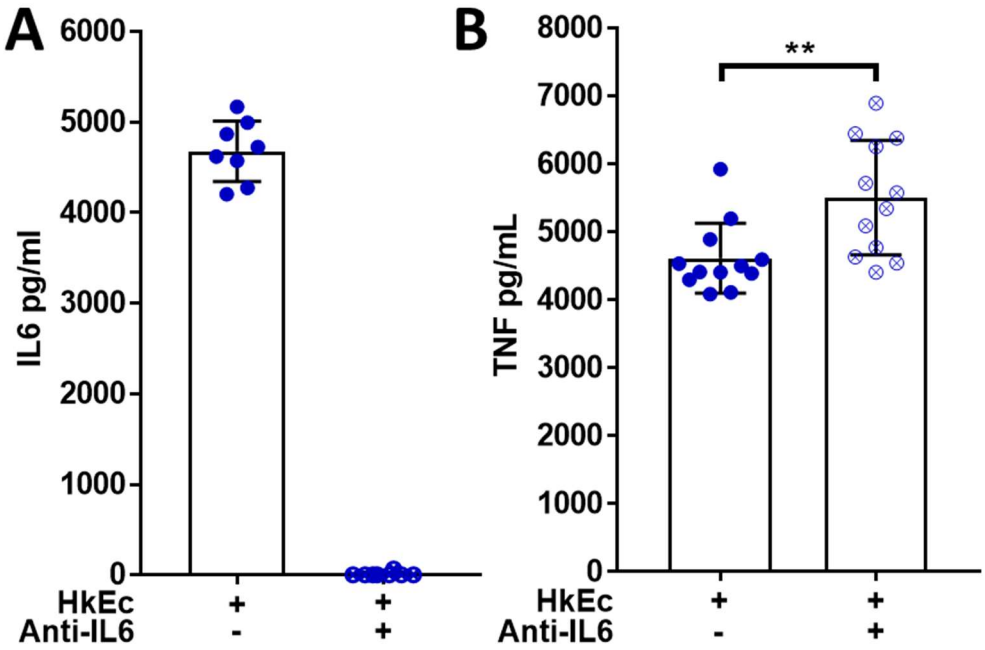

Figure 6-7: Neutralization of IL6 increases the levels of TNF. Neutralization of IL6 by an anti-IL6 antibody resulted in undetected levels of IL6 in the supernatant (A) and hypersecretion of TNF (B). Results shown are representative of 1 (A) and 2 (B) independent experiments and shown as mean ± SEM, *p<0.05, **p<0.01, ***p<0.001, ****p<0.0001; (two-tailed, unpaired t-test).

Finally, we investigated the effects of directly activating STAT3 through the inclusion of rIL6 on TNF secretion. Addition of rIL6 showed a reduction in TNF gene expression resulting in a level similar to HkEc alone, therefore normalizing the effect of NaB (Figure 6-8A). The half-life of recombinant IL6 in cell culture is very short. Five thousand picograms added to cell culture dropped to less than a half during the first 4 hours (Figure 6-8B). In order to evaluate the effects of IL6 in a way more similar to what happens in a normal condition, an experiment was designed with IL6 being added at the same time as HkEc stimulation or after 12 hours (IL6 ±) of bacterial challenge in the presence or absence of NaB (Figure 6-8C). The total time of HkEc stimulation was 24 h in all cases. Addition of IL6 after 12 hours of HkEc stimulation was chosen because it simulates

what was seen in IL6 dynamics (Figure 3-16G), which showed a boost in its secretion between the period from 12 h to 24 h.

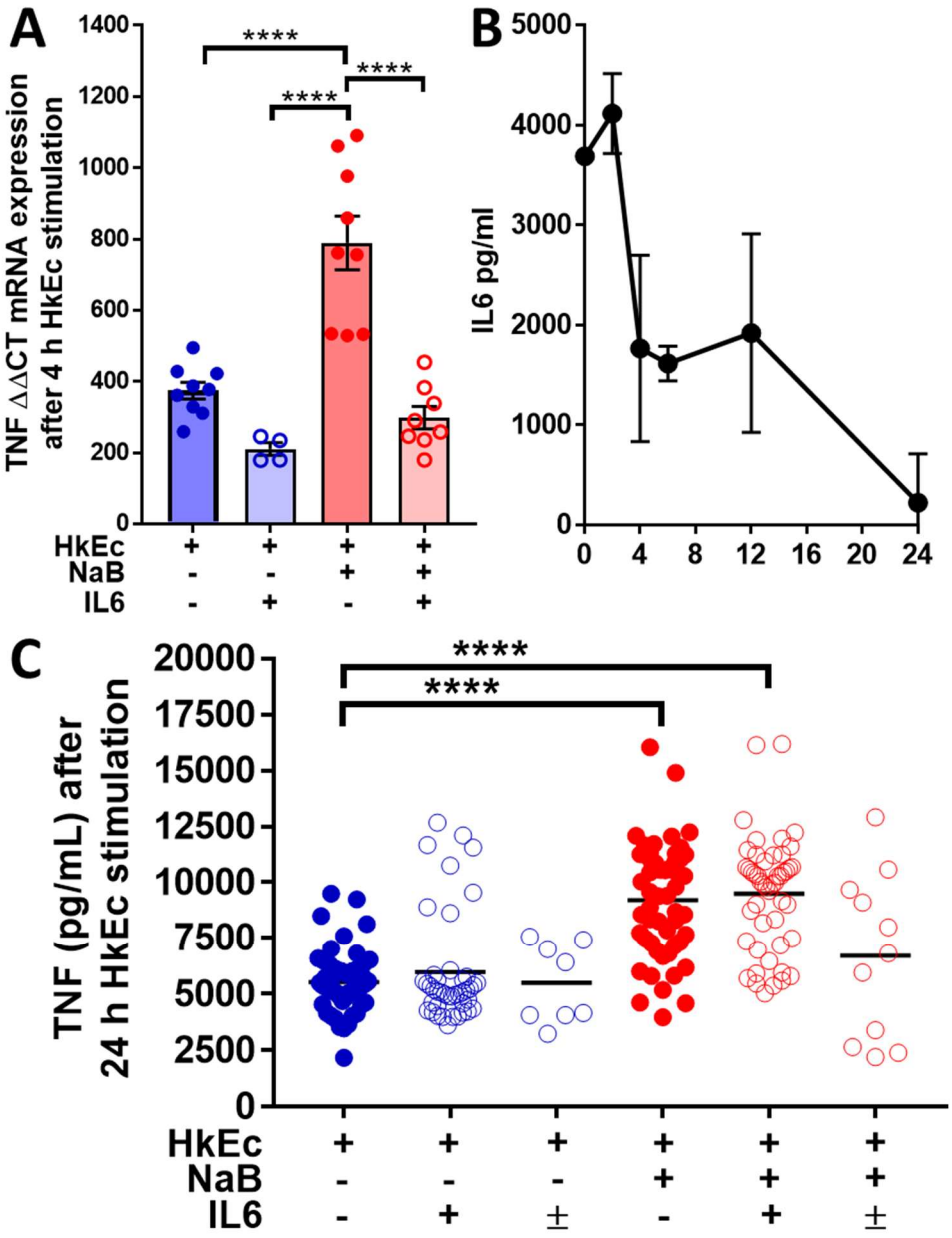

Figure 6-8: Effects of recombinant IL6 in TNF response. Co-stimulation of 10 ng/mL of IL6 with HkEc brought the elevated levels of TNF mRNA induced by NaB back to normal (A). IL6 showed a short half-life in THP-1 culture, more than half of the initial dose of 5000 pg/mL added to the cell culture could not be detected anymore at 4 hours, dropping to almost zero at 24 hours. Addition of IL6 at the same time of HkEc stimulation (IL6 +), does not change the levels of TNF after 24 hours, probably due to its short life in cell culture. However, when IL6 was added later at 12 hours (IL6 ±), TNF levels were brought to normal levels observed without NaB exposure (C). Results shown are mean ± SEM, n= 3 (A), n=1 (B) and n=3 (C)

independent experiments and analysed using one-way ANOVA with Tukey's test (*p<0.05, **p<0.01, ***p<0.001, and ****p<0.0001).

6.2 Discussion

In Chapter 5, it was shown that there is a hyper-active TNF response to HkEc stimulation and NaB exposure. Although it can explain the initial high levels of TNF, TNF remains elevated for a longer period in NaB treated samples and do not show a similar reduction rate than the one observed in HkEc only. It led us to investigate a second mechanism that would add to the one previously described. This mechanism would be related to IL6 deficiency and impaired STAT3 signalling.

In this chapter, it was shown that STAT3 signalling downstream of IL6r binding negatively regulates TNF secretion. Firstly, we demonstrated STAT3 phosphorylation upon IL6 stimulation. Secondly, STAT3 can be activated not only by IL6 but for other cytokines secreted by the cell. STAT3 phosphorylation is observed at 2 h (at this time, no IL6 has been produced by THP-1 cells) after HkEc stimulation and this signal is unaffected by NaB. Brefeldin A, a potent inhibitor of cytokine secretion, completely abolishes STAT3 phosphorylation at an early and late stage, while preserving a normal signal downstream of TLR activation. We have provided convincing evidence of activation of STAT3 by cytokines occurs by autocrine/paracrine stimulation and not by any other signal.

Yoon *et. al.* proposed a mechanism of activation of STAT3 by ROS and autophagy, which would induce IL6 secretion and could be inhibited by knockdown of $P22^{phox}$ and antioxidants[219]. Our results support exactly the contrary, ROS induce IL6 secretion and IL6 (and other cytokines) thus activate STAT3. Blockage of cytokine secretion completely inhibits STAT3 activation.

The STAT3 inhibitor AG490 increased the message and the secretion of TNF in HkEc stimulated cells. Neutralization of IL6 by an IL6 antibody had a similar effect to AG490 in reducing TNF secretion. On the other hand, IL6 negatively regulated TNF at both, the message and protein level.

Thirdly, NaB-induced IL6 deficiency attenuates the activation of STAT3 at later stages (6-24 h) of the immune response. Several studies support the role of STAT3 in controlling inflammation induced by TLR stimulation[216,220,221,222,223]. In human monocytes, STAT3 activation reduces TNF production induced by LPS through IL10/STAT3 signalling[216,221]. Cardiomyocytes from mice with restricted STAT3 knockout showed higher levels of TNF than wild-type controls upon LPS stimulation[222]. Here we showed that IL6 rather than IL10 (which was secreted only in very small concentrations - see Figure 3-3) seemed to exert some type of control in TNF regulation through STAT3 activation.

Chapter 7 Quantitative proteomic profiling of THP-1 cells stimulated with LPS and NaB

7.1 Introduction

THP-1 is a human monocytic cell line that can be differentiated in macrophages. The classical monocyte-macrophage differentiation inducer is PMA, but other stimulants, such as LPS and HkEc, can also induce differentiation as shown in Figure 3-1. Activation of THP-1 cells with LPS or HkEc stimulation stops cell proliferation (Figure 3-2) and differentiate them into a pro-inflammatory phenotype (Figure 3-16 and 3-20). This activation leads the cell to undergo maturation into macrophage-like cells, which upregulate membrane receptors such as ICAM-1 and CD80/CD86 and synthesizes pro-inflammatory cytokines[224].

To have a better understanding of the overall changes caused by LPS stimulation and the effects of NaB, two quantitative proteomic profiles of THP-1 cells were carried out, one to evaluate the dynamic changes in a time course with LPS stimulation, and another with samples stimulated for 0 (untreated), 12 and 24 h in the presence or absence of NaB using LC-MS/MS. This is an ongoing study in collaboration with Professor Lilley and Dr Mulvey (University of Cambridge). Data analysis is not completed yet and extra experiments will be added to support the findings.

7.2 LPS stimulation decreases the levels of proteins related to the cell cycle and increases proteins associated with innate immunity

THP-1 cells were stimulated with LPS from *Salmonella abortus equi* S-form, which is a smooth form of LPS. This smooth LPS requires TLR4 internalization and is CD14-dependent (see section 1.3.2.2), leading to a type I interferon response through TRIF signalling pathway.

THP-1 cells were stimulated with 200 ng/mL of LPS for 0 (untreated), 2, 4, 6, 12, 24 hours. This investigation led to the identification of 4292

proteins with 556 proteins (≈13%) regulated by LPS. The biggest fold changes happened between 0 and 24 hours. Statistical analysis was based on p-value calculated between 0 and 24 hours and adjusted for a false discovery rate using the method of Benjamini–Hochberg[158], with a q value=0.05 (Figure 7-1).

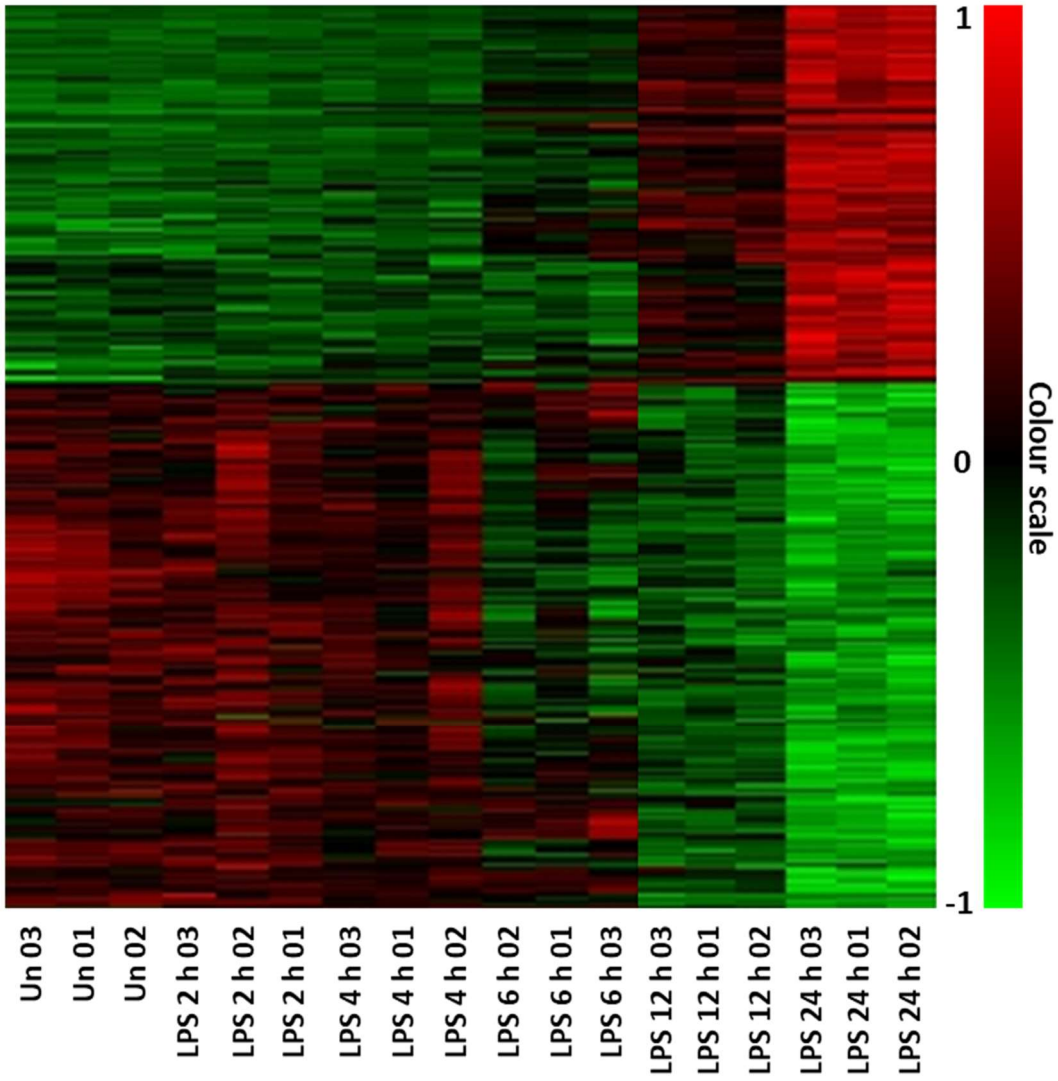

Figure 7-1: Heatmap of 556 differentially expressed genes influenced by LPS stimulation (adjusted p<0.05). Most of the changes happened between 12 and 24 hours with 322 proteins downregulated and 234 upregulated proteins.

The heatmap showed that the biggest changes occurred between untreated and 24 h stimulation, with 2 and 4 h showing a similar profile to untreated, 6 h presented a transitional stage, and 12 h was almost similar to 24 h. Due to these results, all subsequent analysis were conducted between untreated and 24 h stimulated groups.

The proteins regulated by LPS stimulation were split into upregulated or downregulation and submitted to cluster analysis of biological processes on STRING website (Figures 7-2 and 7-3)[225].

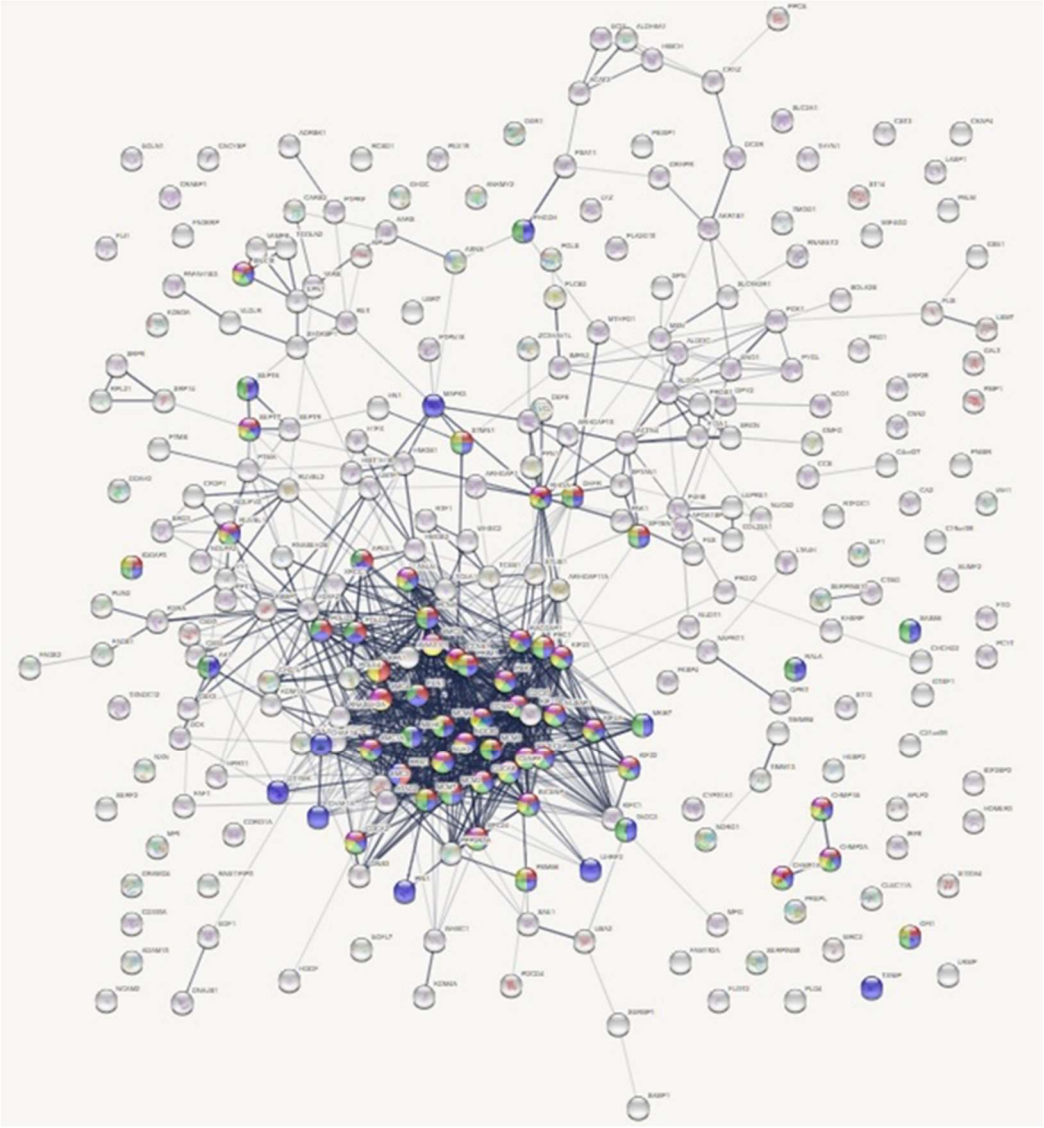

Figure 7-2: Cluster analysis of proteins down-regulated by LPS stimulation. The top five clusters of biological processes with the lowest p-value were associated with the cell cycle (mitotic cell cycle process, mitotic cell cycle, mitotic nuclear division, cell division, cell cycle process). Coloured spheres are related to one of the five clusters and many of them were involved in three or more clusters. Image generated on STRING website.

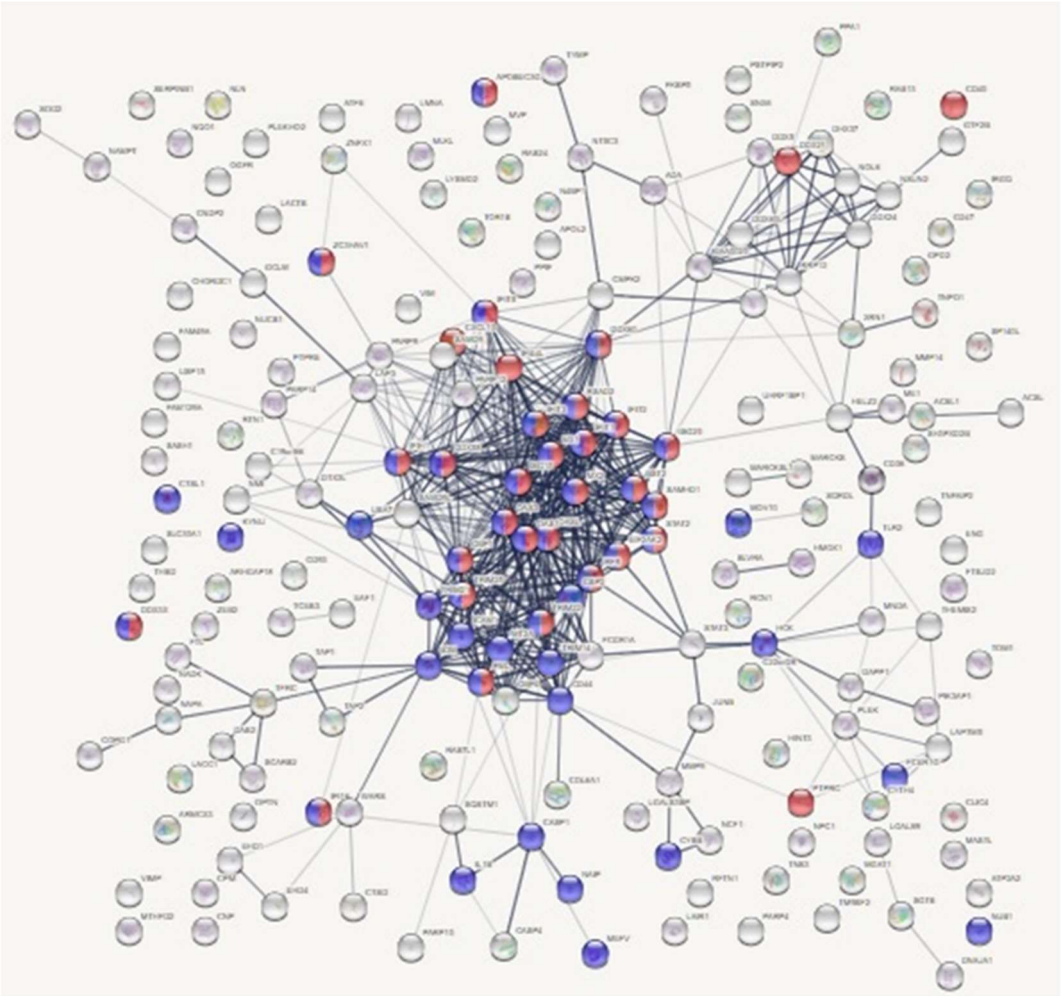

Figure 7-3: Cluster analysis of proteins upregulated by LPS stimulation. There were two main clusters identified in the upregulated group: response to virus with 33 proteins and a p-value $4.22E^{-26}$ (red spheres) and innate immune response (49 proteins, p-value $2.8E^{-21}$, blue spheres). Image generated on STRING website.

Taking the results of Figures 7-2 and 7-3 together, LPS stimulation mainly caused a reduction in the cell cycle, which is expected during monocyte/macrophage differentiation and triggered the immune response, especially by activating the TRIF pathway leading to a type I interferon response, a usual response observed in viral infection.

To validate the findings of the proteomics data, western blots were carried out for the proteins optineurin (OPTN gene) and P62 (SQSTM1 gene), which were chosen because of their strong up-regulation induced by LPS stimulation (Figure 7-4).

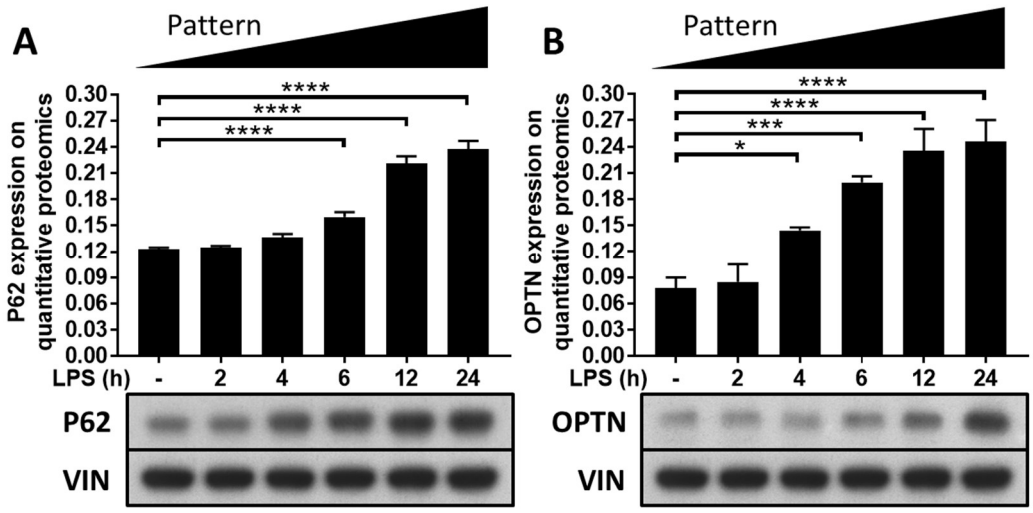

Figure 7-4: Validation of proteomics data by western blot. The bar graphs are related to protein quantification by proteomics samples. Both proteins, P62 (A) and optineurin (B), showed a similar pattern with an increasing expression over time. Results shown in the immunoblots are of an individual experiment. The results of a single experiment are limited to establish a proper cause-effect of the experimental conditions.

Optineurin and P62 expression increased after LPS stimulation in the proteomic analysis and these results matched with the expression of the same proteins in immunoblots.

Since the majority of the changes were observed between untreated samples and LPS stimulation for 12 and 24 hours, these time points were chosen for studying the effects of NaB, but to reduce the size of the thesis, the 12 hours samples were not included in further analysis.

7.3 NaB attenuates the overall response to LPS and affects the amino acid metabolism

In a repeated experiment, untreated and 24 h LPS stimulated ± NaB were analysed in triplicate. LPS stimulation resulted in an alteration in 762 out of 6865 proteins with 473 proteins downregulated and 289 proteins regulated with a cut off adjusted p-value <0.05.

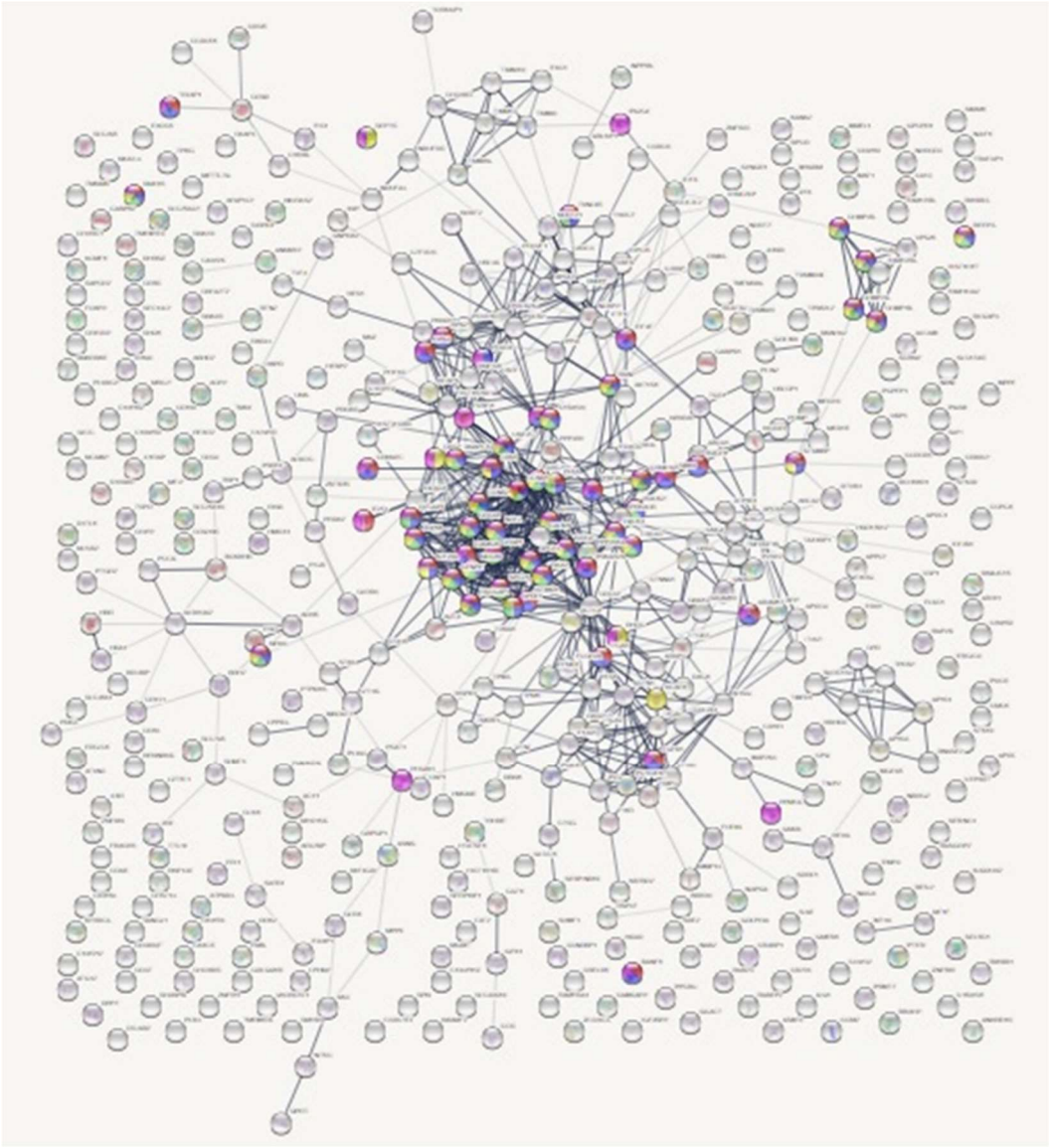

Figure 7-5: Cluster analysis of proteins down-regulated by LPS stimulation. The top five clusters of biological processes with the lowest p-value were associated with the cell cycle (mitotic cell cycle process, mitotic cell cycle, mitotic nuclear division, cell division, cell cycle process). Coloured spheres are related to one of the five clusters and many of them were involved in three or more clusters. Image generated on STRING website.

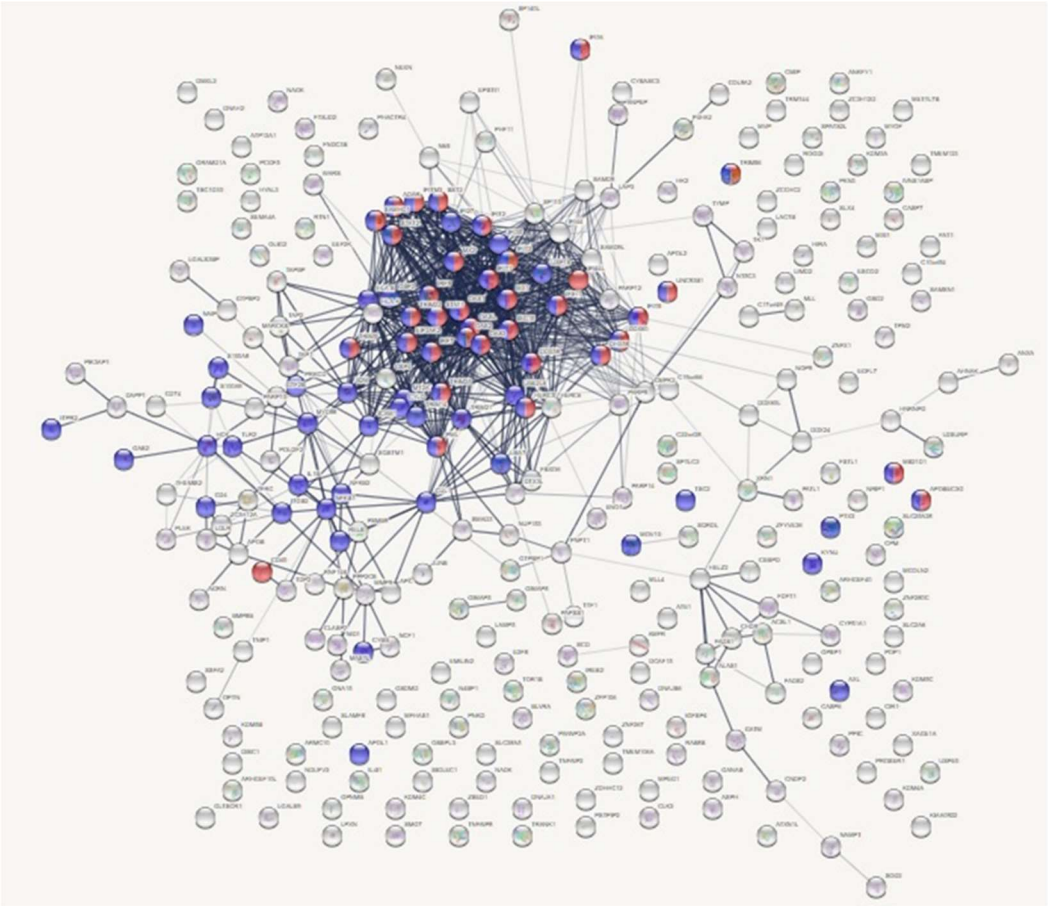

Figure 7-6: Cluster analysis of proteins up-regulated by LPS stimulation. Up-regulated proteins were less abundant and clustered in a response to virus and innate immunity. Image generated on STRING website.

The response to LPS stimulation in this repeated experiment was very similar to that previously observed and explained in Figures 7-2 and 7-3. It is important to note that TNF was not detected in any of the proteomics samples. It is because TNF is not stored within the cell as shown in Figures 3-24 and 3-25. Without any agent to trap the TNF inside the cell (e.g. Brefeldin A), only a small amount of TNF is found within the cell, which seems to be below the detection limit of the proteomic study.

In order to restrict the analysis and focus on the most significant changes, the p-value was reset to <0.01 in the volcano plot (Figure 7-7)

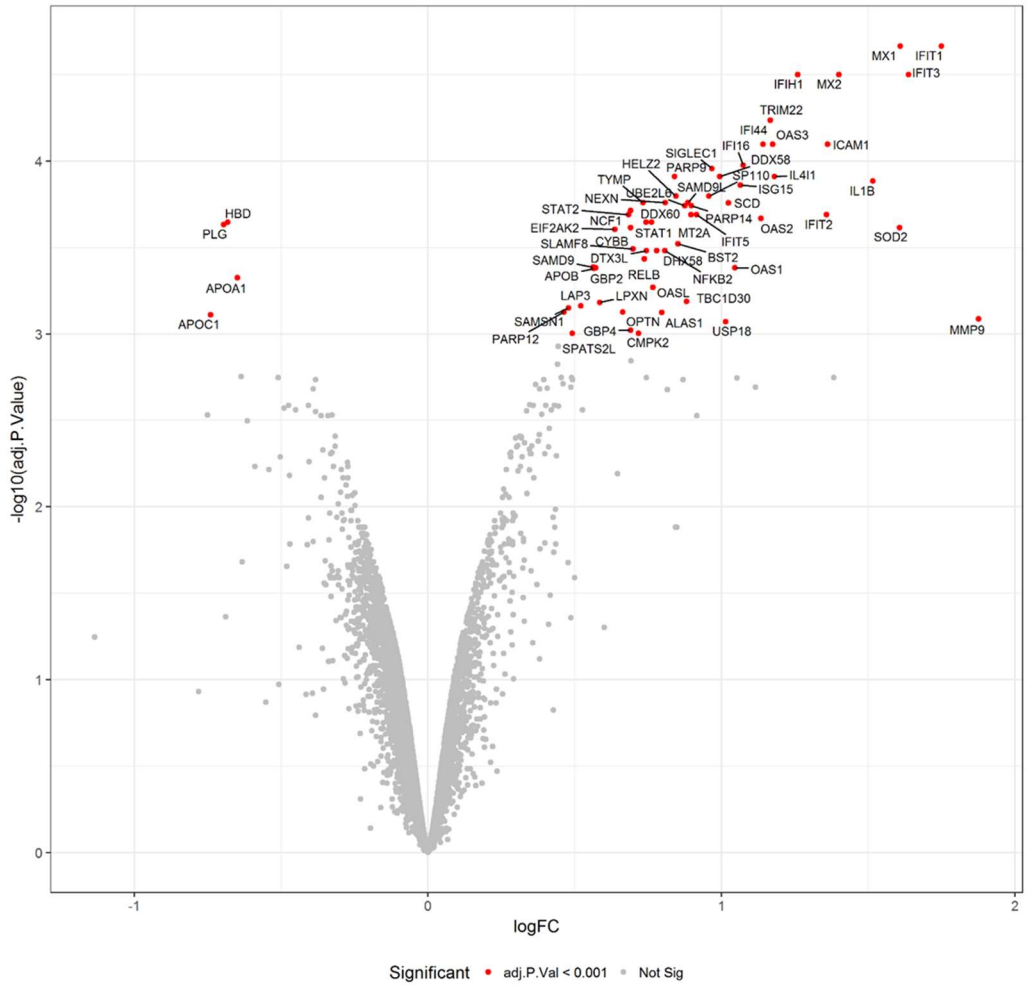

Figure 7-7: Volcano plot showing the changes in protein expression upon LPS stimulation for 24 h. There were 58 proteins upregulated and only 4 were found to be reduced after LPS stimulation. Proteins were labelled based on an adjusted p-value <0.001 (grey dots, not significant; red dots, statistically significant).

To evaluate the functional implication of these proteins, a cluster analysis was carried out and showed the main proteins were related to virus defence and innate immunity (Figure 7-8).

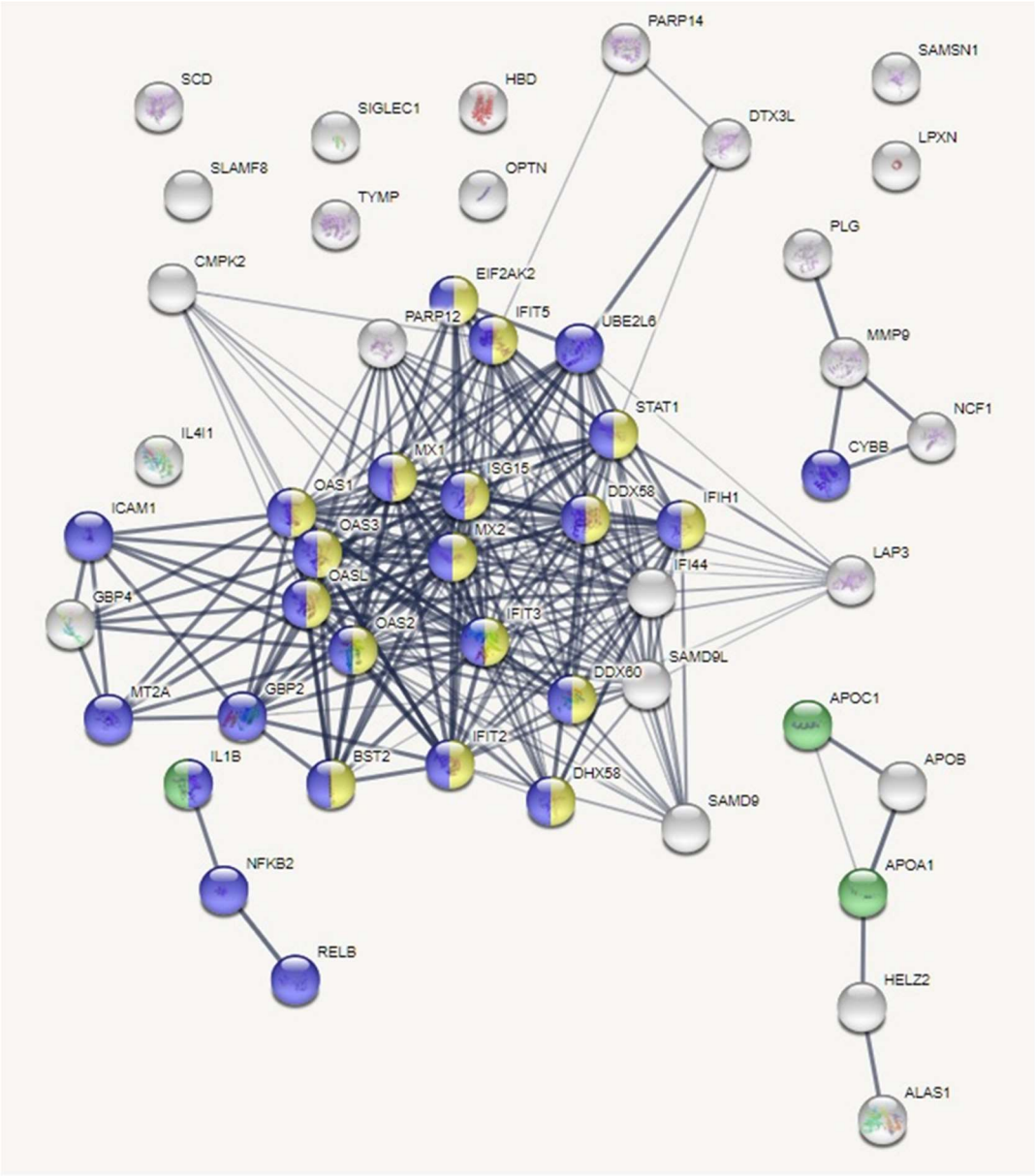

Figure 7-8: Cluster analysis of proteins regulated by LPS stimulation. Two clusters dominated most of the proteins with high interactions, defence to virus with 17 proteins and a p-value $1.87E^{-20}$ (yellow spheres) and innate immune response (25 proteins, p-value $5.37E^{-18}$, blue spheres). All were upregulated. On the other hand, 2 out of 4 proteins down-regulated by LPS were involved in regulation of lipid catabolic process (APOA1 and APOC1, green spheres. Image generated on STRING website.

Similarly to what was observed in the previous analysis (Figures 7-3 and 7-6), using a more restricted p-value (>0.001), the predominant responses to LPS was related innate immunity and response to virus.

NaB in combination with LPS caused fewer changes in protein expression compared to LPS alone, with only 27 proteins up-regulated and none down-regulated (Figure 7-9). All of the up-regulated proteins resulting

from the inclusion of NaB were also elevated in the LPS alone dataset. Cluster analysis showed proteins related to virus defence and innate immunity similar to LPS alone (Figure 7-10).

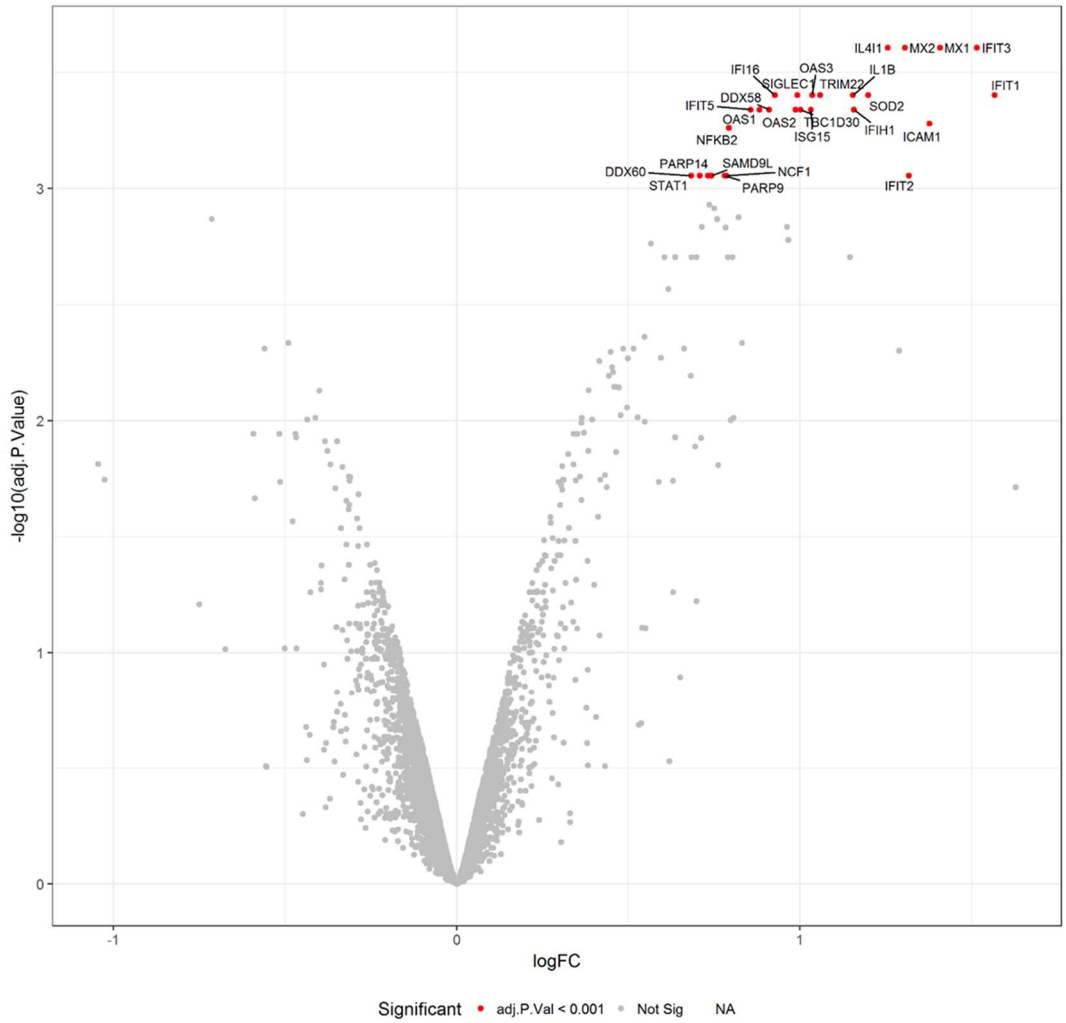

Figure 7-9: Volcano plot showing the changes in protein expression in NaB treated samples upon LPS stimulation for 24 h. There were 27 proteins regulated by LPS stimulation with all of them overexpressed. The cut off was set based on an adjusted p-value <0.001 (grey dots, not significant; red dots, statistically significant).

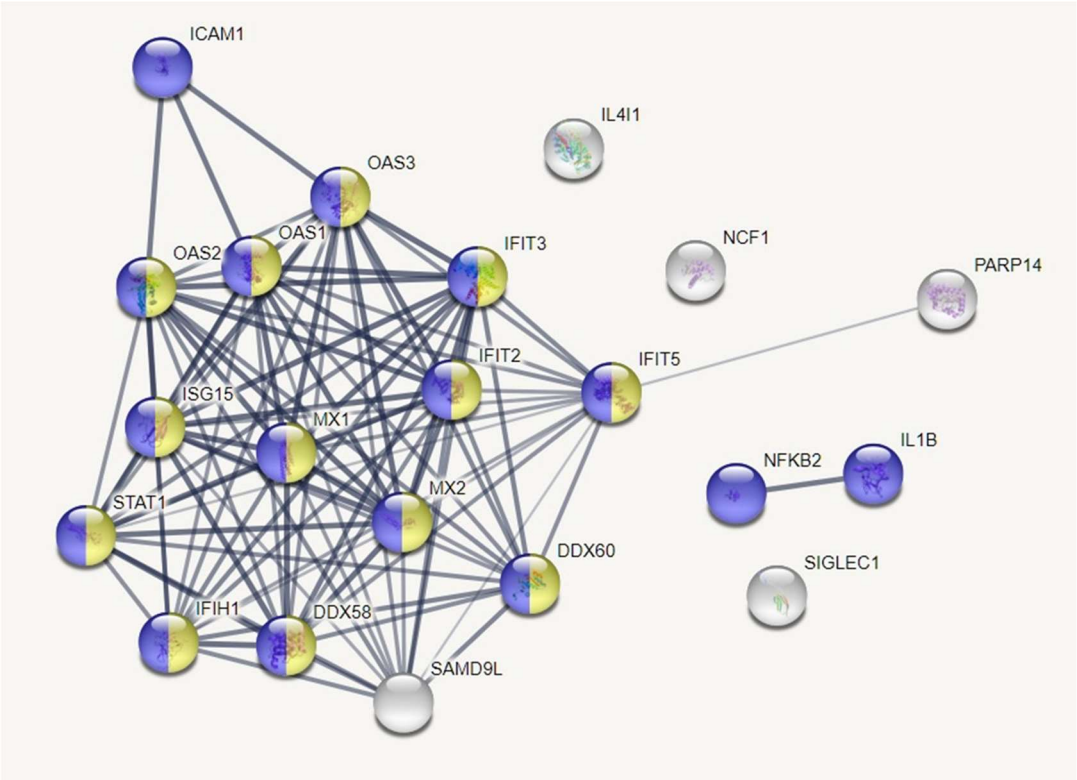

Figure 7-10: Cluster analysis of proteins regulated by LPS stimulation upon NaB exposure. Two clusters dominated most of the proteins with high interactions, defence to virus with 13 proteins and a p-value $3.04E^{-19}$ (yellow spheres) and innate immune response (16 proteins, p-value $2.58E^{-15}$, blue spheres), with all proteins upregulated. Image generated on STRING website.

LPS stimulation in combination with NaB exposure caused a similar but attenuated response than that observed with LPS alone.

To analyse the effect of NaB itself on THP-1 cells, untreated THP-1 cells were compared with cells exposed to NaB only (Figure 7-11). Only one cluster with a p-value <0.05 was identified in the NaB exposed dataset and was related to biosynthesis of amino acids (Figure 7-12).

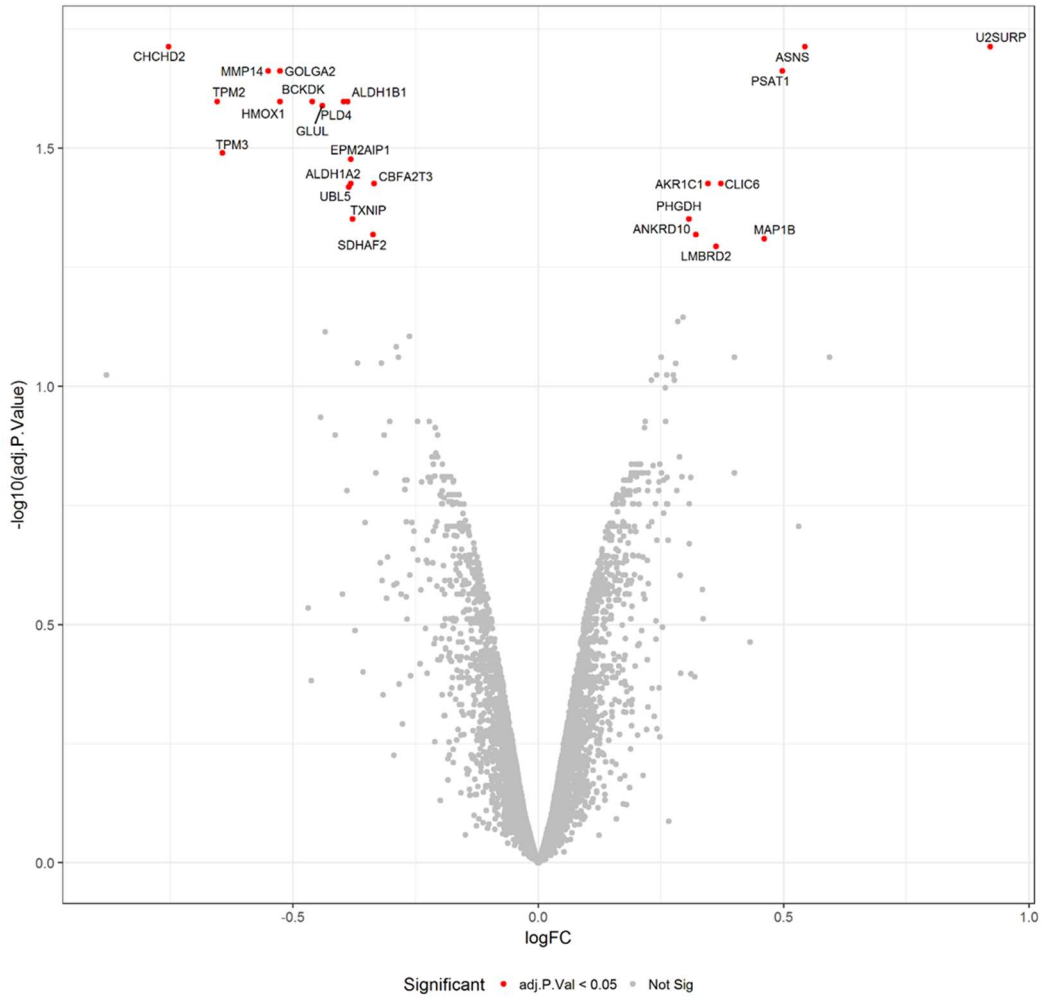

Figure 7-11: Volcano plot showing the changes in protein expression due to NaB exposure. Cells were incubated with or without 5 mM NaB for 24 h. There were 24 proteins regulated by NaB exposure, 16 downregulated and 8 upregulated. The cut off was set based on an adjusted p-value <0.05 (grey dots, not significant; red dots, statistically significant).

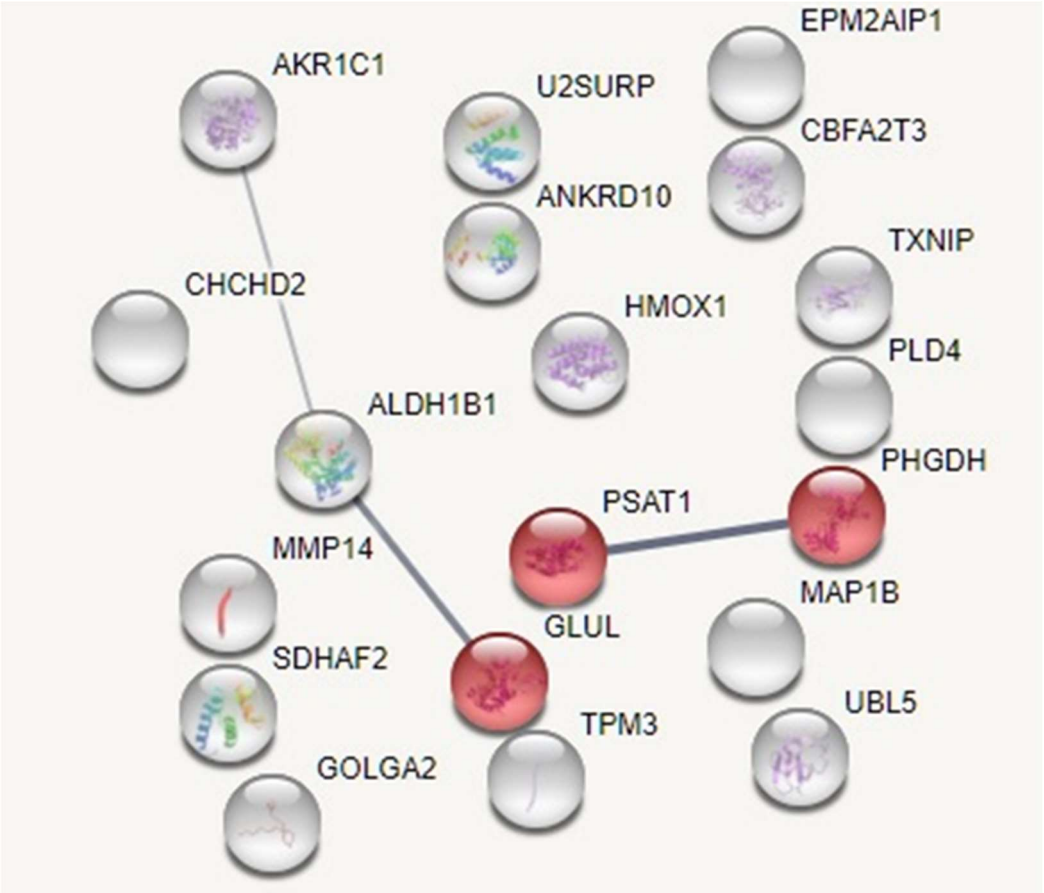

Figure 7-12: Cluster analysis of proteins regulated by NaB exposure. A single cluster related to biosynthesis of amino acids (red spheres) was found with a p-value <0.05. PSAT1 and PHGDH were up, while GLUL downregulated. Image generated on STRING website.

NaB exposure led to a predominant down-regulation in proteins levels detected by mass spectrometry. When these down-regulated proteins were investigated further, only one cluster was found, which was related to amino acid biosynthesis. These proteins will be better investigated later in this chapter.

Next, the effect of NaB was evaluated in combination with LPS stimulation (Figures 7-13 and 7-14).

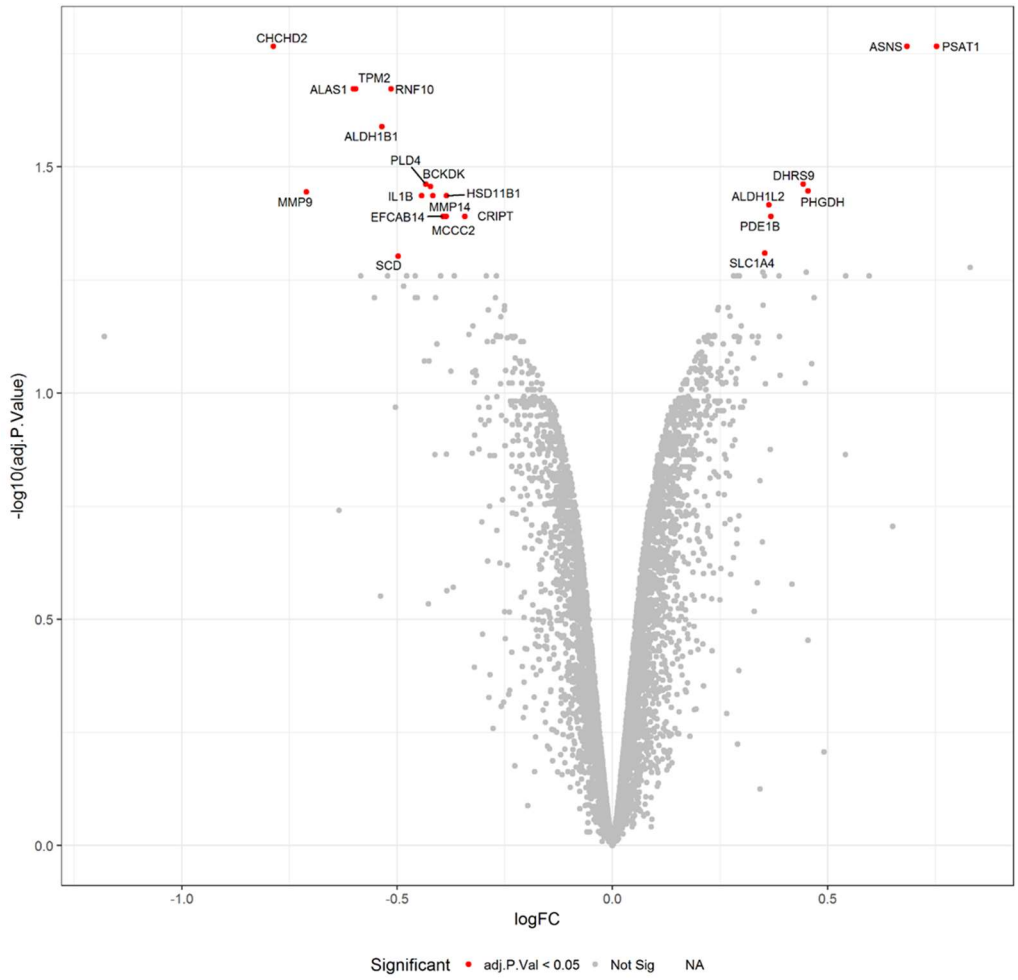

Figure 7-13: Volcano plot showing the changes in protein expression due to NaB exposure upon LPS stimulation. Cells were incubated with 5 mM NaB for 24 h. There were 24 proteins regulated by NaB exposure, 16 downregulated and 8 upregulated. The cut off was set based on an adjusted p-value <0.05 (grey dots, not significant; red dots, statistically significant).

The proteomics data showed that IL1β was upregulated on stimulation with LPS (Figure 7-9) and NaB exposure impaired its synthesis (Figure 7-13). This results in a decreased secretion of IL1β as shown in Figure 3-20A, which links these findings in the proteomics to a functional consequence of NaB exposure. Other proteins that show a similar pattern are part of the matrix metallopeptidase (MMP) family, MMP9 and MMP14, MMP9 is upregulated after LPS stimulation and comparison with NaB treated samples showed a reduction in these two metalloproteases, which are known to play a role in inflammation and innate immunity.

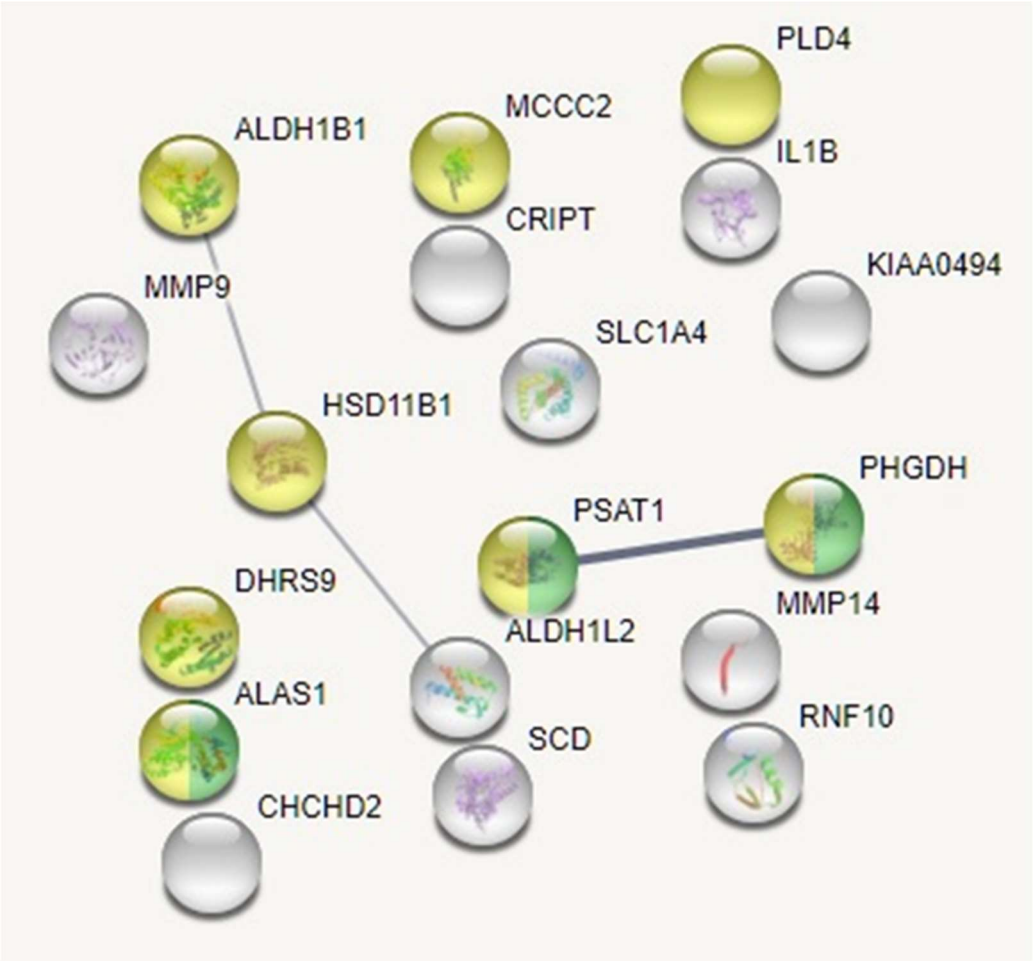

Figure 7-14: Cluster analysis of proteins regulated by NaB exposure upon 24 h LPS stimulation. Metabolic pathways dominated the clusters. The glycine, serine and threonine metabolism showed 3 proteins (green spheres, p-value 0.000735) and metabolic pathways (8 proteins, p-value 0.000735, yellow spheres). Image generated on STRING website.

PSAT1 deficiency has been associated with human diseases such as phosphoserine aminotransferase deficiency[226] and Neu-Laxova Syndrome 2[227]. PSAT1 is a protein involved in the synthesis of L-serine from 3-phospho-D-glycerate. L-serine synthesis has three steps: step 1 involves the D-3-phosphoglycerate dehydrogenase (PHGDH); step 2, PSAT1 and step 3, phosphoserine phosphatase (PSPH) (Figure 7-15A). All three proteins were upregulated upon NaB exposure regardless LPS stimulation (Figure 7-15B-D).

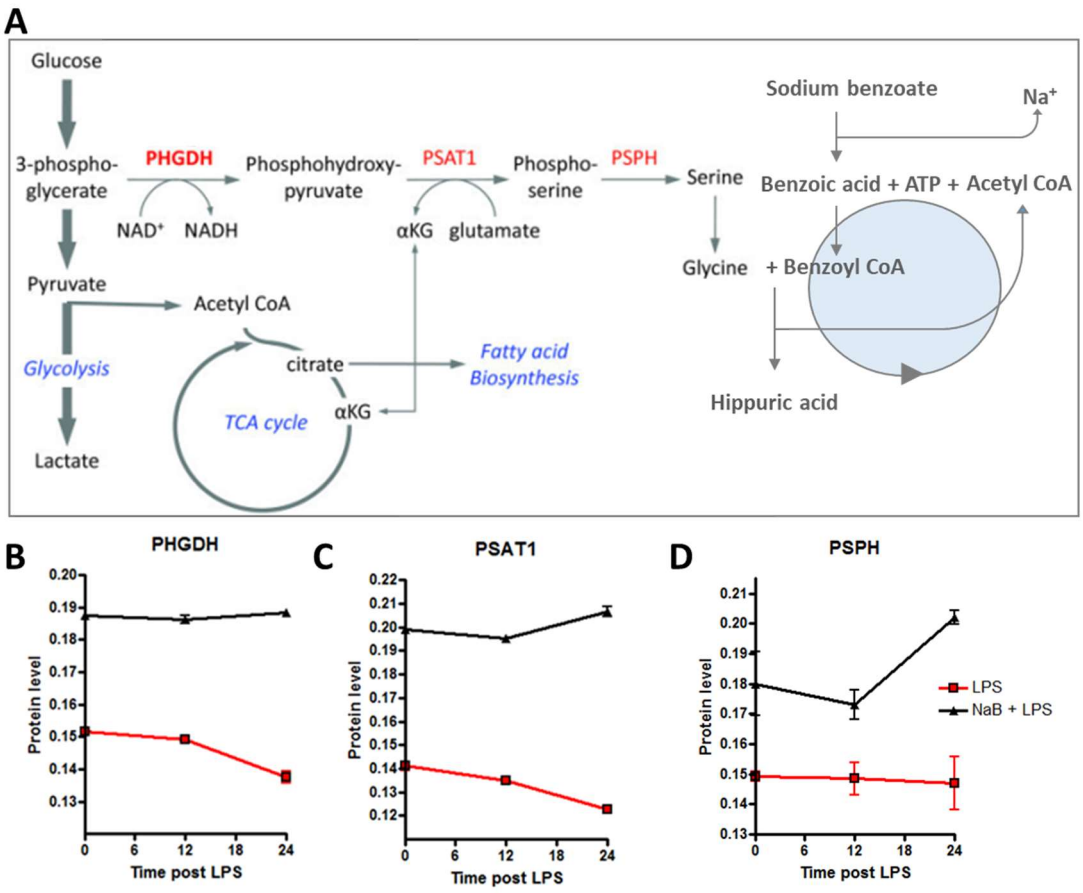

Figure 7-15: Proteins involved in the serine biosynthetic pathway (A) PHGDH, PSAT1, and PSPH are regulated by NaB exposure. PHDG, PSAT1, and PSPH were overexpressed in NaB samples, these proteins are responsible for step 1-3 in L-serine synthesis subpathway, respectively (B-D). Image adapted from Luo, J (2011)[228].

PSAT1 was found reduced in all NaB treated samples since they were pre-incubated for 24 h prior stimulation. To evaluate the expression of PSAT1, THP-1 cells were exposed to NaB and analysed by western blot (Figure 7-16).

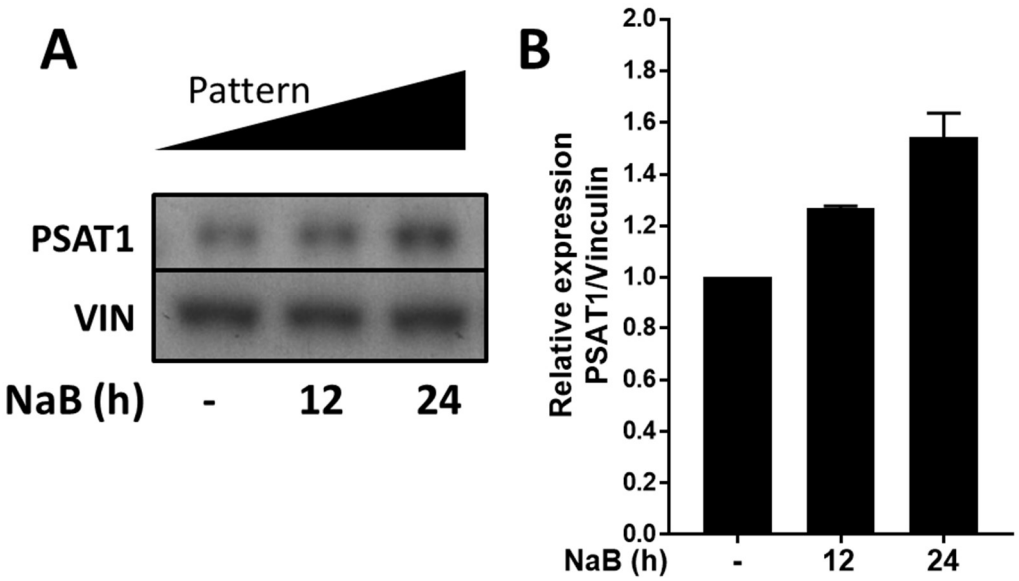

Figure 7-16: Expression of PSAT1 was investigated by western blot upon NaB treatment. PSAT1 expression increases after NaB exposure (A). Protein quantification showed a continuous increase in PSAT1 expression over 24 h. Results shown are representative of 2 independent experiments.

Studies in human volunteers and animal models have demonstrated that administration of NaB leads to NaB metabolism to hippuric acid[104,105,106], which here can be translated by elevation of all three main proteins involved in the serine biosynthetic pathway: PHGDH, PSAT1, and PSPH. It suggests that NaB exposure alters the cell metabolism requiring more efforts to its breakdown.

Changes in cellular metabolic pathway showed the highest number of proteins regulated by NaB in LPS-stimulated cells (Figure 7-14). It was also shown that stimulation with LPS leads the cell to produce proteins related to innate immunity, with just 4 proteins downregulated during this process and two of them, the APOA1 and APOC1, involved in a lipid catabolic process.

7.4 Discussion

To my knowledge, this is the first ever study using quantitative proteomics to study the global response of cells to NaB. Our preliminary analysis has provided evidence to support the notion that NaB can alter

the metabolic processes of immune cells and also impact on the overall immune response to LPS stimulation. In addition, I have also been able to characterise the change in the proteome of THP-1 cells upon sLPS exposure, which has provided a crucial information on how these cells adapt their proteins in order to respond to the antigenic challenge. The quantitative proteomics reflected a number of known alterations in monocyte to macrophage differentiation such as a down-regulation of many proteins associated with the cell cycle and the up-regulation in classical differentiation markers[229]. These findings provide some confidence that the use of mass spectrometry and TMT multiplex labelling can provide quantitative results, which are reliable and reproducible.

NaB exposure without an immune challenge does not cause THP-1 cells differentiation or activation. Only a few random proteins were affected by NaB exposure and were related to its metabolism. The response to LPS was dominated by the up-regulation of proteins related to the innate immunity reinforcing the immune competence of THP-1 cells[230].

Another important finding was the up-regulation of proteins related to the anti-viral response. The predominance for the elevation of the anti-viral proteins was attributed to the use of the smooth form of LPS used in these experiments. Smooth LPS expresses the O-chains, is CD14-dependent and requires internalization for efficient immune activation[125,143], which activates the MYD88-independent (TRIF) pathway (see section 1.3.2.2). Activation of the TRAM/TRIF pathway downstream TLR4 activation induces a type I interferon response, in a similar manner to other intracellular nucleic acids sensing TLRs, such as TLR3, 7, 8, 9, and 13. The classical cytokine profile induced by the type I interferon response involves the potent secretion of interferon-α/β and IP10, which are induced by IRFs. The overall response to LPS in combination with NaB is not very different from the observed with LPS alone but seems to be attenuated[4,81,95].

NaB exposure seems to intensify the metabolism pathway which is responsible for the generation of hippuric acid as observed by an increase in the three key proteins involved in L-serine synthesis subpathway, the

PHGDH, PSAT1, and PSPH. These proteins are elevated by the presence of NaB and their levels increase further upon LPS stimulation. It is difficult to say if this increase is due to an increase in NaB uptake or if it results from a higher metabolic demand resulting from the activation/differentiation induced by LPS.

In any case, it adds an unnecessary metabolic demand to an already over requisitioned cell. It might incur an extra energy expenditure and depletion of important metabolites, amino acids and enzymes which could impact on the cells ability to mount an immune response. Insufficient capacity to deal with the metabolic demand of NaB and thus, accumulation of intermediate products and reduced availability of metabolic enzymes is behind the main mechanism responsible for NaB toxicity[13,105,106,107].

Chapter 8 NaB exposure disturbs the linear relationship between IL6 and TNF in PBM-DM

8.1 Introduction

All the previous work with NaB was carried out in undifferentiated THP-1 cells, which tend to be less responsive than differentiated macrophage-like cells and primary PBM-DM. Another difference between working with cell lines and primary cells is that they are likely to show a more similar response because there is no individual variation.

In order to investigate if NaB would cause a similar effect in primary cells, a pilot study was carried out with healthy individuals and the findings analysed in combination with previous data obtained from patients with CGD, OFG, and healthy controls.

8.2 Primary macrophages tolerate high concentrations of NaB

NaB toxicity was tested in primary MDM (prepared as described in section 2.1.2) using concentrations from 0-32 mM of NaB and incubated for 24 h (Figure 8-1).

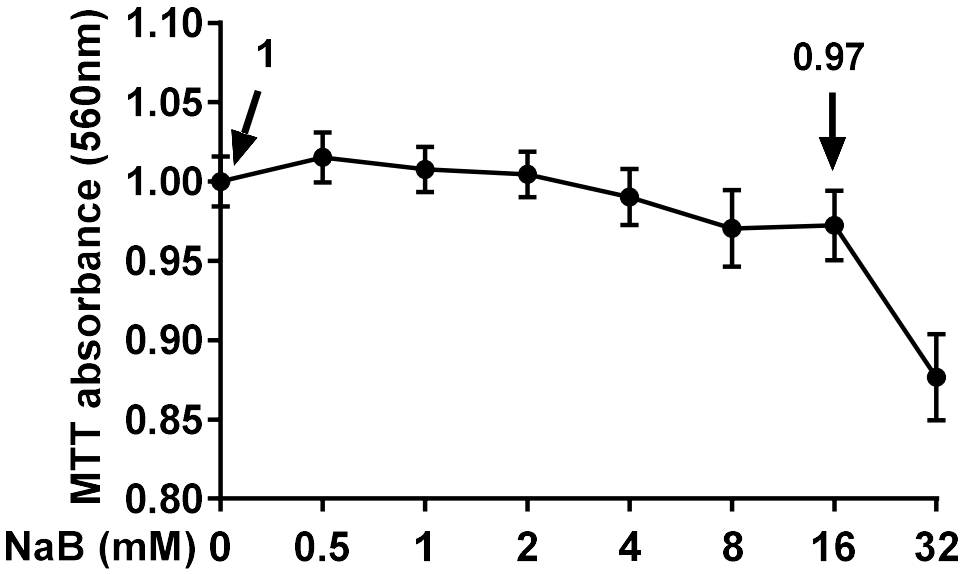

Figure 8-1: The effects of NaB on MDM viability. MDMs were treated with a range of NaB concentrations (0-32 mM) and incubated for 24 h. NaB is

well-tolerated at concentrations ≤ 16 mM, with an average cell loss around 3%. Results shown are mean ± SEM of an individual experiment, n=8.

PBM-DM appeared to tolerate higher concentrations of NaB than THP-1 cells (see section 3.3), showing only 3% of cell loss at a concentration of 16 mM. Although we tested other concentrations of NaB in MDM, 5 mM was established as the standard dose.

8.3 NaB disturbs the positive correlation between TNF and IL6

PBM-DMs were stimulated with HkEc (MoI 20:1) in the presence or absence of NaB (no NaB pre-incubation was done in PBM-DM) and the levels of IL6 and TNF measured by ELISA (Figure 8-2).

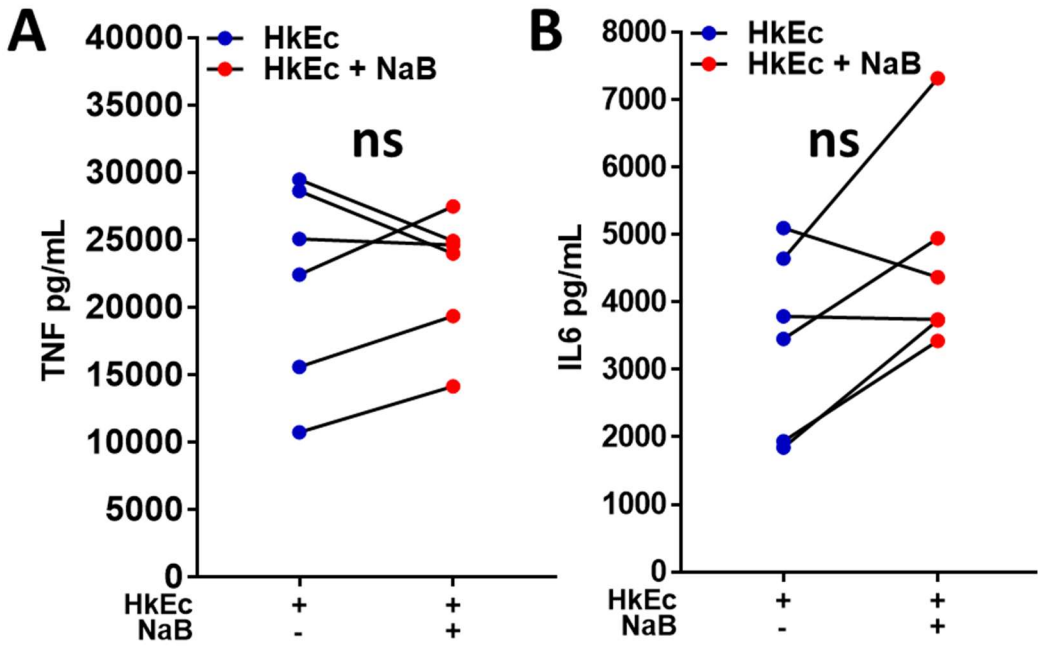

Figure 8-2: The effects of 5 mM NaB on cytokine secretion upon HkEc stimulation. Response to NaB showed individual variance, without reaching significance. Results shown are mean ± SEM of an individual experiment (n=6); ns, non-significant; (two-tailed, paired t-test).

The levels of IL6 and TNF of MDM of patients with OFG and healthy controls (HC) were evaluated upon 24 h HkEc stimulation (Figure 8-3).

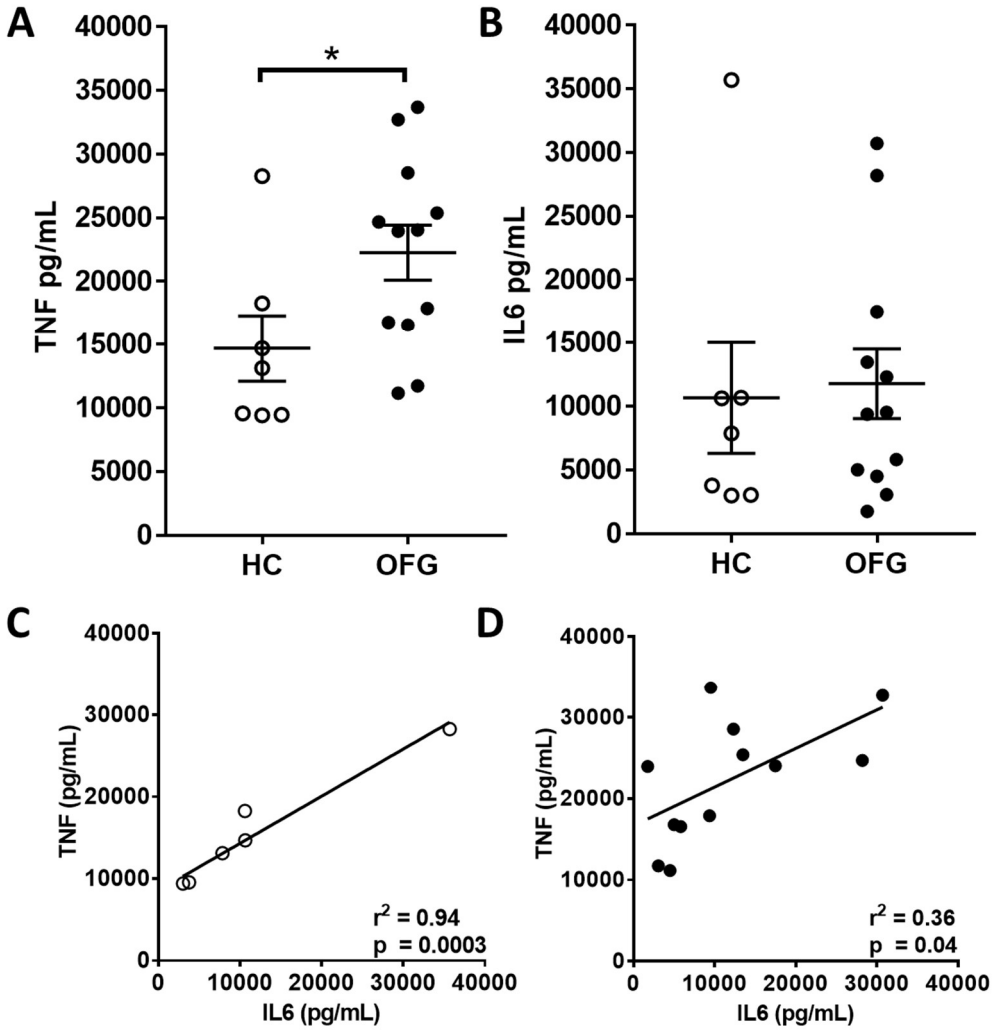

Figure 8-3: The levels of IL6 and TNF in PBM-DM stimulated with HkEc (MoI 20:1) in 7 HC and 12 OFG patients were measured by multiplex immunoassay. OFG patients showed higher levels of TNF. The positive linear correlation between IL6 and TNF was disturbed in OFG patients. Results shown in A and B are mean ± SEM, two-tailed, unpaired t-test). C and D, simple linear regression analysis, *p<0.05, **p<0.01, ***p<0.001, ****p<0.0001. Data from two HC samples varied only in a maximum of 40 pg/mL and they appear overlapping in 8-3C.Data kindly provided by Dr Helen Petersen.

NaB exposure in PBM-DM rather than showing a reduction in IL6, it seems to disturb the correlation between IL6 and TNF, which is already disturbed in OFG patients (Figure 8-4).

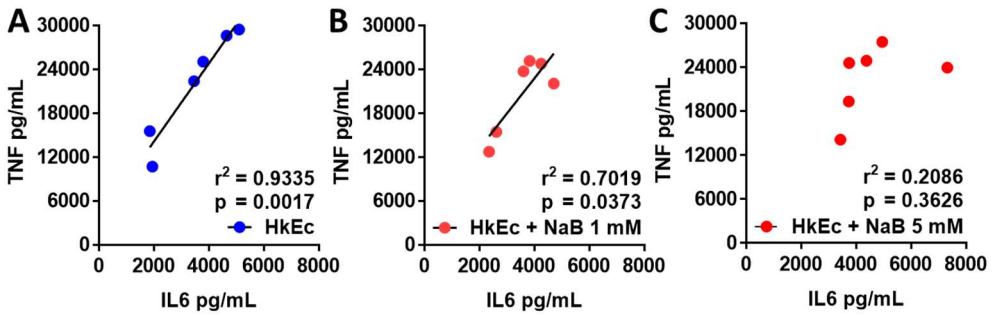

Figure 8-4: Correlation analysis between TNF and IL6 under two different concentrations of NaB in PBM-DM stimulated with HkEc. The positive correlation found TNF and IL6 (A) is disturbed by co-incubation of 1 mM of NaB (B) and lost at a concentration of 5 mM (C). Results shown are simple linear regression analysis.

8.4 Discussion

Monocyte to macrophage differentiation prepares the cell to actively participate in the inflammatory and the immune response[231229]. This process results in the up-regulation of a number of cellular processes, such as antigen presentation, that makes the macrophage much more efficient to deal with harmful stimuli than monocytes[164,229].

Interestingly I was able to demonstrate that PBM-DM were more resistant to NaB toxicity, tolerating higher doses than THP-1 cells. This may be due to change in the oxidative stress response within these cells or an increase in the metabolic processes needed to remove NaB from the cells. I used a dose of 5 mM of NaB, in accordance with the studies on THP-1 cells, which in hindsight may have been too low to study the effects of ROS depletion in PBM-DM. The results with 5 mM were highly variable in the PBM-DM and did not replicate the THP-1 data. The main effects of NaB, which are the modulation of IL6 and IL1β, are directly linked to its ability to neutralize ROS, if 5 mM was insufficient to achieve this then I would not observe the same phenotype as when THP-1 cells were used. Interestingly, one of the major up-regulated processes are seen in monocyte to macrophage maturation are the components of the NADPH oxidase. TLR4 stimulation results in the activation of the NADPH oxidase

and the generation of ROS, which may require higher levels of NaB in order to suppress the ROS dependent signalling in PBM-DM.

In this pilot study, the concentration of NaB needs to be optimized according to the mature macrophage condition. Another methodologic change that requires optimization is the incubation time with NaB. In all experiments with PBM-DM, NaB was administered concomitant with HkEc stimulation. THP-1 cells showed an immediate response to NaB, which was potentialized by pre-incubation for 12-24 h.

Although without a clear effect on IL6 or TNF secretion, NaB exposure did disrupt the linear correlation between these two cytokines, in a similar manner as to what I observed in THP-1 cells. Disruption in macrophage cytokine release is known to contribute to the pathogenesis of CD[178]. PBM-DM of OFG patients stimulated with HkEc secrete higher levels of TNF than healthy controls and the linear correlation between IL6 and TNF is compromised. NaB exposure causes a similar disruption in cytokine secretion, which can potentiate the already disturbed inflammatory response observed in patients with OFG[47,56,58].

This is only a preliminary data that still requires optimization. The lack of statistical significance can be explained by the higher variation observed in individuals and the reduced sample size. Using a power of 0.8, statistical difference is expected to be observed with 10 samples for IL6 secretion. Besides that, NaB still showed an effect on cytokine secretion that resembles the alteration observed in OFG patients and further investigation is warranted.

Chapter 9 Conclusion

The present study demonstrates that NaB does influence human monocytes, which includes small metabolic changes without the need for an immune stimulation, and a much bigger effect on the immune response causing an important attenuation of cytokine secretion upon bacterial challenge and TLR activation.

At high doses, NaB is toxic to THP-1 cells in a time- and dose-dependent manner, but at 5 mM, NaB is well-tolerated by these cells. The biological effects of NaB on cytokine secretion and ROS neutralization are also dose-dependent.

IL6 and IL1β are the major cytokines that are down-regulated at both the message and secretion levels in THP-1 cells. This is in agreement with the majority of the literature which used a range of cell types and stimuli. It is, therefore, possible to conclude that NaB has a similar effect on almost all cells and this is probably due to its ability to neutralize ROS within the cytosol. The concentration of NaB needed to achieve this neutralization will probably be cell-type specific and also be influenced by secondary events such as infection and environmental effects (UV radiation exposure, medication etc). ROS are normally generated by the cells during mitochondrial respiration and are controlled by antioxidant enzymes produced by the cells. Upon TLR or rTNF stimulation, there is an increase in ROS generation. These extra ROS molecules can act as signalling molecules and influence the immune response. My data has identified IL6 and IL1β as highly dependent on the ROS signal and other cytokines such as IP10 and IL8 being independent of this pathway. NaB ability to react and neutralize ROS, impairs the secondary signal, and thus IL6 and IL1β are not properly induced. This mechanism of action and effects on cytokine secretion is reproduced by other antioxidants and dependent on their ability to control ROS.

TNF is hyper-secreted by THP-1 cells at NaB concentrations above 5 mM and appears to be related to ERK1/2 and STAT3 signalling. These two signals are not directly connected, but combine their effects resulting

in the elevation of TNF. NaB itself disturbs the ERK1/2 signal, and upon HkEc stimulation, it seems to maintain a steady state of hyperphosphorylation, disturbing the function of this signalling pathway on TNF regulation. The importance of the ERK1/2 pathway is evident through the inclusion of the MEK1 and MEK2 inhibitor PD98059, which results in the loss of TNF induction. ERK1/2 signalling is only required for the initial induction of TNF and this is hyperactivated in the presence of NaB. The prolonged secretion of TNF, that is also evident from the inclusion of NaB during an immune response, results from an alteration in the IL6/IL6R STAT3 pathway. This secondary mechanism involved in TNF deregulation is an indirect effect of NaB since this signal comes from IL6. IL6 is released at a later stage of the immune response and activates STAT3 through an autocrine/paracrine mechanism which requires the expression of the IL6R. STAT3 activation results in the down-regulation of TNF. Due to the inhibitory effects of NaB on IL6 secretion, this signal is impaired and thus this regulatory control of TNF via STAT3 is attenuated. STAT3 activation by IL6 or STAT3 inhibition by the JAK/STAT3 inhibitor AG490 and by neutralization of IL6 signalling using an anti-IL6 antibody showed a downregulation or upregulation of TNF levels respectively.

A quantitative proteomics analysis on THP-1 cells stimulated by LPS identified a major alteration in the proteome, which involved a number of highly relevant cellular processes such as the down-regulation of the cell cycle, while proteins related to innate immunity, especially those associated with an anti-viral response were upregulated. The inclusion of NaB during an LPS stimulation results in a similar response as that seen with LPS alone, but the change in the proteome is milder, suggesting that the overall immune response is attenuated. Another consequence of NaB exposure is the activation of enzymes associated with its metabolism. The proteins PHGDH, PSAT1, and PSPH that are associated with the L-serine synthesis subpathway, and more importantly they are also involved with the metabolism of NaB to hippuric acid, are all overexpressed upon NaB exposure. This metabolism requires energy expenditure, which suggests an additional burden on the cells exposed to NaB.

Although still requiring optimization, a pilot study in PBM-DM suggests that NaB exposure disturbs the linear correlation between IL6 and TNF secretion in THP-1 cells, this correlation was also found to be disturbed in patients with OFG and might be associated with the negative effects of NaB-containing foods on patients with OFG.

ROS generation and IL6 secretion are a combination found underlying many chronic inflammatory diseases, our results suggest that NaB (or any other substance capable of neutralizing ROS) can be an effective therapy to control the chronic inflammation associated with diabetes, atherosclerosis, rheumatoid arthritis, neurodegenerative disorders, and so on.

9.1 Future directions

The work presented in this thesis has identified important mechanisms involved with NaB effects on the innate immune response that can be expanded with further investigations, such as:

- Optimization of NaB exposure to MDM and investigation of its effect on immune response upon bacterial/TLR stimulation
- We have obtained ethical approval to carry out a clinical investigation in OFG patients, which intends to test patients' sensitivity to benzoates using patch tests, collect peripheral blood and study biopsy samples to evaluate gene expression profiles. Testing the effects of NaB on the immune response in white blood cells from individuals with OFG and compare them to healthy controls.
- The results presented here demonstrated an important role of ROS in the modulation of the immune response. It suggests that the control of ROS generation can be a promising mechanism to treat diseases associated with chronic inflammation, specifically NDD. This would be a worthwhile avenue to continue in the longer term.

References

1. Brahmachari, S., Jana, A. & Pahan, K. Sodium benzoate, a metabolite of cinnamon and a food additive, reduces microglial and astroglial inflammatory responses. *J. Immunol.* **183,** 5917–5927 (2009).
2. Cosmetic Ingredient Review Expert Panel. Final Report on the Safety Assessment of Benzyl Alcohol , Benzoic Acid , and Sodium Benzoate 1. *Int. J. Toxicol.* **20,** 23–50 (2001).
3. Enns, G. M. *et al.* Survival after Treatment with Phenylacetate and Benzoate for Urea-Cycle Disorders. *N. Engl. J. Med.* **356,** 2282–2292 (2007).
4. Pahan, K. Immunomodulation of experimental allergic encephalomyeletis by cinnamon metabolite sodium benzoate. *Immunopharmacol. Immunotoxicol.* **33,** 586–593 (2011).
5. Lin, C.-H. *et al.* Benzoate, a D-Amino Acid Oxidase Inhibitor, for the Treatment of Early-Phase Alzheimer Disease: A Randomized, Double-Blind, Placebo-Controlled Trial. *Biol. Psychiatry* **75,** 678–685 (2014).
6. Jana, A. *et al.* Up-regulation of neurotrophic factors by cinnamon and its metabolite sodium benzoate: Therapeutic implications for neurodegenerative disorders. *J. Neuroimmune Pharmacol.* **8,** 739–755 (2013).
7. Rezaei, N. *et al.* In Vitro Effects of Sodium Benzoate on Th1/Th2 Deviation in Patients with Multiple Sclerosis. *Immunol. Invest.* **45,** 679–691 (2016).
8. Kundu, M., Mondal, S., Roy, A., Martinson, J. L. & Pahan, K. Sodium Benzoate, a Food Additive and a Metabolite of Cinnamon, Enriches Regulatory T Cells via STAT6-Mediated Upregulation of TGF-β. *J. Immunol.* **197,** 3099–3110 (2016).
9. Campbell, H. E. *et al.* Review article: Cinnamon- and benzoate-free diet as a primary treatment for orofacial granulomatosis. *Aliment. Pharmacol. Ther.* **34,** 687–701 (2011).
10. Campbell, H. *et al.* Dietary intervention for oral allergy syndrome as a treatment in orofacial granulomatosis: A new approach? *J. Oral Pathol. Med.* **42,** 517–522 (2013).
11. White, A. *et al.* Improvement in orofacial granulomatosis on a cinnamon- and benzoate-free diet. *Inflamm. Bowel Dis.* **12,** 508–514 (2006).
12. National Center for Biotechnology Information. PubChem Compound Database; CID=517055, http://pubchem.ncbi.nlm.nih.gov/compound/517055 (accessed May 2, 2015).
13. Chipley, J. R. in *Antimicrobials in Food* (eds. Davidson, P. M., Sofos,

J. N. & Branen, L. A.) 11–48 (Taylor & Francis Group, 2005).

14. Fujii, T., Harada, T. & Namie, K. Process for preparation of benzoic acid. 1975 (1975).
15. Butterhof, C., Martin, T., Milius, W. & Breu, J. Microphase separation with small amphiphilic molecules: Crystal structure of preservatives sodium benzoate (E 211) and potassium benzoate (E 212). *Zeitschrift fur Anorg. und Allg. Chemie* **639,** 2816–2821 (2013).
16. PR Newswire Association LLC. Global Sodium Benzoate Market Report 2017: Rise in Concerns about Use of Synthetic Preservatives Globally is Driving Growth - Research and Markets. (2017). Available at: http://www.prnewswire.com/news-releases/global-sodium-benzoate-market-report-2017-rise-in-concerns-about-use-of-synthetic-preservatives-globally-is-driving-growth----research-and-markets-300446147.html. (Accessed: 28th September 2017)
17. Davidson, P. M. Chemical preservatives and natural antimicrobial compounds. In Food Microbiology Fundamentals and Frontiers, 2nd Ed., Doyle, M. P., Beuchat, L. R., and Montville, T. J., Eds., ASM Press, Washington, D.C., p. 593. (2001).
18. European parliament and council directive No 95 ⁄ 2 ⁄EC of 20 February 1995 on food additives other than colours and sweeteners. (1995).
19. Campbell, H. E. *et al.* Development of a low phenolic acid diet for the management of orofacial granulomatosis. *J. Hum. Nutr. Diet.* **26,** 527–537 (2013).
20. Amirpour, M., Arman, A., Yolmeh, A., Ma, A. & Moradi-Khatoonabadi, Z. Sodium benzoate and potassium sorbate preservatives in food stuffs in Iran. *Food Addit Contam Part B Surveill* 2015 (2015).
21. Technavio. *Global Sodium Benzoate Market 2017-2021: Market Insights and Forecasts by Technavio*. (2017).
22. IHS Markit. Benzoic acid - Chemical Economics Handbook. (2015). Available at: https://www.ihs.com/products/benzoic-acid-chemical-economics-handbook.html. (Accessed: 28th September 2017)
23. Praphailong, W. & Fleet, G. H. The effect of pH, sodium chloride, sucrose, sorbate and benzoate on the growth of food spoilage yeasts. *Food Microbiol.* **14,** 459–468 (1997).
24. Krebs, H. A., Wiggins, D., Stubbs, M., Sols, A. & Bedoya, F. Studies on the mechanism of the antifungal action of benzoate. *Biochem. J.* **214,** 657–63 (1983).
25. Brul, S. & Coote, P. Preservative agents in foods: Mode of action and microbial resistance mechanisms. *Int. J. Food Microbiol.* **50,** 1–17 (1999).
26. Kitko, R. D. *et al.* Cytoplasmic acidification and the benzoate transcriptome in Bacillus subtilis. *PLoS One* **4,** 18–21 (2009).
27. Beilen, J. W. A. Van, Mattos, M. J. T. De, Hellingwerf, K. J. & Brul,

S. Distinct effects of sorbic acid and acetic acid on the electrophysiology and metabolism of Bacillus subtilis. *Appl. Environ. Microbiol.* **80,** 5918–5926 (2014).

28. Stratford, M. & Anslow, P. a. Evidence that sorbic acid does not inhibit yeast as a classic 'weak acid preservative'. *Lett. Appl. Microbiol.* **27,** 203–206 (1998).
29. Eklund, T. The effect of sorbic acid and esters of para-hydroxybenzoic acid on the proton motive force in Escherichia coli membrane vesicles. *J. Gen. Microbiol* **131,** 73–76 (1985).
30. Gunders, D. Wasted: How America is losing up to 40 percent of its food from farm to fork to landfill. *NRDC Issue Pap.* 1–26 (2012). doi:12-06-B
31. FAO. *Global food losses and food waste - Extent, causes and prevention. SAVE FOOD: An initiative on Food Loss and Waste Reduction* (2011). doi:10.1098/rstb.2010.0126
32. Fast, T., News, C. & Nov, L. L. Calcuatling the new cost of food spoilage. 1–3 (2016).
33. Böhme, K. *et al.* Detection of food spoilage and pathogenic bacteria based on ligation detection reaction coupled to flow-through hybridization on membranes. *Biomed Res. Int.* **2014,** (2014).
34. WHO. WHO estimates of the global burden of foodborne diseases. *Who* 1–255 (2015). doi:10.1016/j.fm.2014.07.009
35. Food Standards Agency. Foodborne disease strategy for the reduction of foodborne disease in the UK. *Version 1.0* 1–24 (2011).
36. Nychas, G.-J. E. & Panagou, E. in *Food and Beverage Stability and Shelf Life* (ed. Kilcast, David Subramaniam, P.) 1–28 (Woodhead Publishing, 2011).
37. Blair, N. F., Cremer, P. D. & Tchan, M. C. Urea cycle disorders: a life-threatening yet treatable cause of metabolic encephalopathy in adults. *Pract. Neurol.* **52,** 1–4 (2014).
38. Martín-Hernández, E. *et al.* Urea cycle disorders in Spain: an observational, cross-sectional and multicentric study of 104 cases. *Orphanet J. Rare Dis.* **9,** 187 (2014).
39. De Kimpe, S. J., Anggârd, E. E. & Carrier, M. J. Reactive oxygen species regulate macrophage scavenger receptor type I, but not type II, in the human monocytic cell line THP-1. *Mol. Pharmacol.* **53,** 1076–1082 (1998).
40. Modi, K. K. Protection of memory and learning by cinnamon. *Diss. Abstr. Int. Sect. B Sci. Eng.* **76,** No-Specified (2016).
41. Fitzpatrick, L. *et al.* Patch testing for food-associated allergies in orofacial granulomatosis. *J. Oral Pathol. Med.* **40,** 10–13 (2011).
42. Fedele, S., Fung, P. P. ., Bamashmous, N., Petrie, a & Porter, S. Long-term effectiveness of intralesional triamcinolone acetonide therapy in orofacial granulomatosis: an observational cohort study. *Br. J. Dermatol.* **4,** 794–801 (2014).

43. Grave, B., McCullough, M. & Wiesenfeld, D. Orofacial granulomatosis - A 20-year review. *Oral Dis.* **15,** 46–51 (2009).

44. Marcoval, J., Viñas, M., Bordas, X., Jucglà, A. & Servitje, O. Orofacial granulomatosis: Clinical study of 20 patients. *Oral Surg. Oral Med. Oral Pathol. Oral Radiol.* **113,** e12–e17 (2012).

45. Leão, J. C., Hodgson, T., Scully, C. & Porter, S. Review article: Orofacial granulomatosis. *Aliment. Pharmacol. Ther.* **20,** 1019–1027 (2004).

46. Tilakaratne, W. M., Freysdottir, J. & Fortune, F. Orofacial granulomatosis: Review on aetiology and pathogenesis. *J. Oral Pathol. Med.* **37,** 191–195 (2008).

47. Patel, P. *et al.* Clinical evidence for allergy in orofacial granulomatosis and inflammatory bowel disease. *Clin. Transl. Allergy* **3,** 26 (2013).

48. Wiesenfeld, D. *et al.* Oro-facial granulomatosis--a clinical and pathological analysis. *Q. J. Med.* **54,** 101–113 (1985).

49. Al Johani, K., Moles, D. R., Hodgson, T., Porter, S. R. & Fedele, S. Onset and progression of clinical manifestations of orofacial granulomatosis. *Oral Dis.* **15,** 214–219 (2009).

50. Saalman, R., Mattsson, U. & Jontell, M. Orofacial granulomatosis in childhood - A clinical entity that may indicate Crohn's disease as well as food allergy. *Acta Paediatr. Int. J. Paediatr.* **98,** 1162–1167 (2009).

51. Lazzerini, M., Bramuzzo, M. & Ventura, a. Association between orofacial granulomatosis and Crohn's disease in children: Systematic review. *World J. Gastroenterol.* **20,** 7497–7504 (2014).

52. Al Johani, K. a., Moles, D. R., Hodgson, T. a., Porter, S. R. & Fedele, S. Orofacial granulomatosis: Clinical features and long-term outcome of therapy. *J. Am. Acad. Dermatol.* **62,** 611–620 (2010).

53. Troiano, G. *et al.* Orofacial Granulomatosis: Clinical Signs of Different Pathologies. *Med. Princ. Pract.* **24,** 117–122 (2015).

54. McCartan, B. E. *et al.* Characteristics of patients with orofacial granulomatosis. *Oral Dis.* **17,** 696–704 (2011).

55. Gibson, J., Wray, D. & Bagg, J. *Oral staphylococcal mucositis: A new clinical entity in orofacial granulomatosis and Crohn's disease. Oral surgery, oral medicine, oral pathology, oral radiology, and endodontics* **89,** 171–176 (2000).

56. Sanderson, J. *et al.* Oro-Facial Granulomatosis: Crohn's Disease or a New Inflammatory Bowel Disease? *Inflamm. Bowel Dis.* **11,** 840–846 (2005).

57. Facchetti, F. *et al.* Non-specific influx of T-cell receptor alpha/beta and gamma/delta lymphocytes in mucosal biopsies from a patient with orofacial granulomatosis. *J. Oral Pathol. Med.* **29,** 519–522 (2000).

58. Freysdottir, J., Zhang, S., Tilakaratne, W. M. & Fortune, F. Oral

biopsies from patients with orofacial granulomatosis with histology resembling Crohn's disease have a prominent Th1 environment. *Inflamm. Bowel Dis.* **13,** 439–445 (2007).

59. Gibson, J. & Wray, D. Human leucocyte antigen typing in orofacial granulomatosis [20]. *Br. J. Dermatol.* **143,** 1119–1121 (2000).

60. Satsangi, J., Parkes, M., Jewell, D. P. & Bell, J. I. Genetics of inflammatory bowel disease. *Clin. Sci. (Lond).* **94,** 473–478 (1998).

61. Mentzer, A. *et al.* Genetic Association Analysis Reveals Differences in the Contribution of NOD2 Variants to the Clinical Phenotypes of Orofacial Granulomatosis. *Inflamm. Bowel Dis.* **22,** 1552–1558 (2016).

62. Gale, G. *et al.* Characterisation of a Swedish cohort with orofacial granulomatosis with or without Crohn's disease. *Oral Dis.* **21,** e98–e104 (2015).

63. Apaydin, R., Bahadir, S., Bilen, N. & Bayramgürler, D. Possible role of Mycobacterium tuberculosis complex in Melkersson – Rosenthal syndrome demonstrated with Gen-Probe amplified Mycobacterium tuberculosis direct-test. *Australas. J. Dermatol.* 94–99 (2004).

64. Ivanyi, L., Kirby, a & Zakrzewska, J. M. Antibodies to mycobacterial stress protein in patients with orofacial granulomatosis. *Journal of oral pathology & medicine : official publication of the International Association of Oral Pathologists and the American Academy of Oral Pathology* **22,** 320–322 (1993).

65. Ramesh, V. Orofacial granulomatosis due to tuberculosis. *Pediatr. Dermatol.* **26,** 108–109 (2009).

66. Ng, S. C. *et al.* A Systematic Review with Meta-analysis: Accuracy of IGRA and ASCA in differentiating Intestinal Tuberculosis from Crohn's Disease in Asians. *J. Gastroenterol. Hepatol.* **29,** 1–24 (2014).

67. Yadav, S., Dogra, S., De, D. & Saikia, U. N. Orofacial Granulomatosis Responding to Weekly Azithromycin Pulse Therapy. **151,** 219–220 (2015).

68. Riggio, M. P., Gibson, J., Lennon, a, Wray, D. & MacDonald, D. G. Search for Mycobacterium paratuberculosis DNA in orofacial granulomatosis and oral Crohn's disease tissue by polymerase chain reaction. *Gut* **41,** 646–650 (1997).

69. Gibson, J., Riggio, M., McCreary, C., Lennon, A. & Toner, M. Looking for Mycobacterium paratuberculosis DNA by polymerase chain reaction (PCR) in orofacial granulomatosis (OFG) and oral Crohns disease tissue in an Irish population. *Ir. Med. J.* **93,** 218 (2000).

70. Muellegger, R. R. *et al.* Granulomatous Cheilitis and Borrelia burgdorferi Polymerase Chain Reaction and Serologic Studies in a Retrospective Case Series of 12 Patients. *Arch. Dermatol.* **136,** 1502–1506 (2000).

71. Lim, S. H., Stephens, P., Cao, Q. X., Coleman, S. & Thomas, D. W.

Molecular analysis of T cell receptor beta variability in a patient with orofacial granulomatosis. *Gut* **40,** 683–686 (1997).

72. Tomka, M. *et al.* Orofacial granulomatosis associated with hypersensitivity to dental amalgam. *Oral Surgery, Oral Med. Oral Pathol. Oral Radiol. Endodontology* **112,** 335–341 (2011).
73. Pryce, D. W. & King, C. M. Orofacial granulomatosis associated with delayed hypersensitivity to cobalt. *Clin. Exp. Dermatol.* **15,** 384–386 (1990).
74. Guttman-Yassky, E., Weltfriend, S. & Bergman, R. Resolution of orofacial granulomatosis with amalgam removal. *J. Eur. Acad. Dermatology Venereol.* **17,** 344–347 (2003).
75. Lazarov, A., Kidron, D., Tulchinsky, Z. & Minkow, B. Contact orofacial granulomatosis caused by delayed hypersensitivity to gold and mercury. *J. Am. Acad. Dermatol.* **49,** 1117–1120 (2003).
76. Wray, D., Rees, S. R., Gibson, J. & Forsyth, a. The role of allergy in oral mucosal diseases. *QJM* **93,** 507–511 (2000).
77. Campbell, H. *et al.* Distinguishing orofacial granulomatosis from crohn's disease: Two separate disease entities? *Inflamm. Bowel Dis.* **17,** 2109–2115 (2011).
78. James, J., Patton, D. W., Lewis, C. J., Kirkwood, E. M. & Ferguson, M. M. Oro-facial granulomatosis and clinical atopy. *J. Oral Med.* **41,** 29–30 (1986).
79. Nettis, E., Colanardi, M. C., Ferrannini, A. & Tursi, A. Sodium benzoate-induced repeated episodes of acute urticaria/angio-oedema: Randomized controlled trial. *Br. J. Dermatol.* **151,** 898–902 (2004).
80. Armstrong, D. K. B., Biagioni, P., Lamey, P. J. & Burrows, D. Contact hypersensitivity in patients with orofacial granulomatosis. *Am. J. Contact Dermat.* **8,** 35–38 (1997).
81. Taibjee, S. M., Prais, L. & Foulds, I. S. Orofacial granulomatosis worsened by chocolate: Results of patch testing to ingredients of Cadbury's chocolate. *Br. J. Dermatol.* **150,** 595 (2004).
82. Mutalib, M., Bezanti, K., Elawad, M. & Kiparissi, F. The role of exclusive enteral nutrition in the management of orofacial granulomatosis in children. *World J. Pediatr.* **12,** 421–424 (2016).
83. Sciubba, J. J. & Said-Al-Naief, N. Orofacial granulomatosis: presentation, pathology and management of 13 cases. *J. Oral Pathol. Med.* **32,** 576–585 (2003).
84. Mignogna, M. D., Fedele, S., Lo Russo, L., Adamo, D. & Satriano, R. a. Effectiveness of small-volume, intralesional, delayed-release triamcinolone injections in orofacial granulomatosis: a pilot study. *J. Am. Acad. Dermatol.* **51,** 265–268 (2004).
85. Elliott, T. *et al.* Experience with anti-TNF-α therapy for orofacial granulomatosis. *J. Oral Pathol. Med.* **40,** 14–19 (2011).
86. Kolho, K. L., Heiskanen, K., Verkasalo, M. & Pitkäranta, A. Orofacial

granulomatosis in children-A challenge for diagnosis and treatment. *Int. J. Pediatr. Otorhinolaryngol.* **75,** 864–867 (2011).

87. Brogden, K. a, Johnson, G. K., Vincent, S. D., Abbasi, T. & Vali, S. Oral inflammation, a role for antimicrobial peptide modulation of cytokine and chemokine responses. *Expert Rev. Anti. Infect. Ther.* **11,** 1097–113 (2013).

88. Banks, T. & Gada, S. A comprehensive review of current treatments for granulomatous cheilitis. *Br. J. Dermatol.* **166,** 934–937 (2012).

89. Beal, M. F., Lang, A. E. & Ludolph, A. C. *Neurodegenerative Diseases*. (Cambridge University Press, 2005). doi:10.1017/CBO9780511544873

90. Li, J., O, W., Li, W., Jiang, Z.-G. & Ghanbari, H. Oxidative Stress and Neurodegenerative Disorders. *Int. J. Mol. Sci.* **14,** 24438–24475 (2013).

91. Awada, R., Parimisetty, A. & D'Hellencourt, C. L. in *Neurodegenerative Diseases* (ed. Kishore, U.) 381–401 (InTech, 2013). doi:10.5772/711

92. Deleidi, M., Jäggle, M. & Rubino, G. Immune ageing, dysmetabolism and inflammation in neurological diseases. *Front. Neurosci.* **9,** 1–14 (2015).

93. Ilieva, H., Polymenidou, M. & Cleveland, D. W. Non-cell autonomous toxicity in neurodegenerative disorders: ALS and beyond. *J. Cell Biol.* **187,** 761–772 (2009).

94. Khasnavis, S. & Pahan, K. Cinnamon Treatment Upregulates Neuroprotective Proteins Parkin and DJ-1 and Protects Dopaminergic Neurons in a Mouse Model of Parkinson's Disease. *J. Neuroimmune Pharmacol.* **9,** 569–581 (2014).

95. Brahmachari, S. & Pahan, K. Sodium Benzoate, a Food Additive and a Metabolite of Cinnamon, Modifies T Cells at Multiple Steps and Inhibits Adoptive Transfer of Experimental Allergic Encephalomyelitis. *J. Immunol.* **179,** 275–283 (2007).

96. Lin, C.-Y. *et al.* Adjunctive sarcosine plus benzoate improved cognitive function in chronic schizophrenia patients with constant clinical symptoms: A randomised, double-blind, placebo-controlled trial. *World J. Biol. Psychiatry* **2975,** 1–12 (2015).

97. Lane, H.-Y. *et al.* Add-on Treatment of Benzoate for Schizophrenia. *JAMA Psychiatry* **70,** 1267 (2013).

98. Ryan, A. *et al.* The efficacy of sodium benzoate as an adjunctive treatment in early psychosis - CADENCE-BZ: study protocol for a randomized controlled trial. *Trials* **18,** 165 (2017).

99. Mourad, M., Häberle, J., Whitehead, M., Stricker, T. & Gropman, A. Brain Biomarkers of Long-Term Outcome of Neonatal Onset Urea Cycle Disorder. *Int. J. Neonatal Screen.* **2,** 10 (2016).

100. Johnston, MD, M., Adams Jr., MD, H. & Fatemi, MD, MBA, A. *Neurobiology of Disease*. **1,** (Oxford University Press, 2017).

101. Nagamani, S. C. S. *et al.* A randomized trial to study the comparative efficacy of phenylbutyrate and benzoate on nitrogen excretion and ureagenesis in healthy volunteers. *Genet. Med.* **0,** 1–9 (2017).

102. Batshaw, M. L., Macarthur, R. B. & Tuchman, M. Alternative pathway therapy for urea cycle disorders: Twenty years later. *J. Pediatr.* **138,** (2001).

103. Poo, J. L. *et al.* Rationale for the use of sodium benzoate in clinical hepatology. *Rev. Invest. Clin.* **42 Suppl,** 101–105 (1990).

104. Tremblay, G. C. & Qureshi, I. A. The biochemistry and toxicology of benzoic acid metabolism and its relationship to the elimination of waste nitrogen. *Pharmacol. Ther.* **60,** 63–90 (1993).

105. Krähenbühl, L., Reichen, J., Talos, C. & Krähenbühl, S. Benzoic acid metabolism reflects hepatic mitochondrial function in rats with long-term extrahepatic cholestasis. *Hepatology* **25,** 278–83 (1997).

106. Cyr, D. M., Egan, S. G., Brini, C. M. & Tremblay, G. C. On the mechanism of inhibition of gluconeogenesis and ureagenesis by sodium benzoate. *Biochem. Pharmacol.* **42,** 645–654 (1991).

107. Griffith, A. D., Cyr, D. M., Egan, S. G. & Tremblay, G. C. Inhibition of pyruvate carboxylase by sequestration of coenzyme A with sodium benzoate. *Arch. Biochem. Biophys.* **269,** 201–207 (1989).

108. O'Connor, J., Costell, M. & Grisolia, S. The potentiation of ammonia toxicity by sodium benzoate is prevented by L-carnitine. *Biochem. Biophys. Res. Commun.* **145,** 817–824 (1987).

109. Praphanphoj, V., Boyadjiev, S. a., Waber, L. J., Brusilow, S. W. & Geraghty, M. T. Three cases of intravenous sodium benzoate and sodium phenylacetate toxicity occurring in the treatment of acute hyperammonaemia. *J. Inherit. Metab. Dis.* **23,** 129–136 (2000).

110. *Janeway's Immunobiology*. (Garland Science, 2008).

111. Sompayrac, L. *How the immune system works*. *Wiley-Clackwell* (Wiley-Blackwell, 2012).

112. Reikine, S., Nguyen, J. B. & Modis, Y. Pattern recognition and signaling mechanisms of RIG-I and MDA5. *Front. Immunol.* **5,** 1–7 (2014).

113. Reuven, E. M., Fink, A. & Shai, Y. Regulation of innate immune responses by transmembrane interactions: Lessons from the TLR family. *Biochim. Biophys. Acta - Biomembr.* **1838,** 1586–1593 (2014).

114. De Nardo, D. Toll-like receptors: Activation, signalling and transcriptional modulation. *Cytokine* (2015). doi:10.1016/j.cyto.2015.02.025

115. Aalaei-andabili, S. H. & Rezaei, N. Toll like receptor (TLR)-induced differential expression of microRNAs (MiRs) promotes proper immune response against infections: A systematic review. *J. Infect.* **67,** 251–264 (2013).

116. Di Gioia, M. & Zanoni, I. Toll-like receptor co-receptors as master

regulators of the immune response. *Mol. Immunol.* (2014). doi:10.1016/j.molimm.2014.05.008

117. O'Neill, L. A. J., Golenbock, D. & Bowie, A. G. The history of Toll-like receptors - redefining innate immunity. *Nat. Rev. Immunol.* **13,** 453–60 (2013).
118. Manavalan, B., Basith, S. & Choi, S. Similar Structures but Different Roles – An Updated Perspective on TLR Structures. *Front. Physiol.* **2,** 1–13 (2011).
119. Motoi, Y. *et al.* Lipopeptides are signaled by Toll-like receptor 1, 2 and 6 in endolysosomes. *Int. Immunol.* **26,** 563–573 (2014).
120. Jin, M. S. *et al.* Crystal Structure of the TLR1-TLR2 Heterodimer Induced by Binding of a Tri-Acylated Lipopeptide. *Cell* **130,** 1071–1082 (2007).
121. Takeda, K. Toll-like receptors in innate immunity. *Int. Immunol.* **17,** 1–14 (2004).
122. Deguine, J. & Barton, G. M. MyD88: a central player in innate immune signaling. *F1000Prime Rep.* **6,** 1–7 (2014).
123. Cheng, K. *et al.* Specific activation of the TLR1-TLR2 heterodimer by small-molecule agonists. *Sci. Adv.* 1–12 (2015).
124. Lucas, K. & Maes, M. Role of the toll like receptor (TLR) radical cycle in chronic inflammation: Possible treatments targeting the TLR4 pathway. *Mol. Neurobiol.* **48,** 190–204 (2013).
125. Godowski, P. J. A smooth operator for LPS responses. *Nat. Immunol.* **6,** 544–546 (2005).
126. Takeuchi, O. & Akira, S. Pattern Recognition Receptors and Inflammation. *Cell* **140,** 805–820 (2010).
127. Toshchakov, V. *et al.* TLR4, but not TLR2, mediates IFN-beta-induced STAT1alpha/beta-dependent gene expression in macrophages. *Nat. Immunol.* **3,** 392–398 (2002).
128. Dziarski, R. & Gupta, D. Role of MD-2 in TLR2- and TLR4-mediated recognition of Gram-negative and Gram-positive bacteria and activation of chemokine genes. *J. Endotoxin Res.* **6,** 401–405 (2000).
129. Park, B. S. *et al.* The structural basis of lipopolysaccharide recognition by the TLR4 – MD-2 complex. *Nature* **458,** 1191–1195 (2009).
130. Regen, T. *et al.* CD14 and TRIF govern distinct responsiveness and responses in mouse microglial TLR4 challenges by structural variants of LPS. *Brain. Behav. Immun.* **25,** 957–970 (2011).
131. Perkins, D. J. & Vogel, S. N. Cytokine Space and time : New considerations about the relationship between Toll-like receptors (TLRs) and type I interferons (IFNs). *Cytokine* 1–4 (2015). doi:10.1016/j.cyto.2015.03.001
132. Vaure, C. & Liu, Y. A comparative review of toll-like receptor 4 expression and functionality in different animal species. *Front.*

Immunol. **5,** 1–15 (2014).

133. West, a P. *et al.* TLR signaling augments macrophage bactericidal activity through mitochondrial ROS. **472,** 476–480 (2012).
134. Morandini, A. C., Chaves Souza, P. P., Ramos-Junior, E. S., Souza Costa, C. A. & Santos, C. F. MyD88 or TRAM knockdown regulates interleukin (IL)-6, IL8, and CXCL12 mRNA expression in human gingival and periodontal ligament fibroblasts. *J. Periodontol.* **84,** 1353–60 (2013).
135. Yesudhas, D., Gosu, V., Anwar, M. A. & Choi, S. Multiple Roles of Toll-Like Receptor 4 in Colorectal Cancer. *Front. Immunol.* **5,** 1–10 (2014).
136. Shaik-Dasthagirisaheb, Y. B. *et al.* Aging and contribution of MyD88 and TRIF to expression of TLR pathway-associated genes following stimulation with *Porphyromonas gingivalis*. *J. Periodontal Res.* **50,** 89–102 (2015).
137. Mosser, D. M. & Edwards, J. P. Exploring the full spectrum of macrophage activation. *Nat. Rev. Immunol.* **8,** 958–969 (2008).
138. Harman, A. N. *et al.* HIV Blocks Interferon Induction in Human Dendritic cells and Macrophages by Dysregulation of TBK1. *J. Virol.* JVI.00889-15 (2015). doi:10.1128/JVI.00889-15
139. Kagan, J. C. *et al.* TRAM couples endocytosis of Toll-like receptor 4 to the induction of interferon-β. *Nat. Immunol.* **9,** 361–368 (2008).
140. Praefcke, G. J. K. & McMahon, H. T. The dynamin superfamily: universal membrane tubulation and fission molecules? *Nat. Rev. Mol. Cell Biol.* **5,** 133–147 (2004).
141. Tanimura, N., Saitoh, S., Matsumoto, F., Akashi-Takamura, S. & Miyake, K. Roles for LPS-dependent interaction and relocation of TLR4 and TRAM in TRIF-signaling. *Biochem. Biophys. Res. Commun.* **368,** 94–99 (2008).
142. Raetz, C. R. H. & Whitfield, C. Lipopolysaccharide Endotoxins. *Annu. Rev. Biochem.* **71,** 635–700 (2002).
143. Zanoni, I. *et al.* Similarities and differences of innate immune responses elicited by smooth and rough LPS. *Immunol. Lett.* **142,** 41–47 (2012).
144. Terraza, A., Gross, A. & Dornand, J. Different Responses of Macrophages to Smooth and Rough. *Microbiology* **72,** 2429–2433 (2004).
145. Schieber, M. & Chandel, N. S. ROS Function in Redox Signaling and Oxidative Stress. *Curr. Biol.* **24,** R453–R462 (2014).
146. Finkel, T. Signal transduction by reactive oxygen species. *J. Cell Biol.* **194,** 7–15 (2011).
147. Mittal, M., Siddiqui, M. R., Tran, K., Reddy, S. P. & Malik, A. B. Reactive Oxygen Species in Inflammation and Tissue Injury. *Antioxid. Redox Signal.* **20,** 1126–1167 (2014).

148. West, a P. *et al.* TLR signalling augments macrophage bactericidal activity through mitochondrial ROS. *Nature* **472,** 476–480 (2011).

149. Forman, H. J. & Torres, M. Signaling by the respiratory burst in macrophages. *IUBMB Life* **51,** 365–371 (2001).

150. SIES, H. Strategies of antioxidant defense. *Eur. J. Biochem.* **215,** 213–219 (1993).

151. Sullivan, L. B. & Chandel, N. S. Mitochondrial reactive oxygen species and cancer. *Cancer Metab.* **2,** 17 (2014).

152. Tsuchiya, S. *et al.* Establishment and characterization of a human acute monocytic leukemia cell line (THP-1). *Int. J. Cancer* **26,** 171–176 (1980).

153. Sewell, G. W. *et al.* Defective tumor necrosis factor release from Crohn's disease macrophages in response to toll-like receptor activation: Relationship to phenotype and genome-wide association susceptibility loci. *Inflamm. Bowel Dis.* **18,** 2120–2127 (2012).

154. Gentleman, R. C. *et al.* Bioconductor: open software development for computational biology and bioinformatics. *Genome Biol.* **5,** R80 (2004).

155. Smyth, G. K. Limma: linear models for microarray data. In: Gentleman R, Carey V, Dudoit S, R, Irizarry WH, eds. Bioinformatics and computational biology solutions using R and Bioconductor. 397–420 (2005).

156. Durinck, S. *et al.* BioMart and Bioconductor: A powerful link between biological databases and microarray data analysis. *Bioinformatics* **21,** 3439–3440 (2005).

157. Johnson, W. E., Li, C. & Rabinovic, A. Adjusting batch effects in microarray expression data using empirical Bayes methods. *Biostatistics* **8,** 118–127 (2007).

158. Benjamini, Y. & Hochberg, Y. Controlling the False Discovery Rate : A Practical and Powerful Approach to Multiple Testing. *J. R. Stat. Soc.* **57,** 289–300 (1995).

159. Livak, K. J. & Schmittgen, T. D. Analysis of relative gene expression data using real-time quantitative PCR and the 2(-Delta Delta C(T)) Method. *Methods* **25,** 402–408 (2001).

160. Levine, A. P., Duchen, M. R., De Villiers, S., Rich, P. R. & Segal, A. W. Alkalinity of neutrophil phagocytic vacuoles is modulated by HVCN1 and has consequences for myeloperoxidase activity. *PLoS One* **10,** 1–20 (2015).

161. Mulvey, C. M. *et al.* Subcellular proteomics reveals a role for nucleo-cytoplasmic trafficking at the DNA replication origin activation checkpoint. *J. Proteome Res.* **12,** 1436–1453 (2013).

162. Park, H. W., Park, E. H., Yun, H. M. & Rhim, H. Sodium benzoate-mediated cytotoxicity in mammalian cells. *J. Food Biochem.* **35,** 1034–1046 (2011).

163. Reed, B. E., Barrett, A. P., Katelaris, C. & Bilous, M. Orofacial

sensitivity reactions and the role of dietary components. Case reports. *Aust. Dent. J.* **38,** 287–291 (1993).

164. Auwerx, J. The human leukemia cell line, THP-1: A multifacetted model for the study of monocyte-macrophage differentiation. *Experientia* **47,** 22–31 (1991).
165. Bosshart, H. & Heinzelmann, M. THP-1 cells as a model for human monocytes. *Ann. Transl. Med.* **4,** 438–438 (2016).
166. Hu, Z.-D. *et al.* Gene expression profile of THP-1 cells treated with heat-killed Candida albicans. *Ann. Transl. Med.* **4,** 170–170 (2016).
167. Huang, D. W., Sherman, B. T. & Lempicki, R. a. Systematic and integrative analysis of large gene lists using DAVID bioinformatics resources. *Nat. Protoc.* **4,** 44–57 (2009).
168. Huang, D. W., Sherman, B. T. & Lempicki, R. a. Bioinformatics enrichment tools: Paths toward the comprehensive functional analysis of large gene lists. *Nucleic Acids Res.* **37,** 1–13 (2009).
169. Yadav, A., Kumar, A., Das, M. & Tripathi, A. Sodium benzoate, a food preservative, affects the functional and activation status of splenocytes at non cytotoxic dose. *Food Chem. Toxicol.* **88,** 40–47 (2016).
170. Li, N. *et al.* Live and heat-killed lactobacillus rhamnosus GG: Effects on proinflammatory and anti-inflammatory cytokines/chemokines in gastrostomy-fed infant rats. *Pediatr. Res.* **66,** 203–207 (2009).
171. Noel, R. F., Sato, T. T., Mendez, C., Johnson, M. C. & Pohlman, T. H. Activation of human endothelial cells by viable or heat-killed gram-negative bacteria requires soluble CD14. *Infect. Immun.* **63,** 4046–53 (1995).
172. Paul-Clark, M. J. *et al.* Differential effects of Gram-positive versus Gram-negative bacteria on NOSII and TNFlpha in macrophages: role of TLRs in synergy between the two. *Br. J. Pharmacol.* **148,** 1067–75 (2006).
173. Coorens, M. *et al.* Cathelicidins Inhibit *Escherichia coli* –Induced TLR2 and TLR4 Activation in a Viability-Dependent Manner. *J. Immunol.* **2,** ji1602164 (2017).
174. Smith, A. M. *et al.* Disordered macrophage cytokine secretion underlies impaired acute inflammation and bacterial clearance in Crohn's disease. *J. Exp. Med.* **206,** 1883–1897 (2009).
175. O'Neil-Andersen, N. J. & Lawrence, D. a. Differential modulation of surface and intracellular protein expression by T cells after stimulation in the presence of monensin or brefeldin A. *Clin. Diagn. Lab. Immunol.* **9,** 243–50 (2002).
176. Mauvezin, C. & Neufeld, T. P. Bafilomycin A1 disrupts autophagic flux by inhibiting both V-ATPase-dependent acidification and Ca-P60A/SERCA-dependent autophagosome-lysosome fusion. *Autophagy* **11,** 1437–1438 (2015).
177. Cardelli, J. A., Richardson, J. & Miears, D. Role of acidic intracellular

compartments in the biosynthesis of Dictyostelium lysosomal enzymes. The weak bases ammonium chloride and chloroquine differentially affect proteolytic processing and sorting. *J. Biol. Chem.* **264,** 3454–3463 (1989).

178. Smith, A. *et al.* Disruption of macrophage pro-inflammatory cytokine release in Crohn's disease is associated with reduced optineurin expression in a subset of patients. *Immunology* 45–55 (2014). doi:10.1111/imm.12338
179. Scheller, J., Chalaris, A., Schmidt-Arras, D. & Rose-John, S. The pro- and anti-inflammatory properties of the cytokine interleukin-6. *Biochim. Biophys. Acta - Mol. Cell Res.* **1813,** 878–888 (2011).
180. Xing, Z. *et al.* Enhanced Acute Inflammatory Responses in IL6–deficient Mice IL6 Is an Antiinflammatory Cytokine Required for Controlling Local or Systemic Acute Inflammatory Responses. *J. Clin. Invest* **101,** 311–320 (1998).
181. Shin, S. & Brodsky, I. E. The inflammasome: Learning from bacterial evasion strategies. *Semin. Immunol.* 1–9 (2015). doi:10.1016/j.smim.2015.03.006
182. Erta, M., Quintana, A. & Hidalgo, J. Interleukin-6, a major cytokine in the central nervous system. *Int. J. Biol. Sci.* **8,** 1254–1266 (2012).
183. Heneka, M. T., Kummer, M. P. & Latz, E. Innate immune activation in neurodegenerative disease. *Nat. Rev. Immunol.* **14,** 463–477 (2014).
184. Lynch, M. A. Neuroinflammatory changes negatively impact on LTP: A focus on IL1β. *Brain Res.* **1621,** 197–204 (2015).
185. Hartman, J. & Frishman, W. H. Inflammation and Atherosclerosis. *Cardiol. Rev.* **22,** 147–151 (2014).
186. Maggio, M., Guralnik, J. M., Longo, D. L. & Ferrucci, L. Interleukin-6 in Aging and Chronic Disease: A Magnificent Pathway. *J. Gerontol. A. Biol. Sci. Med. Sci.* **61,** 575–584 (2006).
187. Montoya, J. G. *et al.* Cytokine signature associated with disease severity in chronic fatigue syndrome patients. *Proc. Natl. Acad. Sci.* 201710519 (2017). doi:10.1073/pnas.1710519114
188. Caprioli, F., Caruso, R., Sarra, M., Pallone, F. & Monteleone, G. Disruption of inflammatory signals by cytokine-targeted therapies for inflammatory bowel diseases. *Br. J. Pharmacol.* **165,** 820–828 (2012).
189. Webb, S., McPherson, J., Pahan, K. & Koka, S. Regulation of TNF-induced IL6 Production in MG-63 Human Osteoblast-like Cells. *J. Dent* **81,** 17–22 (2002).
190. Segata, N. *et al.* Composition of the adult digestive tract bacterial microbiome based on seven mouth surfaces, tonsils, throat and stool samples. *Genome Biol.* **13,** R42 (2012).
191. Catalina Suarez-Cuervo, Harris, K. W., Hallman, L., HK, V. & Selander, K. S. Tumor necrosis factor-alpha induces interleukin-6

production via ... *Breast Cancer Res Treat* **80,** 71–78 (2003).

192. Turner, N. A. *et al.* Mechanism of TNFα-induced IL-1α, IL1β and IL6 expression in human cardiac fibroblasts: Effects of statins and thiazolidinediones. *Cardiovasc. Res.* **76,** 81–90 (2007).
193. Forman, H. J. & Torres, M. Redox signaling in macrophages. *Mol. Aspects Med.* **22,** 189–216 (2001).
194. Naik, E. & Dixit, V. M. Mitochondrial reactive oxygen species drive proinflammatory cytokine production: Figure 1. *J. Exp. Med.* **208,** 417–420 (2011).
195. Bulua, A. C. *et al.* Mitochondrial reactive oxygen species promote production of proinflammatory cytokines and are elevated in TNFR1-associated periodic syndrome (TRAPS). *J. Exp. Med.* **208,** 519–533 (2011).
196. Zhou, T., Chuang, C.-C. & Zuo, L. Molecular Characterization of Reactive Oxygen Species in Myocardial Ischemia-Reperfusion Injury. *Biomed Res. Int.* **2015,** 1–9 (2015).
197. Mailloux, R. J. & Harper, M.-E. Uncoupling proteins and the control of mitochondrial reactive oxygen species production. *Free Radic. Biol. Med.* **51,** 1106–1115 (2011).
198. Zhang, J. *et al.* ROS and ROS-Mediated Cellular Signaling. *Oxid. Med. Cell. Longev.* **2016,** (2016).
199. Blaser, H., Dostert, C., Mak, T. W. & Brenner, D. TNF and ROS Crosstalk in Inflammation. *Trends Cell Biol.* **26,** 249–261 (2016).
200. Swindle, E. J., Hunt, J. A. & Coleman, J. W. A Comparison of Reactive Oxygen Species Generation by Rat Peritoneal Macrophages and Mast Cells Using the Highly Sensitive Real-Time Chemiluminescent Probe Pholasin: Inhibition of Antigen-Induced Mast Cell Degranulation by Macrophage-Derived Hydrogen Pero. *J. Immunol.* **169,** 5866–5873 (2002).
201. Behe, P. *et al.* The LRRC8A mediated 'swell activated' chloride conductance is dispensable for vacuolar homeostasis in neutrophils. *Front. Pharmacol.* **8,** 1–16 (2017).
202. Barzegar, A. & Moosavi-Movahedi, A. A. Intracellular ROS protection efficiency and free radical-scavenging activity of curcumin. *PLoS One* **6,** 1–7 (2011).
203. Ak, T. & Gülçin, I. Antioxidant and radical scavenging properties of curcumin. *Chem. Biol. Interact.* **174,** 27–37 (2008).
204. McCoy, M. K. & Tansey, M. G. TNF signaling inhibition in the CNS: implications for normal brain function and neurodegenerative disease. *J. Neuroinflammation* **5,** 45 (2008).
205. Bryan, H. K., Olayanju, A., Goldring, C. E. & Park, B. K. The Nrf2 cell defence pathway: Keap1-dependent and -independent mechanisms of regulation. *Biochem. Pharmacol.* **85,** 705–717 (2013).
206. Wang, Q. *et al.* Dimethyl fumarate protects neural stem/progenitor cells and neurons from oxidative damage through Nrf2-ERK1/2

MAPK pathway. *Int. J. Mol. Sci.* **16,** 13885–13907 (2015).

207. Petri, S., Körner, S. & Kiaei, M. Nrf2/ARE Signaling Pathway: Key Mediator in Oxidative Stress and Potential Therapeutic Target in ALS. *Neurol. Res. Int.* **2012,** 1–7 (2012).
208. Loboda, A., Damulewicz, M., Pyza, E., Jozkowicz, A. & Dulak, J. Role of Nrf2/HO-1 system in development, oxidative stress response and diseases: an evolutionarily conserved mechanism. *Cell. Mol. Life Sci.* **73,** 3221–3247 (2016).
209. Yoshida, Y. *et al.* Reactive oxygen intermediates stimulate interleukin-6 production in human bronchial epithelial cells. *Am J Physiol Lung Cell Mol Physiol* **276,** L900-908 (1999).
210. Yang, Y. *et al.* An overview of the molecular mechanisms and novel roles of Nrf2 in neurodegenerative disorders. *Cytokine Growth Factor Rev.* **26,** 47–57 (2015).
211. Butterfield, D. A. Oxidative Stress in Neurodegenerative Disorders. *Antioxid. Redox Signal.* **8,** 1971–1973 (2006).
212. Ferrante, J. V & Ferrante, A. Cutting Edge: Novel Role of Lipoxygenases in the Inflammatory Response: Promotion of TNF mRNA Decay by 15-Hydroperoxyeicosatetraenoic Acid in a Monocytic Cell Line. *J. Immunol.* **174,** 3169–3172 (2005).
213. Dumitru, C. D. *et al.* TNF-α induction by LPS is regulated posttranscriptionally via a Tpl2/ERK-dependent pathway. *Cell* **103,** 1071–1083 (2000).
214. Jeong, S. H. *et al.* Up-regulation of TNFlpha secretion by cigarette smoke is mediated by Egr-1 in HaCaT human keratinocytes. *Exp. Dermatol.* **19,** 206–212 (2010).
215. Mackenzie, S., Ferna, N. & Espel, E. Post-transcriptional regulation of TNF- □ during in vitro differentiation of human monocytes / macrophages in primary culture differentiated in vitro . A significant increase in LPS-. *J. Leukoc. Biol.* **71,** 1026–1032 (2002).
216. Nishiki, S. *et al.* Selective activation of STAT3 in human monocytes stimulated by G-CSF: implication in inhibition of LPS-induced TNFlpha production. *Am. J. Physiol. Cell Physiol.* **286,** C1302-11 (2004).
217. Hunter, C. a & Jones, S. a. IL6 as a keystone cytokine in health and disease. *Nat. Publ. Gr.* **16,** 448–457 (2015).
218. Yu, H., Kortylewski, M. & Pardoll, D. Crosstalk between cancer and immune cells: role of STAT3 in the tumour microenvironment. *Nat. Rev. Immunol.* **7,** 41–51 (2007).
219. Yoon, S. *et al.* STAT3 transcriptional factor activated by reactive oxygen species induces IL6 in starvation-induced autophagy of cancer cells. *Autophagy* **6,** 1125–1138 (2010).
220. Rébé, C., Végran, F., Berger, H. & Ghiringhelli, F. STAT3 activation: A key factor in tumor immunoescape. *Jak-Stat* **2,** e23010 (2013).
221. de Jong, P. R. *et al.* STAT3 regulates monocyte TNFlpha production

in systemic inflammation caused by cardiac surgery with cardiopulmonary bypass. *PLoS One* **7,** 1–9 (2012).

222. Jacoby, J. J. *et al.* Cardiomyocyte-restricted knockout of STAT3 results in higher sensitivity to inflammation, cardiac fibrosis, and heart failure with advanced age. *Proc. Natl. Acad. Sci. U. S. A.* **100,** 12929–34 (2003).
223. Huynh, L. *et al.* Opposing regulation of the late phase TNF response by mTORC1-IL-10 signaling and hypoxia in human macrophages. *Sci. Rep.* **6,** 1–14 (2016).
224. Park, E. K. *et al.* Optimized THP-1 differentiation is required for the detection of responses to weak stimuli. *Inflamm. Res.* **56,** 45–50 (2007).
225. Szklarczyk, D. *et al.* The STRING database in 2011: Functional interaction networks of proteins, globally integrated and scored. *Nucleic Acids Res.* **39,** 561–568 (2011).
226. Hart, C. E. *et al.* Phosphoserine aminotransferase deficiency: a novel disorder of the serine biosynthesis pathway. *Am. J. Hum. Genet.* **80,** 931–937 (2007).
227. El-Hattab, A. W. Serine biosynthesis and transport defects. *Mol. Genet. Metab.* **118,** 153–159 (2016).
228. Luo, J. Cancer's sweet tooth for serine. *Breast Cancer Res.* **13,** 317–319 (2011).
229. Richter, E., Ventz, K., Harms, M., Mostertz, J. & Hochgräfe, F. Induction of Macrophage Function in Human THP-1 Cells Is Associated with Rewiring of MAPK Signaling and Activation of MAP3K7 (TAK1) Protein Kinase. *Front. Cell Dev. Biol.* **4,** 1–15 (2016).
230. Reales-Calderón, J. A., Vaz, C., Monteoliva, L., Molero, G. & Gil, C. Candida albicans Modifies the Protein Composition and Size Distribution of THP-1 Macrophage-Derived Extracellular Vesicles. *J. Proteome Res.* **16,** 87–105 (2017).
231. Takashiba, S. *et al.* Differentiation of Monocytes to Macrophages Primes Cells for Lipopolysaccharide Stimulation via Accu. **67,** 5573–5578 (1999).

Appendix 1 – Presentations, Prizes and Publications

Oral presentation

International Congress of Immunology
Melbourne, Australia 2016

PhD Research Symposium - Eastman Dental Institute
London, United Kingdom 2016

Poster presentation

50 Annual Scientific Meeting of the European Society for Clinical Investigation
Paris, France 2016

Infection, Immunology and Inflammation (III) Symposium
London, United Kingdom 2016

Eastman Research Away Day
London, United Kingdom 2016

2nd Prize for poster presentation

Eastman Research Away Day
London, United Kingdom 2015

Publication

Shaw L, Ribeiro ALR, Levine AP, Pontikos N, Balloux F, Segal AW, Roberts AP, Smith AM. The Human Salivary Microbiome Is Shaped by Shared Environment Rather than Genetics: Evidence from a Large Family of Closely Related Individuals. MBio 12;8(5) 2017. doi: 10.1128/mBio.01237-17

AMERICAN SOCIETY FOR MICROBIOLOGY | mBio®

RESEARCH ARTICLE

The Human Salivary Microbiome Is Shaped by Shared Environment Rather than Genetics: Evidence from a Large Family of Closely Related Individuals

Liam Shaw,[a,b] Andre L. R. Ribeiro,[c,d] Adam P. Levine,[e] Nikolas Pontikos,[a,f,g] Francois Balloux,[a] Anthony W. Segal,[e] Adam P. Roberts,[c,h] Andrew M. Smith[c]

UCL Genetics Institute, UCL, London, United Kingdom[a]; Centre for Mathematics and Physics in the Life Sciences and Experimental Biology (CoMPLEX), UCL, London, United Kingdom[b]; UCL Eastman Dental Institute, UCL, London, United Kingdom[c]; School of Dentistry, University Center of Pará – CESUPA, Belém, Brazil[d]; Division of Medicine, UCL, London, United Kingdom[e]; Institute of Ophthalmology, UCL, London, United Kingdom[f]; Moorfields Eye Hospital, London, United Kingdom[g]; Department of Parasitology, Liverpool School of Tropical Medicine, Liverpool, United Kingdom[h]

ABSTRACT The human microbiome is affected by multiple factors, including the environment and host genetics. In this study, we analyzed the salivary microbiomes of an extended family of Ashkenazi Jewish individuals living in several cities and investigated associations with both shared household and host genetic similarities. We found that environmental effects dominated over genetic effects. While there was weak evidence of geographical structuring at the level of cities, we observed a large and significant effect of shared household on microbiome composition, supporting the role of the immediate shared environment in dictating the presence or absence of taxa. This effect was also seen when including adults who had grown up in the same household but moved out prior to the time of sampling, suggesting that the establishment of the salivary microbiome earlier in life may affect its long-term composition. We found weak associations between host genetic relatedness and microbiome dissimilarity when using family pedigrees as proxies for genetic similarity. However, this association disappeared when using more-accurate measures of kinship based on genome-wide genetic markers, indicating that the environment rather than host genetics is the dominant factor affecting the composition of the salivary microbiome in closely related individuals. Our results support the concept that there is a consistent core microbiome conserved across global scales but that small-scale effects due to a shared living environment significantly affect microbial community composition.

IMPORTANCE Previous research shows that the salivary microbiomes of relatives are more similar than those of nonrelatives, but it remains difficult to distinguish the effects of relatedness and shared household environment. Furthermore, pedigree measures may not accurately measure host genetic similarity. In this study, we include genetic relatedness based on genome-wide single nucleotide polymorphisms (SNPs) (rather than pedigree measures) and shared environment in the same analysis. We quantify the relative importance of these factors by studying the salivary microbiomes in members of a large extended Ashkenazi Jewish family living in different locations. We find that host genetics plays no significant role and that the dominant factor is the shared environment at the household level. We also find that this effect appears to persist in individuals who have moved out of the parental household, suggesting that aspects of salivary microbiome composition established during upbringing can persist over a time scale of years.

KEYWORDS environmental microbiology, microbiome, oral microbiology

Received 18 July 2017 **Accepted** 9 August 2017 **Published** 12 September 2017

Citation Shaw L, Ribeiro ALR, Levine AP, Pontikos N, Balloux F, Segal AW, Roberts AP, Smith AM. 2017. The human salivary microbiome is shaped by shared environment rather than genetics: evidence from a large family of closely related individuals. mBio 8:e01237-17. https://doi.org/10.1128/mBio.01237-17.

Editor Claire M. Fraser, University of Maryland, School of Medicine

Address correspondence to Adam P. Roberts, adam.roberts@lstmed.ac.uk.

L.S. and A.L.R.R. contributed equally to this work.

The human microbiome is the name given to the collected communities of bacteria that live on and in the human body. The oral microbiome is one of the most diverse (1) of any human-associated microbial community (2). The oral microbiome is a causative factor in conditions such as dental caries (3), periodontal disease (4), and halitosis (5) and has also been implicated as a reservoir for infection at other body sites (2) and in the pathogenesis of nonoral diseases, such as inflammatory bowel disease (6). Strictly speaking there is no single "oral microbiome," as its composition is highly heterogeneous at different sites in the mouth (7, 8), but the term is commonly used to encompass all of these sites. Site-specific microbiomes can be observed in the periodontal sulcus, dental plaque, tongue, buccal mucosa, and saliva (9). The salivary microbiome exhibits long-term stability and can be considered an important reservoir that contains microorganisms from all distinct ecological niches of the oral cavity. Characterizing and understanding the factors defining the composition of the salivary microbiome are thus crucial to understanding the oral microbiome (10, 11).

Some factors that are thought to influence the human microbiome include environment, diet, disease status, and host genetics (12). The relative importance of these factors for the oral microbiome is still under debate, with the majority of previous studies focusing on the gut microbiome (7–9), although it seems reasonable to assume some potential interaction between the salivary microbiome and microbial communities in other parts of the human body, including the intestinal tract (10).

There is evidence that genetically related individuals tend to share more gut microbes than unrelated individuals do, whether or not they are living in the same house at the time of sampling (13, 14). However, the levels of covariation are similar in monozygotic and dizygotic twins, suggesting that a shared early environment may be a more important factor than genetics (13, 15). The effect of cohabitation with direct and frequent contact is greatest when considering the skin microbiome, with a less-evident effect on the gut and salivary microbiomes (11).

There is also evidence that genetic variation is linked to microbiome composition across other body sites, including the mouth (12), with a recent genome-wide association study (GWAS) identifying several human loci associated ($P < 5 \times 10^{-8}$) with microbial taxonomies in the gut microbiome (16). However, no study thus far has incorporated both genetic relatedness (as a continuous variable) and shared environment into the same analysis of the salivary microbiome.

Despite high diversity between individuals, the salivary microbiome appears to have little geographical structure at the genus level at the global scale (17). Nevertheless, at smaller geographical scales, it appears that the environment plays a role in the oral microbiome. Song et al. studied 60 household units and found that the bacterial composition of dorsal tongue bacterial samples was more similar between cohabiting family members than for individuals from different households, with partners and mother-child pairs having significantly more similar communities (18). However, this did not include information on genetic relatedness in addition to family relationships. It appears that household-level differences in the salivary microbiome may also apply to genetically unrelated individuals and nonpartners, with a similar pattern observed in analysis of 24 household pairs of genetically unrelated individuals, only half of whom were considered romantic couples at the time of sampling (19).

The establishment of the oral microbiome appears to proceed rapidly in the first few years of life, with a notable increase in diversity from 0 to 3 years (18), especially after the eruption of teeth (20). The plaque microbiome also appears stable within adult individuals over a period of at least 3 months, with a unique "fingerprint" of oligotypes discernible even within a single bacterial genus (21). Another study indicates that the salivary microbiome is relatively stable over a year, despite measurable effects of interventions like flossing (22). Taken together, these findings suggest the intriguing hypothesis that once a particular oral microbiome is established earlier in life, it can potentially persist for months and perhaps even years, particularly if external factors such as diet remain fixed. If this were true, shared upbringing effects would continue

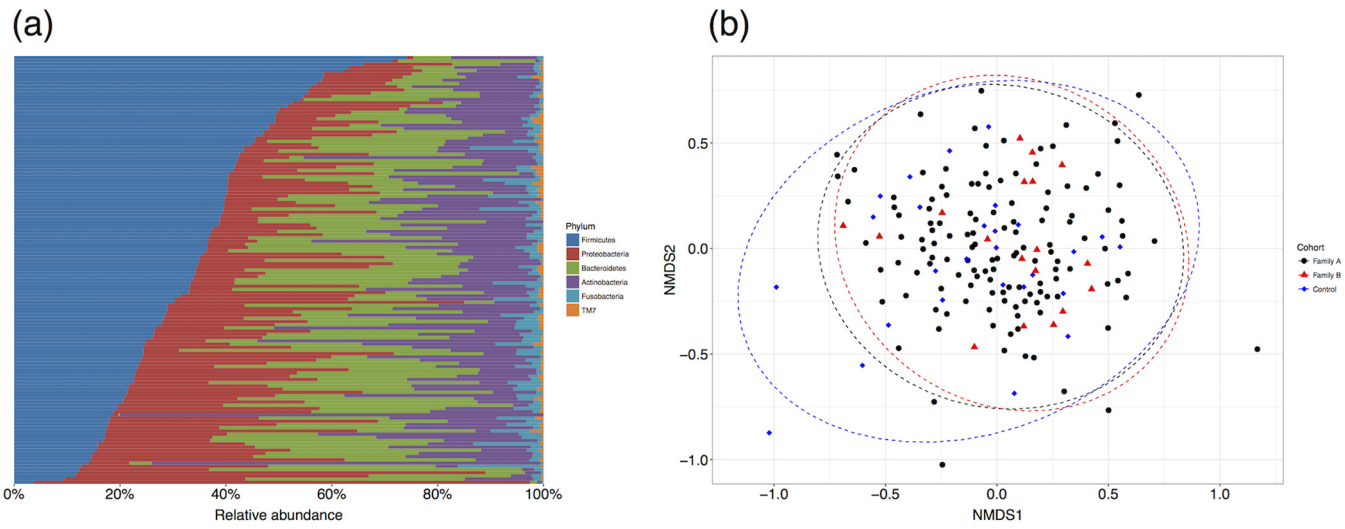

FIG 1 The family within this study contains a representative sample of variation in salivary microbiome composition compared to controls. (a) Relative abundance of the six bacterial phyla found in saliva samples from family A sorted by decreasing *Firmicutes* content. The color scheme used here was adapted from that in Stahringer et al. (15). The 271 MED phylotypes were assigned to taxa using RDP based on the HOMD database. (b) Nonmetric multidimensional scaling based on Bray-Curtis dissimilarity between samples shows high overlap between family A, family B, and unrelated Ashkenazi Jewish controls. NMDS1, nonmetric multidimensional scaling axis 1.

to be detected in the salivary microbiome even after individuals are no longer living in the same household (15).

A recently described large Ashkenazi Jewish family (23) offers an opportunity to investigate the effect of both environment and genetics in closely related individuals. The availability of host genetic data for this cohort means that we can calculate similarity between individuals based on single nucleotide polymorphisms (SNPs), rather than using measures of relatedness from pedigrees that do not precisely correspond to shared genetic content (24). We hypothesized that using this more accurate measure of host genetic similarity could lead to different conclusions about the proportion of shared microbiome composition attributable to genetics compared to previous studies. While, like other studies, we lack information on potential confounders such as diet and lifestyle (17), due to shared cultural practices between members of the ultraorthodox Ashkenazi Jewish community (25), we believe that confounding factors are likely to be more controlled for in this cohort than in others. For this reason, this cohort represents a unique opportunity to compare the salivary microbiome within a large number of individuals living in separate locations but nevertheless sharing a similar diet, lifestyle, and genetic background and to investigate the long-term effect of shared upbringing on salivary microbiome composition.

RESULTS

Description of cohort. The families analyzed in this study have been already described in detail by Levine et al. (23). All individuals sampled were from the ultraorthodox Ashkenazi Jewish community. Family A comprised more than 800 individuals living in at least eight cities in four countries. Family B comprised more than 200 individuals living in at least four cities in three countries. The unrelated controls were sampled from the same community as the two families. In total, data were generated from samples from 133 individuals in family A, 18 individuals in family B, and 27 controls.

Using minimum entropy decomposition (see Materials and Methods), we found 271 phylotypes in the total microbiome data set, all of which were present when considering just family A. Of these 271 phylotypes, 49 were present in >95% of individuals within family A, with the *Firmicutes* the most abundant phyla (Fig. 1a) as observed in previous oral microbiome studies (15, 26). The most abundant genera were *Streptococcus* (30.4%), *Rothia* (18.5%), *Neisseria* (17.1%), and *Prevotella* (17.1%). The composi-

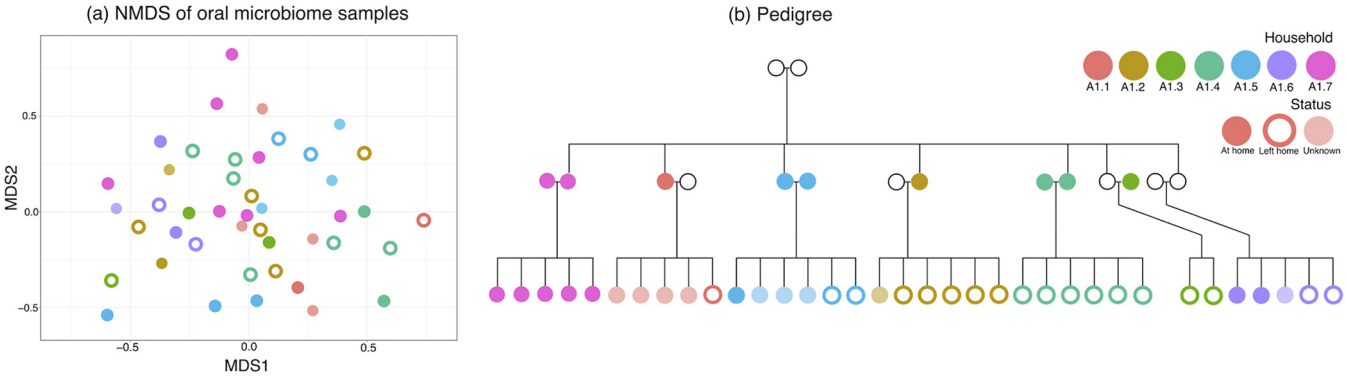

FIG 2 Salivary microbiome composition appears associated with household in an exploratory analysis. Salivary microbiome samples cluster somewhat by household (shown by different colors) despite large overlap between them, shown by a nonmetric multidimensional scaling based on Bray-Curtis dissimilarity between samples from individuals in a particular subfamily ($n = 44$) within family A (a). This figure includes individuals who are currently living together (filled circles), those who had moved out of their childhood home (empty circles), and those for whom data were missing (faint circles). This clustering could be due to shared environment or also due to shared genetics, as is obvious from the pedigree (b).

tion of samples was similar between the two families (families A and B) and the unrelated controls (Fig. 1b). These groupings had a small but significant effect in an analysis of variance ($R^2 = 0.015$; $P < 0.01$), but this is typical of comparisons between such large groups that may differ in an unknown number of confounded variables (e.g., diet, genetics, lifestyle). We concluded that family A was at the very least a representative sample capturing the majority of the variation present in the wider Ashkenazi Jewish population, if not also individuals who are not Ashkenazi Jewish (for comparison with Human Microbiome Project data, see Fig. S3 in the supplemental material).

This cohort was originally collected for a study of the genetics of Crohn's disease (23), and 28 individuals within our sample had a diagnosis of the disease at the time of saliva sample acquisition. We found no significant effect of Crohn's disease on salivary microbiome composition with an exploratory analysis of variance ($R^2 = 0.009$; $P = 0.101$; $n = 148$) accounting for other variables. It was therefore not included as a covariate in further analysis.

Host genetic similarity is weakly correlated with salivary microbiome similarity. We performed an exploratory analysis on individuals in family A with both genetic and microbiome data available ($n = 111$) (Fig. S4) and found that genetic kinship was weakly but significantly associated with salivary microbiome dissimilarity computed using Bray-Curtis dissimilarity (Fig. S5a; r = 0.065 by Mantel test; $P = 0.001$). This analysis does not take into account confounding by the shared environment and therefore sets a probable upper bound on the variation that can be attributed to host genetics. An exploratory analysis of microbiome variation across a subfamily within family A ($n = 44$) showed that individuals from the same household had a more similar microbiome composition as measured by Bray-Curtis dissimilarity (mean ± standard deviation [SD], 0.623 ± 0.088) compared with individuals from different households (0.652 ± 0.084), and this difference was significant ($P < 0.001$ by two-sided t test). An exploratory visual representation of this variation showed further clustering by household, although there was large overlap between households in two dimensions (Fig. 2). However, such an analysis is insufficient; household is obviously correlated with variation in host genetics (Fig. S6) because parents tend to live with their children. This emphasizes the need for a quantitative approach looking at the effect of both household and genetics simultaneously as well as other potential confounders.

The approach we chose to use was adonis, which performs a permutational analysis of variance in community composition using a sequential sum-of-squares approach (27). We used Bray-Curtis dissimilarities to quantify differences in salivary microbiome composition between individuals. The following sections present our analyses attempting to quantify the effects of shared environment and genetics. The analysis groups were effectively nested as follows: individuals cohabiting with at least one other

TABLE 1 Permutational analysis of variance (adonis) results for 26 cohabiting individuals who lived in the same household with at least one other individual[a]

	City only		Household only		City and household[c]	
Variable[b]	R^2	*P*	R^2	*P*	R^2	*P*
Sequencing plate	0.048	0.190	0.048	0.075	0.048	0.458
Gender	0.032	0.724	0.032	0.4	0.032	0.467
Age	0.069	0.017	0.069	0.004	0.069	0.013
MDS1	0.031	0.757	0.031	0.537	0.031	0.727
MDS2	0.050	0.142	0.050	0.052	0.050	0.099
MDS3	0.030	0.807	0.030	0.585	0.030	0.862
MDS4	0.049	0.162	0.049	0.054	0.049	0.097
MDS5	0.029	0.824	0.029	0.614	0.029	0.791
City	0.080	0.400			0.080	0.178
Household			0.300	0.001	0.220	0.001
Residuals	0.582		0.362		0.362	
Total	1.000		1.000		1.000	

[a]Sharing a household was always significant and explained the most variance of any variable (>18%) even in a model that nests permutations within cities.
[b]The order of variables in the model is given by their order in the table. MDS1 to MDS5 are the five axes of metric multidimensional scaling (MDS).
[c]Permutations stratified by city in this analysis.

individual (n = 26; Table 1), individuals who had cohabited with at least one other individual, either at the time of sampling or beforehand (n = 61; Table 2), individuals living in four different cities who were not necessarily cohabiting with another individual (n = 82; Table S1), and individuals with host genetic information available (n = 111; Table 3).

Shared household is the dominant factor affecting salivary microbiome composition. We performed a permutational analysis of variance on the salivary microbiome dissimilarities for 26 individuals within family A, each of whom lived in a household with at least one other individual in the cohort. At the time of sampling, these cohabiting individuals lived in a total of 16 households in four cities (cities I, II, III, and IV). To account for host genetics, we included axes from a metric multidimensional scaling (MDS) of pairwise genetic distances between individuals as explanatory variables (see Materials and Methods and Fig. S6). The magnitude of the effect of a significant variable is given by the amount of variance explained (R^2 in tables).

TABLE 2 Permutational analysis of variance (adonis) results for 61 individuals who had at least cohabited at some point[a]

	City only		Household only		City and household[c]	
Variable[b]	R^2	*P*	R^2	*P*	R^2	*P*
Sequencing plate	0.029	0.018	0.029	0.012	0.029	0.013
Gender	0.018	0.258	0.018	0.219	0.018	0.257
Age	0.038	0.002	0.038	0.001	0.038	0.002
MDS1	0.014	0.668	0.014	0.607	0.014	0.740
MDS2	0.017	0.362	0.017	0.305	0.017	0.440
MDS3	0.020	0.173	0.020	0.141	0.020	0.263
MDS4	0.020	0.150	0.020	0.118	0.020	0.147
MDS5	0.012	0.783	0.012	0.744	0.012	0.943
City	0.056	0.149			0.056	0.934
Household			0.239	0.021	0.183	0.044
Residuals	0.777		0.594		0.594	
Total	1.000		1.000		1.000	

[a]Sharing a household was always significant and explains the most variance of any variable (>18%) even in a model that nests permutations within cities.
[b]The order of variables in the model is given by their order in the table.
[c]Permutations stratified by city in this analysis.

TABLE 3 Comparison of pedigree-based and genome-wide measures of kinship to take host genetics into account in a permutational analysis of variance (adonis) on salivary microbiome dissimilarities of 111 individuals[a]

Variable[b]	Pedigree (kinship2)		Genome-wide SNPs (LDAK)	
	R^2	P	R^2	P
Sequencing plate	0.028	<0.001	0.028	<0.001
Gender	0.011	0.094	0.011	0.096
Age	0.023	<0.001	0.023	<0.001
MDS1	0.010	0.174	0.011	0.119
MDS2	0.007	0.706	0.010	0.231
MDS3	0.012	0.063	0.011	0.131
MDS4	0.016	0.009	0.011	0.111
MDS5	0.009	0.325	0.007	0.617
Parental household	0.215	<0.001	0.217	<0.001
Residuals	0.670		0.671	
Total	1		1	

[a]Using pedigree information to produce kinship results in a significant association with human genetics via the fourth MDS axis, which is not present using kinships calculated with LDAK based on genome-wide SNPs.

[b]The order of variables in the model is given by their order in the table.

There was no significant effect of any of the MDS axes, suggesting that host genetics in closely related individuals does not significantly affect microbiome composition. We investigated the effect of environment using two levels of geography: city and household (Table 1). A city-only model showed no significant effect of environment (R^2 = 0.08; P = 0.4), whereas a household-only model showed a significant effect (R^2 = 0.30; P = 0.001). This was reproduced in a model containing both geographical variables, with permutations stratified by city, where household was still a significant effect (R^2 = 0.22; P = 0.001), suggesting that differences at the level of household are more important than at larger geographical scales. We confirmed that city-level effects were small by extending our sample to 82 individuals across the four cities who were not necessarily cohabiting with others (48 individuals for city I, 13 for city II, 12 for city III, and 9 for city IV) and found that city still had a small effect, although it was significant (R^2 = 0.053; $P < 0.01$). In this analysis, we also found no significant effect of genetics, but age was significant (R^2 = 0.028; P = 0.0101) (Table S1).

Spouses share taxa at the subgenus level. Restricting the analysis to only married couples within family A (n = 16; eight couples), shared household explained even more of the variance (R^2 = 0.591; P = 0.001). Subtle variations in the relative abundance of phylotypes within the same genus between households were observable, even within the same city location. For example, *Leptotrichia* phylotypes qualitatively varied consistently between spouse pairs, and these patterns were also seen in children living at home (Fig. 3). Minimum entropy decomposition (MED) phylotype X2772 was present in both spouses in household A1.7 and was also present in the two youngest children within that household (≤10 years old). Similarly, within household A2.4, the *Leptotrichia* phylotypes of the two children who were ≤10 years old were more similar than the *Leptotrichia* phylotype of an older child. Quantitatively, repeating the permutational analysis of variance based only on the composition of phylotypes within *Leptotrichia* showed that spousal pair explained 68.4% of variance, although this was not significant (R^2 = 0.684; P = 0.068), and spouses had significantly more similar subgenus phylotype composition than nonspouses did (Fig. S7b). Similar patterns with spouses were also visible in other abundant genera (Fig. S7a), with spouses on average having a significantly more similar subgenus phylotype composition than nonspouses did (mean ± standard error [SE] difference in Bray-Curtis dissimilarity for each genus, −0.048 ± 0.013; Fig. S7b).

Household effects persist in individuals who are no longer cohabiting. There were an additional 35 individuals who had grown up in a household with at least one

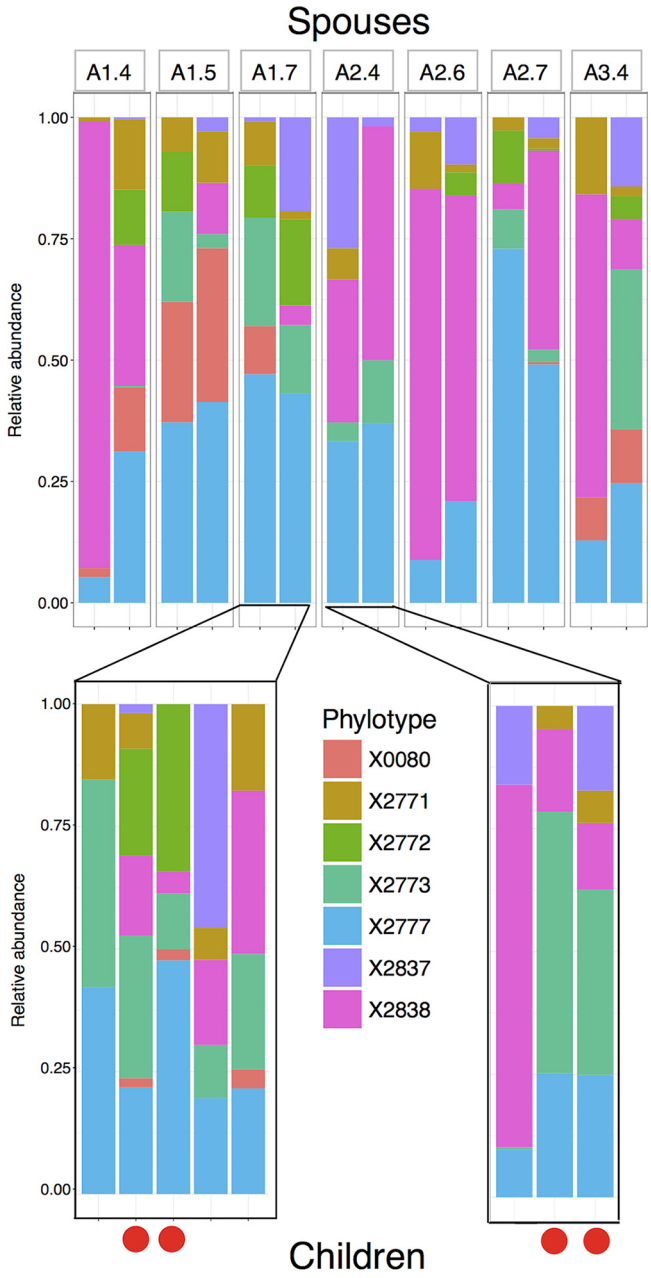

FIG 3 Variation within a genus shows household-level differences in relative abundances of phylotypes, shown here with the relative abundance of phylotypes within *Leptotrichia*. The relative abundance of phylotypes within seven pairs of spouses shows clear associations with household, with spouses significantly more similar in phylotype composition within *Leptotrichia* ($P = 0.039$ by two-sided t test). These patterns are to some extent recapitulated in their children. Looking at children still living at home, MED phylotype X2772 is not observed in any individual from household A2.4 but is found in both spouses and two children living in household A1.7. Solid red circles indicate children ≤10 years at the time of sampling, who appear more similar to each other than other pairs of children. For variation within the top 12 most abundant genera between spouses, see Fig. S7 in the supplemental material.

other individual present but who no longer lived together at the time of sampling. To see whether the effects of household persisted, we repeated analysis of variance with these individuals included along with the cohabiting individuals ($n = 61$; Table 2). The effect of household remained significant ($R^2 = 0.183$; $P = 0.044$), and no axes of human genetic variation were significant ($P > 0.05$). Age had a significant effect ($R^2 = 0.038$; $P < 0.01$).

Other variables such as age and sequencing plate had smaller effects than household in all our analyses of variance. However, we chose the order of variables as presented in our tables (Tables 1, 2, and 3) to test for the effect of household after controlling for other variables. Because of the sequential sum-of-squares approach used by adonis, this ordering of variables can have an effect with an unbalanced design. To check that this was not biasing our results and therefore our conclusions about the important factors for salivary microbiome composition, we also investigated the effect of randomly permuting the order of variables in our model formula (see supplemental material). The results of this analysis confirmed that household was always significant (false-discovery rate [q] < 0.05, with Benjamini-Hochberg multiple testing correction), as was age.

Relying on pedigree kinships produces a genetic signal. To test whether our conclusions required using kinships estimated from genome-wide SNP data for individuals or whether pedigree information was sufficient, we also repeated our analyses using pedigree kinships (see Materials and Methods). Using pedigree kinships resulted in a small but significant amount of variation in microbiome composition being attributable to host genetics via MDS axis 4 ($R^2 = 0.016$; $P < 0.01$; Table 3).

DISCUSSION

We have conducted, to our knowledge, the first simultaneous investigation of the role of environment and host genetics in shaping the human salivary microbiome in a cohort of closely related individuals within a large Ashkenazi Jewish family. We found a weak correlation between host kinship and salivary microbiome dissimilarity before taking shared household into account and an apparent small but significant effect of genetics when using kinships based on the family pedigree as proxies for genetic similarity. However, when using kinship estimates based on genome-wide SNPs between individuals and simultaneously controlling for shared household with a permutational analysis of variance, we find no support for any clear effect of human genetics, suggesting that shared environment has a much larger effect than genetics and is the dominant factor affecting the salivary microbiome. Typically shared household had an order of magnitude greater effect compared with other significant variables. For example, in our analysis where city was also used as an environmental variable, the variance explained was as follows: household (18.3%), age (3.8%), and sequencing plate (2.9%) (Table 2).

We also observed that younger children living in the same household shared subtle variations in phylotype abundance within genera with their parents (Fig. 3). However, despite a persistence of household effects, it would be wrong to conclude that the salivary microbiome is completely fixed once established, as it clearly has aspects that can change over time. For example, shared household explained more variation for spousal pairs (likely due to frequent contact between them) and that phylotypes observed in younger children and their parents were not seen in older children (likely due to less frequent contact between them). Taken together, these observations support the view that human genetics does not play a major role in shaping the salivary microbiome, at least not in individuals of the same ethnicity, compared to the environment and contact with other individuals.

Our results confirm the seemingly paradoxical situation that the salivary microbiome is largely consistent across global geographical scales but can show large variation between households in the same city. Previous studies have also found evidence of small variations in salivary microbiome composition comparing samples across a global scale (17). As noted previously, this variation could be influenced by differences in environmental or cultural factors, in which case controlling for these differences would decrease the amount of geographical variation. All individuals in our study follow a traditional Ashkenazi Jewish lifestyle and subsequently are thought to share a similar diet and lifestyle regardless of geographical location (25), which may reduce the variation attributable to city-level differences.

The establishment of the oral microbiome early in life may lead to the persistence

of a similar composition over several years. The microbial composition of sites within the mouth has been previously observed to be persistent within individuals over periods of months (21) to a year (22), and we see similar strain-level variation between spouses and their young children as observed between individuals by Utter et al. (21) (Fig. 3). Our results indicate the persistence of household effects in individuals no longer cohabiting, suggesting that the salivary microbiome composition established early in life via shared upbringing is able to persist for at least several years. It has been observed that monozygotic twins do not have significantly more similar gut microbiomes than dizygotic twins (13). Stahringer et al. observed the same effect in the salivary microbiome and also found that the salivary microbiomes of twins became less similar as they grew older and ceased cohabiting, concluding that "nurture trumps nature" in the salivary microbiome (15). Our findings from a large number of related individuals rather than twins support this view, including the persistence of shared upbringing effects. Shared upbringing appears to be the dominant factor affecting microbiome composition in both the gut and the mouth, rather than genetic similarity. This may have implications for understanding the familial aggregation of diseases such as inflammatory bowel disease, which has been suggested to have an environmental component (28).

The salivary microbiome appears to be far more resilient to perturbation than the gut microbiome is, with a rapid return to baseline composition after a short course of antibiotics (29). While this could be because of the pharmacokinetics of the antibiotics involved, Zaura et al. speculate that this difference may be due to the salivary microbial ecosystem's higher intrinsic resilience to stress, as the mouth is subject to more frequent perturbation (30). Our work supporting the dominant role of the environment in affecting salivary microbiome composition suggests that another important factor in long-term persistence may be the regular reseeding of the ecosystem with bacteria from the external environment.

The fact that we reached our conclusion about the lack of effect of genetics only after including kinship based on genome-wide SNP markers casts doubt on the reliability of pedigrees for calculating relatedness. There are several possible reasons for a discrepancy between kinship estimates from pedigrees and allele sharing (24). One possibility is errors in the pedigree, most likely due to extrapair paternities, although this explanation can be ruled out in this data set. More importantly, inherent stochasticity in the Mendelian process of inheritance means that although parents always pass on 50% of their genes to their offspring, SNPs are inherited together in blocks (i.e., haplotypes), meaning that the relatedness between two offspring in a family can be substantially different from 50%. Finally, and most importantly for this closely related population, shallow pedigrees cannot fully capture complex inbreeding patterns. Thus, while pedigrees are a good model for host relatedness in microbiome studies of large randomly mating populations, they should be used with caution in closely related large families like this one.

Limitations. Because all individuals in our main cohort were members of the same extended Ashkenazi Jewish family, the genetic variation in our data set is therefore much lower than between individuals from a wider population. It is conceivable that host genetics between more distantly related individuals may play a significant role in affecting salivary microbiome composition. However, we note that a recent study of the nasopharyngeal microbiome among Hutterite individuals (a founder population in North America) detected associations between host variation and microbial composition with a similar cohort size (31), demonstrating that limited genetic variation can be associated with the composition of other microbiomes; it may simply be that the salivary microbiome is relatively unaffected by such variation.

Furthermore, our study looked at only overall genetic similarity, assessed using community comparison metrics based on taxon abundances. They therefore do not preclude the existence of fine-scale links between particular microbial taxa and individual genetic loci, particularly in immune-sensing genes such as those identified in the

gut microbiome by Bonder et al. using a much larger cohort (32), although our study was not designed or have the statistical power to detect such associations.

Additionally, we lack detailed information on diet and lifestyle factors of individuals in this study. However, the shared cultural practices within this ultraorthodox Ashkenazi Jewish family mean that it is not unreasonable to assume that they share similar lifestyles and diet despite living in different locations around the world (25).

The apparent persistence of shared upbringing could be confounded by the fact that individuals may continue living near the household where they grew up. If this were the case, then our observation could instead be due to the persistence of a shared environment beyond the household at a level intermediate between household and city, rather than the persistence of a stable salivary microbiome following environmental change. Finally, our samples represent only a single cross-sectional snapshot in time. More long-term longitudinal studies like the work of Stahringer et al. on twins (15) are necessary to investigate the persistence of the salivary microbiome after its establishment early in life in a variety of relatedness settings.

Conclusion. In summary, our results incorporating a measure of genetic relatedness using SNPs demonstrate that the overall composition of the human salivary microbiome in a large Ashkenazi Jewish family is largely influenced by shared environment rather than host genetics. An apparent significant effect of host genetics using pedigree-based estimates disappears when using genetic markers instead, which shows that in future microbiome research, the use of pedigree relatedness as a proxy for host genetic similarity should be done with caution. Geographical structuring occurs to a greater extent at the household level within cities than between cities on different continents. Living in the same household is associated with a more similar salivary microbiome, and this effect persists after individuals have left the household. This is consistent with the long-term persistence of the salivary microbiome composition established earlier in life due to shared upbringing.

MATERIALS AND METHODS

Ethics. Ethical and research governance approval was provided by the National Research Ethics Service London Surrey Borders Committee and the UCL Research Ethics Committee. Written informed consent was provided by all participants.

Cohort. Our cohort contained data from 133 individuals within the same extended family (family A) living in four disparate cities (I, II, III, and IV) across three continents (see reference 23 for more information). We also had samples available from 18 individuals from a separate smaller family (family B) and 27 unrelated Ashkenazi Jewish controls. All individuals studied were of genetically confirmed Ashkenazi Jewish ancestry (23, 25). When information was not directly available, shared household was inferred according to age; individuals within this community marry and subsequently leave the family home at a median age of 21 years (95% confidence interval, 19 to 26 years) (25). Therefore, we assumed that individuals aged 18 or younger at the time of sampling were living with their parents and individuals aged 25 or older were not.

For analysis of the effects of household, we included only households with two or more individuals so as to remove the possibility that we were measuring only interindividual differences, which can be large in the salivary microbiome (17, 21). Twenty-six individuals were living with at least one other individual at the time of sampling in a total of nine households. An additional 35 individuals who had grown up in a shared household with at least one other individual in the cohort but who were no longer living together were subsequently included in the analysis.

Sampling. Saliva samples were collected in sterile tubes containing saliva preservative buffer by the method of Quinque et al. (33). For the full protocol, see the supplemental material. Five hundred milliliters of saliva/preservative buffer was used with PurElute bacterial genomic kit (Edge Biosystems, Gaithersburg, MD) for DNA extraction. After bacterial DNA extraction, three spike DNAs were added to all samples at a final concentration of 4 pg/ml, 0.4 pg/ml, and 0.08 pg/ml, respectively.

PCR amplification, purification, and sequencing. The Mastermix 16S basic PCR kit containing MolTaq 16S DNA polymerase (Molzym GmbH & Co. KG, Bremen, Germany) was used to generate PCR amplicons. PCR amplicons were purified in two rounds using the Agencourt AMPure system (Beckman Coulter, Inc., Beverly, MA) in a Hamilton StarLet (Hamilton Company, Boston, MA) automated liquid handler. DNA quantitation and quality control were performed using the Agilent 2100 Bioanalyzer system (Agilent Technologies, Santa Clara, CA).

We used 785F (F stands for forward) and 1175R (R stands for reverse) 16S rRNA primers (see Text S1 in the supplemental material) that amplified the V5-V7 region of the 16S rRNA gene on the Illumina MiSeq system (Illumina, San Diego, CA).

Quality control. To assess technical variation across runs, we spiked samples during library preparation with a fixed amount of synthetic DNA (see supplemental material). Three unique spike sequences (length of 350 bases) that could be easily identified for quality control purposes were designed. We found, as expected, that the number of spike sequences and the number of putative 16S sequences (length between 350 and 380 bases) were negatively correlated with each other due to the limited total sequencing depth of the Illumina MiSeq system (Fig. S1a). The variation in reads corresponding to this spike across samples was independent of run. We also resequenced a subset of samples without spikes to verify whether spikes affected our analyses and observed the same qualitative differences (Fig. S1b), implying that the addition of spikes did not have a negative impact on downstream analysis. Paired-end reads were merged with fastq-mergepairs in VSEARCH v1.11.1 (34), discarding reads with an expected error of >1. As the expected length of the V5-V7 region was 369 bases, we discarded sequences with <350 or >380 bases.

Clustering and taxonomic classification. Sequences were clustered with minimum entropy decomposition (MED) (35). MED requires that the variation in read depth across samples does not differ by several orders of magnitude, so we discarded samples with fewer than 5,000 reads and subsampled to a maximum number of 20,000 sequences, resulting in 6,353,210 sequences. We ran MED v2.1 with default parameters (see Text S1 in the supplemental material), identifying 271 phylotypes in the data set (Table S2). MED offers higher resolution than operational taxonomic unit (OTU) picking methods do, and it has previously been shown to differentiate the composition of the oral microbiomes of individuals over time even within the same genus in a study of plaque samples (21). We verified that using MED phylotypes gave very similar compositional dissimilarities compared to using *de novo* OTUs clustered at 98.5% sequence similarity (Fig. S2) but allowed slightly increased statistical power in analysis of variance (see supplemental material), consistent with the literature (35). MED phylotypes had taxonomy assigned using RDP (36) against the Human Oral Microbiome Database (HOMD) (37). Comparison to Human Microbiome Project (HMP) samples from various sites in the mouth also indicated that Ashkenazi Jewish individuals do not have a significantly different oral microbiome from those of other populations, with Ashkenazi Jewish saliva samples clustering with nonplaque samples from individuals in the HMP (Fig. S3). However, the use of different primers makes it difficult to reach a robust conclusion on this point.

Inclusion of host genetics. We investigated the effect of relatedness between individuals on salivary microbiome composition using both genetic kinships (based on SNPs) and pedigree kinships (based on the pedigree). We calculated pedigree kinships with kinship2 (38) and genetic kinships with LDAK v5.94 (39) using genome-wide SNP data from either the Illumina HumanCytoSNPv12 (Illumina, USA) or the Illumina HumanCoreExome-24, as described previously (23). These genetic kinships k_g are normalized to have a mean of zero and correspond to genetic similarity between individuals. k_g correlates with the pedigree kinship k_p, but there can be substantial spread around the expected values due to the random nature of genetic inheritance (Fig. S5b), making k_g a more accurate measure of true genetic similarity between individuals (24). We converted these kinships to dissimilarities and then Euclidean distances (supplemental material) which were used in a multidimensional scaling (MDS) ordination (Fig. S6). Following Blekhman et al. (12), we used MDS with five axes as covariates in a permutational analysis of variance of salivary microbiome dissimilarities.

Statistical analysis. We calculated Bray-Curtis dissimilarities between samples based on relative abundances of phylotypes, excluding samples with fewer than 1,000 reads. Variance explained in Bray-Curtis dissimilarities was calculated using the adonis function from the vegan v2.4.1 package in R, which performs a permutational analysis of variance of distance matrices (27). We used 9,999 permutations, with permutations stratified by geographical sample location where appropriate.

SUPPLEMENTAL MATERIAL

Supplemental material for this article may be found at https://doi.org/10.1128/mBio.01237-17.

TEXT S1, DOCX file, 0.04 MB.
FIG S1, TIF file, 11.8 MB.
FIG S2, TIF file, 11.3 MB.
FIG S3, TIF file, 13.1 MB.
FIG S4, TIF file, 41.5 MB.
FIG S5, TIF file, 14.9 MB.
FIG S6, TIF file, 5.9 MB.
FIG S7, TIF file, 14 MB.
TABLE S1, DOCX file, 0.05 MB.
TABLE S2, XLSX file, 0.3 MB.

ACKNOWLEDGMENTS

We thank all the individuals who kindly participated in this study.

This project was supported through the following charities and research councils: EFFORT (Eastman Foundation for Oral Research and Training), the Charles Wolfson Charitable Trust, and the Medical Research Council (MR/L000261/1). A.P.L. was sup-

ported by the Irwin Joffe Memorial Fellowship. L.S. was supported by the Engineering and Physical Sciences Research Council (EP/F500351/1). A.L.R.R. was supported by the CAPES Foundation of the Ministry of Education of Brazil (0698130).

The funders had no role in study design, data collection and interpretation, or the decision to submit the work for publication.

REFERENCES

1. Human Microbiome Project Consortium. 2012. Structure, function and diversity of the healthy human microbiome. Nature 486:207–214. https://doi.org/10.1038/nature11234.
2. Wade WG. 2013. The oral microbiome in health and disease. Pharmacol Res 69:137–143. https://doi.org/10.1016/j.phrs.2012.11.006.
3. Yang F, Zeng X, Ning K, Liu K-L, Lo C-C, Wang W, Chen J, Wang D, Huang R, Chang X, Chain PS, Xie G, Ling J, Xu J. 2012. Saliva microbiomes distinguish caries-active from healthy human populations. ISME J 6:1–10. https://doi.org/10.1038/ismej.2011.71.
4. Teles R, Teles F, Frias-Lopez J, Paster B, Haffajee A. 2013. Lessons learned and unlearned in periodontal microbiology. Periodontol 2000 62: 95–162. https://doi.org/10.1111/prd.12010.
5. Ren W, Zhang Q, Liu X, Zheng S, Ma L, Chen F, Xu T, Xu B. 2016. Supragingival plaque microbial community analysis of children with halitosis. J Microbiol Biotechnol 26:2141–2147. https://doi.org/10.4014/jmb.1605.05012.
6. Lucas López R, Grande Burgos MJ, Gálvez A, Pérez Pulido R. 2017. The human gastrointestinal tract and oral microbiota in inflammatory bowel disease: a state of the science review. APMIS 125:3–10. https://doi.org/10.1111/apm.12609.
7. Eren AM, Maignien L, Sul WJ, Murphy LG, Grim SL, Morrison HG, Sogin ML. 2013. Oligotyping: differentiating between closely related microbial taxa using 16S rRNA gene data. Methods Ecol Evol 4:1111–1119. https://doi.org/10.1111/2041-210X.12114.
8. Mark Welch JL, Rossetti BJ, Rieken CW, Dewhirst FE, Borisy GG. 2016. Biogeography of a human oral microbiome at the micron scale. Proc Natl Acad Sci U S A 113:E791–E800. https://doi.org/10.1073/pnas.1522149113.
9. Krishnan K, Chen T, Paster BJ. 2017. A practical guide to the oral microbiome and its relation to health and disease. Oral Dis 23:276–286. https://doi.org/10.1111/odi.12509.
10. Takeshita T, Kageyama S, Furuta M, Tsuboi H, Takeuchi K, Shibata Y, Shimazaki Y, Akifusa S, Ninomiya T, Kiyohara Y, Yamashita Y. 2016. Bacterial diversity in saliva and oral health-related conditions: the Hisayama Study. Sci Rep 6:22164. https://doi.org/10.1038/srep22164.
11. Belstrøm D, Holmstrup P, Bardow A, Kokaras A, Fiehn N-E, Paster BJ. 2016. Temporal stability of the salivary microbiota in oral health. PLoS One 11:e0147472. https://doi.org/10.1371/journal.pone.0147472.
12. Blekhman R, Goodrich JK, Huang K, Sun Q, Bukowski R, Bell JT, Spector TD, Keinan A, Ley RE, Gevers D, Clark AG. 2015. Host genetic variation impacts microbiome composition across human body sites. Genome Biol 16:191. https://doi.org/10.1186/s13059-015-0759-1.
13. Turnbaugh PJ, Hamady M, Yatsunenko T, Cantarel BL, Duncan A, Ley RE, Sogin ML, Jones WJ, Roe BA, Affourtit JP, Egholm M, Henrissat B, Heath AC, Knight R, Gordon JI. 2009. A core gut microbiome in obese and lean twins. Nature 457:480–484. https://doi.org/10.1038/nature07540.
14. Yatsunenko T, Rey FE, Manary MJ, Trehan I, Dominguez-Bello MG, Contreras M, Magris M, Hidalgo G, Baldassano RN, Anokhin AP, Heath AC, Warner B, Reeder J, Kuczynski J, Caporaso JG, Lozupone CA, Lauber C, Clemente JC, Knights D, Knight R, Gordon JI. 2012. Human gut microbiome viewed across age and geography. Nature 486:222–227. https://doi.org/10.1038/nature11053.
15. Stahringer SS, Clemente JC, Corley RP, Hewitt J, Knights D, Walters WA, Knight R, Krauter KS. 2012. Nurture trumps nature in a longitudinal survey of salivary bacterial communities in twins from early adolescence to early adulthood. Genome Res 22:2146–2152. https://doi.org/10.1101/gr.140608.112.
16. Zhernakova A, Kurilshikov A, Bonder MJ, Tigchelaar EF, Schirmer M, Vatanen T, Mujagic Z, Vila AV, Falony G, Vieira-Silva S, Wang J, Imhann F, Brandsma E, Jankipersadsing SA, Joossens M, Cenit MC, Deelen P, Swertz MA, Weersma RK, Feskens EJM, Netea MG, Gevers D, Jonkers D, Franke L, Aulchenko YS, Huttenhower C, Raes J, Hofker MH, Xavier RJ, Wijmenga C, Fu J. 2016. Population-based metagenomics analysis reveals markers for gut microbiome composition and diversity. Science 352:565–569. https://doi.org/10.1126/science.aad3369.
17. Nasidze I, Li J, Quinque D, Tang K, Stoneking M. 2009. Global diversity in the human salivary microbiome. Genome Res 19:636–643. https://doi.org/10.1101/gr.084616.108.
18. Song SJ, Lauber C, Costello EK, Lozupone CA, Humphrey G, Berg-Lyons D, Caporaso JG, Knights D, Clemente JC, Nakielny S, Gordon JI, Fierer N, Knight R. 2013. Cohabiting family members share microbiota with one another and with their dogs. Elife 2:e00458. https://doi.org/10.7554/eLife.00458.
19. Abeles SR, Jones MB, Santiago-Rodriguez TM, Ly M, Klitgord N, Yooseph S, Nelson KE, Pride DT. 2016. Microbial diversity in individuals and their household contacts following typical antibiotic courses. Microbiome 4:39. https://doi.org/10.1186/s40168-016-0187-9.
20. Cephas KD, Kim J, Mathai RA, Barry KA, Dowd SE, Meline BS, Swanson KS. 2011. Comparative analysis of salivary bacterial microbiome diversity in edentulous infants and their mothers or primary care givers using pyrosequencing. PLoS One 6:e23503. https://doi.org/10.1371/journal.pone.0023503.
21. Utter DR, Mark Welch JL, Borisy GG. 2016. Individuality, stability, and variability of the plaque microbiome. Front Microbiol 7:564. https://doi.org/10.3389/fmicb.2016.00564.
22. David LA, Materna AC, Friedman J, Campos-Baptista MI, Blackburn MC, Perrotta A, Erdman SE, Alm EJ. 2014. Host lifestyle affects human microbiota on daily timescales. Genome Biol 15:R89. https://doi.org/10.1186/gb-2014-15-7-r89.
23. Levine AP, Pontikos N, Schiff ER, Jostins L, Speed D, NIDDK Inflammatory Bowel Disease Genetics Consortium, Lovat LB, Barrett JC, Grasberger H, Plagnol V, Segal AW. 2016. Genetic complexity of Crohn's disease in two large Ashkenazi Jewish families. Gastroenterology 151:698–709. https://doi.org/10.1053/j.gastro.2016.06.040.
24. Speed D, Balding DJ. 2015. Relatedness in the post-genomic era: is it still useful? Nat Rev Genet 16:33–44. https://doi.org/10.1038/nrg3821.
25. Levine A. 2015. The genetics of inflammatory bowel disease in extended multiplex Ashkenazi Jewish kindreds. PhD thesis. University College London, London, United Kingdom.
26. Dewhirst FE, Chen T, Izard J, Paster BJ, Tanner AC, Yu WH, Lakshmanan A, Wade WG. 2010. The human oral microbiome. J Bacteriol 192: 5002–5017. https://doi.org/10.1128/JB.00542-10.
27. Oksanen J, Kindt R, Legendre P, O'Hara B, Henry M, Stevens H. 2016. vegan: community ecology package version 2.4.1.
28. Nunes T, Fiorino G, Danese S, Sans M. 2011. Familial aggregation in inflammatory bowel disease: is it genes or environment? World J Gastroenterol 17:2715–2722. https://doi.org/10.3748/wjg.v17.i22.2715.
29. Zaura E, Brandt BW, Teixeira de Mattos MJ, Buijs MJ, Caspers MPM, Rashid M-U, Weintraub A, Nord CE, Savell A, Hu Y, Coates AR, Hubank M, Spratt DA, Wilson M, Keijser BJF, Crielaard W. 2015. Same exposure but two radically different responses to antibiotics: resilience of the salivary microbiome versus long-term microbial shifts in feces. mBio 6:e01693-15. https://doi.org/10.1128/mBio.01693-15.
30. Marsh PD, Head DA, Devine DA. 2015. Dental plaque as a biofilm and a microbial community—implications for treatment. J Oral Biosci 57: 185–191. https://doi.org/10.1016/j.job.2015.08.002.
31. Igartua C, Davenport ER, Gilad Y, Nicolae DL, Pinto J, Ober C. 2017. Host genetic variation in mucosal immunity pathways influences the upper airway microbiome. Microbiome 5:16. https://doi.org/10.1186/s40168-016-0227-5.
32. Bonder MJ, Kurilshikov A, Tigchelaar EF, Mujagic Z, Imhann F, Vila AV, Deelen P, Vatanen T, Schirmer M, Smeekens SP, Zhernakova DV, Jankipersadsing SA, Jaeger M, Oosting M, Cenit MC, Masclee AAM, Swertz MA, Li Y, Kumar V, Joosten L, Harmsen H, Weersma RK, Franke L, Hofker MH, Xavier RJ, Jonkers D, Netea MG, Wijmenga C, Fu J, Zhernakova A. 2016.

The effect of host genetics on the gut microbiome. Nat Genet 48: 1407–1412. https://doi.org/10.1038/ng.3663.
33. Quinque D, Kittler R, Kayser M, Stoneking M, Nasidze I. 2006. Evaluation of saliva as a source of human DNA for population and association studies. Anal Biochem 353:272–277. https://doi.org/10.1016/j.ab.2006.03.021.
34. Rognes T, Flouri T, Nichols B, Quince C, Mahé F. 2016. VSEARCH: a versatile open source tool for metagenomics. PeerJ 4:e2584. https://doi.org/10.7717/peerj.2584.
35. Eren AM, Morrison HG, Lescault PJ, Reveillaud J, Vineis JH, Sogin ML. 2015. Minimum entropy decomposition: unsupervised oligotyping for sensitive partitioning of high-throughput marker gene sequences. ISME J 9:968–979. https://doi.org/10.1038/ismej.2014.195.
36. Wang Q, Garrity GM, Tiedje JM, Cole JR. 2007. Naive Bayesian classifier for rapid assignment of rRNA sequences into the new bacterial taxonomy. Appl Environ Microbiol 73:5261–5267. https://doi.org/10.1128/AEM.00062-07.
37. Chen T, Yu W-H, Izard J, Baranova OV, Lakshmanan A, Dewhirst FE. 2010. The Human Oral Microbiome Database: a web accessible resource for investigating oral microbe taxonomic and genomic information. Database (Oxford) 2010:baq013. https://doi.org/10.1093/database/baq013.
38. Sinnwell JP, Therneau TM, Schaid DJ. 2014. The kinship2 R package for pedigree data. Hum Hered 78:91–93. https://doi.org/10.1159/000363105.
39. Speed D, Hemani G, Johnson MR, Balding DJ. 2012. Improved heritability estimation from genome-wide SNPs. Am J Hum Genet 91:1011–1021. https://doi.org/10.1016/j.ajhg.2012.10.010.